The Tidal Features of the Magellanic Cloud System

Gemma Bagheri

Submitted to the University of Hertfordshire in partial fulfilment of the requirements of the degree of Doctor of Philosophy

Research Supervisors : Dr Ralf Napiwotzki, Dr Maria-Rosa Cioni, Dr Leo Girardi

January 2014

Contents

Abstract

The Magellanic System at a distance of $\sim$ 50 kpc from the Milky Way (MW), is a prime target in the study of stellar populations, star formation histories and galactic dynamics in low metallicity environments. The Large Magellanic Cloud (LMC) and Small Magellanic Cloud (SMC) have been observed in great depth, however there has been somewhat less interest in the Magellanic Bridge connecting the two and only more recently has the interest surged in the Magellanic Stream, which trails the Clouds between them and the MW.

The Magellanic Bridge has a known younger stellar population dating back to Irwin's observations (Irwin et al., 1990), only more recently has an older population been confirmed in the Bridge by Bagheri et al. (2013) and Noël et al. (2013), while the Magellanic Stream is known to contain gas only with no stellar component. The estimated ages of the Bridge and Stream are 200 Myr (Bekki, 2007) and 2 Gyr (Diaz and Bekki, 2012) respectively, with the postulated Bridge formation from a tidal interaction between the Clouds. The formation of the Stream is less well understood with different models using varying assumptions and parameters such as Besla et al. (2012) and Nidever et al. (2010), including possibilities that the Clouds were historically bound or un-bound, and that the MW may or may not have been involved in the Stream formation.

The work in this thesis makes use of different methods of removing the Galactic foreground population in the direction of the Magellanic Bridge and Stream to create cleaned catalogues of these regions. Various methods of analysis are applied to the cleaned catalogues in this work to identify stellar populations in the

Bridge and Stream and density variations in the Bridge, including the production of CMDs and two-colour diagrams, fitting isochrones to the observational data, creating stellar density maps and studying spatial variations.

This work contains the first published confirmation that the Bridge contains an older population of stars from public catalogues, which is supported with observations of the older population in recent deeper surveys, and confirmed with spectroscopic follow up observations. The young population has ages within the age of the Bridge ($\sim 200 - 500$ Myr) and are likely to have formed in-situ, in regions of high density gas closest to the SMC. The number of young blue objects in the Bridge tiles is greater towards the SMC and decreases towards the LMC. Populations identified here reach ages up to 3 Gyr are likely to have been drawn into the Bridge from the Clouds at formation.

The key results from this work are that an older Bridge stellar population has been identified and confirmed, indicating that stars as well as gas were drawn into the Bridge at its creation. The fact that the younger population has the highest density away from the main concentration of hydrogen show that the gas within the Bridge has been displaced by ram pressure, most likely due to the Clouds moving through the Galactic halo. Less concrete results in this work reveal a puzzling populetion of objects within the Magellanic Stream, which could be stellar in nature and with follow up work, could be the first observation of Stream objects. This work contributes to our understanding of the interaction between the LMC and SMC via the Stellar populations between them.

Acknowledgements

Many people have contributed in the production of this thesis directly or indirectly. Firstly, I would like to thank my primary supervisors, Maria-Rosa Cioni and Ralf Napiwotzki, both of whom have contributed much time and feedback to the work. Maria-Rosa allowed me to develop this project in my own way and gave me the freedom to follow topics of my interest from the very start, while Ralf has been a constant presence, always available to confer and advise on matters in hand. Outside of my primary supervision I would like to thank Elias Brinks and Leo Girardi who have provided knowledge and support at various times, as well as many other Astronomers who's work has provided me with inspiration.

Away from the office I would not have made it to the end without my mum Debbie or my fiancee Simon, who continue to support me and put up with me through all times. My father Siya has always been a constant presence in my academic life and has always encouraged me to work hard and never give up, this work ethic helped me through the tough times when the PhD felt like a never ending task. Finally, it only feels right to dedicate this PhD to Mr. Kiriakopolous (Mr. K.), my A-level Physics teacher. Without Mr. K. I would have never discovered the wonder that is Astrophysics. And although Mr. K. is sadly no longer with us, his lively spirit will live on in all of the students he has taught, we are all lucky to have been in your class.

List of Figures

List of Tables

Chapter 1

Introduction

The Magellanic system comprises the LMC, the SMC, the Magellanic Bridge and Magellanic Stream with Leading Arm (Fig. 1.1). It is widely believed that the Stream and Bridge were formed tidally. The Magellanic Clouds, at a distance of approximately 50 kpc from the MW, are a prime template for observing Star Formation History (SFH), evolution and interactions of the Clouds themselves and between the Clouds and the MW. The evolution of these galaxies is strongly affected by interactions as seen for example, by the formation of the Bridge between the LMC and SMC.

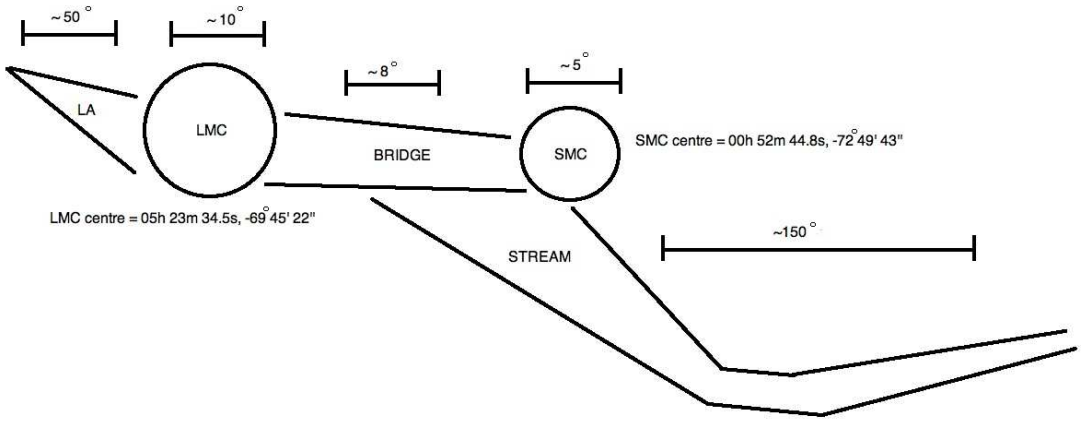

Figure 1.1: A rough schematic diagram of the LMC, SMC, Magellanic Bridge, Stream and Leading arm with the galaxy centres and angular sizes.

The Magellanic Clouds have been observed from ancient times as far back as

the year 964 by the Persian astronomer Al Sufi, noted in his 'Book of fixed stars'. Figure 1.1 shows the rough scale of the Magellanic System in terms of sizes and the total masses of the LMC and SMC are roughly 5 and 2 billion solar masses respectively, compared to the Galactic mass of 1250 billion solar masses, with the total Bridge mass at approximately 0.2 billion solar masses. The LMC and SMC are visible to the human eye in the sky of the southern hemisphere with apparent magnitudes of 0.9 for the LMC and 2.7 for the SMC (Irwin et al., 1990). The LMC is thought to have a fairly constant distance to the Galaxy at approximately 50 kpc, however there is less certainty of the distance of the SMC and whether in fact the SMC has been tidally effected to the point that it includes two separate masses with a depth of up to 10 kpc (Mathewson, 1985).

The star formation histories of the LMC and SMC indicate there after an initial burst of star formation, there was an inert period from 12 to 5 Gyr ago, at which point star formation resumed has continued until the present at an average rate of 0.2 solar masses per yr (Harris and Zaritsky, 2009). Due to the fact that star formation resumed in both the LMC and SMC approximately 5 Gyr ago indicates that there must have been a dramatic event in the Magellanic System at that time. There are peaks in both the LMC and SMC star formation rate at 2 Gyr and 500 Myr ago which coincide with suggestions that these two times were when the Clouds underwent their close encounters together to create the Bridge and Stream. Since these encounters, the LMC and SMC appear to have had a joint dynamical history leading to the current day.

The close proximity of the Magellanic Clouds to the Galaxy makes them prime targets for investigating interactions as well as the ongoing star formation within each of the Clouds. Recent measurements of the proper motions of the Clouds (Kallivayalil et al., 2013) suggest that they are on their first passage past the MW which challenges previous scenarios that the Magellanic Stream was formed from an interaction between the Clouds and the Galaxy. The Magellanic Stream appears to date to be a purely gaseous feature (Guhathakurta and Reitzel, 1998).

However, the Magellanic Bridge contains a known stellar population (Irwin et al., 1990). Different populations observed in the Magellanic Bridge can constrain the tidal event between the Clouds that led to its formation.

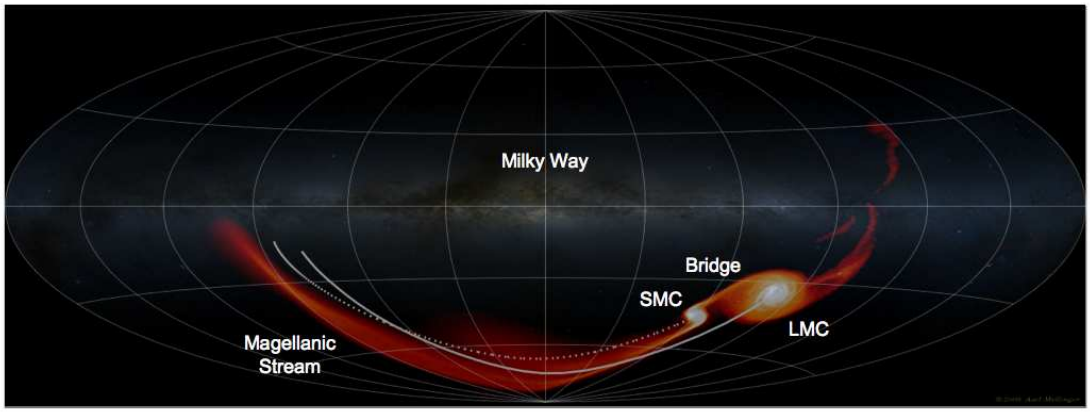

Figure 1.2: Besla et al. (2013), Hammer-Aitoff projection of the total gas distribution of the simulated Magellanic System (red) plotted over an image of the MW (Mellinger 2009). The orbital trajectory of the LMC(SMC) is indicated by the solid(dotted) white line.

Due to the expansion of the universe, the particles that exist in space are moving away from each other, unless there is enough matter for gravitational forces to overcome the expansion, causing mass to become more dense and to collapse and grow. It is possible that larger structures formed first, the size of galactic clusters that then fragmented to form galaxies and dwarf galaxies, or that smaller dwarf galaxies formed first and merged to produce larger galaxies and clusters. These competing scenarios and refereed to as top down and bottom up scenarios respectively, with a combination of the two fitting in with observations. The first protogalaxies existed 13 to 14 Gyr ago, with dark matter and ordinary matter separating at this point due to their different interactions. Elliptical galaxies were created with rapid star formation exhausting all of the gas supplies in an initial burst, forming a smooth elliptical shape. Spiral galaxies are created with star formation occurring slowly with gas collisions conserving angular momentum forming the spiral shape with ongoing star formation at the present time such as in the Milky Way.

Galactic interactions include mergers, cannibalism and harassment. If two galax-

ies are of equal size they can undergo a merger, this is a possibility of what has happened and is ongoing between the LMC and SMC. Harassment could occur if the Magellanic Clouds are travelling past the Galaxy fast enough that they do not undergo cannibalism by the Galaxy which is likely to occur in the future of the Clouds. Due to the relative size of the Magellanic Clouds and the Galaxy, the Clouds will be greatly effected by the tidal forces from the Galaxy.

Tidal interactions are an important feature of galaxy evolution as they can reshape galaxies and trigger star formation events (Smith et al., 2010). There are a number of tidal features involved in galaxy dynamics including spirals, bridges and tails (Smith et al., 2006). Many galaxies exhibit these tidal features as described in Byrd and Salo (1994) and Bekki (2008), and in the case of the Magellanic Clouds it is an important task to understand the Magellanic Bridge and Stream as these features will have an impact on the stellar populations, future shaping and dynamical evolution of the Clouds and perhaps the MW.

Nidever at al. (2011) discover stars that belong to the SMC out to distances twice as far as previous detections. They find an intermediate component of older stars that dominate a ring in the SMC from 3° to 7.5° that follow an elliptical pattern, and also a outer circle of objects from 7.5° to 10.6° which the authors postulate, could be a bound stellar halo. Work such as this indicates that there may be more to the SMC than we have previously observed, and as the SMC feeds into the Bridge, this work is of interest to understand more the extent of the interaction between the Clouds and the Galaxy but also, between the LMC and SMC.

At the start of the work in this thesis, only young populations had been observed in the Bridge region (Irwin et al., 1990), which implied that at the time of the tidal interaction, only gas was drawn in from the Clouds to create the Bridge, and that the inter-Cloud population of the Bridge formed some time afterwards. An older Bridge population has been identified in this work (Bagheri et al., 2013), and also in other new work (Noël et al., 2013), which indicates that stars, as well as gas, were stripped from the LMC and/or SMC in the event that formed the Bridge.

As tidal interactions should affect stars and gas, an older population would be expected within the Bridge which has been confirmed in this thesis with further observations of this older Bridge population with deeper catalogues. In the case of the Magellanic Stream, a stellar population would be expected if tidal interactions were involved in the Stream creation. To date, no stellar component has been observed in the Stream which supports the formation without tidal forces, but more likely from ram pressure. This work investigates the contribution of tidal interactions in the formation of both the Magellanic Bridge and Stream by searching for a stellar counterpart in the Stream and with the identification and confirmation of the older population in the Bridge.

Chapter 2 places this work into context by describing previous and current work on the Magellanic Bridge and Stream as well as a description of stellar evolution and different populations. Chapter 3 describes the acquisition of data to be analysed in this work and the creation of catalogues with the application of quality flags, including a description of the surveys and instruments used in each catalogue. A study of the removal of Galactic foreground objects in the direction of the Magellanic Clouds is outlined in Chapter 4 including an investigation into different methods and different foreground regions in order to create accurate un-contaminated catalogues for analysis. Chapter 5 describes a study of the Magellanic Bridge with public catalogues along with the identification of an older population. Chapter 6 investigates the stellar content of the Magellanic Bridge with the VMC survey, including an analysis of younger and older populations. Follow up spectroscopic observations are analysed in Chapter 7 of red giant objects identified from Chapter 5. The Magellanic Stream is studied in Chapter 8 using both public catalogues and the VMC survey to search for a stellar population for the first time. A summary of the work in this thesis is presented in Chapter 9.

Chapter 2

Tidal features of the Magellanic System

2.1 The Magellanic Bridge

To date, the Magellanic Bridge has been investigated in terms of neutral and ionised gas and stellar populations. The existence of a young population of stars in the Bridge has been known for decades (Irwin et al., 1990), however the existence of an older stellar component in the Bridge has only recently been identified during the writing this thesis by Bagheri et al. (2013) and Noël et al. (2013). The work in this thesis aims to complement previous work on the Magellanic Bridge by identifying and confirming the existence of an older Bridge population, as well as investigating the spatial distribution of the young and older stellar population, and looking in more detail at the different populations present in the Bridge. This work will differentiate between the formation of these features from ram pressure exerted on the Clouds gas when they move through the warm Galactic halo, or tidal forces on the Magellanic Cloud stars from the gravitational pull of them from each other and from the Galaxy.

2.1.1 Stellar populations

Hindman et al. (1963a), reported about observations and digital reduction for a survey of HI in the direction of the Magellanic Clouds and noted a considerable amount of gas between the two Clouds (Fig. 2.1). In a follow up paper Hindman et al. (1963b) also reported that the Magellanic Clouds were encompassed by a halo of gas. They also observed double peaks in the velocity of the SMC gas possibly indicating two separate masses one behind the other. Irwin et al. (1990) showed that the stellar population of the SMC wing extends towards the LMC halo which is supported by the detection of young blue stars in several areas between the Clouds (Fig. 2.2). Grondin et al. (1991), carried out CCD photometry in B and V bands of three regions within the Bridge and found populations of young stars, approximately 100 Myr old. This study also yielded the result that the stellar population in the Bridge has a distance gradient from the SMC wing tip to the LMC halo with the populations on the SMC side being more dense, confirming that associations on this side formed first.

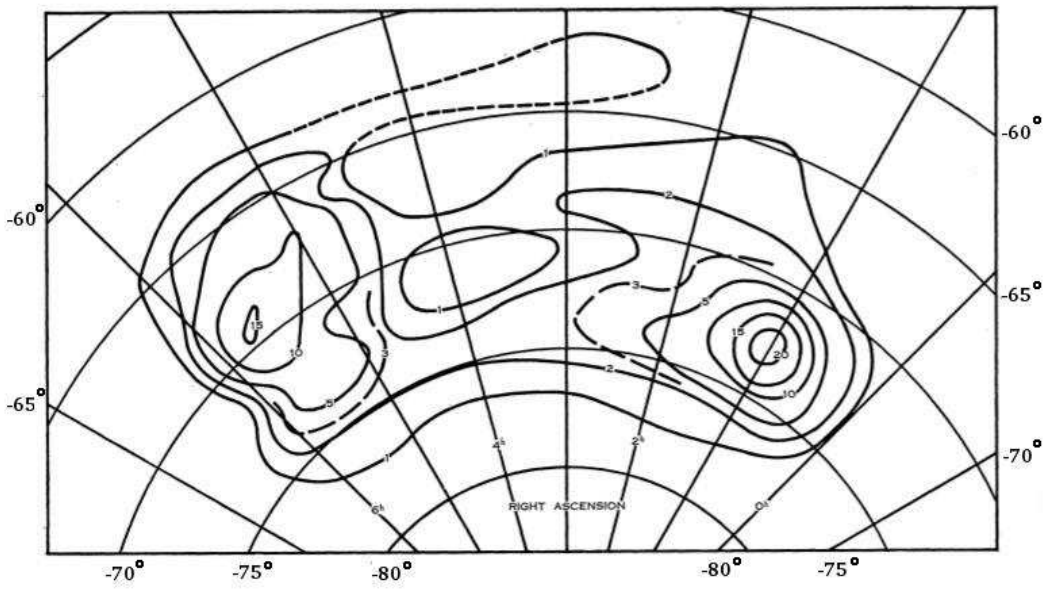

Figure 2.1: Contours of integrated brightness of HI in the Magellanic System from Hindman et al. (1963b). Contour units are $2 \times 10^{-16}\mathrm{Wm}^{-2}\mathrm{sr}^{-1}$.

Grondin et al. (1992) studied B, V photometry of two regions of stars in the SMC wing and one in the central Bridge region, and isochrone fittings showed that some associations are as young as 16 Myr in the resulting colour-magnitude diagrams (CMDs). This study also observed that the inter-Cloud stars were, not homogeneously distributed, and were likely to have formed from the SMC. Mathewson (1985) proposed that the SMC had a close encounter with the LMC warping the LMC disk and forming the Bridge while tidally fissioning the SMC in a process of irreversible disintegration. It was also postulated here that the Clouds were not bound to the Galaxy and were approaching from the direction of Andromeda after a close encounter that triggered a massive starburst in the Magellanic Clouds at that time. Matthewson also stated that the Stream was swept out of the Cloud region by ram pressure from the gaseous halo of the MW and that if dynamic friction captured the Clouds on a MW collision, a polar ring would form which is not observed. Grondin et al. (1991) proposed a scenario that a close encounter of the LMC and SMC occurred, triggering star formation in the densest parts of the inter-Cloud region, leaving denser gas on the SMC side (Fig. 2.3). Their optical data analysis confirmed that the Bridge associations on the west side formed first. It was then suggested by Grondin et al. (1992) that a tidal interaction between the Clouds was on a milder scale than seen elsewhere in external galaxies but caused the formation of a disk around the SMC which was then stripped to form the Bridge.

Grondin and Demers (1993) showed that a collision of the Clouds with the Galactic halo would give sufficient energy to form large structures such as the SMC wing but that this process is not likely to yield star formation in the Bridge. Hambly et al. (1994) found that Bridge stars have a lower metallicity than typical SMC stars, which could mean that the material in the Bridge came from less chemically evolved parts of the SMC. They postulated the age of the Bridge to be approximately 7 Myr, which implies that continuing star formation is present in the Bridge and that the previous scenario of the close encounter between the

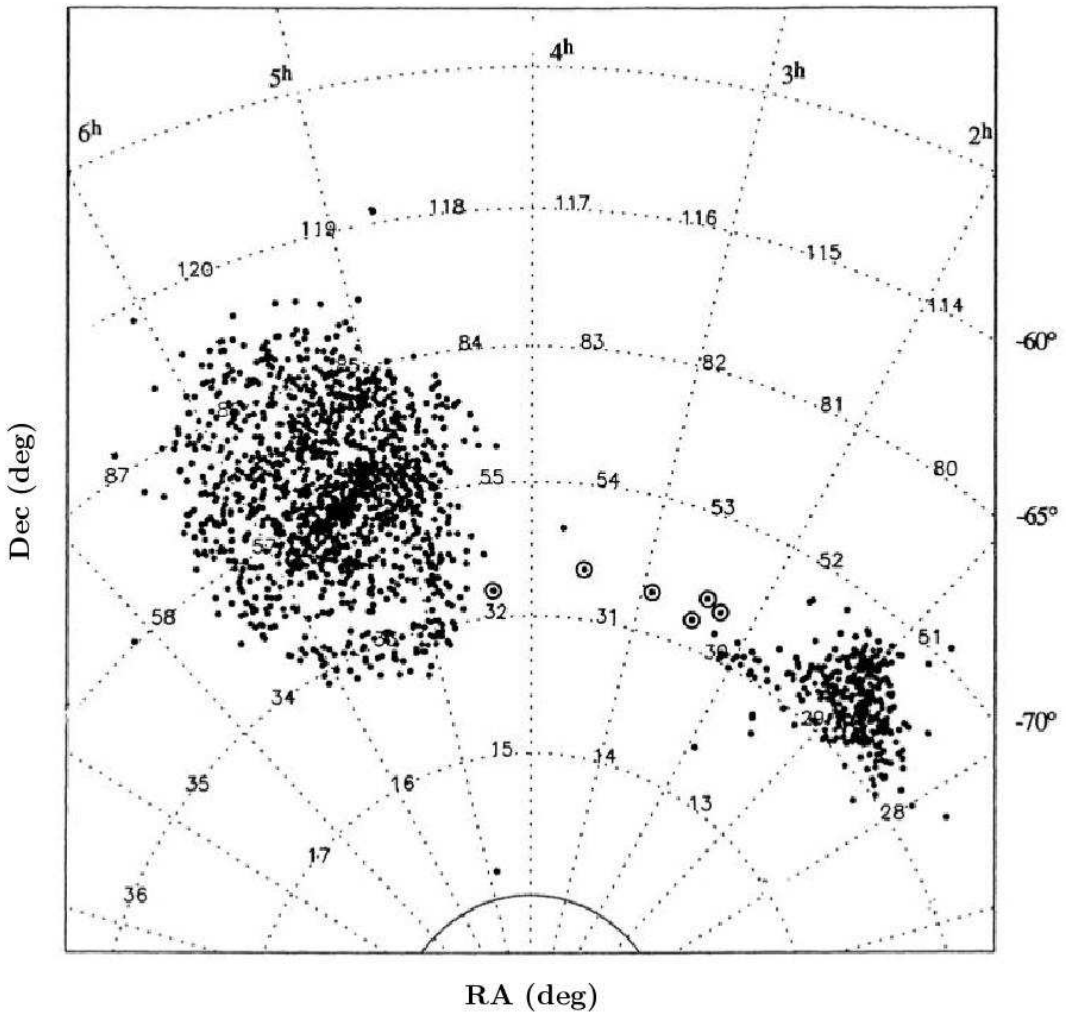

Figure 2.2: Irwin (1991) distribution of Magellanic Cloud clusters on a grid of UKST field numbers. Blue stellar associations found by Irwin et al. (1990) are shown with encircled symbols.

Clouds 200 Myr ago is not the only cause of starbursts within the Bridge. Authors since (e.g. Christodoulou et al. (1997) and Mizuno et al. (2006)), have postulated that the Bridge may have been formed from a close encounter 200 Myr ago between the LMC and SMC, which is challenged with postulations that the Bridge was formed later due to the difference between the Bridge and SMC populations and that the ages of associations in the Bridge are closer to 6 Myr. It is possible that the Bridge was formed in the close encounter 200 Myr ago but that star formation was triggered by an event $6 - 7$ Myr ago.

Bica and Schmitt (1995) carried out a survey of extended objects in the Bridge

and SMC using the ESO/SERC R and J Sky Survey Atlases and found 1188 objects. The authors assume a border between the SMC and Bridge at $\alpha = 2^h$ and of the total Bridge objects, they find 11 stellar clusters, 97 emissionless associations and 6 objects relating to emission nebulae. The results in this work suggest different SFHs between the Bridge and SMC given different ratios of objects in each, although the low gas density in the Bridge and different average mass function are likely to have an effect.

Harris (2007) used the MOSAIC II camera on the 4m telescope at CTIAO to look at 12 regions in the Magellanic Bridge to look at the younger Bridge population which he detected in each of his observing fields (Fig. 2.4). Harris also searched for an older population, which would have been stripped from the SMC as stars. The 12 fields observed here follow the HI gas ridge line in the Bridge and are extended to $\alpha = 3^h$, where the HI surface density falls to below the critical threshold for star formation determined by Kennicutt (1989). The work showed no clear detection of an older population in the Bridge indicating perhaps the stars in the Bridge were all formed in-situ due to the SMC being highly bound centrally with a looser gaseous halo. From modeling of H-R diagrams, they expected that star formation in the Bridge occurred as far back as the tidal interaction that formed the Bridge 200 Myr ago, so an older population, greater than 200 Myr, would be expected to have originated from SMC stripping.

2.1.2 The gas component of the Magellanic Bridge

The Bridge has a confirmed stellar population, but the hydrogen features within the Bridge are also of interest. Muller et al. (2003) used the 64m Parkes telescope and the Australia Telescope Compact Array (ATCA) to observe two velocity components within the Bridge HI gas similar to the SMC. Shell like structures were observed in the Bridge and interpreted as Hα shells with an unknown origin. Proposed explanations include gravitational and pressure instabilities, collisions between High Velocity Clouds (HVC) and ram pressure effects. They propose

that a shell within a gas cloud can be formed through a range of mechanisms (Shu, 1992) involving young energetic stars or clusters that ionise their surrounding gas into a hot, high pressure region. This produces a spherical shock wave which propagates into the ambient neutral gas, giving a relatively low density sphere enclosed by a higher density hydrogen shell which moves through the ambient gas at supersonic velocities. Hα shells have also been observed in the SMC (Staveley-Smith et al., 1997). The Bridge is observed here to have shells, lumps, filaments and holes ranging from 98″ to approximately 7°. A bi-modal velocity in the Bridge HI gas is also observed here which converges at about 3.6 kpc from the SMC towards the LMC. Also a large HI loop exists that is 1 kpc in diameter containing over 150 smaller shells which are expanding at a lower rate and have kinematics similar to those in the SMC. The HI column density correlates well with the O and B type star (OB) distributions, however the shells do not.

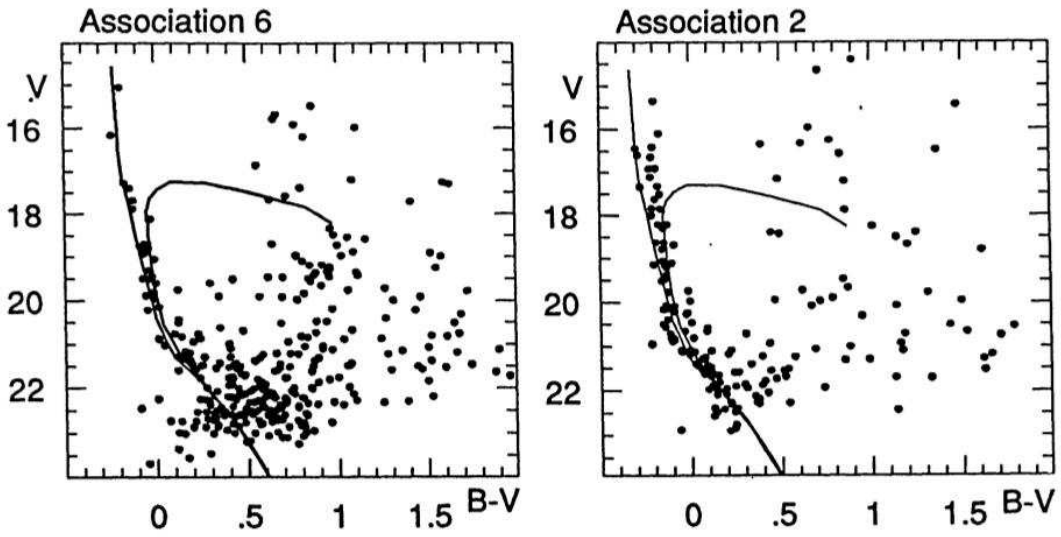

Figure 2.3: CMD, $(B-V)$ vs V of Bridge associations from Grondin et al. (1991). Isochrones are for 150 Myr with $Y = 0.3$ and $Z = 0.004$ and the ZAMS from Schmidt-Kaler (1982).

Muller et al. (2004) performed a statistical analysis to show that the northern and southern parts of the Magellanic Bridge represent two distinct arms of gas emanating from the SMC which challenges previous ideas that the Bridge was formed of a single filamentary feature. The southern part of the Bridge has brighter and

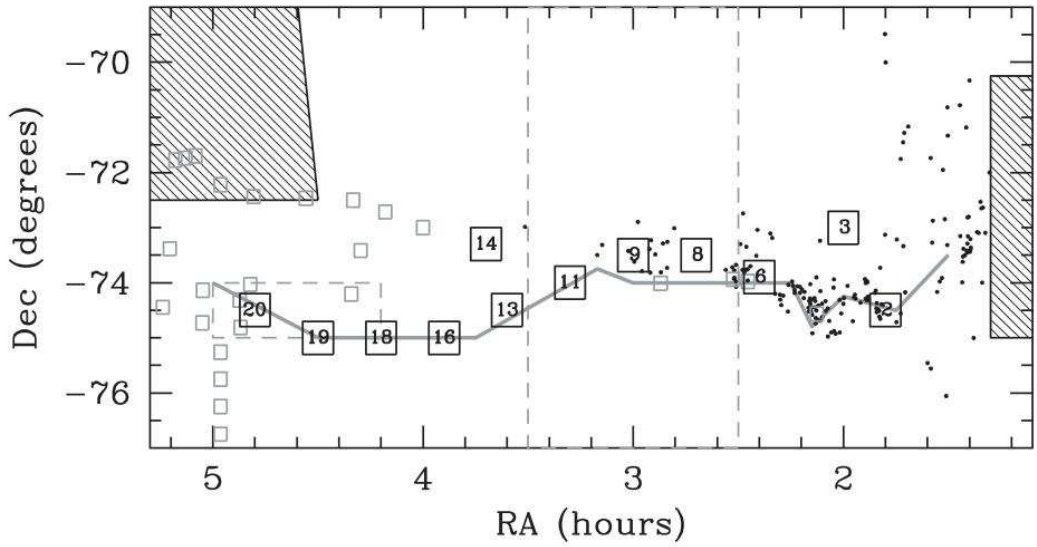

Figure 2.4: Harris (2007, Fig. 1), Schematic view of the Magellanic Bridge region. The positions of the 12 observed CTIO 4 m fields are shown as numbered boxes. The inter-Cloud fields previously observed by Demers & Battinelli (1998) are shown as grey boxes. Star clusters from Bica & Schmitt (1995) are shown as points. The grey line is an approximate trace of the HI ridge-line through the inter-Cloud region, from Fig. 1 in Putman (2000). The hatched areas represent the portions of the regions covered by the Magellanic Clouds Photometric Survey (LMC at left, Zaritsky et al. 2004; SMC at right, Zaritsky et al. 2002).

more turbulent HI similar to the SMC, however the northern part is more tenuous. This study continues with Muller et al. (2004) and Muller and Bekki (2007) who also find a velocity bimodality within the Bridge (Fig. 2.5) and large HI loops up to 1.3 kpc in diameter, spanning across the northern and southern parts of the Bridge. They postulate that the northern part of the Bridge gas is a radially extended arm of the SMC and is not connected to the LMC but that the southern part was drawn from the SMC in a LMC−SMC interaction. Muller and Parker (2007) investigate the different hydrogen features within the Magellanic Bridge and conclude that the stellar population of the Bridge does not contribute significantly to the turbulent energy balance of the inter-stellar medium (ISM) and that the low emission measurements of the HI features suggest that the ISM in the Bridge is not being greatly mixed by the deposition of energy via turbulent motions and stellar winds, implying that the ISM within the Magellanic Bridge is

mostly a purely turbulent feature on all scales. Hambly et al. (1994) use the 3.9m Anglo-Australian telescope to look at one main sequence (MS) B star and one B type supergiant with Echelle spectra to determine their chemical composition to get the temperature structure of the ISM within the Bridge. They find that the stars have a mild He deficiency of $0.1 - 0.2$ dex and a heavy element depletion of $0.5 - 1$ dex which reflect the compositions within the SMC and not the LMC.

Kobulnicky and Dickey (1999) detect cold atomic hydrogen in the Bridge using 21cm absorption spectroscopy towards the radio source B0312-770. The results from this study represent a cold atomic phase probably accompanied by molecular condensation in the ISM within the Bridge. It is possible that the young OB stars observed in the Bridge could have formed from this gas phase opposed to formation within the SMC before the tidal stripping, representing a small scale version of star formation in tidal tails of interacting galaxies. The dynamical structures of the Magellanic Clouds are complex, with an SMC depth up to 10 kpc (North et al., 2009). The thermodynamic state and metallicity of the Magellanic Bridge are poorly understood and it is not clear whether the stellar populations in the Bridge were formed in-situ or stripped from the SMC as stars. There is no evidence of star forming gas clouds within the Bridge, but molecular condensation would be possible, initiating the production of Bridge stars from cold atomic hydrogen. Muller et al. (2003) used the MOPRA 22m and SEST 15m telescopes to map a region of CO emission embedded within a cloud of HI in an IRAS region in the Magellanic Bridge. They determine that the Bridge is not as evolved as the SMC but that this region is the first evidence of star formation in the Bridge from molecular cloud collapse. They confirm that there is a difference in abundances of the SMC and Bridge indicating that the Bridge is formed of SMC gas and a component from the un-enriched SMC outer halo. CO regions can be associated with tidally extruded HI and Braine et al. (2001) show that CO emissions correlate with regions of high HI column density. This may be accurate for the Bridge as the regions of high HI column density are well correlated to the young stellar

associations.

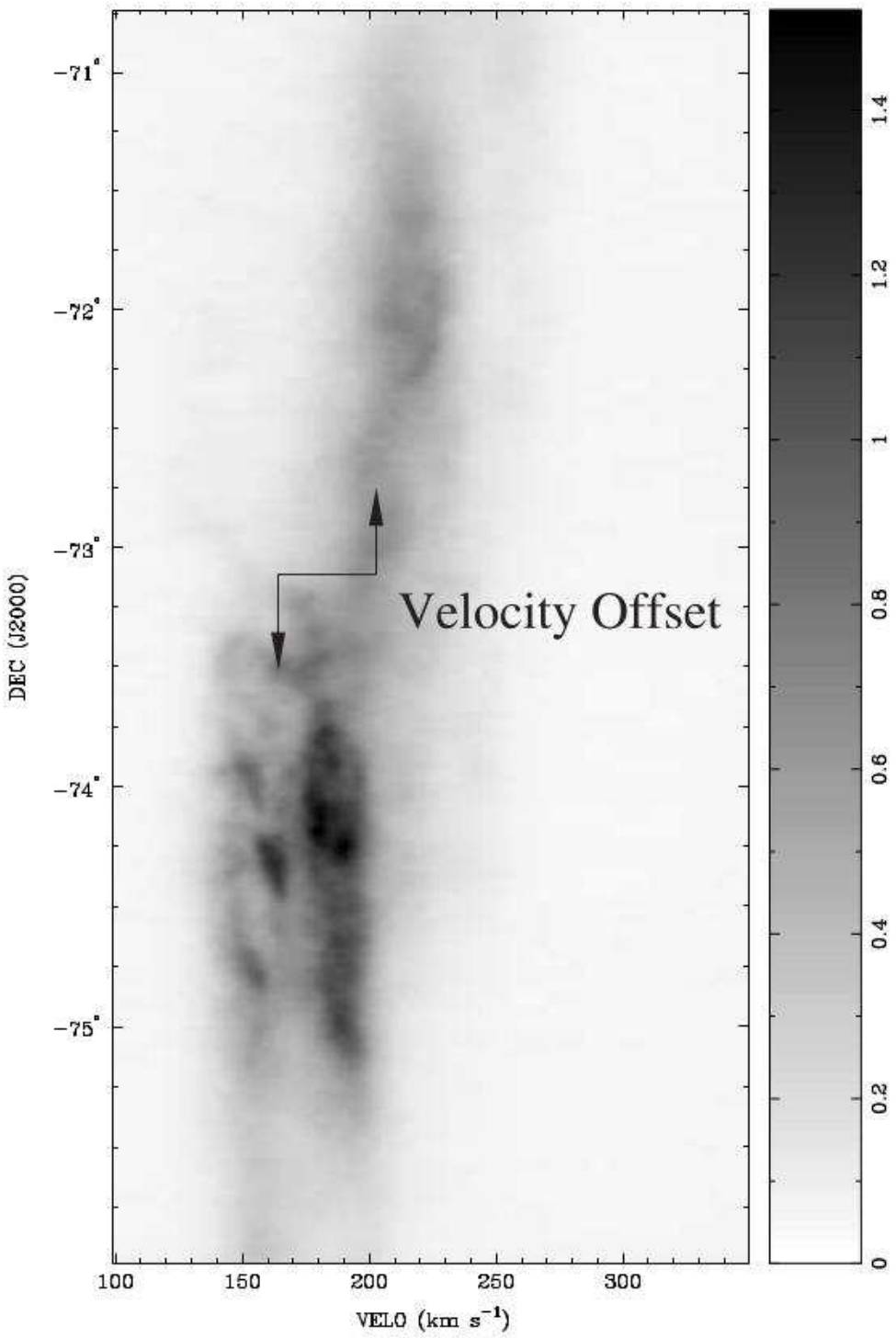

Figure 2.5: Muller et al. (2004)[Fig. 2], Integrated intensity map of the declination-velocity projection of the combined ATCA-Parkes data cube. The northern part of the HI in the Bridge is clearly offset to higher velocities with respect to the southern part by $40-50$ km s^{-1}. Since this map is integrated along the image x-axis, the labels on the declination axis are correct only for RA=02h 08m 08s.

The detections of CO within the Bridge are well matched to those in the SMC with a correlation between velocity width and integrated CO intensity which are greater in the SMC, which is expected from the progenitor galaxy with star formation occurring in the Bridge through molecular cloud collapse. The above results with the velocity bimodality and existence of Hα shells support the theoretical understanding that the Bridge was formed primarily from material of the SMC and not the LMC. This supports scenarios that the Bridge formed from a tidal interaction between the Clouds 200 Myr ago stripping gas from the SMC to form the Bridge and that an event closer to 6 Myr ago triggered star formation from molecular condensations with the presence of CO. It is also possible that the northern part of the Bridge not connected to the LMC may have been stripped from a different region of the SMC that contained stars at the time of the stripping event.

2.1.3 Massive star formation

Chen et al. (2010b) combine mid-IR Spitzer IRAC and MIPS observations, with 2MASS and IRSF JHK catalogs with archival UKST BRI data, to identify massive young stellar objects (YSOs) in the Magellanic Bridge. The authors identify 20 candidates, most of which are found near regions with high HI column density. The identification of some of these objects in regions with low HI column density, but near diffuse Hα emission implies triggered star formation in these locations. Barger and Haffner (2011) also look at Hα regions in the Bridge to investigate warm ionised gas using spectra from the Wisconsin H-alpha Mapper observatory. This work is part of an ongoing investigation of the ionised gas in the Magellanic Bridge and the source of ionisation. They find that the Magellanic Bridge has a complex gas distribution with multi-peak spectral features which could indicate active local star formation.

2.1.4 The detection of an older population

Together with the study described in this thesis for which preliminary results were published in Bagheri et al. (2013), evidence for an older stellar population associated to the Magellanic Bridge was found by Noël et al. (2013). Bagheri et al. (2013) search for an older stellar population in the Bridge using NIR catalogues from 2MASS and WISE across the entire Bridge, while Noël et al. (2013) analyse B and R band images of 6 fields merged into 2 larger fields of 0.75×0.75 degrees in the Bridge using the ESO Wide Field Imager (WFI) at La Silla. Both of these studies identify an older population in the Bridge with ages up to ~ 10 Gyr indicating that these objects were drawn into the Bridge tidally at formation, or that the Bridge is older than the current estimate of ~ 200 Myr. New work in this thesis from the VISTA survey of the Magellanic Clouds (Cioni et al., 2011) will make use of deeper NIR magnitudes than DENIS, 2MASS and WISE to further explore the recently identified older Bridge population.

2.2 The Magellanic Stream

The Magellanic Stream is a $\sim 140^{\circ}$ long (Nidever et al., 2010) gas feature trailing the Magellanic Clouds. The Magellanic Stream has no observed stellar population to date however, if the Stream was formed from a tidal interaction between the Magellanic Clouds and the Galaxy, some form of stellar population would be expected. If there remains no detection of stars in the Stream after deeper observations, this may imply a different formation mechanism of the Stream which should be investigated.

A number of formation mechanisms for the Magellanic Stream have been postulated, Murai and Fujimoto (1980) assume that the Stream is tidal debris stripped from the Magellanic Clouds approximately 2 billion years ago when they were at pericentre one orbit ago. The model requires a high transverse motion of the Clouds, which has been measured by Jones et al. (1994). They confirm that the

Magellanic Stream is trailing the Magellanic Clouds. Mathewson et al. (1987) postulated that the Stream consists of material swept from the inter-Cloud region of the Magellanic Clouds from ram pressure stripping by repeated collisions with high velocity clouds (HVC) in the Galactic halo. This scenario predicts a number of clumps within the Stream and requires a high density of gas at large distances from the Clouds. For a long time the most prominent model was that the Stream formed tidally from an interaction between the Magellanic Clouds and the Galaxy (Mathewson et al., 1987). However, this model fails to reproduce observed features of the Stream including the absence of a more substantial counter-Stream expected from tidal stripping. Radial velocities of the Stream are not consistent with the observed orbital parameters of the Magellanic Clouds, yet stripped material from the LMC would still maintain LMC internal velocities. If the Stream formed from the LMC a thick plane of the Stream around the MW would be observed, yet the observations show that the Stream is a tightly confined feature.

2.2.1 The Magellanic Leading Arm

As well as the main body if the Magellanic Stream, a counter-Stream feature exists which has been named the Leading Arm (LA). The LA was first discovered by Putman et al. (1999) with observations from the HI Parkes All-Sky-Survey (HIPASS) of the global HI distribution in the vicinity of the Magellanic Clouds and the southern part of the Galaxy. This work identified a narrow continuous counter-Stream leading the direction of motion of the Magellanic Clouds supporting the gravitational model of the Magellanic Stream where the Stream and LA are torn from the Clouds. Studies of the LA have been ongoing since its discovery including more recent work from McClure-Griffiths et al. (2010) and For et al. (2013). The LA is an important feature of the Magellanic System as the inclusion of the LA in model simulations of the Clouds will lead to a more accurate representation of their dynamical history.

2.2.2 Features of the Magellanic Stream

The Stream exhibits uniform variations along its length and to date no stellar component has been observed, which conflicts with the model of tidal formation. Moore and Davis (1994) present numerical investigations to test models for the origin of the Magellanic Stream. They suggest an alternative model that the Stream formed from ram-pressure stripping during its last passage through an extended ionised disk of the Galaxy about 500 Myr ago. The authors also postulate the existence of an extended dilute halo of diffuse ionised gas surrounding the Galaxy to prevent the stripped material from leading the Clouds and causing a large infall velocity. Sofue (1994) proposed a ram-pressure accretion model of intergalactic gas clouds by galaxies with extended gaseous halos showing that gaseous debris from tidally disturbed galaxies is accreted by a nearby galaxy. The above two models do not accurately produce the amount of gas within the Stream and cannot explain the existence of the leading arm (LA). Mastropietro et al. (2004) studied the simultaneous effects of gravitational and hydrodynamical forces acting on the LMC as it moves through the halo of the Galaxy and they also looked at the internal changes in the structure of the LMC neglecting any effects from the SMC due to its small mass. From this work the Stream is reproduced without a significant amount of stars and the LA is possibly formed, but the study remained unable to reproduce the Stream accurately in terms of size and extension.

Recent measurements of the proper motion of the Magellanic Clouds by Kallivayalil et al. (2006, 2013) show with HST data that the Clouds are on their first passage past the MW and are likely to have been bound to each other for a Hubble time. This challenges models of Stream formation from a tidal interaction between the Clouds and the Galaxy alone as if the Clouds are on their first passage, perhaps the Stream was created by tidal forces between the Clouds and was just extended by the Clouds moving through the Galactic halo. Mathewson et al. (1974) observed the Stream to have six discrete complex HI concentrations and more recently Putman and Gibson (1999) used HIPASS to reveal a complex net-

work of filaments and clumps. Putman et al. (2002) performed the first complete survey of the Magellanic Stream and found bifurcation along the main body along with the discovery of dense, isolated gas clouds along the whole length with head-tail structures and a complex filamentary web at the end closest to the Magellanic Clouds, where gas is freshly stripped away from the SMC and the Magellanic Bridge (Fig. 2.6). Two filaments observed here separately stripped from the SMC and the Bridge, may also indicate that the Bridge is older than previously thought. They also detected a velocity gradient in the Stream from 700 km/s closest to the Clouds down to approximately 400 km/s at the tail end. This gradient is greater than would be expected from Galactic rotation implying that the Stream has a non-circular orbit. Putman et al. (2002) also observed that the most elongated gas clouds within the Magellanic Stream have position angles that are aligned along the Stream which suggests shearing motion from tidal forces or interaction with the Galactic halo.

The first metallicity measurements of the Stream were taken using the HST by Gibson et al. (2000). This work made use of observations of three background sources in the direction of the Stream. They found that their measurements were consistent with the LMC and SMC values for the present day, but that if the Stream formed 1.5 Gyr ago, its metal abundance is approximately two times higher than expected. However, systematic uncertainties in the HI column density measurements could weaken this argument. Stanimirović et al. (2002) studied the morphology and confinement mechanisms of Stream gas clouds by looking at 21cm HI emission with the Arecibo telescope in two regions of the northern tip of the Stream away from the Magellanic Clouds (Fig. 2.7). They found that the gas clouds could not be gravitationally confined as this would require large amounts of dark matter, or that the gas clouds were in free expansion. They postulated that the most likely confinement mechanism is pressure from the hot Galactic halo gas. Stanimirović et al. (2008) used the Arecibo telescope to find four large scale streams extending over 20°, each with different morphologies and

velocity gradients. This finding again supports models of a tidal origin of the Magellanic Stream suggesting spatial and kinematic bifurcation. Three of their internal streams appeared to form from a three way split but the fourth is younger and looks to have originated from the Magellanic Bridge less than $200 - 500$ Myr ago.

More recently Matthews et al. (2009) detected the first cold atomic gas within the Stream through 21cm absorption with the ATCA towards the background source $J0119 - 6809$. The spin temperature in the Stream is higher than similar components in the LMC, SMC and Bridge. They found cool atomic hydrogen in only one of the four fields examined and state that most Stream gas clouds are too tenuous for active star formation. This detection does not rule out that some regions within the Stream could possibly support star formation. Stanimirovic et al. (2010) revisit the topic of the small scale structure within the Stream and whether the gas is fed back into the Magellanic Clouds via accretion. The authors also examine the ageing process of Stream gas through hydrodynamic instabilities and interstellar turbulence and how the gas fails to form stars although it remains cool. Processes that occur on small scales within the complex HI gas within the Stream could affect star formation, although it is not known how or over what periods of time. Stanimirovic et al. (2010) suggest that the Magellanic Stream gas is being replenished continually and that this should eventually lead to the formation of Stream stars, but that further observations are required to constrain properties of the gas in the Stream and halos of the Magellanic Clouds.

2.2.3 The formation of the Stream

The debate on the correct formation mechanism for the Stream has become a widely discussed topic recently. The latest HST proper motions (Kallivayalil et al., 2013) open up the question of the Stream formation, as previous models of the Stream rely on a number of close encounters between the LMC, SMC and MW. The HST proper motions imply that the Magellanic Clouds are on their first

passage past the MW and therefore models of the Cloud's past need to be revisited. The different possible scenarios that are currently presented by different research groups, are the formation of the Stream from a purely tidal perspective, and the formation with the inclusion of ram pressure. Below is a summary of four of the more prominent models and scenarios for the formation of the Stream.
Ruzicka et al. (2011) investigate the parameter space of the interaction between the Magellanic Clouds and the Galaxy with the inclusion of a new free parameter, the local standard or rest (LSR) circular velocity. The results in this work involve two close encounters between the LMC and SMC within the last 4 Gyr, the first of which formed the Stream tidally about 2.5 Gyr ago, with a more recent interaction at $\sim$ 150 Myr ago creating the Magellanic Bridge. This work still leaves open questions on the modeling of the Stream and state that further free parameters are required for increased model accuracy such as dissipative hydrodynamical processes and although tidal processes included here reproduce the LA to some extent, the inclusion of ram pressure may produce more accurate results.
Nidever et al. (2010) use the Green Back Telescope to study the extent of the Magellanic Stream in a 21-cm survey. They discover that it is some 40° longer than previously known, and that with the inclusion of the LA, the entire system is at least 200° long. This work provides an age estimate of $\sim$ 2.5 Gyr for the Stream which coincides with an epoch of star formation in the Clouds from a close encounter that could have formed the Stream. Besla et al. (2010) state that with the HST proper motions from Kallivayalil et al. (2006), it appears that the Clouds are either on their first passage past the Galaxy or that they are on an eccentric long period orbit about the Galaxy (Fig. 2.8). The authors state that in this scenario, the Stream cannot be formed from tidal stripping from the MW with a contribution from ram pressure, but that it could have been formed from the effect of LMC tides acting on the SMC prior to accretion by the Galaxy. This work concludes that a tidal scenario between the Clouds alone is sufficient to reproduce a Magellanic Stream without the need for hydrodynamical interactions

or MW tides, however the present day Stream observations are not replicated in detail.

Diaz and Bekki (2011) investigate the possibility that the Magellanic Clouds are not in bound orbits after the more recent HST proper motions (Kallivayalil et al., 2006), and calculate models in which the Clouds have only recently been bound to each other, although separately bound to the MW for over 5 Gyr (Figs. 2.9, 2.10). This work finds that tidal stripping dominated by the LMC can form the Stream and LA during a recent dynamical coupling of the two Clouds. This work follows the common tidal model of the system with the inclusion of LMC and SMC proper motions to 1σ of the HST values, and a parameterization of the MW isothermal halo with an increased circular velocity of 250 kms^{-1}. The main difference in these models is that the Magellanic Cloud pericentric passage about the MW does not contribute to the tidal stripping of the SMC disk, but the stripping occurs during the formation of an LMC−SMC binary pair $\sim$ 1.2 Gyr ago. The authors also state that their model should be classed as a stepping stone between traditional models and more robust models due to their neglection of self-gravity, gas physics and use of an isothermal atmosphere. In a later paper Diaz and Bekki (2012) present a further model in which the LMC and SMC are more recently an interacting binary pair as recently as $\sim$ 3 Gyr ago. This more recent work also finds that a bound association with the Galaxy is required for a bifurcation in the Magellanic Stream and also that additional HI structures are formed in the tidal interactions including a counter-Bridge. This work is able to reproduce the Stream morphology and bifurcation as well as its new longer extent, using proper motion values from Vieira et al. (2010). Diaz & Bekki show that there are many parameters to be considered when modeling the Stream and that the more observations we have, the more accurate models we can produce.

In an overview of the Magellanic Stream, Mathewson (2012) discusses the discovery of the Stream and the different potential formation mechanisms. The author describes how previous observations of the Magellanic Clouds led to a

Stream age of 0.3 Gyr. However, the more recent observations of the true extent of the Stream lead to a new Stream age of 1.5 Gyr. Mathewson states that we are no closer to understanding the formation of the Stream than ~ 40 years ago when it was first discovered. Finding an explanation for the formation mechanism of the Stream and estimating a time of formation has proven to be a difficult task. Over the past years, observations of the Stream have improved, and to date the estimated length of the Stream (without the LA) is somewhere around 140° (Nidever et al., 2010). Due to the hyperbolic orbit of the Clouds, the longer the Stream is, the older it has to be to explain its extent. The production of the Stream from the Bridge by ram pressure would support the lack of a stellar component of the Stream. However, a model for the formation of the Stream that involves just ram pressure, fails to produce an old enough Stream age to explain its length. Newer tidal models for the Stream formation can produce an older Stream age, but other aspects cannot be reproduced accurately like the LA in terms of length and position. Perhaps a deeper search for a Stream stellar population in this thesis can shed light on the above problems and aid the models in reproducing the formation and evolution of the Stream to mirror current observations of this intriguing feature. The detection of a stellar population older than the age of the Stream would evidence the presence of tidal forces at the time of creation, and a younger population would indicate stars formed in-situ. As the Stream is such a large feature, the observation of a stellar component would give a location of interest within the Stream for further study to build up the picture of the Stream formation and expected evolution.

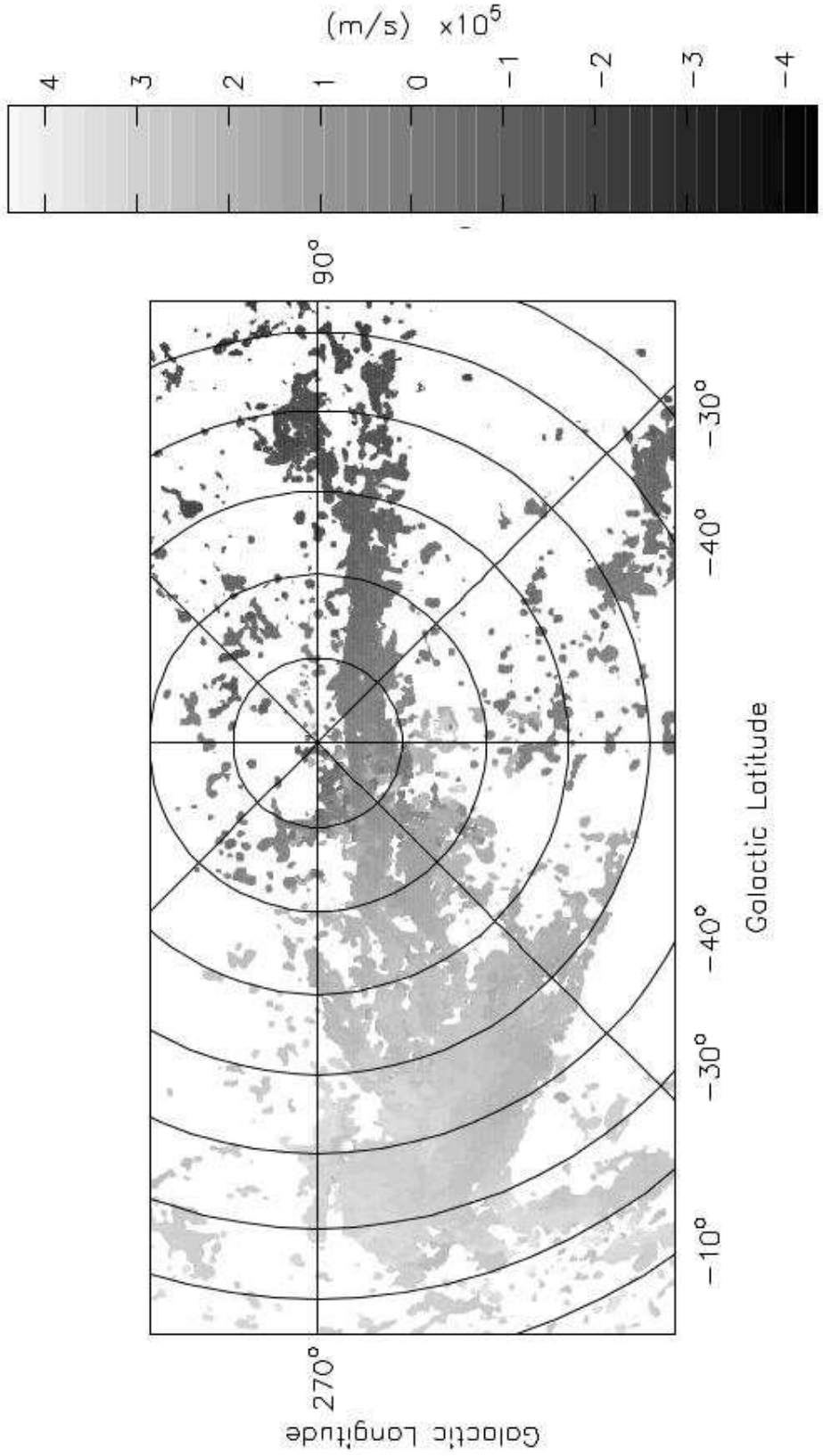

Figure 2.6: Velocity distribution of the Magellanic System from Putman et al. (2003, Fig. 7), with velocities ranging from $v_{LSR} = +380$ km s^{-1} (light grey) to -450 km s^{-1} (dark).

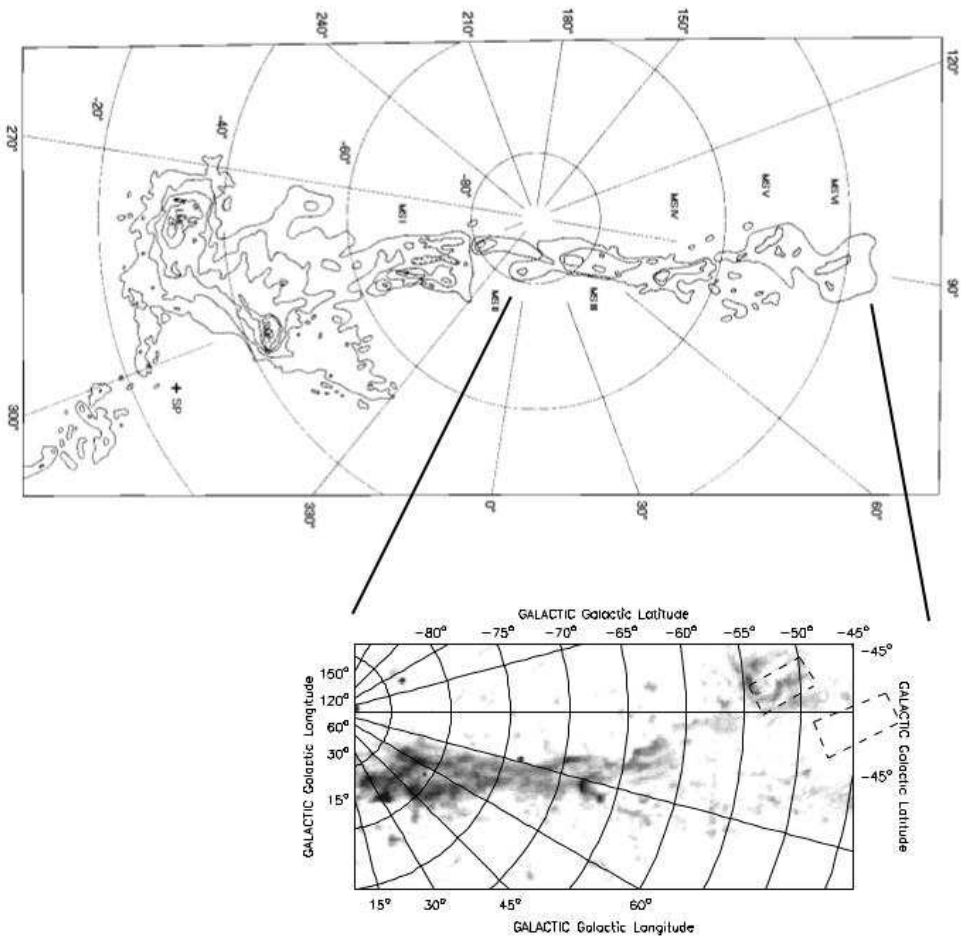

Figure 2.7: From Stanimirović et al. (2002, Fig. 1), Top: HI distribution of the Stream from Mathewson & Ford (1984). Bottom: Clouds MS III-MS VI, as seen by the Parkes HIPASS survey (Putman et al. 2002).

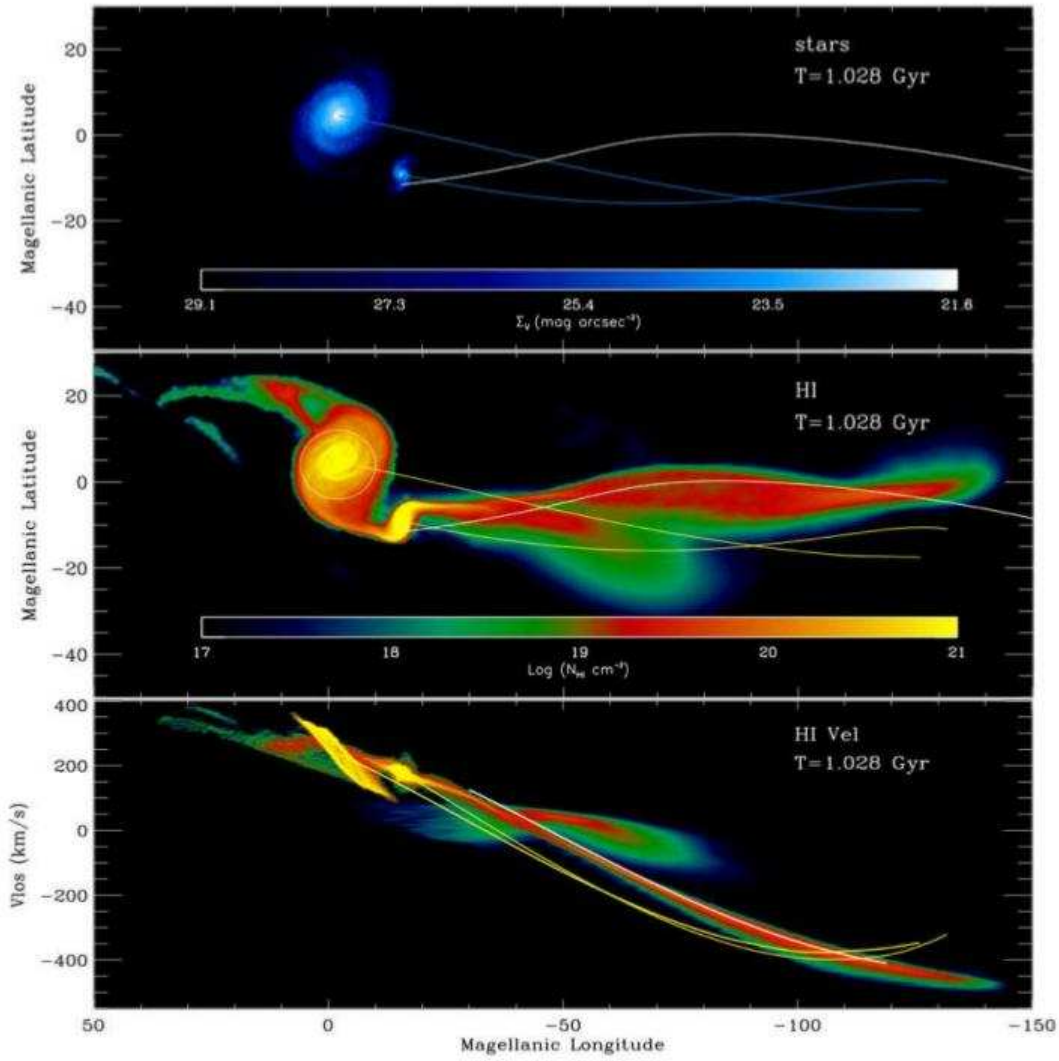

Figure 2.8: From Besla et al. (2010, Fig. 2), the stellar surface brightness, HI gas column densities and line-of-sight velocities of the simulated Magellanic system. Top panel: The resulting stellar distribution is projected in Magellanic coordinates, a variation of the Galactic coordinate system where the Stream is straight. The distribution is colour-coded in terms of V-band surface brightness. The past orbit of the LMC and SMC are indicated by the blue lines. Middle panel: The HI gas column densities of the simulated stream range from $1018 - 1021$ /cm^2. The white circle indicates the observed extent of the LMC HI disk: the simulated LMC is more extended than observed, indicating ram pressure likely plays a role to truncate the disk. In both the top and middle panels, the solid white line indicates the past orbit of the SMC according to the old theoretically derived proper motions. The true orbits for the LMC and SMC are indicated by the yellow lines. Bottom panel: The line-of-sight velocities along the simulated stream are plotted. The LMC disk is too extended, causing a larger velocity spread than observed. The line-of-sight velocities along the past orbits of the LMC and SMC are indicated by the yellow lines, which do not follow the true velocities along the Stream. The Stream is kinematically distinct from the orbits of the Clouds.

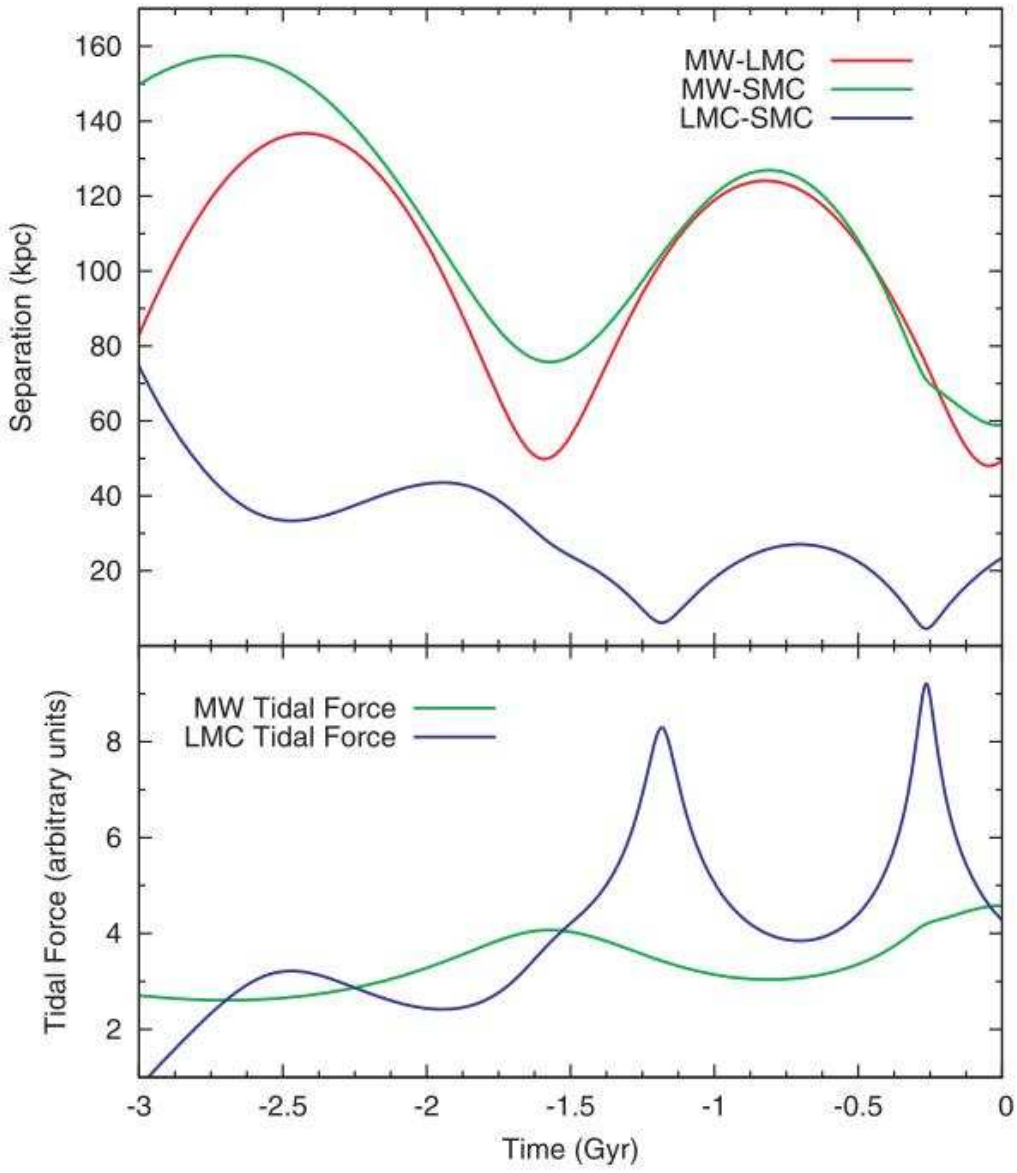

Figure 2.9: From Diaz and Bekki (2011, Fig. 1), Separations between the LMC, SMC and MW during their 3 Gyr orbital interaction (top panel), and the tidal forces experienced by the SMC (bottom panel).

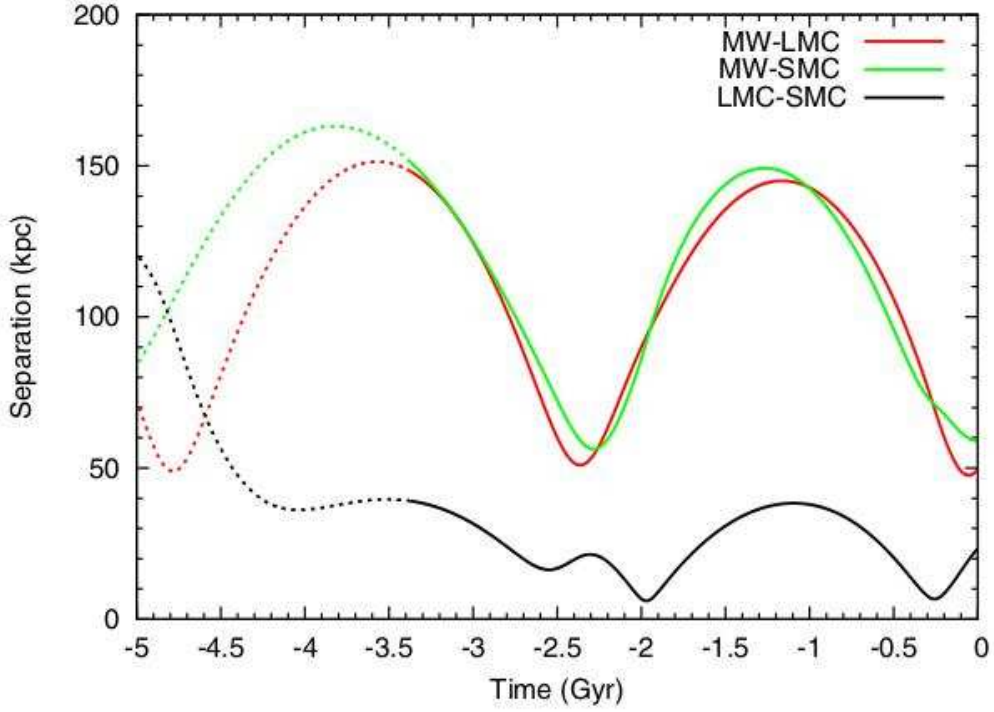

Figure 2.10: From Diaz and Bekki (2011, Fig. 3), Orbital separations between the LMC and MW (red), SMC and MW (green), and LMC and SMC (black). Solid lines indicate the time window in which the N-body models are evolved, 3.37 Gyr. Dotted lines indicate the continuation of the orbit integrations to 5 Gyr in the past.

2.3 Stellar populations

Understanding stellar populations is important, as differentiating objects from the Magellanic Clouds to those in the Galaxy makes up a large part of this work. This section describes the evolution of stars of different masses, the creation of stellar tracks and the different populations observed in CMDs. Different factors are also discussed that may effect the reliability of identifying populations from observations.

2.3.1 Stellar evolution

Stellar evolution is the sequence of events from which a star is born, to stellar maturity and death. There are basic steps in stellar evolution which are common to all stars, and some stages that will only occur if a star has a specific initial mass. The initial mass of a star after it is born from a dust cloud will determine the evolutionary path the star will follow and also the duration of the stellar life. The simplest way to understand stellar evolution is with the use of an H-R diagram. Various forms of the H-R diagram exist, showing populations of stars as a function of temperature, luminosity, magnitude, spectral type and other parameters that can describe a star. The most common form of the H-R diagram as seen in Fig. 2.11 is with the axes representing temperature and luminosity.

The main stages of stellar evolution seen in H-R diagrams are the Main Sequence (MS) phase, the giant and supergiant, or horizontal branch (HB) phases. Depending on their mass, stars end their lives as WDs or neutron stars/black holes after going through a planetary nebula phase or supernova explosion respectively. The duration that a star spends in each phase, depends sensitively on the initial mass of the star. The MS phase is the longest lived most stable period of the stellar life-cycle with stars migrating away from various points of the MS (Fig. 2.12) onto the giant and supergiant phases. Stellar evolution is governed by nuclear processes occurring internally within the star.

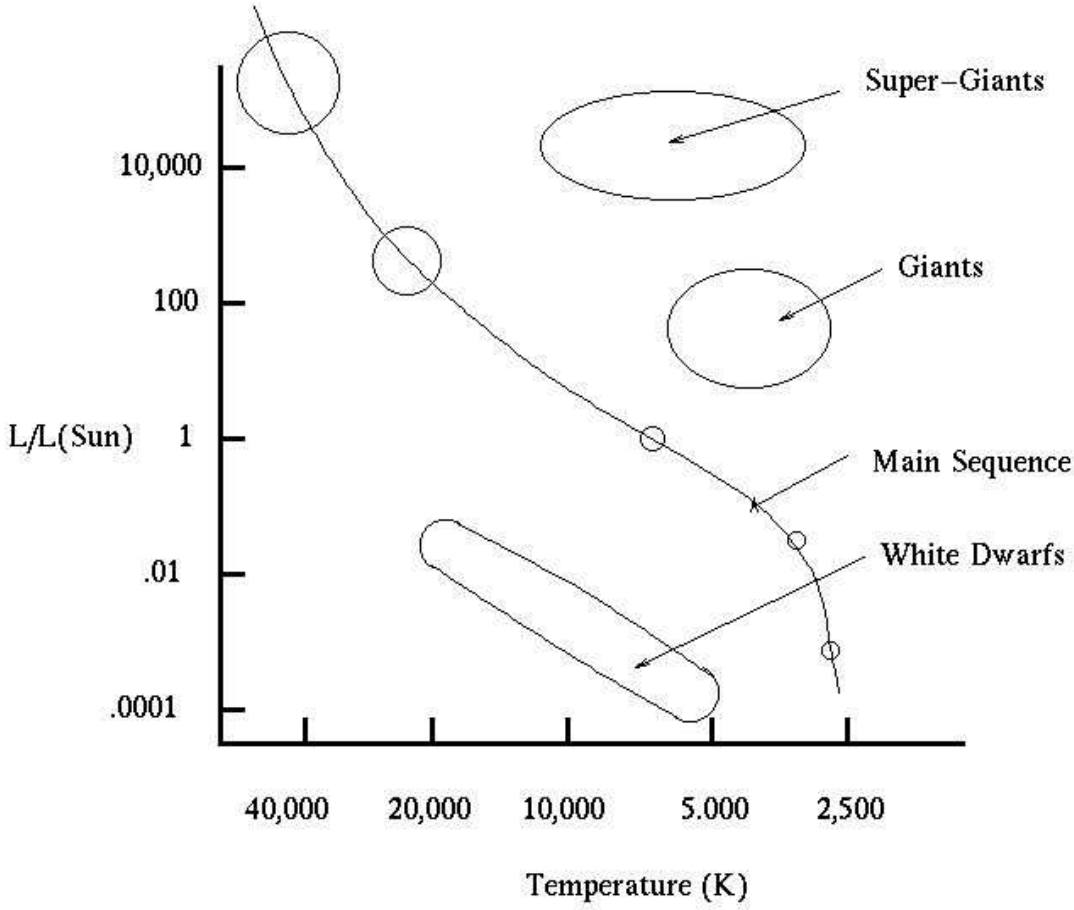

Figure 2.11: A schematic H-R diagram showing the main phases of stellar evolution (http://www.tim-thompson.com/hr.html).

The evolution of stars can be divided into three regimes for low mass (M less than $\sim 2.5M_{\odot}$), intermediate mass (M$\sim 2.5M_{\odot}$ to ~ 8.0) and high mass (M greater than $\sim 8.0M_{\odot}$) stars according to their different evolutionary paths taken. The longest lasting most stable phase in the stellar lifetime is the MS phase when the star is in thermal and hydrostatic equilibrium. The stellar core is converting hydrogen into helium via nuclear fusion and a star will remain on the MS for $\sim 100,000$ years to 100 billion years for high and low mass stars respectively. Higher mass stars have more gravitational potential energy which means that they collapse faster and higher pressure and central temperatures lead to energy production at a higher rate leading to a shorter MS lifetime.

The balance of external gravity with the internal nuclear fusion on the MS from the conversion of hydrogen to helium (via the p-p chain for low mass stars or

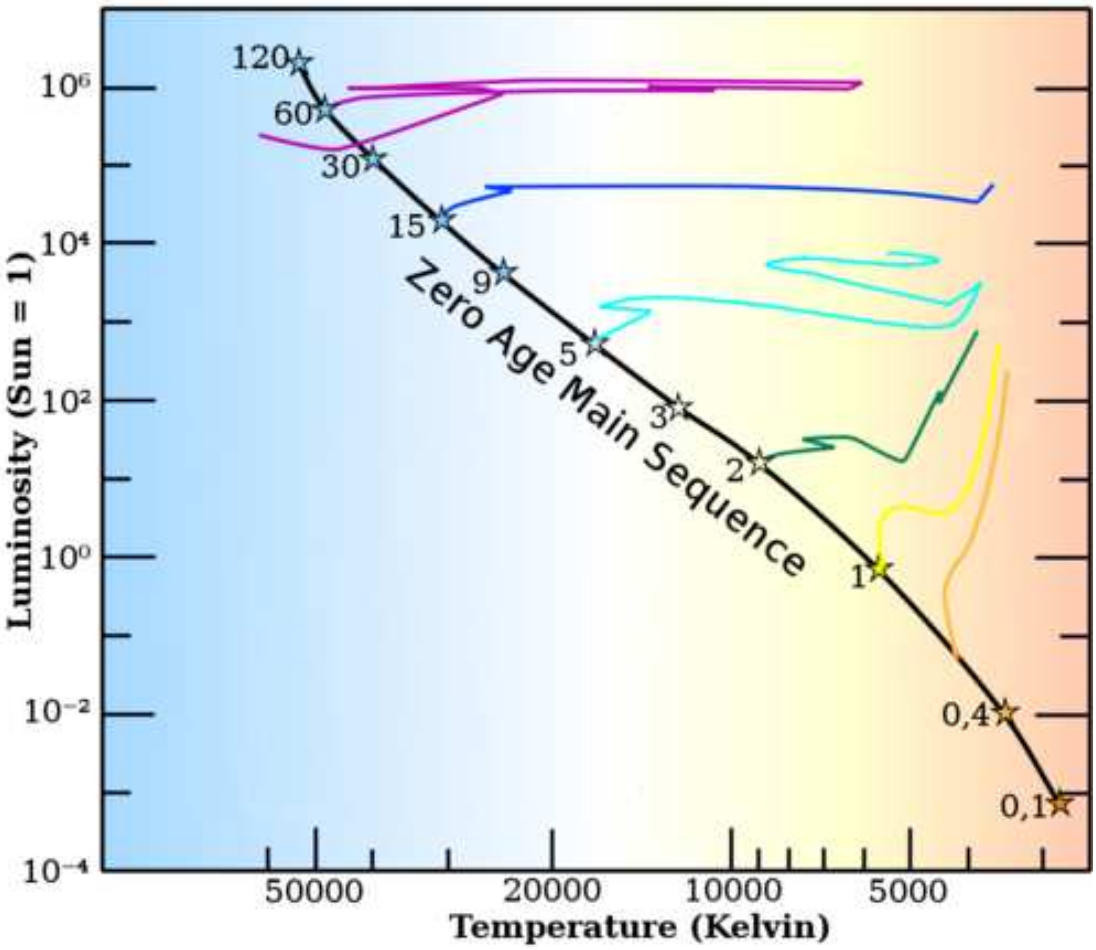

Figure 2.12: A schematic H-R diagram showing the main phases of stellar evolution from the zero age main sequence by initial mass as a function of solar mass. The yellow track represents the stellar evolution of the Sun which is on the red giant branch (http://en.wikipedia.org/wiki/Stellar_evolution).

CNO cycle for high mass stars) stops when the hydrogen is used up, and the gravity dominates, causing the stellar core, and outer layers to contract and heat up. Fusion then begins in the shell outside of the core, with more rapid fusion causing the stellar luminosity and temperature to increase, with the expansion of the outer layer from the internal pressure. This phase sees the expansion of a star into the red giant phase.

Low mass stars such as the Sun undergo a helium flash at the tip of the RGB. Low mass RGB stars have degenerate cores and helium ignition leads to a run-away process causing the helium flash, with the increasing temperature lifting degenaracy and the star moves onto the HB burning helium in their cores (via the

triple alpha process). All core burning low mass stars have a helium core mass of 0.48 $M_{\odot}$ and the same luminosity. Envelope mass and opacity determine the size and therefore the temperature of the star. Low metallicity stars are found on the HB, however higher mass, higher metallicity stars are found on the (primary) red clump (like is a red extension of the HB). Intermediate mass stars do not have a well defined helium core mass and can be higher or lower than 0.48 $M_{\odot}$.

After a star has used up the helium in its core, fusion continues in a shell around the hot core of carbon and oxygen. This phase is known as the AGB phase and is parallel to the RGB phase in the H-R diagram. Low and intermediate mass stars are not massive enough to start carbon fusion. Most of their envelope is lost by a strong stellar wind at the end of the AGB phase. Eventually the remaining envelope begins to shrink and the temperature increases. Once the star is hot enough, a planetary nebula is formed followed at the end of the stars life by the WD cooling sequence. Intermediate and high mass stars have cores large enough that helium ignition occurs before electron degeneracy pressure becomes prevalent.

The gravitational forces on the cores of higher mass stars increase the pressure and temperature enough for further fusion reactions to take place, from carbon and oxygen to neon, silicon and iron. The temperature and pressure required to keep hydrostatic equilibrium can no longer be sustained and the core collapses, with protons and electrons converted into neutrons. This results in a supernova with a remaining neutron core, or if the stellar mass was large enough, a black hole.

Stellar evolutionary models are a powerful tool in aiding our understanding of stellar evolution. The models can provide the stellar evolutionary path or track that a star will follow for a giving initial mass, depending on a range of physical inputs e.g. metallicity. An isochrone is a track on an H-R diagram or CMD representing a population of stars of the same age. Isochrones are a very useful tool in analysing stellar populations, for example with a given metallicity in a

given photometric system, a set of isochrones can aid in determining the ages of populations present.

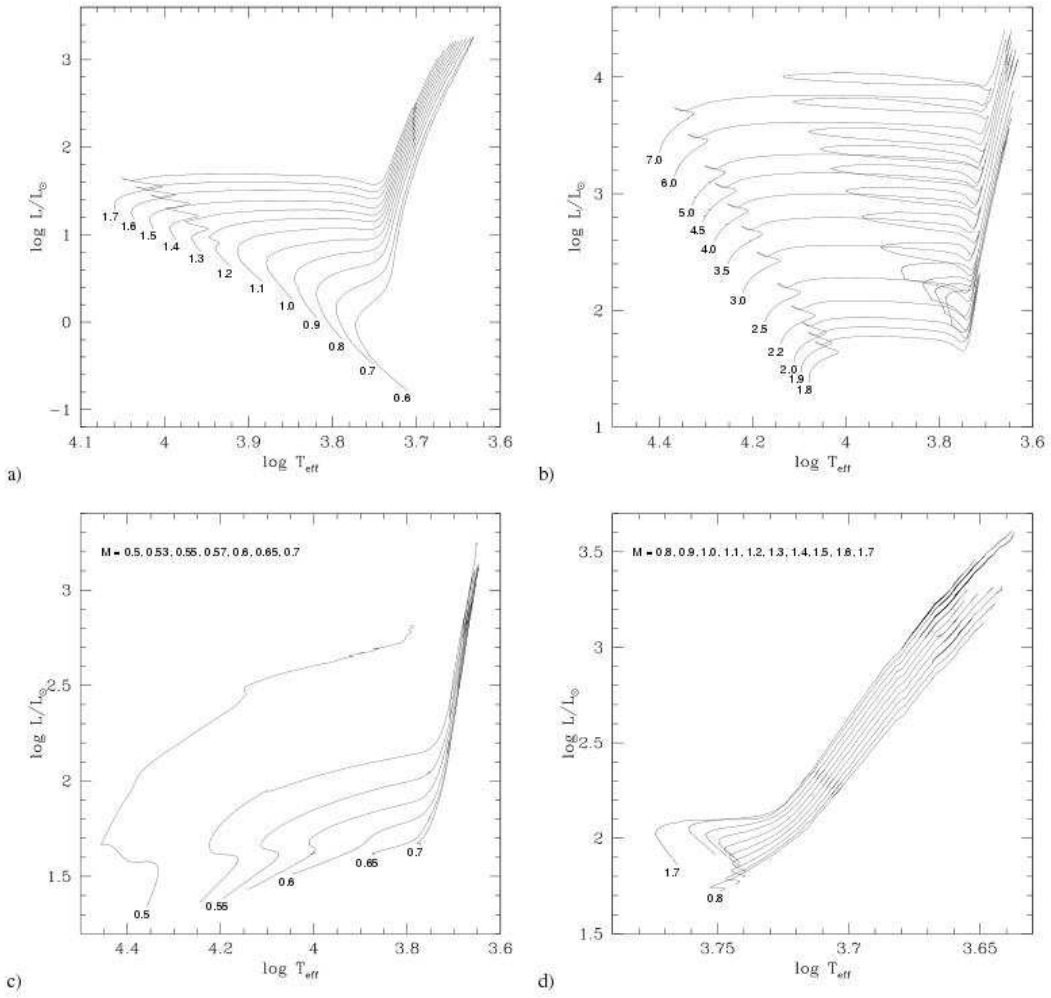

Figure 2.13: From Girardi et al. (2000, Fig. 2), evolutionary tracks in the H-R diagram, for the composition [$Z = 0.0004$,$Y = 0.23$] for most tracks of low-mass stars up to the RGB-tip (panel a), and intermediate-mass ones up to the TP-AGB (panel b), the stellar mass (in $M_\odot$) is indicated at the initial point of the evolution. For the low-mass tracks from the ZAHB up to the TP-AGB (panels c and d), we indicate the complete range of stellar masses in the upper part of the plots.

Girardi et al. (2000) present a large grid of stellar evolutionary tracks that enable the modeling of stellar populations with initial masses from $0.15 - 7$ $M_\odot$ and metallicities of $Z = 0.0004 - 0.03$ (Fig. 2.13). These stellar tracks extend from the zero-age MS (ZAMS), to the thermally pulsing AGB (TP-AGB) phase (or carbon ignition), with isochrones derived for the Johnson-Cousins $UBVRIJHK$ broadband photometric system. The input physics for the tracks is homogeneous

with the consideration of moderate convective overshooting from the stellar cores and mass loss from massive stars. The tracks are evolved from the ZAMS at constant mass with the detailed evolution through the hydrogen and helium burning phases, until either the thermally pulsing AGB phase in intermediate mass stars, or at the onset of carbon ignition in a helium exhausted core for the most massive stellar tracks.

For models of M$<$ 0.6 $M_{\odot}$, the MS evolution takes place on timescales larger than the Hubble time (13.7 Gyr), and so the tracks are terminated at $\sim$ 25 Gyr. For low mass stars (M$>$ 0.6 $M_{\odot}$), the evolution is interrupted at the stage of the helium flash in the electron degenerate core (as the computation of the complete evolution through the helium flash required too much CPU time), and is re-started from a zero age HB (ZAHB) model with the same core mass and surface chemical composition as the last RGB model. The initial ZAHB models also presents a core in which 5% (in mass fraction) of helium has been burnt into carbon, taking into account the approximate amount of nuclear fuel required to lift the core degeneracy during the helium flash. This evolution is followed by the TP-AGB phase.

Additional helium burning models with 0.5 $<$(M/$M_{\odot}$)$<$ 0.6 have been computed from a ZAHB model with the same core mass and surface chemical composition as the last 0.6 $M_{\odot}$ model. In intermediate mass stars, the evolution goes from the ZAMS up to either the TP-AGB or carbon ignition (for M$\sim$ 5 $M_{\odot}$). For stellar masses in which the evolution goes through the TP-AGB phase, a small number of thermal pulses is followed ($\sim 2-5$), with some sequences containing just one significant pulse, to others with up to 19 pulse cycles. The pulses last typically a few thousand years and cause mixing of the core material with outer layers (dredge-up). Most of the time the hydrogen shell is burning, accumulating helium. When enough helium has been produced, helium burning ignites in a helium shell flash.

The authors define $M_{\rm Hef}$ as the maximum mass for a star to develop an electron

degenerate core after the MS and this parameter sets a limit between low and intermediate mass stars, with M_{up} representing the maximum mass for a star to develop an electron degenerate core after the core helium burning phase and sets the limit between intermediate and high mass stars. Stars with $M > M_{up}$ should ignite carbon and avoid the TP-AGB phase. In these models, as soon as a small amount of carbon burning occurs in stars with $M < 4 - 5$ $M_{\odot}$, it cannot be determined with confidence whether shell burning will increase or fade away (leaving an AGB star), so a range of possible M_{up} is presented with a lower limit representing stars that are likely to end up in the double-shell thermal pulsing phase, and an upper limit which will burn carbon explosively.

The tracks here are extended for low and intermediate mass stars through the TP-AGB phase, with mass loss and stellar winds during the RGB phase only considered at the stage of isochrone construction using an empirical formula. From the RGB tip to the ZAHB, the authors integrate the mass loss rate along the RGB of each track to estimate the total amount of mass to be removed and the mass of the models is scaled down to the value of ZAHB stars. The TP-AGB path is constructed synthetically by evolving the mass, total mass, effective temperature and luminosity of each star from the first thermal pulse on the AGB, to the stage of complete envelope ejection.

Castellani et al. (2003) provide a supplement to computational evolutionary models of the Magellanic Cloud stars with metallicities (Z) of 0.004 and 0.008 for the SMC and LMC respectively with the same input physics as Girardi et al. (2000).

Stellar tracks are a useful tool in identifying different stellar populations in this work and the tracks described above from Girardi et al. (2000) prior to 2012, and more recently Bressan et al. (2012) are used for Magellanic Cloud metallicities and distances.

2.3.2 Stellar populations and the CMD

As well as the H-R diagram, CMDs are a very useful, and more specific way to study stellar populations of objects with observations carried out in certain wavebands (Fig. 2.14). Both observational and theoretical CMDs allow for accurate classification and separation of different stellar populations.

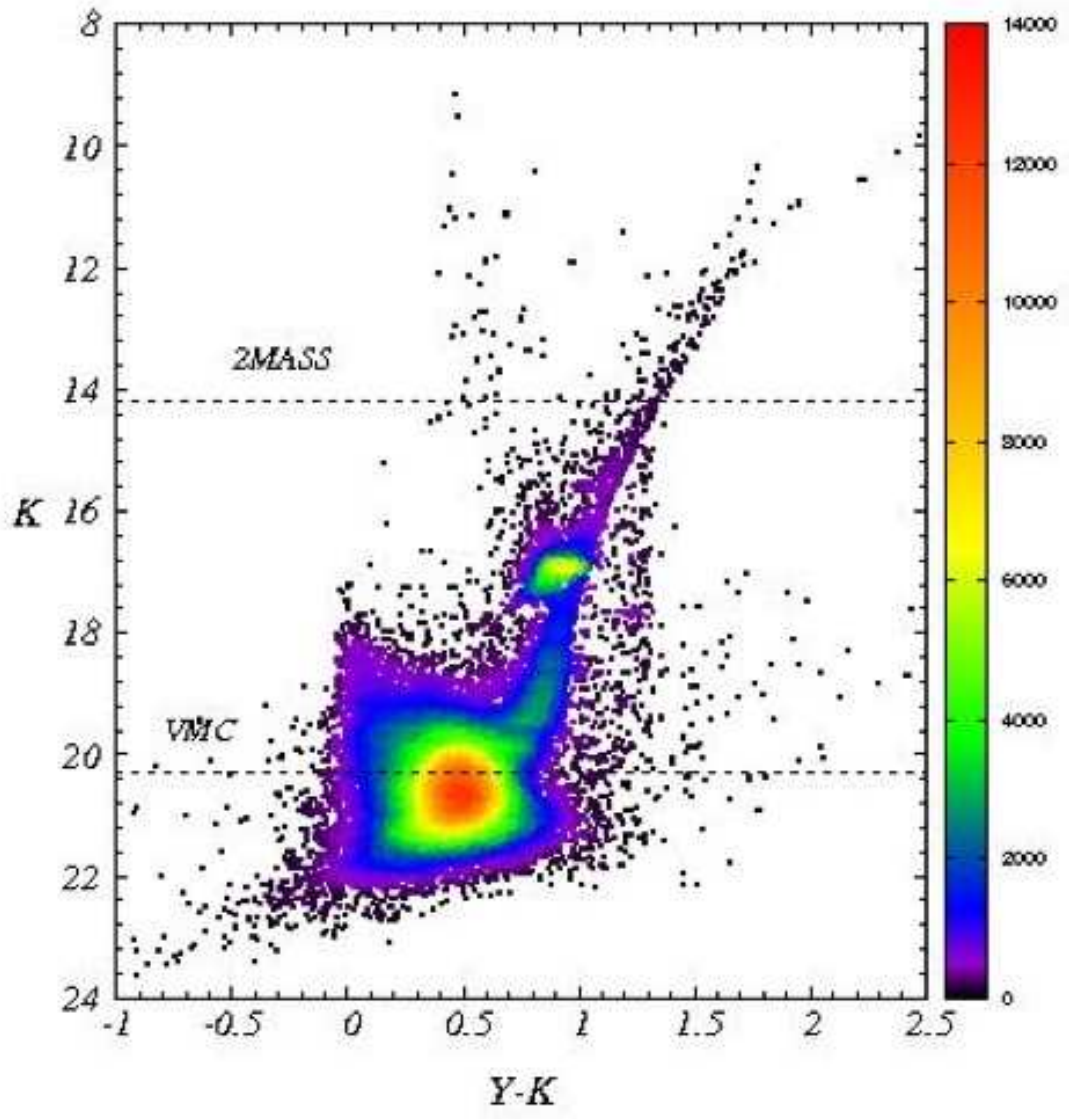

Figure 2.14: Simulated CMD for a 0.8 deg sq. area of the LMC. The total number of stars is $\sim$ 55000 where the colours correspond to the density of stars in a logarithmic scale (star.herts.ac.uk/ mcioni/vmc/project, Fig. 1).

Nikolaev and Weinberg (2000) use a CMD of the LMC to reliably identify stellar populations from 2MASS observations (Fig. 2.15). They find 12 regions of different populations in the LMC ($J - K_s$) vs K_s CMD (A to L) using isochrones

and distance estimates to separate the LMC and MW populations. Region A contains blue supergiants, ZAMS LMC dwarfs, evidencing recent star formation. Region B contains a large number of MW disc dwarfs with a presence of LMC supergiants. The objects in region C are made up of MW disc dwarfs and K giants with young supergiants from the LMC bar. Region D is the most heavily populated CMD region with MW disc dwarfs again, but with RGB and early AGB stars from the LMC to the right of this region. Region E covers the RGB including the tip of the RGB with a relatively smooth spatial distribution and a small number of foreground disc dwarfs. Regions F and G are made of LMC oxygen rich AGB stars and AGB stars respectively. Region H contains relatively young LMC supergiants, with some MW dwarfs and giants. At the centre of the CMD, region I contains the red clump in the LMC and intermediate-mass red supergiant stars, with MW dwarfs. Region J contains LMC carbon stars that have descended from regions F and G, with an extension into region K containing very red, dusty AGB stars. Region L sources are made up of reddened LMC M giants with a small number of MW dwarfs and a significant number of background galaxies. These regions identified by Nikolaev and Weinberg (2000) are beneficial when describing the populations observed in the Magellanic Bridge from 2MASS in Chapter 5.

The SMC populations are described in Noel et al. (2005) with the use of deep $B-R$ vs R CMDs reaching the oldest MS turn-off for 12 fields with B and R band observations. The authors apply three sets of isochrones from Pietrinferni et al. (2004) for three different metallicities ($Z = 0.001, 0.002, 0.004$), at a distance modulus of 18.9 ($m - M$). They find a population of young stars corresponding to the most recent LMC-SMC interaction ($\sim 100 - 300$ Myr) and intermediate population up to ~ 10 Gyr. Gardiner and Hatzidimitriou (1992) study the outer SMC and find the majority of stars have ages $\sim 10-12$ Gyr, with smaller number of objects from a very old population of ~ 15 Gyr.

As well as the work in Nikolaev and Weinberg (2000), Bessell and Brett (1988)

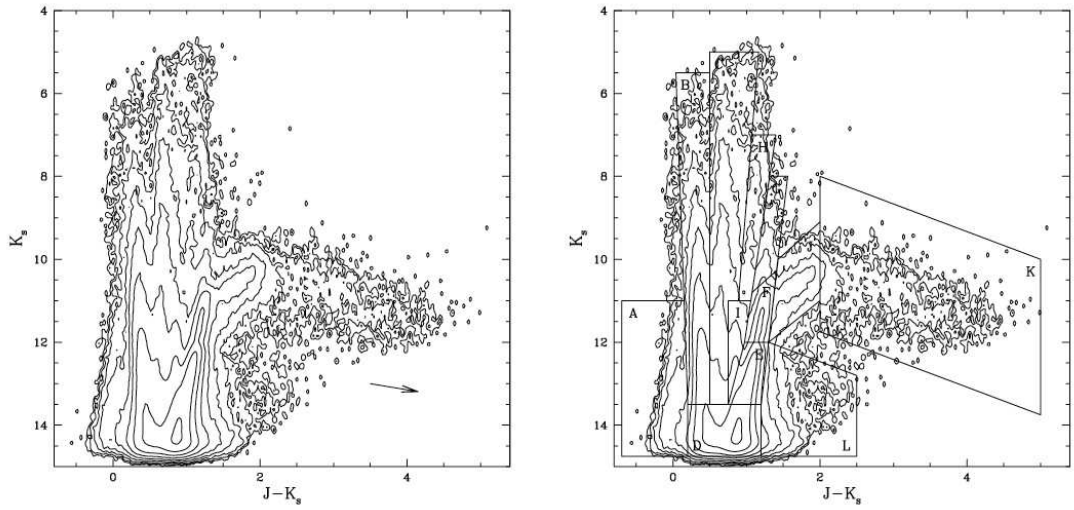

Figure 2.15: From Nikolaev and Weinberg (2000, Fig. 3), CMD of the LMC (left) with logarithmic density levels from $2-6$, spaced by 0.5. The reddening vector corresponds to $E_{B-V} = 1.0$, with the 12 highlighted regions (right) of major CMD features.

describe the positions of MW objects in CMD and two-colour space. They investigate the relations between colours in a number of $JHKL$ systems, deriving a method of transformation between different NIR colours.

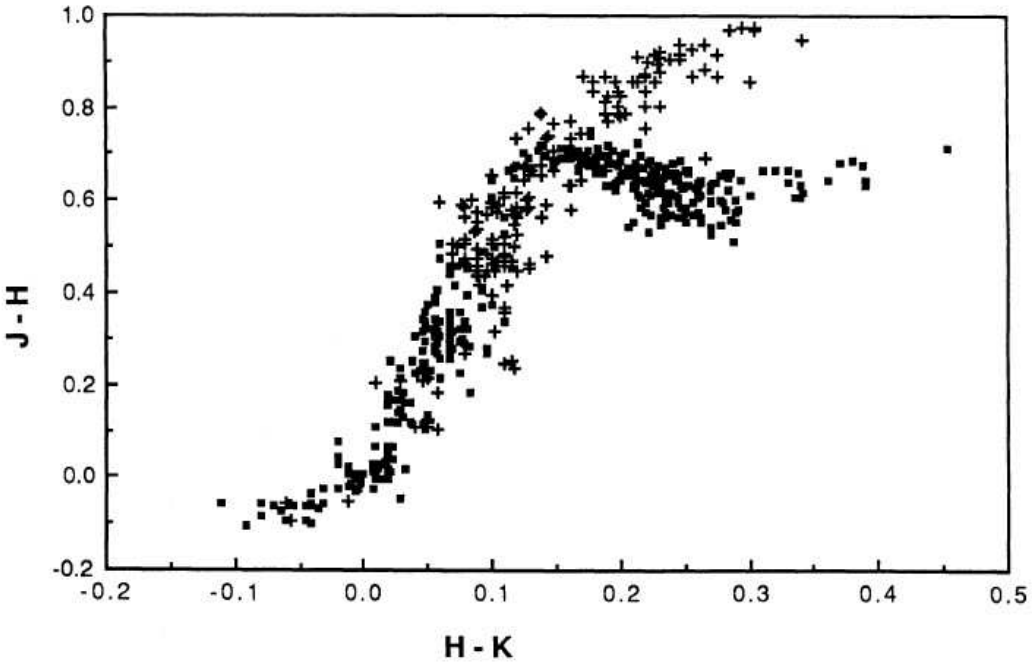

Figure 2.16: From Bessell and Brett (1988, Fig. 5), two-colour diagram $(H-K)$ vs $(J-H)$ of combined data for giants, supergiants and dwarfs.

Bessell and Brett (1988) produce a variety of two-colour diagrams presenting different stellar populations, including intrinsic colours and the $(H-K)$ vs $(J-H)$ two-colour diagram which can be used to describe MW populations of dwarfs and giants (Fig. 2.16), which can aid in the removal of Galactic foreground from NIR catalogues in the direction of the Magellanic System.

A useful tool in the identification of stellar populations from observations, is the application of synthetic populations. Girardi et al. (2002) describe the method of transferring the stellar tracks into different photometric systems, which can be used to categorize stellar populations from observations. A number of input parameters are required when creating synthetic populations including the initial mass function (IMF), star formation rate (SFR) and age-metallicity relation (AMR). The IMF describes the distribution of initial masses for stellar populations and peaks at a few tenths of the solar mass with a power law tail towards higher masses (Larson, 2006).

Girardi et al. (2005) describes how synthetic populations can be applied to create simulated photometric data in different photometric systems. The TRILEGAL population synthesis code creates a synthetic galactic population in terms of stellar density and intrinsic luminosity function at a given line of sight distance. The primary goal of TRILEGAL was to simulate star counts in different passbands using the work in Girardi et al. (2002), and to produce deep and shallow photometry with the inclusion of very low mass stars to WDs. In TRILEGAL the Galaxy is split into the disc, bulge and halo components, specified by their initial distributions of stellar ages (SFR) and metallicities (AMR), masses (IMF), space densities and interstellar absorption. TRILEGAL interpolates and searches for stars of a given mass, age and metallicity within a database of tracks, and converts these properties into absolute photometry via interpolation and grids of isochrones and converted to magnitudes via bolometric corrections and distance moduli. The input datasets for TRILEGAL consist of tables of tracks, tables of bolometric corrections, IMF, SFR and the geometry of Galactic components.

TRILEGAL is a useful tool in simulating Galactic populations from a number of different photometric systems and contains all of the systems used in this work.

2.3.3 Reddening and Metallicity

The categorisation of stars into different populations is complicated by factors that effect the position of objects in CMD space, particularly in colour, by factors such as reddening (or extinction) and metallicity which need to be considered in order to make an accurate classification of objects into different populations.

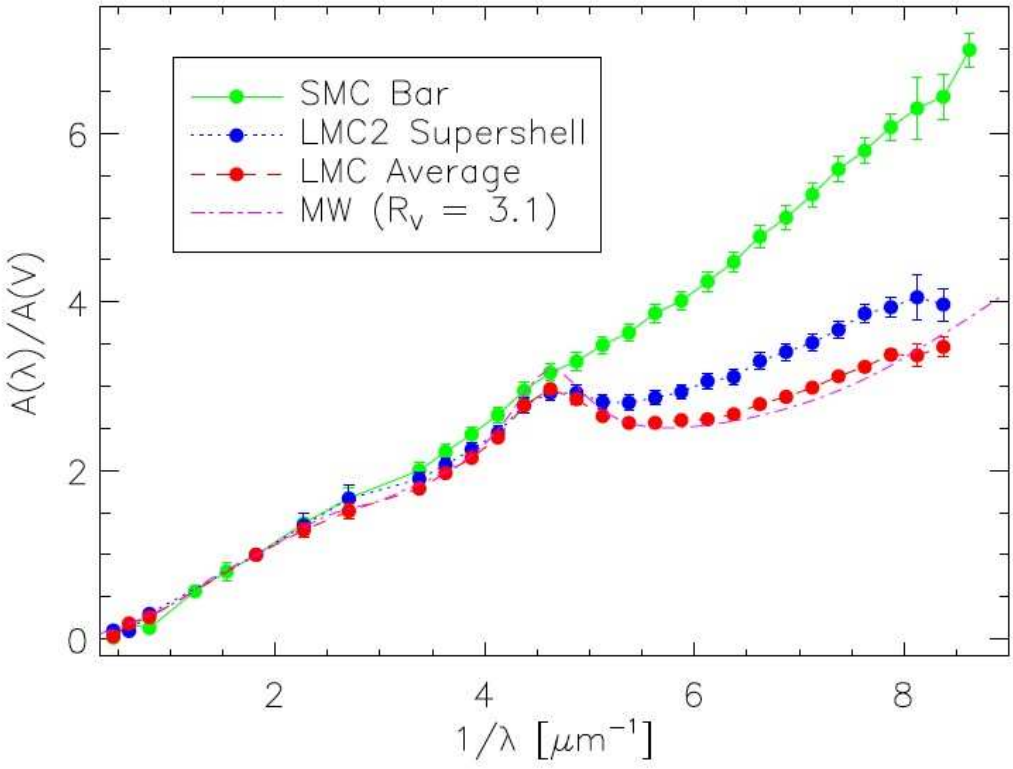

Figure 2.17: From Gordon et al. (2003, Fig. 5), comparison of the extinction laws in the MW, LMC and SMC.

Extinction is the product of scattering and absorption of light from stars by interstellar dust. The efficiency of scattering and absorption, are highest for dust grains the same size as, and larger than, the wavelength of incident radiation respectively. The number of dust grains in the ISM is much larger for smaller grains, so extinction is stronger at shorter wavelengths which leads to the effect

of reddening. The most common measure of reddening is the colour excess:

$$E(B-V) = A_B - A_V = (B-V) - (B-V)_0 \tag{2.1}$$

Where $(B-V)_0$ denotes the intrinsic colour index of a given star. A_B and A_V are the total extinctions in the photometric B and V bands. The extinction law depends on location (Gordon et al., 2003), for example between the MW, LMC and SMC (Fig. 2.17). Extinction toward stellar populations can be estimated and CMDs can be corrected for the effect of extinction, by measuring interstellar reddening. This thesis makes use of work from Schlegel et al. (1998), who created full sky dust maps and give extinctions per waveband for a number of photometric bands, to estimate the effect of MW foreground absorption.

Another factor that can effect the classification of stars into populations in CMDs is metallicity. The metallicity (Z) of an object is the proportion of its matter made up of chemical elements other than hydrogen and helium. Metallicity can be used to determine the age of a star as older stars have lower metallicities than younger stars. Due to the replenishment of different metals into galaxies in the form of supernovae and planetary nebulae at the end of a stellar lifetime, younger stars will have higher metallicity that older objects. Objects with higher metallicity will have redder colours and objects with lower metallicity have bluer colours due to the absorption properties of different metals. This means that in a CMD, the metallicity of an object can effect the position in the CMD and therefore the classification of the stellar population. In this work, metallicity effects are not of large significance due to the fact that broad colour ranges are selected.

Chapter 3

Wide-field catalogues

3.1 Data

The aim of this work was to establish source catalogues in the region of the Magellanic Bridge and Stream prior to the analysis of observations using VISual and Infrared Telescope for Astronomy (VISTA), (Emerson et al., 2004) as part of the VISTA survey of the Magellanic Cloud system (VMC; Cioni et al., 2011). As such, the main source of data used in this work is NIR photometry from the Two Micron All Sky Survey (2MASS) and the Deep Near-Infrared survey of the Southern sky (DENIS) respectively. Optical SuperCOSMOS data are also used for comparison. The 2MASS, DENIS and SuperCOSMOS catalogues are publicly available. With the availability of a number of VMC observing tiles, the Bridge was also analysed using these tiles complemented by the NASA Wide-field Infrared Survey Explorer (WISE) data, which also became publicly available during this work. The Bridge area was chosen from previous definitions of the Bridge coverage by Kerr and de Vaucouleurs (1955), McGee and Newton (1981) and Harris (2007). This corresponds to an area between the LMC and SMC from 20° to 70° in right ascension (α) and from $-69°$ to $-77°$ in declination (δ). A more central Bridge region was also used in places to reduce contamination from the outer LMC and SMC with α from 30° to 60°. In the case of the Magellanic

Stream, due to the large length of the Stream, as a starting point observations from the above public catalogues were carried out in two regions of the Stream that were to be observed as part of the VMC survey (Sect. 3.3).

3.1.1 DENIS

DENIS (Fig. 3.1) is a complete survey in one optical band I (0.8μm) and two NIR bands, J (1.25μm) and K_s (2.16μm) of the southern sky (Epchtein, 1994). The 10σ limiting magnitudes of the survey are 18.5, 16.5 and 14.0 mag in I, J and K_s bands, respectively with a 1σ photometric uncertainty of < 0.1 mag and a pixel size of $1''$ in I and $3''$ in J and K_s with image sampling of $1''$ in each waveband (Cioni et al., 2000). The J and K_s images are dithered to a $1''$ pseudo-resolution, using a micro-scanning mirror. They consist of a set of 9 frames each obtained in a 1 s integration time, shifted by $+/-$ 1/3 pixel in RA plus $+/-$ 7/3 pixel in Dec [1].

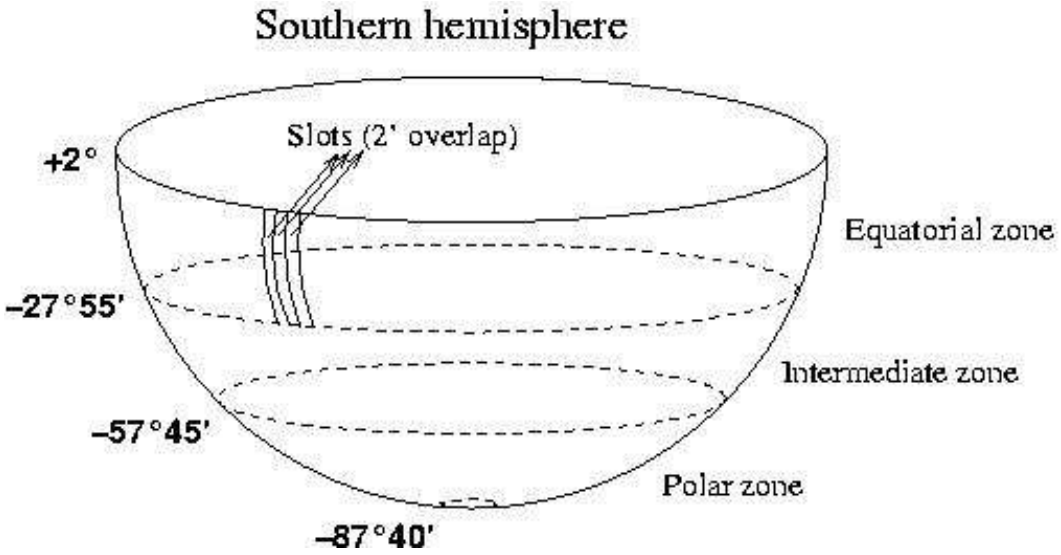

Figure 3.1: Schematic of the DENIS observing strategy which observes 5112 slots of $12''$ in α and $30°$ in δ from CDS.

[1] http://irsa.ipac.caltech.edu/Missions/denis.html

3.1.2 2MASS

2MASS collected raw imaging data covering 99.998% of the celestial sphere (Fig. 3.2) in the NIR at J (1.25μm), H (1.65μm) and K_s (2.16μm) between 1997 and 2001 (Skrutskie et al., 2006). The 10σ photometric uncertainty is < 0.03 mag for bright sources with a pixel size of 2.0″. The point 10σ source detection level is 15.8, 15.1, and 14.3 mag at the J, H, and K_s bands, respectively, for the vast majority of observations[2].

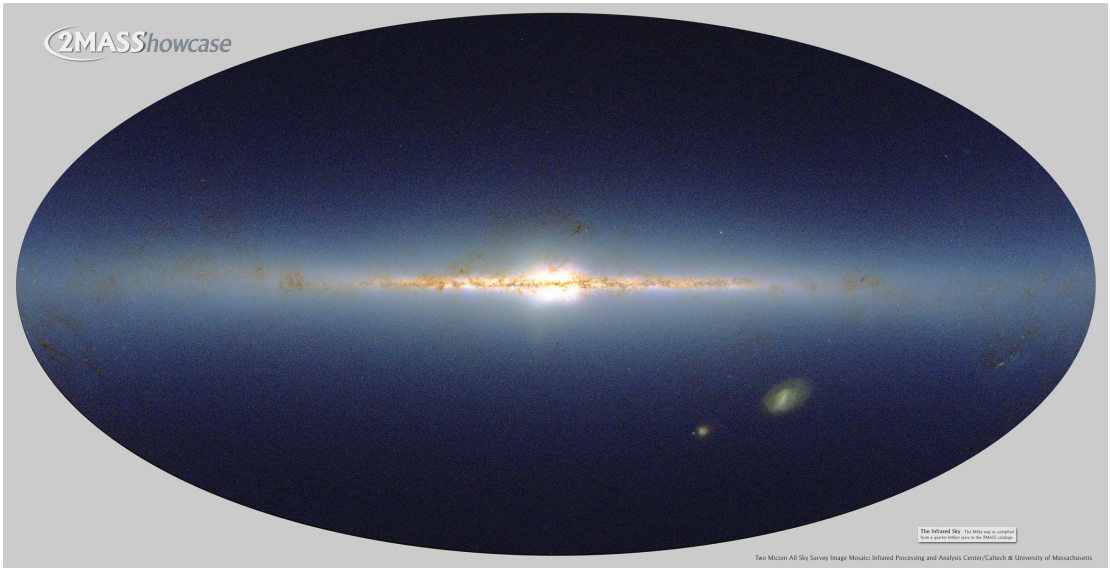

Figure 3.2: 2MASS image mosaic highlighting the point source coverage from IPAC/Caltech and University of Massachusetts.

3.1.3 SuperCOSMOS

For completeness in the analysis of the Magellanic Bridge, a comparison of the NIR data above was done with the optical SuperCOSMOS catalogue which covers this region with reasonable depth (Fig. 3.3). SuperCOSMOS is an advanced photographic plate digitising machine which digitised sky survey plates taken with the UK Schmidt telescope (UKST), the ESO Schmidt, and the Palomar Schmidt telescope for the entire sky. The pixel size of the SuperCOSMOS surveys is 0.7″. The SuperCOSMOS Sky Surveys are beneficial due to the small pixel size and

[2]http://irsa.ipac.caltech.edu/Missions/2mass.html

the availability of proper motions and variability information. For this work the UKST catalogue was used with band pass filters B (0.45μm), R (0.66μm) and I (0.8μm) and limiting magnitudes of $B = 22.5$, $R = 20.0$ and $I = 19.5$ mag (Hambly et al., 2001) with 10σ photometric errors of $0.3 - 0.5$ mag [3].

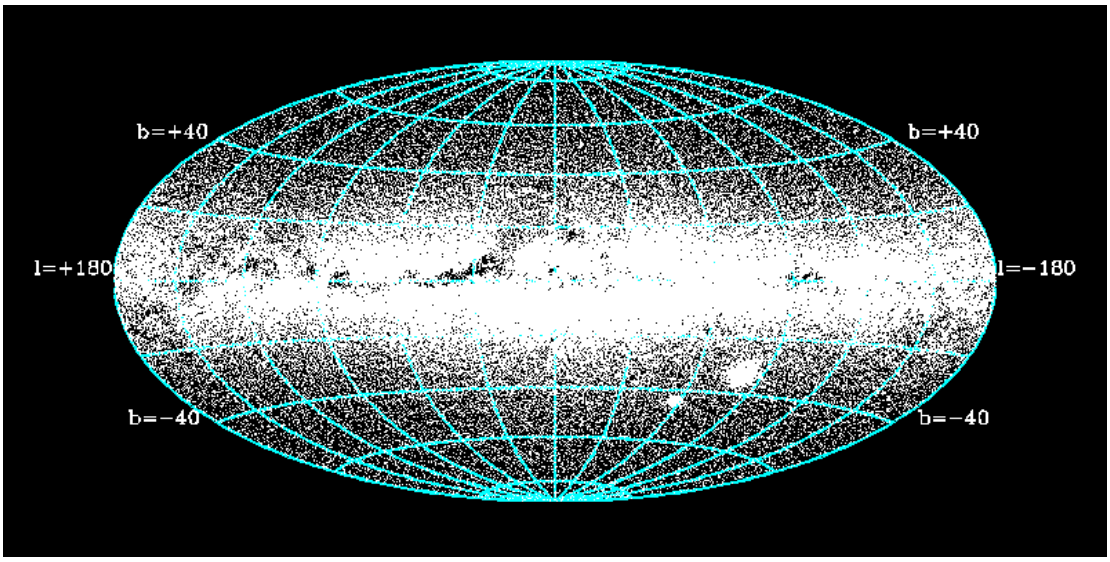

Figure 3.3: SuperCOSMOS observing sky coverage from the SuperCOSMOS Science Archive containing $\sim$ 6.4 billion individual object detections merged into $\sim$ 1.9 billion multi-colour, multi-epoch sources and covering the entire sky in BRI.

3.1.4 WISE

WISE, (Wright et al., 2010) is the NASA Wide-field Infrared Survey Explorer and was created to survey the entire sky in the mid-IR. Although the main goals of WISE are to probe far regions of the universe and search for local objects such as asteroids and brown dwarfs, it can also be used to look for stellar populations in local galaxies due to its all-sky coverage and IR photometry. The use of WISE complements this study as it has recently become publicly available in the direction of the Magellanic Clouds and covers IR bands with longer wavelengths than the VMC survey (1.02μm$-$2.15μm). Fig. 3.7 shows the normalised spectral responses of the four WISE bands. The WISE photometric bands $W1$, $W2$, $W3$

[3] http://www-wfau.roe.ac.uk/sss/

and $W4$ are at 3.4μm, 4.6μm, 12μm and 22μm to depths of 16.5, 15.5, 11.2 and 7.9 mag respectively, with 5σ sensitivities of 120, 160, 650 and 2600 μJy [4].

Figure 3.4: NASA/JPL-Caltech image of the WISE spacecraft on a work stand.

[4]http://www.nasa.gov/mission_pages/WISE/main/index

3.1.5 VMC

VISTA is the largest wide-field near-IR imaging telescope in the world and it is designed to perform survey observations (Emerson and Sutherland, 2010). VISTA observes a continuous area of the sky by filling in the gaps between the detectors using a sequence of six offsets, each by a significant fraction of a detector. The combined image corresponds to a VISTA tile that covers ~ 1.5 deg^2. VMC is a NIR, Y (1.02μm), J (1.25μm), $K_{\rm s}$ (2.15μm) public survey covering an area of 170 deg^2 across the Magellanic Clouds (Cioni et al., 2011). The 10 sigma sensitivity (Vega) in Y, J and $K_{\rm s}$ are 21.1, 21.3 and 20.7 respectively. Figure A.1 shows the photometric errors in the three VMC bands which can be used in order to make magnitude cuts near brightness and sensitivity limits when creating catalogues of the Bridge and Stream. The filters chosen for this survey will allow colour-colour diagrams to be created and also contains a large colour base which will enable a good characterization of populations within the Magellanic Clouds. Fig. 3.8 shows the VMC filter curves compared to those of 2MASS and DENIS. Combining the VMC survey with wide spectroscopic and optical photometric surveys, will increase our understanding of the Magellanic System [5].

3.1.6 UKIDSS

The UKIRT Infrared Deep Sky Survey (UKIDSS) is included in this section as it is used in this work as a tool for the removal of Galactic foreground objects. The similar photometric wavebands in UKIDSS to the VMC bands make it a useful survey for the Galactic foreground removal in the absence of a suitable VMC offset field. UKIDSS is considered to be the successor of 2MASS and upon completion will have surveyed 7500 square degrees of the northern sky in JHK to $K = 18.3$ mag. The Large Area Survey (LAS), is one of six UKIDSS surveys and will survey 4000 square degrees at high Galactic latitudes which makes it a suitable survey away from the Galactic plane for finding foreground regions. The

[5] http://star.herts.ac.uk/ mcioni/vmc/

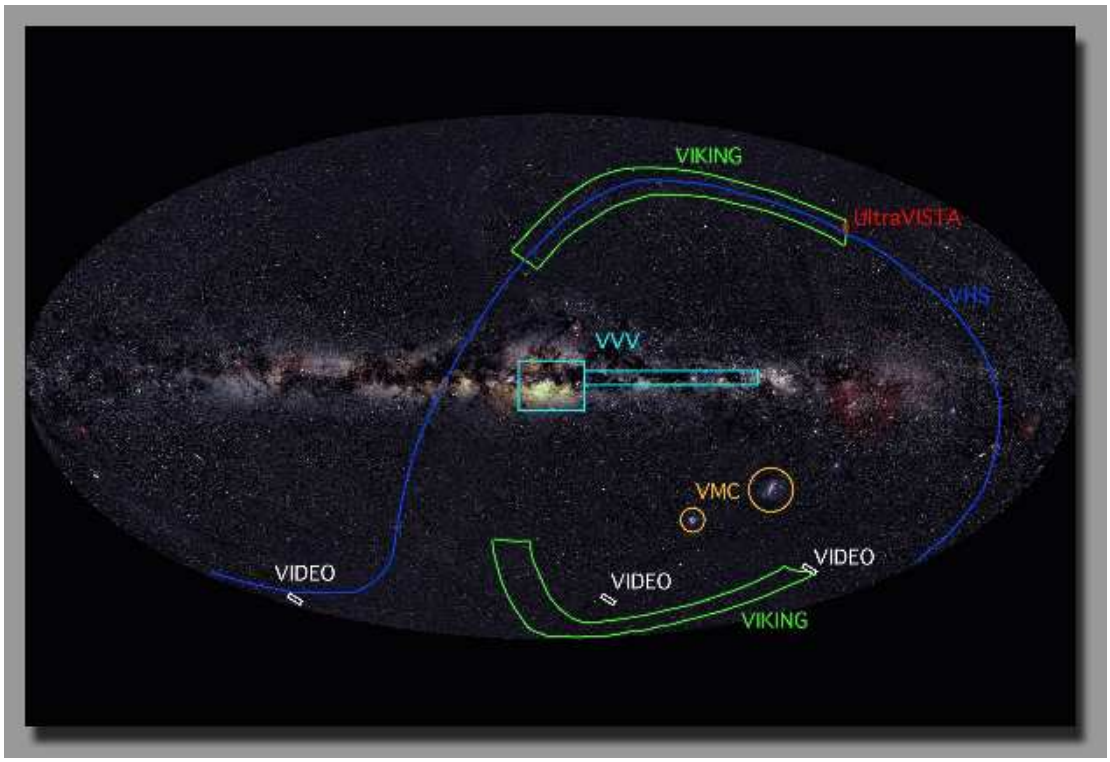

Figure 3.5: Image of the VISTA surveys and their coverage including the VMC survey of the Magellanic System from VISTA/ESO.

magnitude limits (vega) of the LAS bands are at 20.5, 20.0 and 18.4 mag for Y, J and K respectively (Hambly et al., 2001), with 3 sigma point source detection limits of 20, 19 and 18. Fig. 3.6 shows the transmission curves for the UKIRT Wide Field Camera (WFCAM) filters in different atmospheric conditions.

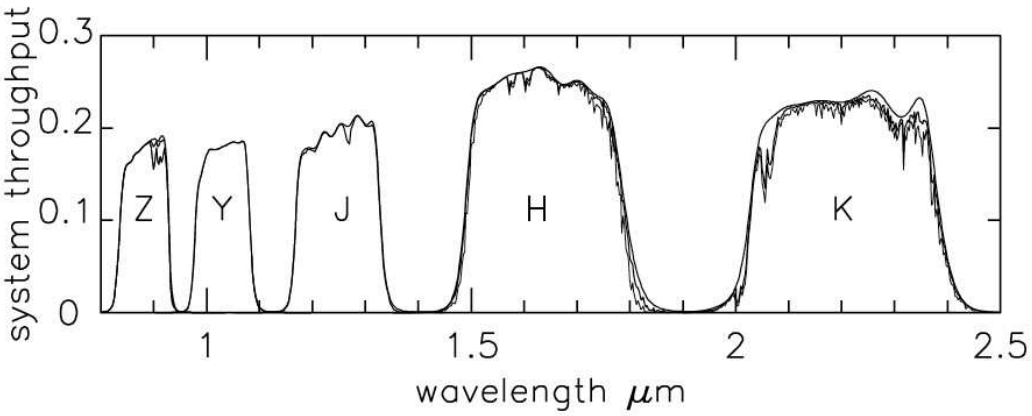

Figure 3.6: From Hewett et al. (2006), transmission curves for the WFCAM filter set. Three curves are shown for each band. The upper, thick, curve is for no atmospheric absorption. The middle, thick, curve is for the default atmospheric conditions (1.3 airmass, 1.0mm water), and the lower, thin, curve is for extreme atmospheric conditions (2.0 airmass, 5.0 mm water).

3.2 Magellanic Bridge catalogues

The catalogues for Chapter 5 of the Bridge region were downloaded from the 2MASS, DENIS, WISE and SuperCOSMOS web interfaces using columns of α, δ, magnitudes and photometric uncertainties.

Various flags were applied to clean each catalogue from the online data sources (Table. 3.1). In 2MASS, flags were used to remove objects with $JHK_{\rm s}$ artifact contamination and/or confusion and contamination from extended sources. The ph_qual flag was used to select objects with a good photometric quality for an object detected in this band with a flux S/N less than 10 (AAA), the rd_flag was used which indicates the origin of the default magnitudes and uncertainties in each band with objects selected that have best quality detections (1,2,3). The cc_flag was applied to select objects with no known contamination from artifacts (0), and objects were selected that had total photometric uncertainties of less than 0.1 mag. DENIS flags were applied to remove multiple observations of sources and maintain image and source quality. The iqual, jqual, kqual flags were used to select objects in each band that have the best quality (100), the iflg, jflg, kflg flags were used to select objects with no known image or source problems (000). Objects were

selected for the DENIS catalogue with total photometric uncertainties less than 0.1 mag.

Table 3.1: Flag cleaning requirements

Catalogue	Flag names	Required respective value
2MASS	ph_qual, rd_flag, cc_flag	AAA, 1,2,3, 0
DENIS	ijk_qual, ijk flag	100, 000
WISE	cc_flag, ext_flag, ph_flag	0, 0, AA
VMC	pp_errbits, p_star	< 256, > 0.90
UKIDSS	pp_errbits, p_star	< 256, > 0.90

The results in this work are mostly affected by the photometric uncertainties in the magnitudes. To further reduce the photometric uncertainties near the sensitivity limits, cuts at $K_\mathrm{s} = 14$ and $R = 17$ mag were applied. The photometric uncertainties of colours are derived from $\sigma_{\mathrm{A-B}} = \sqrt{\sigma_\mathrm{A}^2 + \sigma_\mathrm{B}^2}$. In order to complete a full study of the Magellanic Bridge the catalogues of 2MASS and DENIS were combined to form a catalogue with I, J, H and K_s bands. Because the 2MASS catalogue reaches fainter magnitudes than DENIS in the J and K_s band, and the photometric errors are smaller in 2MASS (Fig. A.1), after cross matching the catalogues, the J and K_s bands of DENIS were discarded. The DENIS I band was favoured over the somewhat deeper SuperCOSMOS I band as the photometric errors in DENIS are less. The 2MASS and DENIS samples were matched using coordinates and a separation of $0.5''$ to ensure that the stars in the combined catalogue were the same stars in each catalogue.

WISE flags were also applied when downloading data from this archive to remove multiple observations of sources, artifacts and maintain image and source quality. The cc_flag was applied to select objects with no known contamination from artifacts (0), the ext_flag was applied to select objects with a shape corresponding to a point source (0), the ph_qual flag was used to select objects with a good photometric quality for an object detected in this band with a flux signal-to-noise ratio less than 10 (AA–). The flag for photometric quality was specified

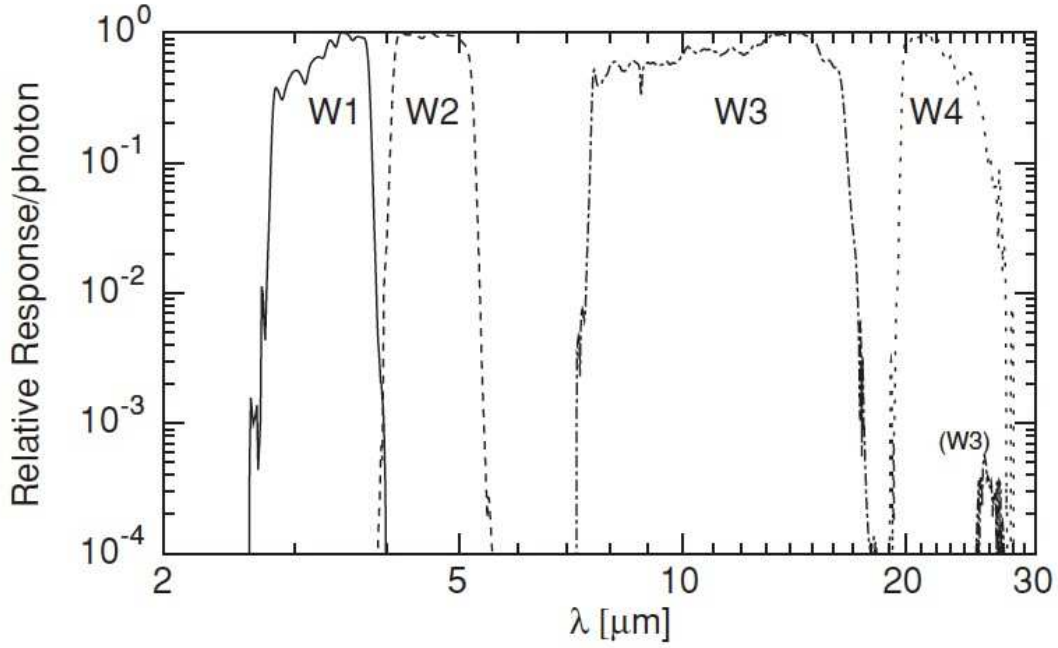

Figure 3.7: From Wright et al. (2010), weighted mean WISE relative spectral response functions after normalizing to a peak value of unity on a logarithmic scale.

for the $W1$ and $W2$ bands only as these are the bands that will be used in this work and are most suitable for detecting a stellar population. From the original $\sim 70,000$ objects in DENIS and $\sim 300,000$ in 2MASS, the combined catalogue contained $\sim 70,000$ objects observed in both 2MASS and DENIS. For the SuperCOSMOS catalogue, the classification flag was used to select only stellar objects (2), the quality flag was also used to select objects with no known quality issues (0). From the original SuperCOSMOS and WISE catalogues, $\sim 450,000$ and $\sim 800,000$ objects remained in the direction of the Bridge respectively.

At the time of writing up this work, there were five available VMC tiles from the Vista Science Archive (VSA) data release VMCv20120126 (Cross et al., 2012), completed in the direction of the Bridge [6]. The available Bridge tiles analysed in Chapter 6 were 2_3, 2_4, 2_8, 3_5 and 3_7 (Table 3.2, Fig. 3.9). The Bridge tile regions were downloaded from the Vista Science Archive (VSA) using columns of α, δ, magnitudes (AperMag) and photometric uncertainties (AperMagErr) with different flags used to only extract stellar objects. Flags were used to remove

[6] http:/surveys.roe.ac.uk/vsa

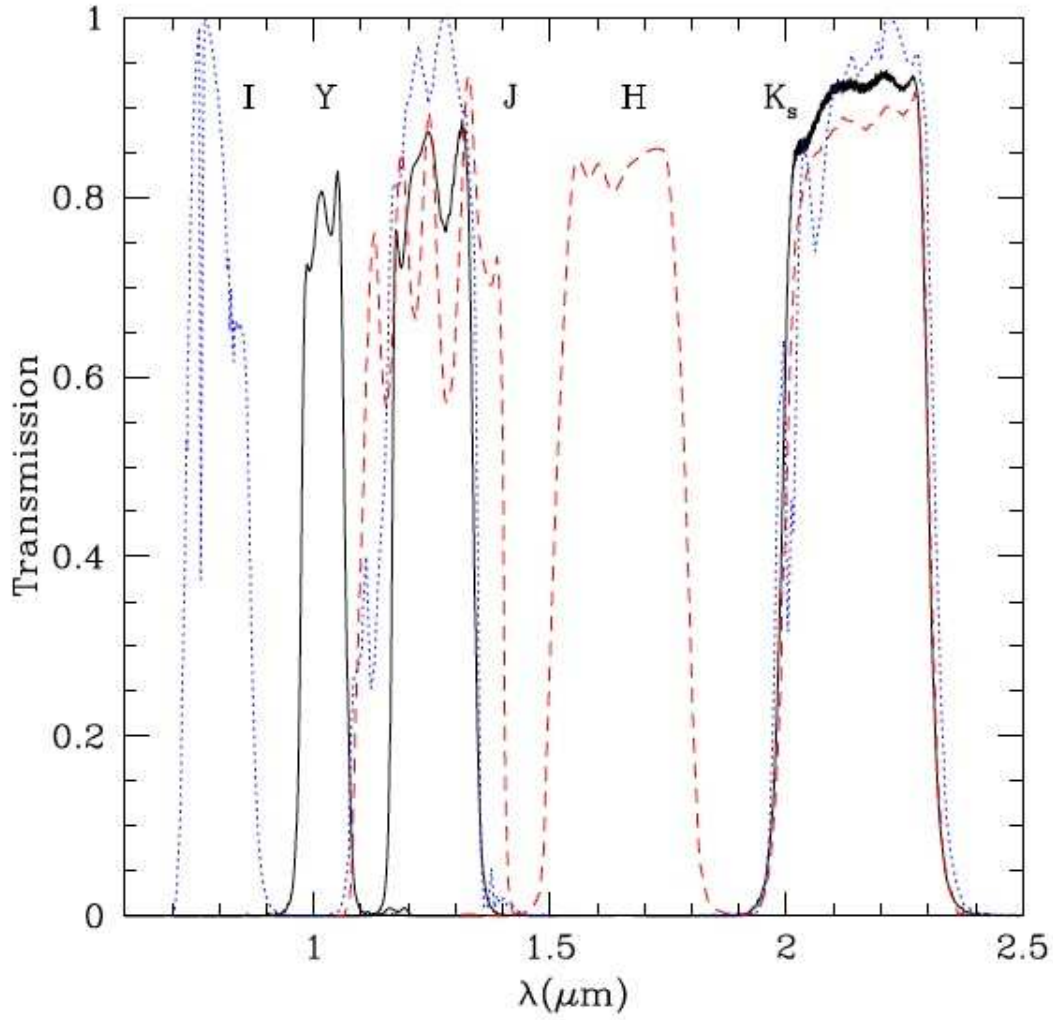

Figure 3.8: From Cioni et al. (2011), Filter transmission curves for the VMC survey (YJK_s black continuous lines) compared with the transmission of the 2MASS (JHK_s red dashed lines) and DENIS (IJK_s blue dotted lines) surveys.

objects with YJK_s artifact contamination and/or confusion and contamination from extended sources and to remove multiple observations of sources and maintain image and source quality. The pp_errbits flags were used to select objects with no known quality issues or just minor, informative, warnings (< 256), also objects were selected to have a high probability of being a stellar source (> 0.90) and observed in all three bands. The same flags used in the VSA were applied for the WFCAM archive for the UKIDSS catalogue for the Galactic foreground regions.

Table 3.2: VMC observation tiles in the Magellanic Bridge

Tile	Central RA (h:m:s)	Central Dec (h:m:s)
2_3	02:14:46.58	−74:00:47.52
2_4	02:35:28.44	−74:13:18.84
2_8	04:00:21.03	−73:46:37.56
3_5	02:57:33.29	−73:12:52.20
3_7	03:37:39.24	−72:59:54.60

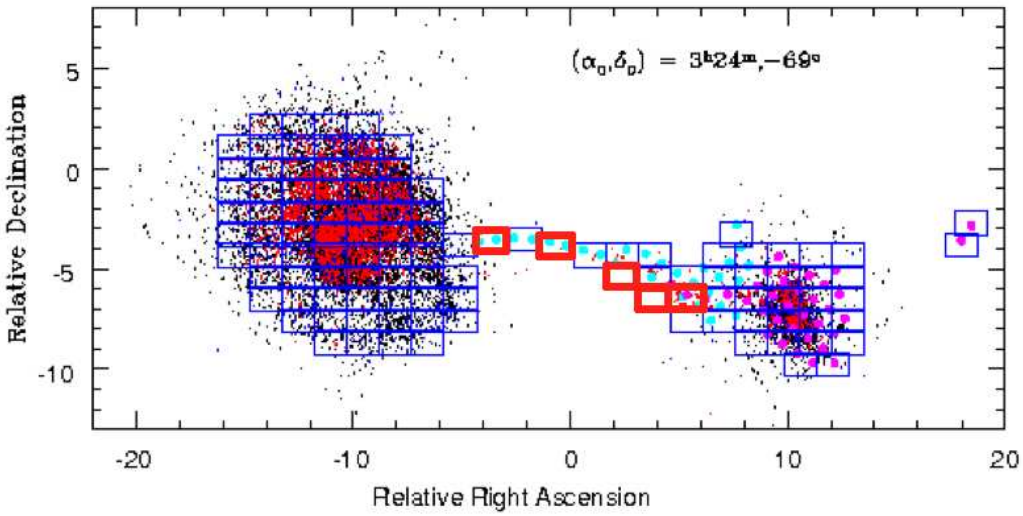

Figure 3.9: .
From Cioni et al. (2011), distribution of VISTA tiles across the Magellanic System (LMC, Bridge, SMC and Stream). Underlying small dots indicate the distribution of carbon stars (black), stellar clusters (blue) and associations (red) while thick dots show the location of observations to be performed with the VLT Survey Telescope (VST) in the optical domain. The red boxes represent the tiles used for analysis in this work. The LMC is to the left and the SMC to the right.

3.3 Magellanic Stream catalogues

The VMC survey observed two tiles in the Stream at $\alpha = 03{:}30{:}03.8$, $\delta = -64{:}25{:}24.8$ (1_1) and $\alpha = 00{:}11{:}59.3$, $\delta = -64{:}39{:}31.8$ (2_1) in all three VMC photometric bands. The positions of the VMC observations within the Stream were chosen based on the work of Mastropietro et al. (2004) as these locations were predicted as the most likely to contain a stellar component. The data for the two Stream regions were downloaded from the VSA using columns of α, δ, magnitudes and

photometric uncertainties with different flags used to only extract stellar objects using the same process as the Bridge above. From the original $\sim 70,000$ and $\sim 80,000$ objects from the VMC catalogues for the Stream tiles 1_1 and 2_1 respectively, the cleaned catalogues contained $\sim 20,000$ and $\sim 21,000$ objects in these respective regions.

In order to complete a fuller search for a stellar population within the Stream, the SuperCOSMOS survey was also studied in the direction of the two VMC tiles to give a comparison and to be able to analyse catalogues over a larger range of photometric bands as it is possible that there may exist a young or older population within the Stream. 2MASS, DENIS and WISE were not analysed in the direction of the Stream as the VMC catalogues cover the Stream in the NIR at deeper magnitudes than 2MASS, DENIS and WISE and were available at the time of this study. Initially catalogues were created just in the direction of the two VMC tiles in SuperCOSMOS, in order to perform a comparison to the VMC catalogue. The Magellanic Stream is a very large feature ($> 100°$), and it is therefore not practical to study the entire Stream at this time. As this work is the first of this kind, this study is limited to a search for a Stream stellar component in the two VMC tile regions. Subsequent work will include the search for stars in other regions of the Stream based on the predictions of various models. There are $\sim 28,000$ and $\sim 35,000$ objects in the SuperCOSMOS catalogue for the Stream tiles 1_1 and 2_1 respectively.

3.4 Summary

A number of catalogues have been created in this work for the analysis of objects in the direction of the Magellanic Bridge and Stream. For work with the Magellanic Bridge, the 2MASS, 2MASS-DENIS, SuperCOSMOS and WISE public catalogues were investigated, with the SuperCOSMOS catalogue also studied in the work with the Magellanic Stream. VMC catalogues were analysed for both the Bridge and

Stream with the application of a UKIDSS foreground region.

Table 3.3: Catalogue objects in the direction of the Magellanic Bridge and Stream

Observation region	Catalogue	No. of objects
Magellanic Bridge	2MASS	$\sim 300,000$
Magellanic Bridge	2MASS-DENIS	$\sim 70,000$
Magellanic Bridge	SuperCOSMOS	$\sim 450,000$
Magellanic Bridge	WISE	$\sim 800,000$
Magellanic Bridge 2_3	VMC	$\sim 22,000$
Magellanic Bridge 2_4	VMC	$\sim 23,000$
Magellanic Bridge 2_7	VMC	$\sim 24,000$
Magellanic Bridge 3_5	VMC	$\sim 21,000$
Magellanic Bridge 3_7	VMC	$\sim 21,000$
Magellanic Stream 1_1	SuperCOSMOS	$\sim 28,000$
Magellanic Stream 2_1	SuperCOSMOS	$\sim 35,000$
Magellanic Stream 1_1	VMC	$\sim 20,000$
Magellanic Stream 2_1	VMC	$\sim 21,000$

Table. 3.3 shows the number of objects remaining in all catalogues after cleaning, prior to the consideration of the removal of Galactic foreground sources. From these catalogues, a search will be conducted for stellar populations in both the Bridge and Stream and subsequent work will include the search for stars in other regions of the Stream e.g. exploiting the entire SuperCOSMOS database and/or driven by the predictions of various models, which will make a significant contribution to our present knowledge of these Magellanic System components.

Chapter 4

The removal of Galactic foreground objects

In the analysis of objects carried out in the direction of the LMC and SMC, the high density of Magellanic Cloud objects in comparison to Galactic objects means that the majority of objects observed and studied truly belong to the Magellanic System with a clear separation between Magellanic and Galactic objects. However, when observing lower stellar density regions such as the Magellanic Bridge and Stream, the contribution from the Galactic foreground stars and background objects can not be neglected as they will account for the vast majority of objects observed. It is possible to choose an offset region that represents the Galactic foreground population which can be removed from the Bridge and Stream regions leaving candidate Magellanic objects remaining.

As stated in Chapter 3, at the commencement of this work there were no VMC Bridge tile observations completed for analysis. For this reason, the Magellanic Bridge was preliminary analysed using catalogues from 2MASS, DENIS and WISE in the NIR as well as the optical SuperCOSMOS catalogue in anticipation for the release of VMC data. In the case of the Magellanic Stream however, VMC tiles were available throughout which supersede 2MASS, DENIS and WISE in terms of NIR magnitude depth and so no attempt was made to analyse these catalogues in

the direction of the Stream. As such, the removal of Galactic foreground objects was only investigated for the VMC and SuperCOSMOS catalogues in the direction of the Magellanic Stream. It should also be noted in the case of the Magellanic Bridge, that as the DENIS catalogue was combined with the 2MASS catalogue, there is no analysis of DENIS alone but as part of the 2MASS-DENIS combined catalogue.

In the cases of 2MASS, SuperCOSMOS and WISE, a target region was chosen to represent a purely Galactic foreground population in the direction opposite to the Magellanic Clouds across the Galactic plane, at the same Galactic longitude but at positive Galactic latitude. The application of a foreground field at opposing latitude assumes that the Galaxy is smooth and symmetric. It should be noted that it is possible that there is a small amount of contamination in this region due to the Galaxy not being perfectly symmetric, however the conservative magnitude cuts applied in each survey should account for this. This region was chosen as it represents a similar location to the Clouds in terms of reddening effects and foreground population, but without the Magellanic System dominating the region, it better represents a purely Galactic population. For this work, public catalogues were downloaded (at 292°, 39°) to cover an area equivalent to that of the central Bridge ($\sim 7° \times 8°$) or VMC tile ($\sim 1° \times 1.5°$) regions. Flags were used to clean up the foreground catalogues as in Sect. 3 for the different surveys used.

For the removal of the Galactic foreground from the VMC catalogue, the process becomes more difficult as there are no offset fields in the VMC survey, which is limited to regions of the Magellanic system. In this case it is possible to use the UKIDSS catalogue for the removal of Galactic foreground objects since the observed bands are the same as the VMC survey, although somewhat shallower in the $K_{\rm s}$ band (Hewett et al., 2006). The UKIDSS magnitudes are at least $2-3$ mag fainter than the general 2MASS catalogue.

Magnitude corrections from the Cambridge Astronomy Survey Unit (CASU) were applied to the UKIDSS magnitudes to correct for the difference between UKIDSS

and the VMC magnitudes. There are a few important differences between VISTA and the UKIRT WFCAM as well as the difference in magnitude systems between the VISTA Y, J, K_s and UKIDSS Y, J and K (Cross et al., 2012). Colour corrections are applied to the WFCAM photometric system to put the magnitudes onto the Vega system[7]. A number of publically available VISTA Hemisphere Survey (VHS) and LAS regions are observed with both VISTA and WFCAM allowing the calculation of colour terms and offsets between the two systems. The corrections were applied to the UKIDSS foreground catalogue to perform a direct comparison to the VMC catalogue.

As the DENIS survey only covers the southern sky, a different foreground field was required for analysis when using the 2MASS-DENIS combined catalogue. Two offset regions were chosen, one above and one below the Bridge to obtain a sample of the foreground population. The offset fields were chosen to be $2^\circ \times 2^\circ$ in size centred at $\alpha = 3{:}26{:}00$, $\delta = -59{:}53{:}0$ and $\alpha = 4{:}01{:}31.91$, $\delta = -80{:}58{:}19.8$. The offset fields were analysed for Galactic dust reddening by examining dust extinction maps (Schlegel et al., 1998) as these fields are assumed to comprise of only Galactic foreground stars. The average absorption ($A_I = 0.073$, $A_J = 0.033$, $A_H = 0.021$, $A_K = 0.014$) are sufficiently low to allow use of these fields in the removal of Galactic foreground stars from the Magellanic Bridge population and this is re-enforced as the Magellanic Clouds lie sufficiently above the Galactic plane for reddening effects to be low and therefore no correction for reddening has been made. Two Bridge fields of $2^\circ \times 2^\circ$ were also chosen to represent the Bridge population from the 2MASS-DENIS catalogue, in a test for the foreground removal process, in the direction of the highest stellar density at $\alpha = 2{:}00{:}00$, $\delta = -75{:}30{:}00$ and $\alpha = 2{:}20{:}00$, $\delta = -70{:}00{:}00$ (from density maps in Chapter 5). It should be noted that the reddening effects of the Bridge were also examined and the average absorption ($A_I = 0.094$, $A_J = 0.043$, $A_H = 0.028$, $A_K = 0.018$) are also low enough here and similar to the offset fields, to continue without a

[7]http://apm49.ast.cam.ac.uk/surveys-projects/vista/technical/photometric-properties

reddening correction for the Bridge region.

The three main methods of foreground removal that are applied to the Bridge and Stream catalogues are described below. Different combinations of methods were used depending on their suitability to the catalogues to be analysed. These foreground removal methods are described here in the direction of the Magellanic Bridge and Stream with a brief description of any remaining Magellanic candidates after removal to be analysed in the following chapters.

4.1 Foreground removal methods

The three methods of removing Galactic foreground objects from a target region used in this work are described here. These methods compare observations from the target region, in this case the Magellanic Bridge or Stream, with a chosen field representing a purely Galactic population as described above. As well as these observation based methods, a method is also described later in this chapter which looks at the application of a synthetic foreground population for removal.

4.1.1 A probability method

This method of foreground removal plots CMDs of a target region and corresponding foreground region of the same size and bins the objects in x (colour) and y (magnitude) bins that are large enough to contain a high enough number of objects but also small enough to achieve reasonable accuracy ($\sim 0.1 \times 0.5 mag$). Then per bin, the probability was calculated of an object belonging to the Magellanic target region, N_{Target}, given the number of objects in the foreground field, $N_{\mathrm{Foreground}}$, (probability = $\frac{N_{\mathrm{Target}} - N_{\mathrm{Foreground}}}{N_{\mathrm{Target}}}$) per colour and magnitude bin. The cut off for an object belonging to the Bridge or Stream was chosen to be 0.75 as this represents the upper quartile. Depending on the photometric bands of the catalogue in each case, different colour and magnitude bins were used.

4.1.2 Using colour cuts

The colour-cut approach compares the target fields to foreground fields using a range of CMDs and two-colour diagrams to find the best separation between Magellanic and Galactic populations. Instead of binning the target and foreground fields, this method makes the use of colour and magnitude cuts to separate the Magellanic and foreground populations and allows an analysis of the separated populations. This method is particularly useful where there is a clear separation between the target region and foreground stars.

4.1.3 Statistical cleaning

The third method of Galactic foreground removal used here is a method that involves foreground removal in colour and magnitude space as in the probability method. However, this method removes objects one by one based on their colour and magnitude position opposed to collecting objects in bins. This statistical method uses a chi-squared analysis (see equation below) to match objects from a foreground field to objects in the target region and if the chi-squared value is within a range corresponding to three sigma (according to a normal distribution), the method removes a given object from the foreground and target field.

$$\chi^2 = (\delta K/\sigma_{\rm K})^2 + (\delta(Y-J)/\sigma_{\rm Y-J})^2 + (\delta(J-K)/\sigma_{\rm J-K})^2 \qquad (4.1)$$

If more than one object is chosen within the chi-squared criteria (14.2 or better with a combination of the colours and magnitude), the closest object is removed. This removal method was only applied to the VMC catalogue for the Magellanic Bridge, as it was developed in the project (This method is also briefly investigated in the direction of the Stream later on). The probability method was satisfactory when applied in work by Bagheri et al. (2013) to 2MASS and WISE catalogues to discover the first candidate older Bridge population however, for the VMC catalogue it is important to explore all channels of foreground removal as this

work will build upon the existing older and younger candidates. As this method is only applied to the VMC catalogue it is adapted to the VMC Y, J and $K_{\rm s}$ bands and colours between. This method uses three dimensions to perform the analysis in the best combinations of colours and magnitudes with $(Y-J)$, $(J-K_{\rm s})$ and $K_{\rm s}$. Objects that do not have a foreground field counterpart in the target Bridge field are considered to be a candidate Bridge object. This removal program also gives the number of objects in the foreground region that do not have a counterpart in the target region. Usually this number is very small (1% or less). This removal code was written in Fortran by the primary project supervisor.

4.2 Foreground removal in the direction of the Magellanic Stream

When observing the Magellanic Stream, quantifying the contribution from Galactic foreground stars is vital as they will account for the vast majority of objects observed. The foreground removal method was investigated here by applying the probability method as described in Sect. 4.1.1.

For the removal of the Galactic foreground from the VMC catalogue, as there are no offset fields in the VMC survey, it is possible to use the UKIDSS data for removal since the observed bands can be adapted the VMC survey with the application of a small correction as described in Chapter 3 (Fig. 4.2).

For the SuperCOSMOS and UKIDSS data, a target region was chosen to represent a purely Galactic foreground population in the direction opposite to the Magellanic Clouds across the Galactic plane, at the same Galactic longitude but at positive Galactic latitude. Flags were used to clean up the catalogues as described in Sect. 3. In each catalogue, a CMD was chosen to carry out the removal by binning objects in colour and magnitude bins of $(B-I)$ vs I in SuperCOSMOS (Fig. 4.1), and $(Y-K_{\rm s})$ vs $K_{\rm s}$ in VMC and UKIDSS to make use of the largest baseline producing the best distinction between populations. The bin sizes were

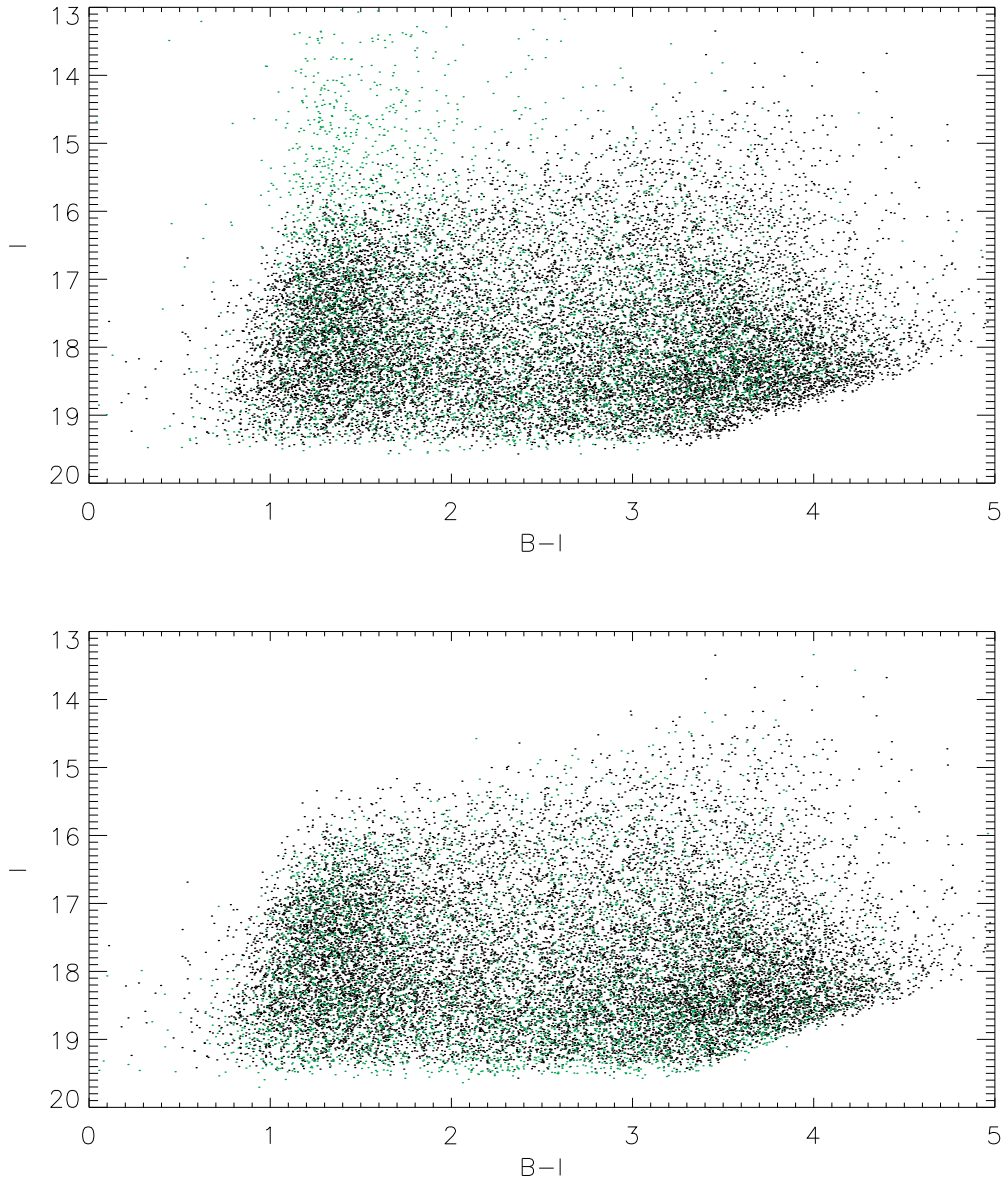

Figure 4.1: CMD, $(B - I)$ vs I of the Magellanic Stream tiles 1_1 (top) and 2_1 (bottom), in SuperCOSMOS before the removal of Galactic foreground objects (green), and also the chosen Galactic foreground field (black) prior to the removal of foreground objects.

chosen to be 0.1×0.5 in colour and magnitude in all cases, as this bin size is large enough to contain a reasonable number of objects in each bin (up to 1000 in this case), but small enough to have enough bins with different probabilities to optimise accuracy (refer to Sect. 4.1.1). Table 4.1 shows the number of objects remaining in each catalogue for the Stream tiles after the removal of foreground objects.

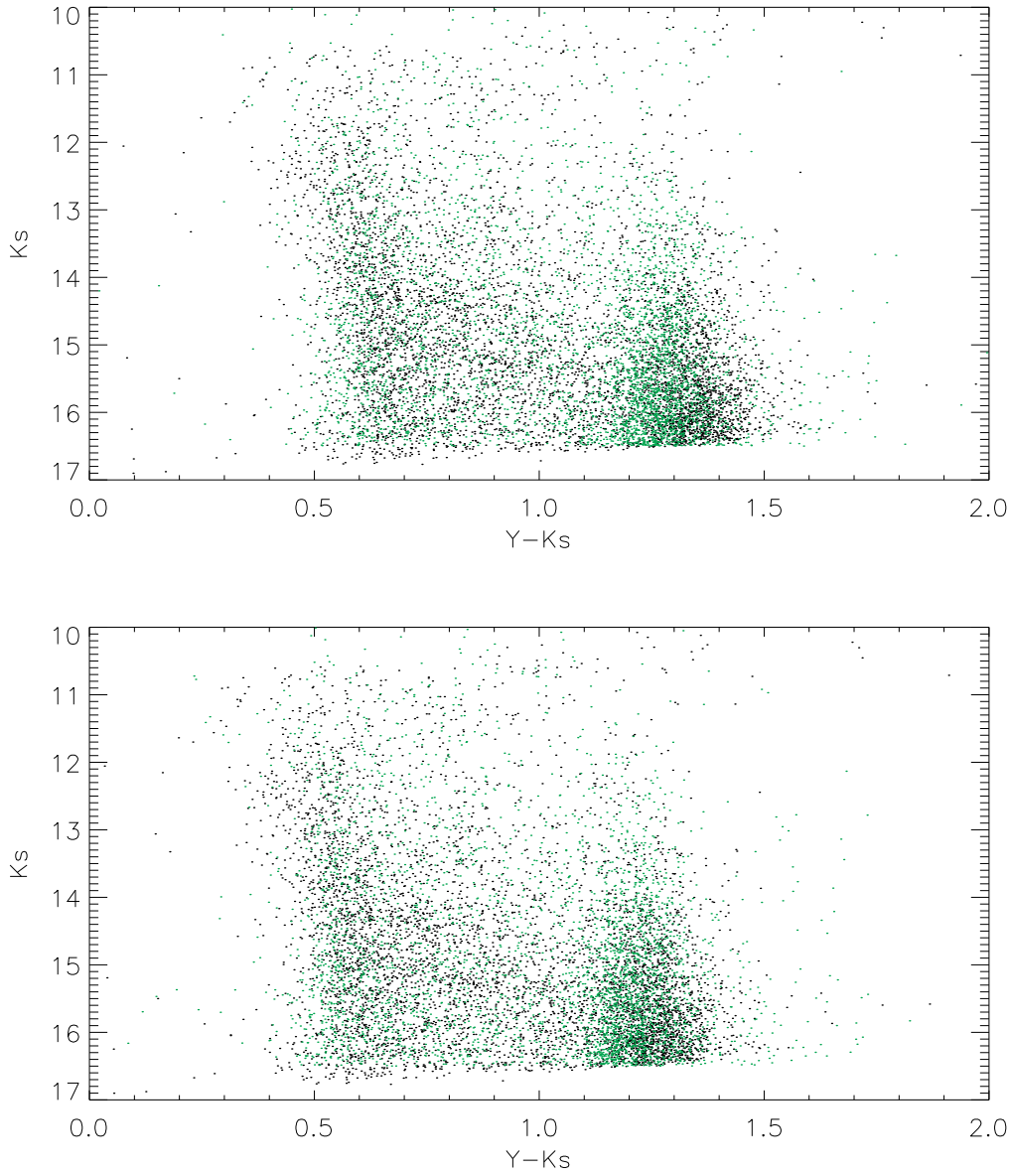

Figure 4.2: CMD, $(Y - K_s)$ vs K_s of the Magellanic Stream tiles 1_1 (top) and 2_1 (bottom), from the VMC catalogue before the removal of Galactic foreground objects (green), and also the chosen Galactic foreground field from UKIDSS (black) prior to the removal of foreground objects.

Table 4.1: Stream candidates after foreground removal

Tile	Catalogue	No. of sources remaining
1_1	SuperCOSMOS	365
1_1	VMC ($K_s < 16.5$)	0
2_1	SuperCOSMOS	4
2_1	VMC ($K_s < 16.5$)	0

The SuperCOSMOS catalogue left just 4 objects in tile 2_1 with $P > 0.75$, but a population of 365 candidates in tile 1_1 indicating the presence of a potential stellar counterpart to the Stream. The Poisson error on the total number of objects ($\sqrt{N}$) for the tile 1_1 catalogue is 255, confirming that the candidates here are above statistical uncertainty. After the Galactic foreground removal was applied to the VMC catalogue using UKIDSS for the two Stream tiles, no Stream stellar candidates remained above statistical errors. For now it appears that there are no candidate redder objects in the Magellanic Stream. This may change with the application of a different method of Galactic foreground removal or the investigation of other parts of the Stream.

The VMC foreground removal in the direction of the Stream is limited to the availability of a suitable foreground field, in this case using UKIDSS. The discovery of a stellar population in the Magellanic Stream would be of great importance as would a reliable non-detection as each result could support a different method of formation of the Stream and as such, would have great implications for the past, present and future interactions between the Magellanic Clouds. It is therefore important to make full use of the depth of the VMC survey catalogue which is not achieved while including the shallower UKIDSS catalogue. Although not possible within the time constraints of this work, a study should be carried out into removing the foreground in the direction of the Stream (and also the Bridge) from the VMC catalogue using a deeper foreground catalogue. An ideal foreground field would be taken from one of the other ongoing VISTA surveys. As the Galactic foreground population across the sky is somewhat inhomogeneous, the use of UKIDSS data to represent the VMC foreground population has limitations. Other VISTA surveys may have suitably located observing tiles which may be used, for example the VHS has some publicly available data in the region close to opposite the Magellanic Stream across the Galactic plane, with depths similar to UKIDSS but do not require any magnitude corrections. From the time of the writing of this thesis, other data will become available for an ongoing study of the foreground

in the direction of the Magellanic System with deeper VISTA magnitudes. The Magellanic Stream can also be analysed in the future by exploiting the entire SuperCOSMOS catalogue regardless of the VMC pointings.

4.3 Foreground removal in the direction of the Magellanic Bridge

The removal of the Galactic foreground objects in the direction of the Magellanic Bridge is split into two main parts. The first application of the Bridge foreground is for public catalogues using the methods described above with foreground fields taken from the catalogues themselves. The second part of the Bridge foreground removal is for the VMC catalogues which, as no offset region is available, uses the Stream tile 2_1 as a foreground field as this tile showed no potential Magellanic candidates. As well as the application of the probability removal method to the VMC Bridge tiles, the statistical method was also applied using the UKIDSS opposite foreground field and the Stream tile 2_1.

4.3.1 Public catalogue observations

As described above, at the beginning of work for this thesis, no VMC observations were available in the direction of the Magellanic Bridge. As such, foundation work was carried out by studying data available from the public catalogues of 2MASS, DENIS and SuperCOSMOS with a contribution from the newly available WISE catalogue (Chapter 3). This section describes the removal of Galactic foreground objects towards the Bridge from the public catalogues and the candidate Magellanic objects remaining after the removal.

2MASS-DENIS and SuperCOSMOS matches

The two offset fields (of $2^\circ \times 2^\circ$) chosen for the 2MASS-DENIS removal ($\alpha =$ 03:26:00, $\delta = -59$:53:0 and $\alpha = 04$:01:31.91, $\delta = -80$:58:19.8), were compared to

two Bridge fields (α = 02:00:00, $\delta = -75$:30:00 and α = 02:20:00, $\delta = -70$:00:00) using a range of CMDs and two colour diagrams to find the best distinctions between the Bridge and the offset field stars. In this work, the DENIS catalogue was also included to make use of the I band for the more robust method of removing Galactic foreground. The foreground was removed from a combined 2MASS-DENIS catalogue. A CMD was also used to make cuts in the $K_{\rm s}$ magnitude for the combined catalogue near the sensitivity and brightness limits to reduce statistical fluctuations in the data (Fig. A.1). These cuts were taken at $K_{\rm s}$ = 9.0 and $K_{\rm s}$ = 13.8 mag for the bright and sensitivity limit respectively. This analysis was repeated for all bands and was used in this work to determine the point at which the photometric uncertainty was too large for the data to be reliable. Figure A.1 shows that the photometric uncertainty increases for stars brighter than $K_{\rm s} \sim 8.5$ mag, and a cut around this level excludes Galactic giant stars as they will appear as very bright objects. The cut at $K_{\rm s}$ = 13.8 mag was chosen as a compromise between the higher photometric uncertainties near the sensitivity limit of the catalogue and not removing faint objects in the Magellanic Bridge. This method for the removal of foreground stars makes primarily use of the different IR colours of late type dwarfs and giants (Bessell and Brett, 1988).

The best separation of the Bridge and Galactic populations was observed in the $(I - K_{\rm s})$ vs $K_{\rm s}$ Hess diagram (Fig. 4.3). A value of $(I - K_{\rm s}) > 1.3$ was initially taken by eye as the best cut to separate the Galactic foreground from the Bridge population. Using this value as a base, a spread of values around this cut were selected, and the best S/N value was calculated using the formula $\mathrm{S/N} = \frac{N_{\rm Bridge}}{\sqrt{N_{\rm Bridge}{}^2 + N_{\rm Foreground}{}^2}}$, comparing the Bridge field to the foreground field. The value with the highest S/N was adopted for the final colour cut. With an optimum S/N of 10, a final Galactic foreground cut of $(I - K_{\rm s}) > 1.1$ mag was applied. Photometric errors of the photometry cause a scattering of foreground stars into clean regions in colour space. The aim was to find an optimal trade off between removing as much Galactic foreground contamination as possible without

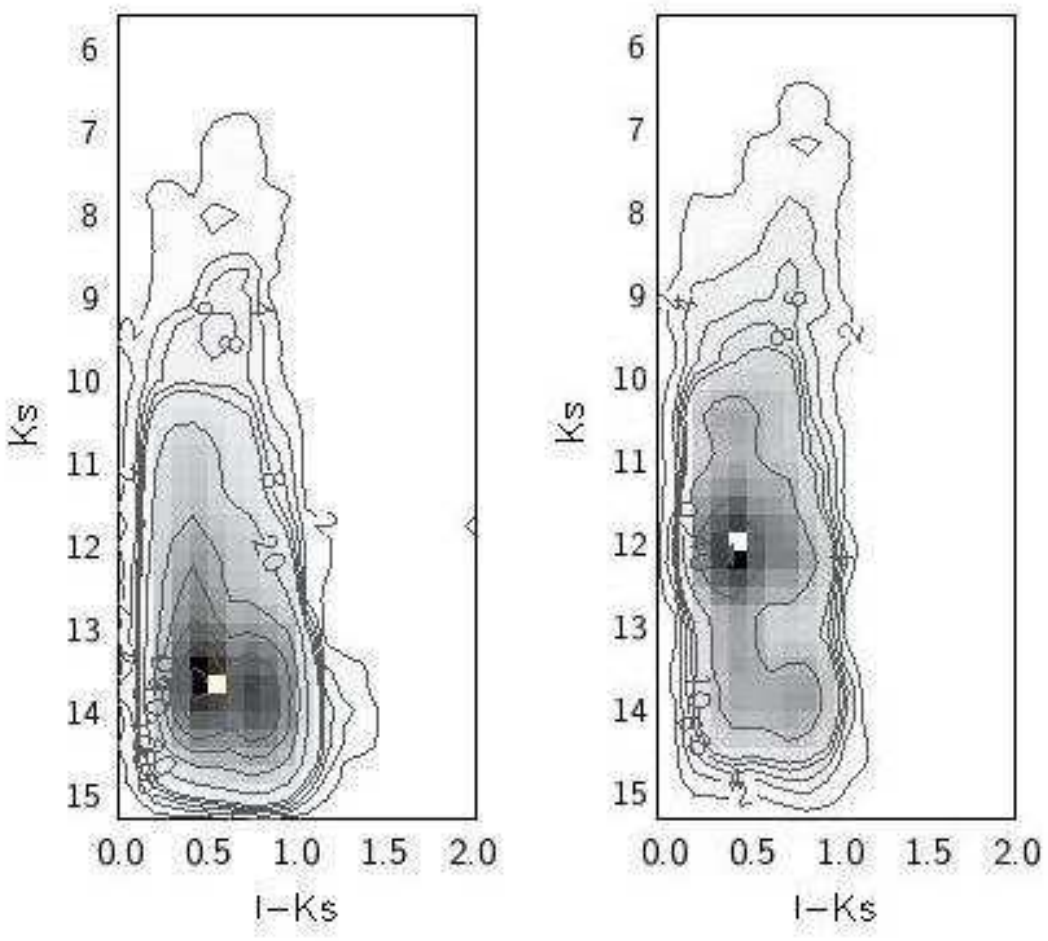

Figure 4.3: $(I - K_s)$ vs K_s Hess diagrams of the Bridge (left) and foreground (right) fields of the 2MASS-DENIS combined catalogue showing the difference in populations. Bin size is 0.1×0.2 in colour and magnitude respectively. Contour levels are at: 2, 4, 6, 8, 10, 20, 40 and 60 stars.

removing too many genuine Bridge stars.

Figure 4.4 shows the two colour diagram $(H - K_s)$ vs $(J - H)$ of the combined 2MASS-DENIS catalogue and the Galactic dwarf and giant sequences (Bessell and Brett, 1988) which aided the Galactic foreground removal process. From this comparison a cut at $(J - H) = 0.70$ was chosen initially by eye to remove the Galactic dwarfs from the catalogue which will cause contamination to the Magellanic objects. Again a range of values around this $(J - H)$ cut were checked for the optimum cut (S/N = 7.9), resulting in a value of $(J - H) > 0.75$ mag. The remaining objects were then further selected in $(H - K_s)$ (S/N = 13) to remove any remaining Galactic population by making a cut at the point in which the two

population arms begin to separate, i.e. the Magellanic giant population begins to divert away from the main bulk of Galactic M dwarf objects. The final colour selection criteria for the 2MASS-DENIS combined catalogue were $(I - K_s) > 1.1$, $(J - H) > 0.75$ and $(H - K_s) > 0.32$ mag which were applied together with the magnitude cuts at $K_s = 9.0$ and $K_s = 13.8$ mag.

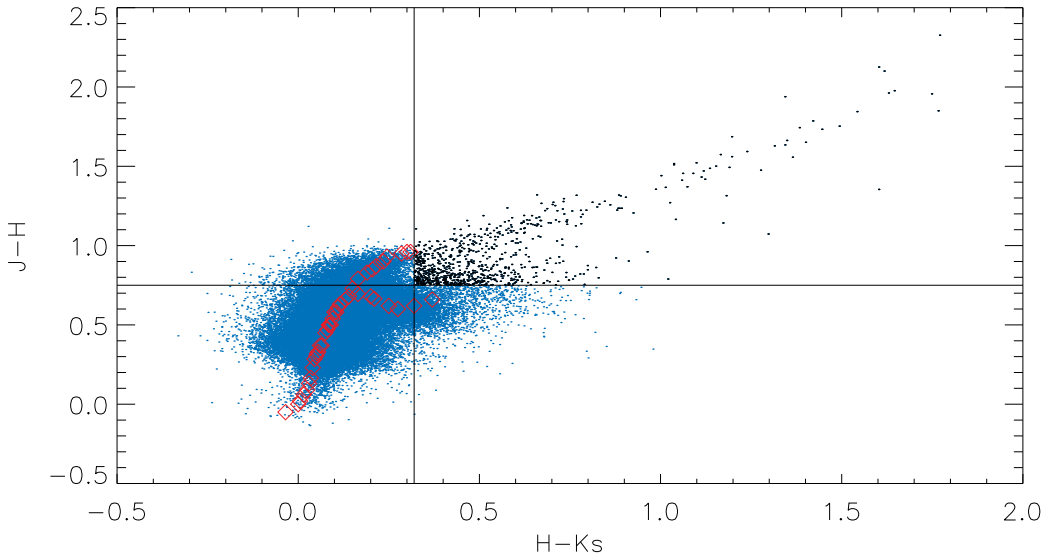

Figure 4.4: $(H - K_s)$ vs $(J - H)$ two colour diagram for the 2MASS-DENIS combined catalogue of the Bridge (dots) with Bessell & Brett (1988) Galactic dwarfs and giants (red diamonds. Bold lines illustrate the foreground removal cuts at $(H - K_s) > 0.32$ and $(J - H) > 0.75$ mag, the blue region is removed as foreground and the black region (top right quartile) is kept as a candidate Bridge population.

A similar method of the removal of Galactic foreground objects was carried out for the optical SuperCOSMOS data using the same Bridge and Galactic foreground fields as with the combined 2MASS-DENIS catalogue. Magnitude cuts in the I band were applied to account for the brightness and sensitivity limits of the catalogue, taken at $I = 18.4$ and $I = 10$ mag, at a similar level with respect to those in the combined 2MASS-DENIS catalogue. A CMD, $(B - I)$ vs I, and two colour diagram, $(R - I)$ vs $(B - R)$, were used to separate the Galactic foreground sources from the Magellanic sources. The cuts in these diagrams were initially taken at $(B - I) < 0.4$, $(R - I) < 0.35$ and $(B - R) < 0.5$ mag. After

checking the spread around these values, cuts of $(B-I) < 0.5$, $(R-I) < 0.3$ and $(B-R) < 0.6$ mag were chosen (with optimum S/N = 24.4, 24.7 and 25.1 respectively) for the final Galactic foreground removal. A cut at the blue end of the catalogue was also applied to remove background galaxies at $(B-R) > -0.5$ mag. This cut was confirmed to be accurate as all sources with $(B-R) < -0.5$ mag are galaxies according to the SIMBAD[8] astronomical database. Note that these selection criteria remove some Magellanic Cloud red giants as well.

The SuperCOSMOS objects have been compared to the colours of known MS and G-M giant objects in Fig. 4.5. A few Galactic runaway stars and hot evolved objects (HB, post-AGB and WD stars) may slip through, but numbers are small as confirmed by the CMD of the foreground fields. It can be seen here that the method of Galactic foreground removal in the SuperCOSMOS catalogue excludes Galactic MS stars and giants.

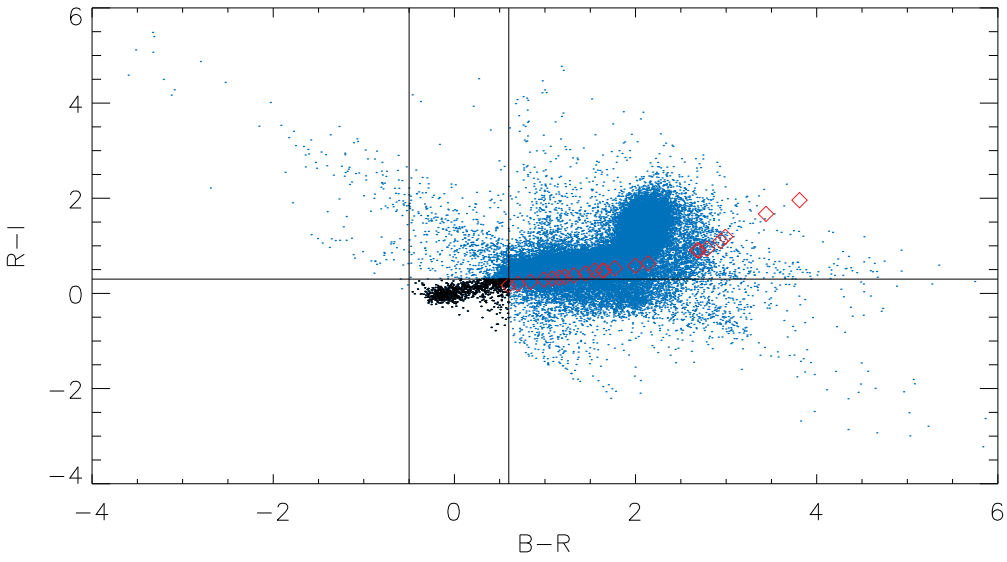

Figure 4.5: $(B-R)$ vs $(R-I)$ colour-colour plot of the SuperCOSMOS catalogue of the Magellanic Bridge with the colours of known MS stars and G-M giants ((red) diamonds). Bold lines represent foreground cuts at $(B-R) < 0.6$ and $(R-I) < 0.3$ mag. The blue region is removed as foreground and the lower central (black) region is kept as a candidate Bridge population.

The number of stars in the Magellanic Bridge area is reduced to 449 in the

[8]http://simbad.u-strasbg.fr/simbad/

combined 2MASS-DENIS catalogue and 274 in the SuperCOSMOS catalogue after the Galactic foreground removal.

Table 4.2: Different populations identified within the Magellanic Bridge from SIMBAD after the removal of Galactic foreground. [1] Irwin et al. (1990), [2] Cannon and Pickering (1918), [3] Hog et al. (1998), [4] Skrutskie et al. (2006), [5] Holmberg et al. (1974), [6] Abraham et al. (1995), [7] Westerlund and Glaspey (1971), [8] Demers and Irwin (1991).

Object	2MASS-DENIS	SuperCOSMOS	Reference
Bridge star	0	63	[1]
SMC star	53	30	[1] [7]
LMC star	21	0	[1]
Magellanic Cloud object	4	11	[1] [8]
Background Galaxy	74	3	[4] [5]
Other known object	0	20	[2] [3] [6]
Unknown	275	129	

A further extension to the Galactic foreground removal process used SIMBAD over the entire Bridge region to investigate the candidate Bridge objects in the 2MASS-DENIS combined catalogue and the SuperCOSMOS catalogue with a breakdown of objects in Table 4.2. Using this method a further 74 objects were removed from the 2MASS-DENIS combined catalogue as background galaxies and 7 objects were removed from the SuperCOSMOS catalogue as Galactic stars and background galaxies. It should be noted that no previous attempt was made to remove background galaxies from the 2MASS-DENIS catalogue beyond using the point source flags. The remaining 365 objects in the 2MASS-DENIS combined catalogue and 267 in the SuperCOSMOS catalogue are all likely to be objects with a Magellanic origin.

2MASS and WISE matches

In the search for an older Bridge population, the decision was made to discard the DENIS catalogue as although the extra I band was a useful tool in analysing the Bridge in terms of stellar densities over a larger waveband range, because no older

population had been observed in the Bridge, the deeper 2MASS data was required at the fullest depth to conduct a thorough search. In this case the 2MASS and WISE catalogues were analysed after the Galactic foreground removal. Flags were used to clean up the catalogues as described in Sect. 3.

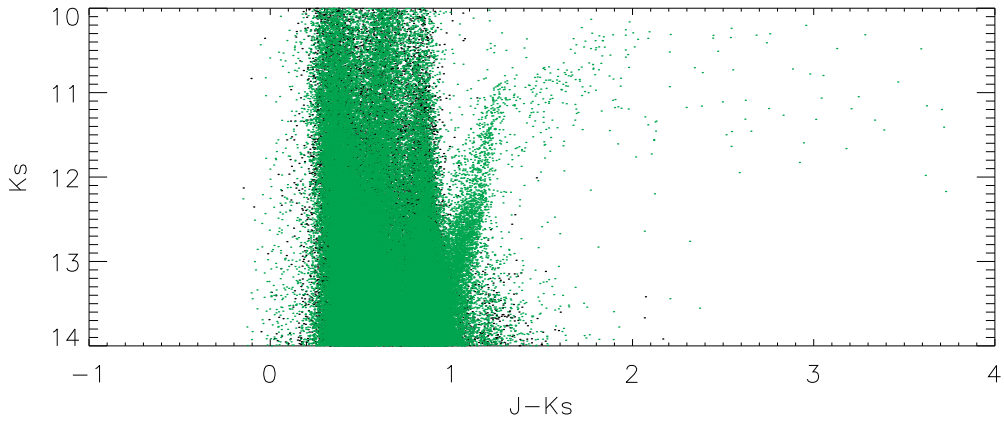

Figure 4.6: CMD, $(J - K_s)$ vs K_s of the Magellanic Bridge from 2MASS before the removal of Galactic foreground objects (green), and also the chosen Galactic foreground field (black) prior to the removal of foreground objects.

Two approaches were applied to the removal of Galactic contamination from the Bridge sample as described above. The first method is a more statistical probability based approach (Sect. 4.1.1), which does not supply information about the individual candidates remaining in the Bridge, but confirms that an over density of objects exists after the removal of the foreground. The second method makes use of a colour-cuts (Sect. 4.1.2) which will remove some genuine Bridge objects, but will leave a sample of Bridge candidates that are almost free of contamination. The second method will enable the characterisation of any remaining Bridge population.

In each catalogue of the Bridge and foreground, the CMD chosen for the removal was that with the largest baseline and separation of objects. These were $(J - K_s)$ vs K_s in 2MASS, and the WISE removal was based on the shorter wavelengths $(W1 - W2)$ vs $W2$ as these bands are more likely to reveal a stellar population in the direction of the Bridge, and have magnitude limits comparable to 2MASS

or slightly better.

The bin sizes chosen for the 2MASS statistical removal were 0.2×0.5 in colour and magnitude in all cases, as this bin size is large enough to contain a reasonable number of objects in each bin (up to 1000 in this case), but small enough to have enough bins with different probabilities to optimise accuracy. From the 2MASS catalogue 2515 objects remained and this method confirms an over density of Bridge objects to the foreground and this method leaves a sequence remaining (Fig. 4.7) that is likely to belong to the Bridge given the position on the CMD.

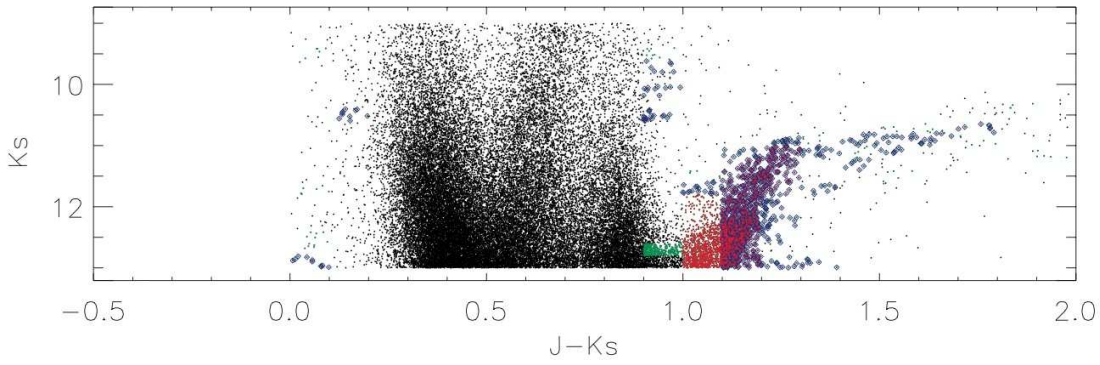

Figure 4.7: CMD, $(J - K_s)$ vs K_s of the Magellanic Bridge in 2MASS before the removal of Galactic foreground objects (black), and also after the application of the probability removal method, keeping only objects with probabilities of $0.75 - 0.85$ (green), $0.85 - 0.95$ (blue) and 0.95 and over (red).

The colour-cut method for the removal of foreground stars makes primarily use of the different IR colours of late type dwarfs and giants (Bessell and Brett, 1988). For NIR 2MASS colours, the intrinsic colours of $(H - K_s)$ and $(J - H)$ show a good separation between Galactic dwarfs and giants to Magellanic Bridge objects, enabling a good removal of foreground from the Bridge. The redder colours of the WISE $W1$ and $W2$ bands do not allow for such a clear separation since this region is dominated by the Rayleigh-Jeans tail towards redder wavelengths.

Figure 4.8 shows the two colour diagram $(H - K_s)$ vs $(J - H)$ with the application of a cut at $(J - H) > 0.78$ to remove the Galactic objects from the 2MASS Bridge catalogue where there is a clear separation between Magellanic and Galactic objects. A cut at $K_s = 13$ mag was also applied near the sensitivity

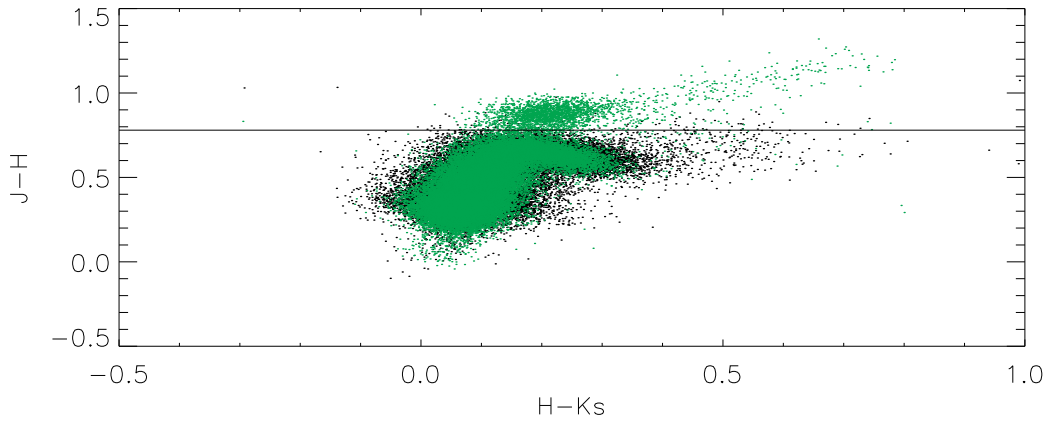

Figure 4.8: Two colour diagram, $(H - K_s)$ vs $(J - H)$ of the 2MASS Galactic foreground field (black) and the Magellanic Bridge (green), in order to apply a colour-cut method of removing the foreground objects. A line at $(J - H) > 0.78$ is shown to indicate the selection criteria that an object belongs to the Magellanic Bridge and not the Galactic foreground.

limit of the 2MASS survey in order to reduce uncertainty. This selection criteria was applied to the 2MASS Bridge catalogue and from this colour-cut removal, 2499 Bridge candidates remain.

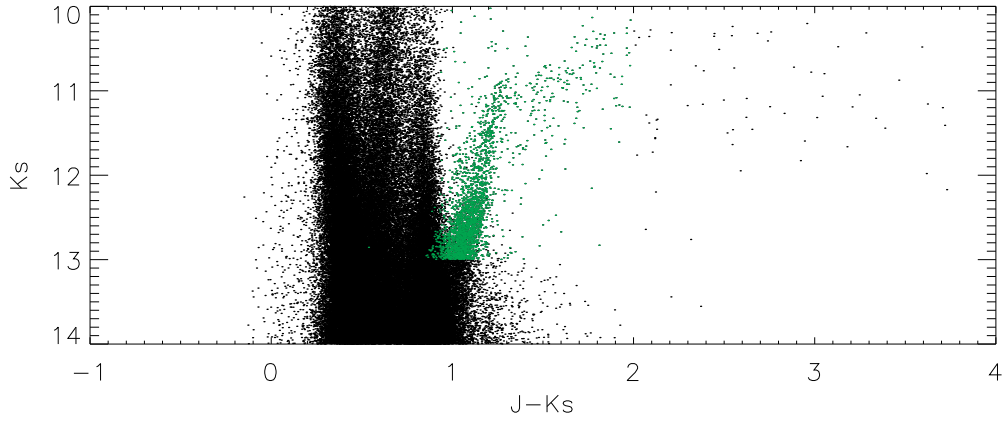

Figure 4.9: CMD, $(J - K_s)$ vs K_s of the Magellanic Bridge in 2MASS before the removal of Galactic foreground objects (black), and also after the application of the colour-cut removal method (green).

After the application of the removal of Galactic foreground objects from the Bridge 2MASS catalogue, the statistical method confirm that there is an over density of Bridge objects to foreground contamination. The colour-cut method of

removal isolates particular populations of Bridge candidates and these remaining objects will be investigated in Sect. 5.3.3.

The same methods of Galactic foreground removal were applied to the WISE catalogues as in 2MASS. The binning in WISE was applied at $(W1 - W2) = 0.1$ and $W2 = 0.2$ mag in order to maximise the number of objects in each bin, while keeping the greatest accuracy. After the application of the probability method of removal to the WISE catalogue, just 75 Bridge candidates remain, which is below the poisson error, to confirm an over density within the Bridge. The colour-cut method of removing the Galactic foreground was investigated using the $W1$ and $W2$ WISE bands.

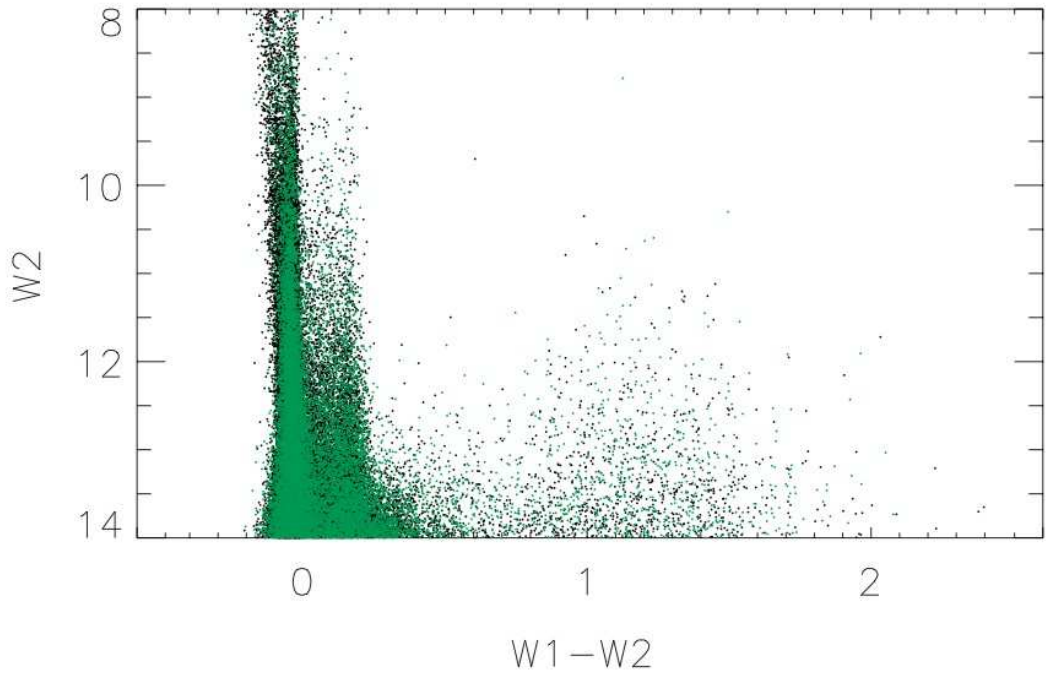

Figure 4.10: CMD, $(W1 - W2)$ vs $W2$ of the Magellanic Bridge in WISE (black), and the Galactic foreground field (green).

It can be seen from Fig. 4.10 that there is very little separation between the Bridge and foreground field in $(W1 - W2)$ vs $W2$. This is also the case in other CMDs and two-colour diagrams meaning that it is not possible to separate the Bridge from Galactic objects using a colour-cut method. From the investigation of WISE at this point, there are no clear Bridge candidates to put forward for

analysis. Due to the longer wavelengths of WISE, the catalogue is strongly dominated by background objects and the Rayleigh-Jeans regime of stellar objects, making it difficult to separate Bridge and foreground objects. The candidates from the 2MASS colour cut removal will be put forward for analysis, in order to characterise their populations.

4.3.2 VMC observations

Due to the confirmation that there appears to be no stellar significant component in Stream tile 2_1, this tile can be used to represent an upper limit on the Galactic foreground population in the direction of the Magellanic Bridge (this will still be the case if a small Stream population exists). As well as performing the foreground removal on the Bridge using a UKIDSS catalogue, tile 2_1 from the VMC survey has also been applied since this tile covers the same area and wavebands as the Bridge catalogues and also has the advantage of being in the vicinity of the Magellanic Clouds in terms of reddening effects. As described, the UKIDSS catalogue is shallower than the VMC observations so for the removal with UKIDSS, a cut at $K_{\rm s} = 17$ is applied to all catalogues to match the magnitude limit of UKIDSS within reasonable photometric errors (~ 0.06 or better). It should be noted that very conservative magnitude cuts are applied when using the UKIDSS catalogue to remove foreground from the VMC catalogue, and as such neither catalogue is utilised to its full depth.

It can be seen from Figs. 4.11 and 4.12 that the remaining Bridge candidate objects occupy different regions of the CMD, which will be investigated in more detail in Sect. 5.3.3. From the removal using the probability method with the UKIDSS foreground field and Stream tile 2_1, all five of the Bridge observing tiles had similar remaining likely candidate stellar populations above statistical uncertainties. The populations remaining occupy three different regions of the CMD, a blue region, a red region and an intermediate region.

Due to the shallower magnitudes in UKIDSS compared to the VMC cata-

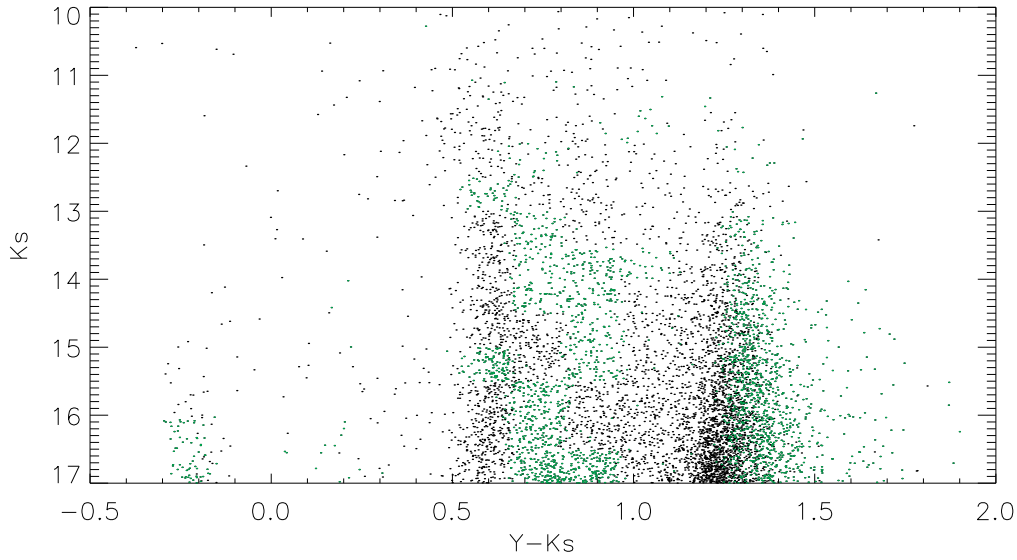

Figure 4.11: CMD, $(Y - K_s)$ vs K_s of the Bridge tile 2_3, after the removal of the Galactic foreground population (blue) using the probability method ($P > 0.75$), from the VMC catalogues with the UKIDSS field representing the foreground population (black) in the direction of the Magellanic Clouds.

logues, the foreground removal with the Stream tile from the VMC data will reveal candidate Bridge objects at fainter magnitudes than the UKIDSS method. These fainter Bridge candidates represent a lower limit on Bridge candidates as no removal of Galactic foreground has been carried out on the Stream tiles at magnitudes fainter than the UKIDSS Y, J and K limiting magnitudes.

It should be noted that at a brief look at the cleaned Bridge sample using both UKIDSS and the tile 2_1, the population of Bridge candidates on the right side of the CMD at redder colours appear to be very well mixed with the foreground population. The work below using the more accurate statistical removal method will explore whether this region is really a candidate Bridge population.

As well as the application of the probability removal method to the VMC Bridge tiles, the statistical method was also applied using the Stream tile. The decision was taken to perform this method of foreground removal with just the Stream tile 2_1 representing the Galactic foreground. After performing the probability removal method with the Stream tile and with the UKIDSS foreground field, similar cleaned populations were recovered in the Bridge indicating there was not

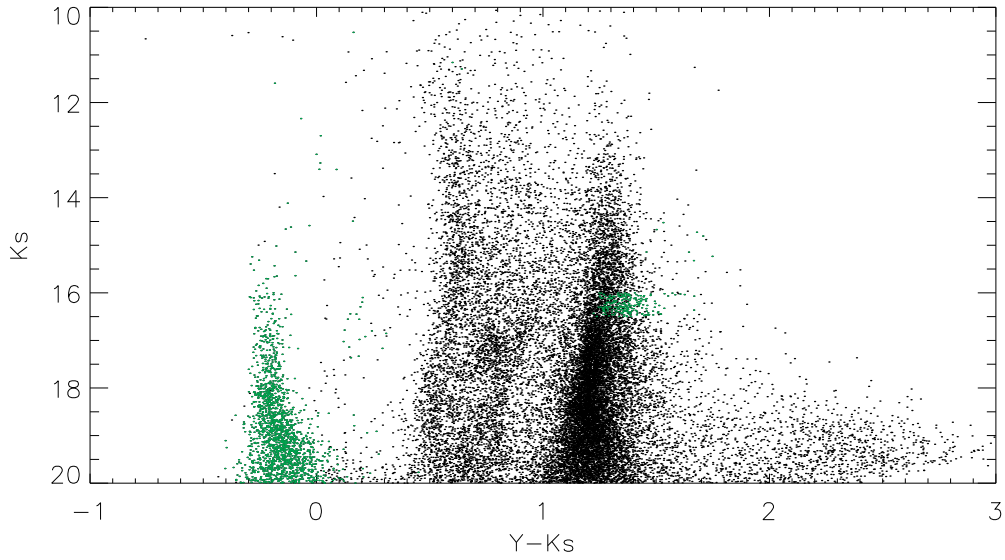

Figure 4.12: CMD, $(J - K_s)$ vs K_s of the Bridge tile 2_3, after the removal of the Galactic foreground population (green) using the probability method ($P > 0.75$), from the VMC catalogues with the VMC Stream tile 2_1 representing the foreground population (black) in the direction of the Magellanic Clouds.

a need to use both, and with the deeper magnitudes, the Stream tile was chosen to represent the Galactic foreground for the statistical method.

The statistical foreground removal method applies a small tolerance in the two colours and magnitude to account for cosmic errors on top of the photometric errors of the VMC catalogue. These tolerances will effect the number of objects recovered in the removal process and if too strict, will result in foreground objects not being matched to their true counterpart. The test for this method was carried out using a VMC field in the SMC. The field chosen (3_3) was not in the centre of the SMC but just outside so as not to be too crowded, but to have enough objects that the contamination from Galactic foreground objects is very low. It is useful to use the SMC to calibrate the foreground method for the Bridge here as it is postulated that the Bridge is likely to have formed primarily from the SMC (Chapter 2). The calibration needed initial values of the tolerances in $(Y - J)$, $(J - K_s)$ and K_s which were chosen to be 0.05, 0.05 and 0.1 respectively. The removal process was then applied to the SMC field using the Stream field 2_1.

In this case the SMC tile was used to calibrate the tolerances in colour and

Table 4.3: Different tolerances for the statistical foreground removal.

Label	Colour tolerance	Magnitude tolerance	Unmatched foreground objects
A	0.05	0.2	411
B	0.1	0.5	310
C	0.1	1.0	306
D	0.2	1.0	70
E	0.5	2.0	0

magnitude by running the foreground removal with a number of different tolerances. It can be seen from Table 4.3 that the number of matched objects increases as the tolerances are relaxed as one would expect, with version E being the most relaxed leaving no foreground objects without a match in the target field.

It can be seen from Fig. 4.13 that using the original tolerance values removes the Galactic foreground population in the direction of the SMC and leaves an SMC population remaining. It can also be seen however that there is a region to the right of the CMD that does not fit the path of the stellar tracks and appears to be a remaining foreground population. This region corresponds to a region of the two-colour diagram which is highlighted in Fig. 4.14 and also appears to be inconsistent with the remaining cleaned population.

If the green population in Fig. 4.14 is neglected, the width of the giant population tail in the top right of the two-colour diagram will give an estimate of the cosmic scatter and as such the tolerances required to calibrate the removal method. The width of the tail is $\sim$ 0.2 in colour which corresponds to a 1σ tolerance of 0.1. These tolerances were applied to the removal process as well as some more relaxed values as seen in Table. 4.3 to determine whether the apparent remnant foreground population can be eradicated from the cleaned sample.

Figure. 4.15 shows the remaining SMC population after removing the Galactic foreground population with the tolerances A, B and E which correspond to the most strict values, the values estimated from the two-colour diagram and the values that leave no un-matched foreground objects respectively. It can be seen

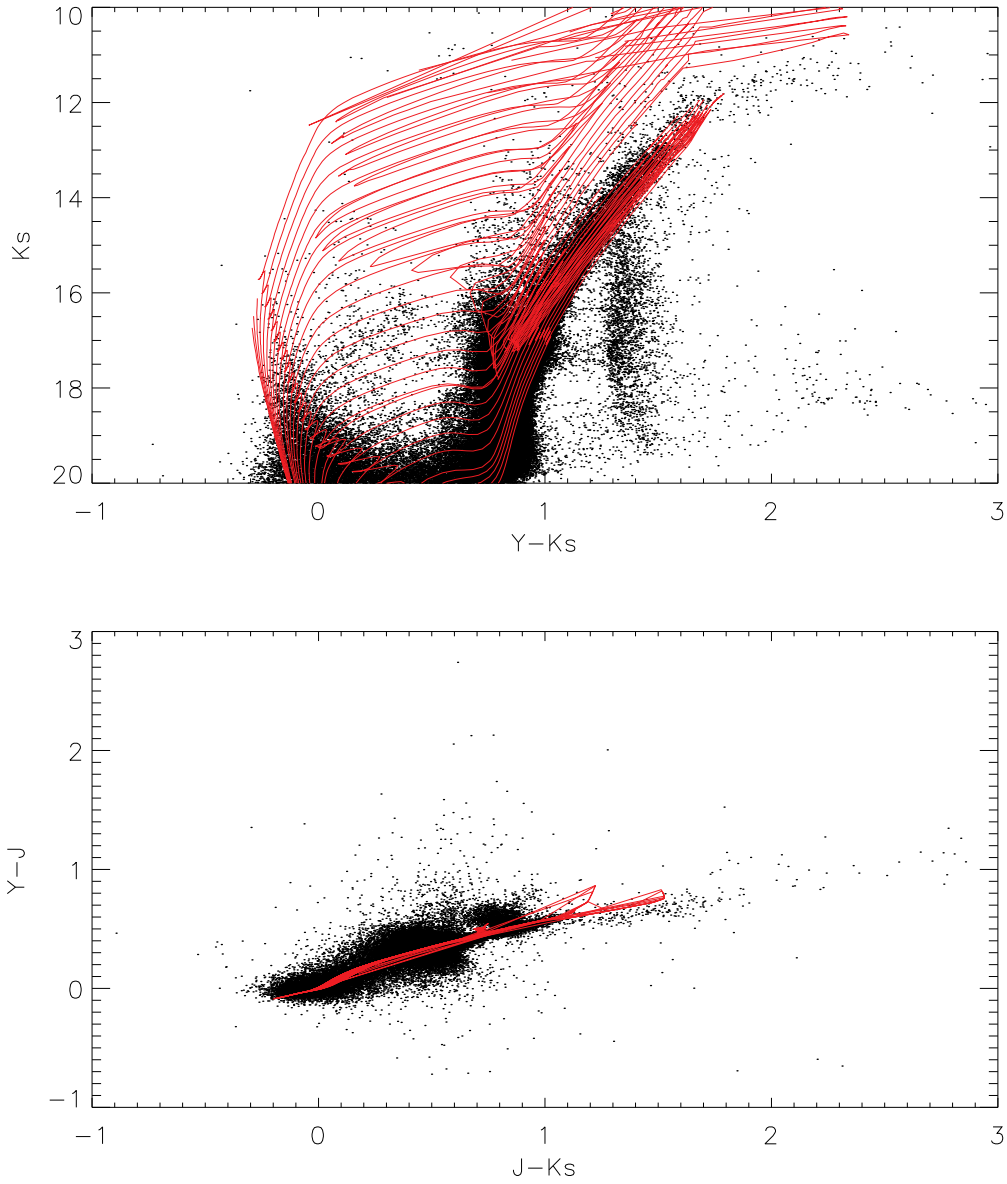

Figure 4.13: CMD, $(Y - K_s)$ vs K_s (top) and two colour diagram $(Y - K_s)$ vs $(Y - J)$ (bottom) of the SMC tile 3_3, after the removal of the Galactic foreground population using the statistical method, from the VMC catalogues with the Stream 2_1 tile representing the foreground population in the direction of the Magellanic Clouds with tolerances A from Table 4.3. Overlaid onto both Figs. are Padova isochrones at a distance of 55 kpc and a metallicity of $z = 0.004$ and ages from 10 Myr to 10 Byr.

that in all three cases the objects that appear to make up a remnant foreground population still remain. This indicates that there is no need to relax the tolerances beyond the predicted cosmic scatter as it will not remove the remaining potential foreground remnants. Changing the magnitude tolerance from 0.5 to 1.0 made

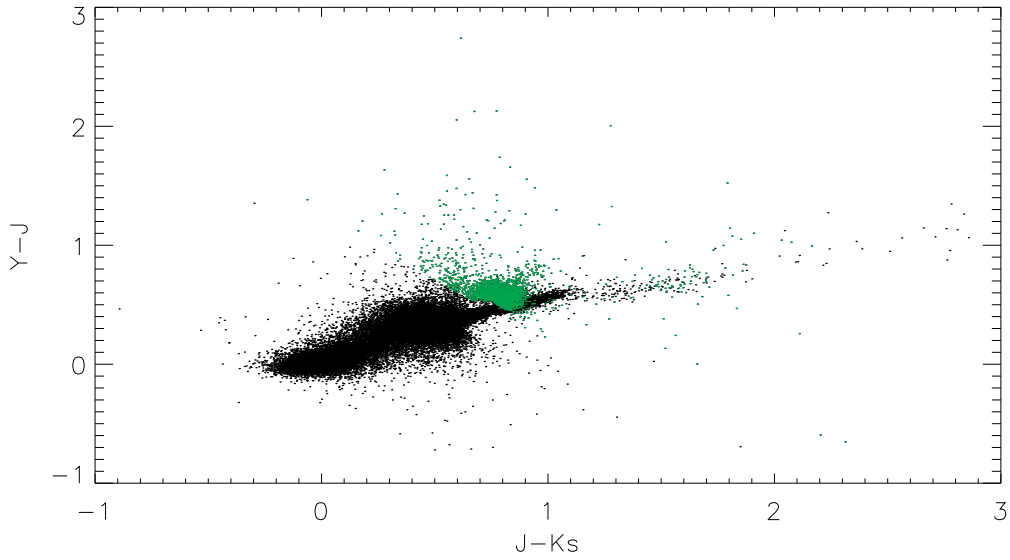

Figure 4.14: Two colour diagram $(Y - K_s)$ vs $(Y - J)$ of the SMC tile 3_3, after the removal of the Galactic foreground population using the statistical method, from the VMC catalogues with the Stream 2_1 tile representing the foreground population in the direction of the Magellanic Clouds with tolerances A from Table 4.3. The population that lies outside of the stellar tracks is highlighted in green here.

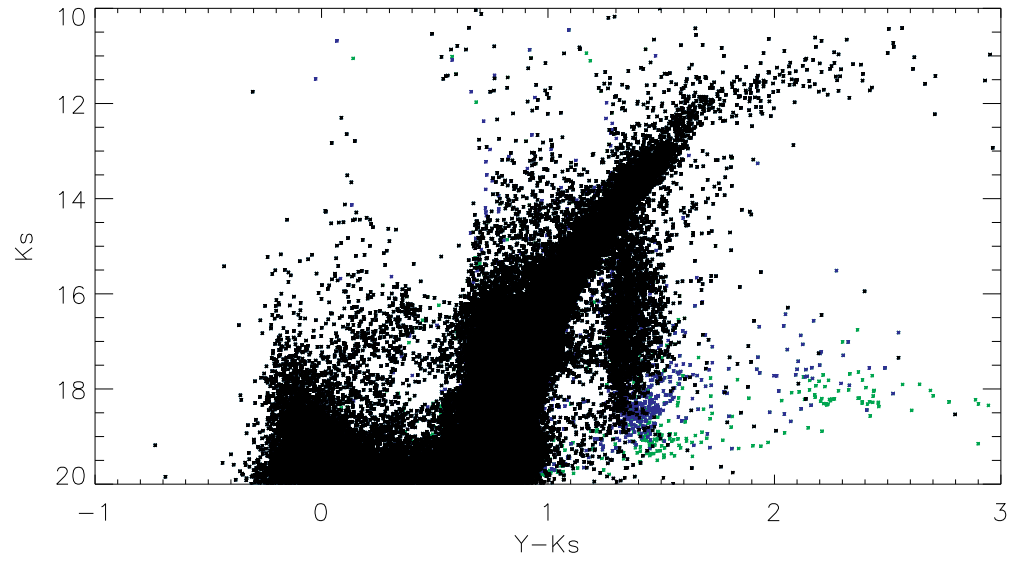

Figure 4.15: CMD, $(Y - K_s)$ vs K_s of the SMC tile 3_3, after the removal of the Galactic foreground population using the statistical method, from the VMC catalogues with the Stream 2_1 tile representing the foreground population in the direction of the Magellanic Clouds with tolerances A (green), B (blue) and E (black) from Table 4.3.

very little difference to the number of objects remaining with the colour tolerance of 0.1 therefore the tolerance of 0.5 in magnitude was deemed acceptable.
It appears that there is a population remaining in the cleaned SMC sample that does not belong to the SMC population as no isochrones from 10 Myr to 10 Gyr at the distance and metallicity of the SMC fit this population which appears to belong to the Galactic foreground. A background population would appear at redder colours and would not reach the bright magnitudes that this population does. These objects are most likely to belong to a population of Galactic K and M dwarfs (Bessell and Brett, 1988) and will be discussed later.
The Magellanic Bridge tile 2_3 was also used in testing the accuracy of the removal, with the tolerances in colour and magnitude of B as these values represent the most accurate values for the cosmic variations as above. The purpose of using the Bridge tiles here is that, if the remaining probable foreground contamination remains in the Bridge tiles, it will rule out any possibility that the excess foreground is isolated to the direction of the SMC tile 3_3 as the Bridge tiles cover a larger range in RA. Using the $(J - K_{\rm s})$ colours of the objects will also aid in the identification of any non-Magellanic populations in the cleaned samples due to the availability of stellar intrinsic $(J - K_{\rm s})$ colours from Bessell and Brett (1988) which do not cover the Y band.

It can be seen from Fig. 4.16 that there are three apparent regions of Bridge populations remaining after the removal of Galactic foreground and that the younger (left) and intermediate (middle) populations fit well with the stellar isochrones indicating that they fit to a candidate Bridge population. However the redder population to the right of the CMD falls outside the region of the stellar tracks as in the SMC tile which indicates that this population is again likely to remain from the Galactic foreground population. The redder feature is also of a similar strength in the Bridge as the SMC tile although the number of Magellanic objects is much smaller. As a test, the SMC tile was again run through the statistical foreground removal process, this time using each of the Bridge tiles as

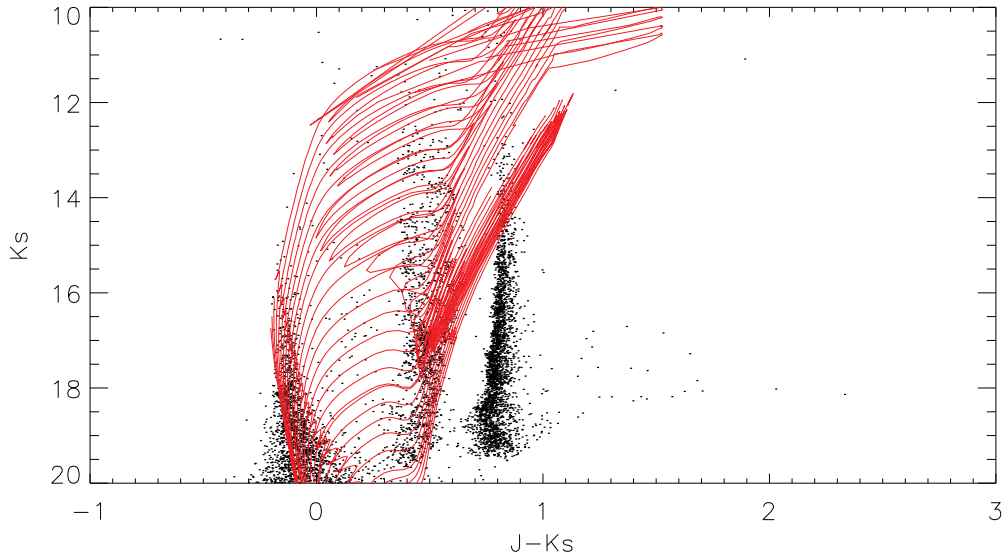

Figure 4.16: CMD, $(J - K_s)$ vs K_s of the Bridge tile 2_3, after the removal of the Galactic foreground population using the statistical method, from the VMC catalogues with the VMC Stream tile 2_1 representing the foreground in the direction of the Magellanic Clouds. Overlaid are Padova isochrones (red) at a distance of 55 kpc and a metallicity of $z = 0.004$ and ages from 10 Myr to 10 Byr.

the foreground field. The $(Y - K_s)$ vs K_s CMD was plotted in this case to show the greatest separation between populations.

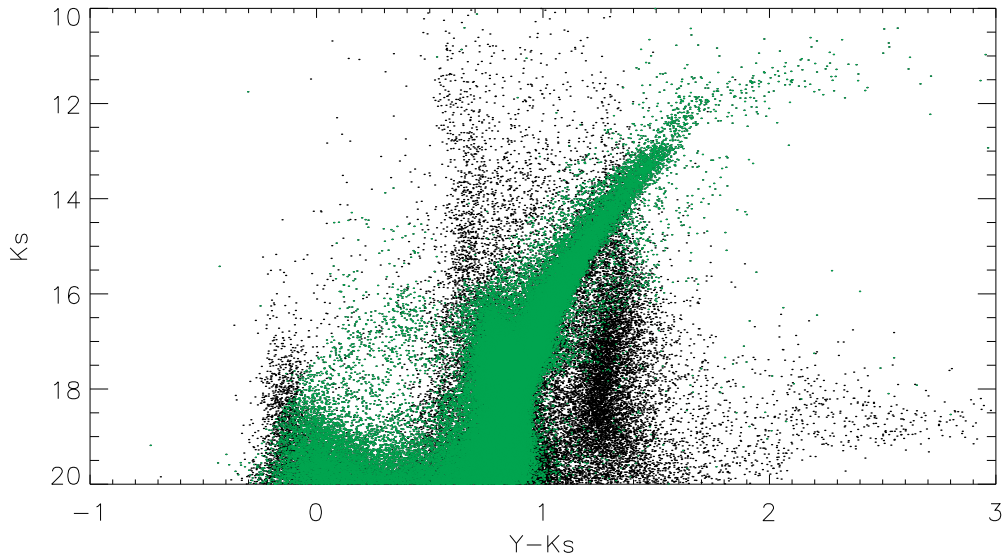

Figure 4.17: CMD, $(Y - K_s)$ vs K_s of the SMC tile 3_3 (green) using the Bridge tiles (black) 2_3 as the Galactic foreground region using the statistical method, from the VMC catalogues.

It can be seen from Fig. 4.17 that the population of potential remnant foreground objects is no longer present in the cleaned SMC population. The younger population to the left of the CMDs varies between the Bridge and SMC however, this can be explained as the younger population is most prominent in tile 2_3 which is the tile closest to the SMC with the highest density of gas and younger Bridge stars that formed in-situ. From Fig. 4.13 it can be seen that the younger population described in the SCM tile here fits very well with the Magellanic object isochrones and is completely absent from any of the foreground regions giving confidence that these objects are Magellanic. The same argument can be applied to the middle aged Magellanic populations which follow the stellar tracks from the younger objects and as such are likely to be related to the younger Magellanic population. By using the Bridge to remove the SMC foreground it appears that the foreground is very similar in the direction of Bridge and SMC but perhaps not in the direction of the Stream tile even though the tile 2_1 lies above the SMC, however with a different Galactic latitude.

From the work above it is clear that there is some difficulty in removing the entire foreground population from the direction of the Magellanic Clouds. It appears that the remaining contaminants, due to their $(J - K_{\rm s})$ colours, belong to a population of K and M dwarfs from the work by Bessell and Brett (1988). The effect of the anomaly in the Galactic foreground is also observed when applying the probability removal method and also both removal methods using the UKIDSS foreground field which is across the Galactic plane. The difference in the foreground and SMC or Bridge region of the redder objects could possibly be due to reddening or metallicity differences between the Bridge and foreground, or an uneven distribution of Galactic dwarfs across Galactic latitudes. The Galactic population is made up of objects from different parts of the MW (disc and halo) in the direction of the Magellanic Clouds, with different distances, that could also have an effect on the foreground removal. The Stream tile used in the foreground removal is at a higher Galactic latitude than the Bridge and SMC and will likely

have a different proportion of objects from the MW disc and halo.

The reddening in each band was checked using work by Schlegel et al. (1998) and the greatest difference in $E(J-K) = 0.014$ across the Bridge tiles, which is consistent with work above stating that the reddening effects across the Bridge do not vary enough to be of concern. Also the greatest difference in $E(J-K) = 0.026$ between the Bridge tiles and the foreground region 2_1 which is well within the value of tolerances that are included in the removal.

In order to investigate the density of the population of Galactic dwarfs that may be effecting the foreground removal, UKIDSS was used to study variations in numbers of these objects in Galactic latitude due to the broad coverage of the LAS. Data were downloaded from the publicly available UKIDSS LAS DR9 between 30° and 60° in Galactic latitude. The number of objects in the region of the $(J-K_{\rm s})$ CMD remaining after cleaning were normalised to the total number of objects in Galactic latitude strips to look for a variation in the Galactic dwarf objects. Fig. 4.18 shows that the normalised number of objects in the region of remaining contamination containing Galactic dwarfs, between 30° and 60° is periodic in nature. Calculations of the standard deviation of the normalised number of objects in each latitude slice indicate that all of the values are within a Gaussian distribution.

After the analysis of UKIDSS, it can be concluded that the number of Galactic dwarfs do not vary greatly across Galactic latitudes (between 30° and 60°) indicating that this effect would not be the cause of the remaining redder foreground population after removal. It appears that the issues in the removal of Galactic foreground for redder colours perhaps has a contribution due to metallicity. An investigation into the metallicity of different foreground and Magellanic objects is beyond the time available for this project.

Aside from the isolated population of Galactic objects remaining in the cleaned samples above, the removal method works well for other regions of CMD space (This is investigated further in Chapter 6). The periodic variation in numbers of

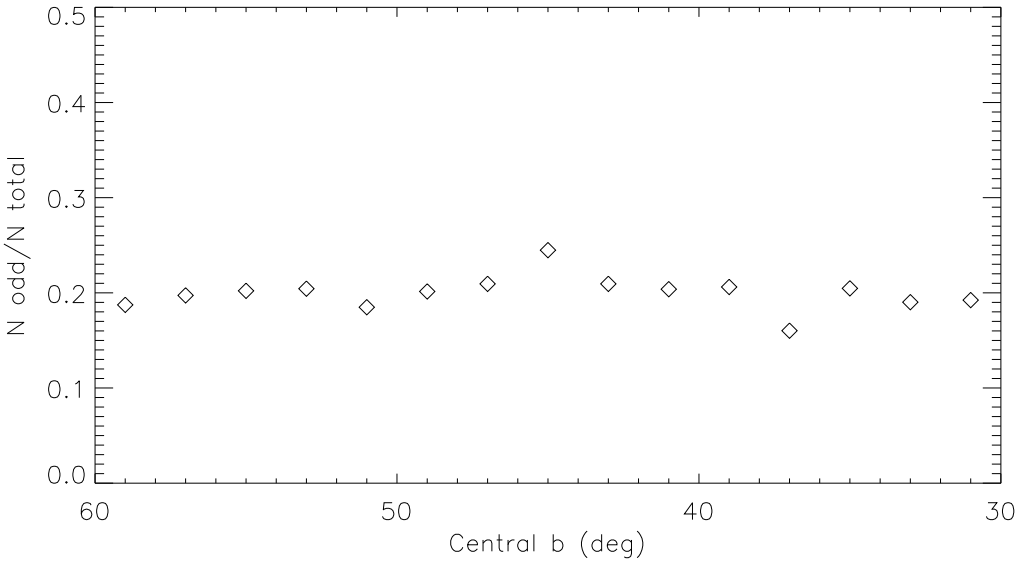

Figure 4.18: Number of objects from UKIDSS in the remaining red region of Galactic contamination, as a fraction of the total number of objects in slices of Galactic latitude vs the central Galactic latitude of each slice.

objects across Galactic latitude from Fig. 4.18 is $\sim 9\%$ from the maximum to minimum values, indicating that there could be some remaining contamination in other regions of the CMD within this range, although the effect appears to be much less at the bluer colours. The results from this removal will be carried forward for analysis in terms of the younger and related intermediate populations of the Magellanic Bridge, which are recovered with the statistical removal and fit well to the stellar tracks. A cut was made at $(J - K_{\rm s}) = 0.65$ and remaining objects with colours redder than this are discarded for now due to the lack of confidence that they are Magellanic objects. A $(J - K_{\rm s})$ colour of 0.65 and larger corresponds to Galactic dwarf populations of K and M dwarfs which make up the remaining contaminants in the cleaned Bridge sample. Objects with $(J - K_{\rm s})$ colours less than this value will be kept for analysis in the direction of the VMC Bridge tiles.

Figures 4.19 - 4.21 show the populations within the Magellanic Bridge tiles that are true Bridge candidates that will be analysed in Chapter 6.

The statistical removal applied here could also be applied to the Bridge and

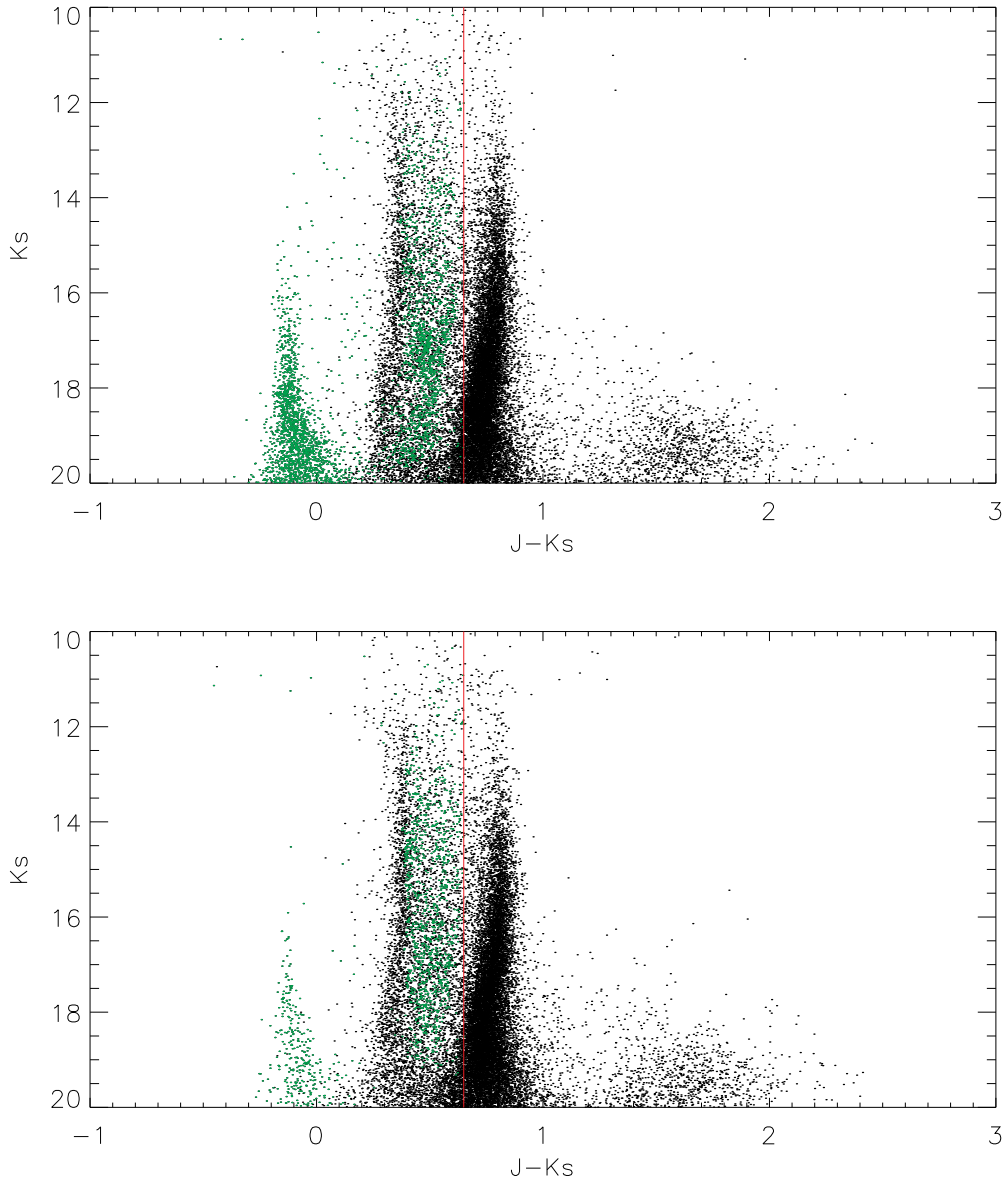

Figure 4.19: CMD, $(J - K_s)$ vs K_s of the Bridge tiles (from top to bottom) 2_3, 2_4 after the removal of the Galactic foreground population (black) using the statistical method isolating just the remaining Bridge populations (green), from the VMC catalogues with the VMC Stream tile 2_1 representing the foreground in the direction of the Magellanic Clouds.

Stream regions using a foreground field from a different source with the same depth as the VMC observations but at a location more like the opposite fields used in the large scale surveys. In future work, a foreground region should be applied from one of the other VISTA surveys which would have a depth comparable to the VMC survey opposed to the shallower UKIDSS field. Future work will also

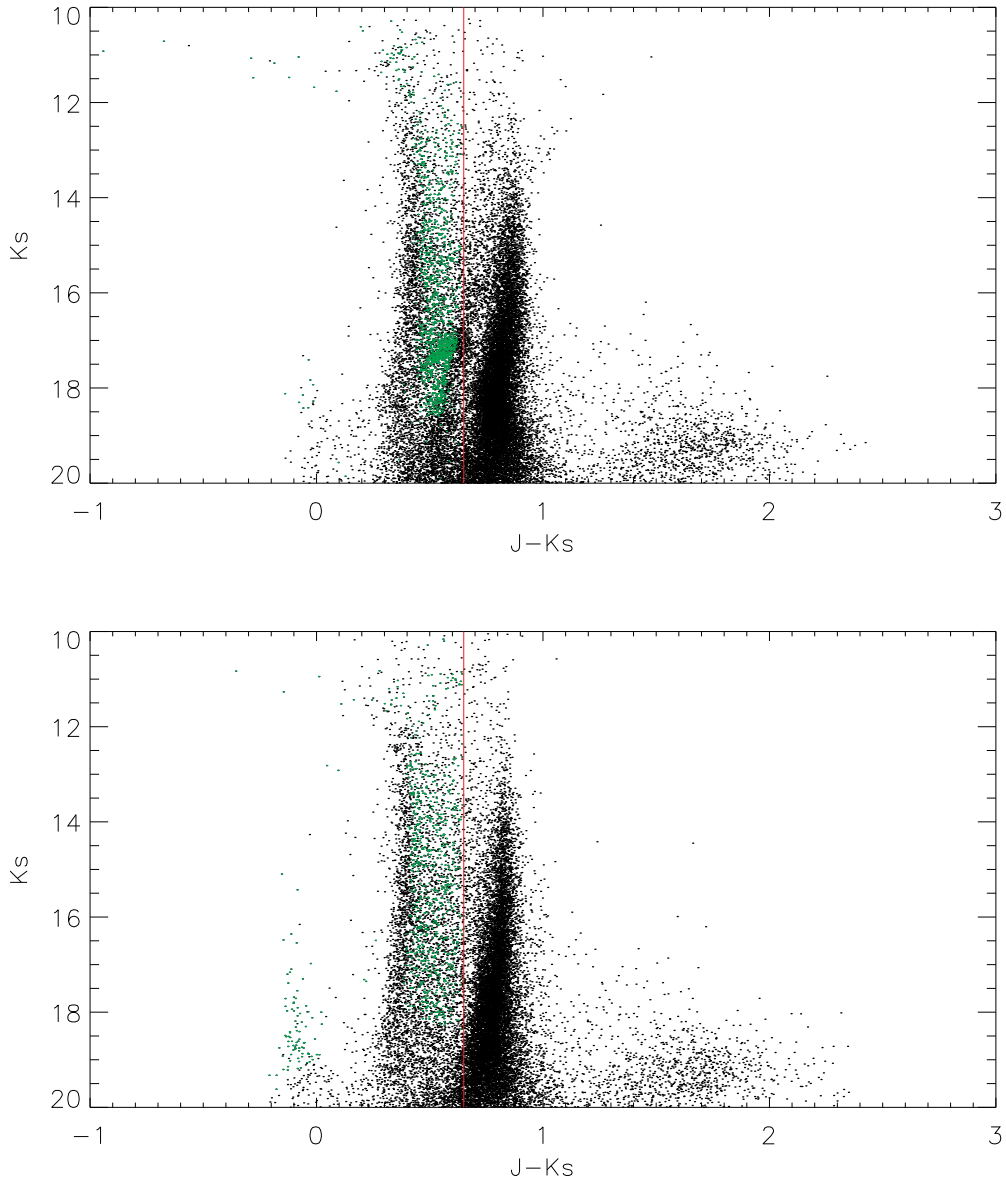

Figure 4.20: CMD, $(J - K_s)$ vs K_s of the Bridge tiles (from top to bottom) 2_8, and 3_5, after the removal of the Galactic foreground population (black) using the statistical method isolating just the remaining Bridge populations (green), from the VMC catalogues with the VMC Stream tile 2_1 representing the foreground population in the direction of the Magellanic Clouds.

require the creation and application of a method to remove the entire foreground population in the direction of the Magellanic Clouds to reveal the entire extent of the remaining populations.

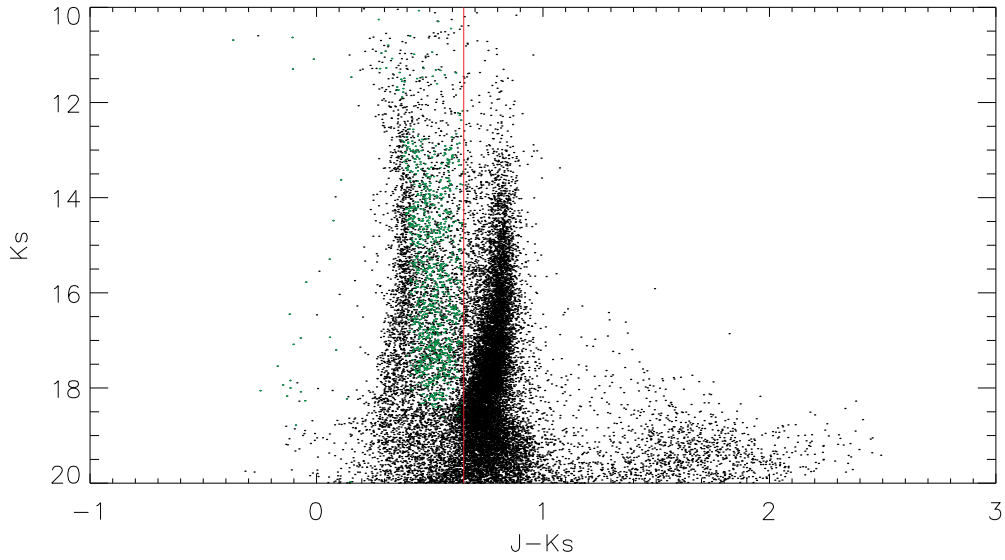

Figure 4.21: CMD, $(J - K_s)$ vs K_s of the Bridge tile 3_7, after the removal of the Galactic foreground population (black) using the statistical method isolating just the remaining Bridge populations (green), from the VMC catalogues with the VMC Stream tile 2_1 representing the foreground population in the direction of the Magellanic Clouds.

4.4 Using population synthesis

Most of the work here uses catalogues created from large area surveys in which an offset field could be chosen to represent a purely Galactic population and were used to verify empirical colour selection criteria. Offset fields can also be used for a statistical removal of foreground stars. As the VMC observations only cover specific tiles across the Magellanic Clouds and do not include an offset region, this work explores another method of Galactic foreground removal, using the TRILEGAL population synthesis model (V1.6) from Girardi et al. (2005) [9].

TRILEGAL simulates the number of Galactic stars in a given target field with a specified area by splitting the Galactic populations into the bulge, thick disk, thin disk and halo components and models each of these separately. The aim of the work with TRILEGAL is to be able to simulate star counts in a number of different passbands (Girardi et al., 2002) for deep and shallow photometry. Stars are created adopting random age, mass and metallicity, drawn from distributions

[9] http://stev.oapd.inaf.it/cgi-bin/trilegal

representing the star formation rate (SFR), age metallicity relation (AMR) and initial mass function (IMF) of each object. Stellar parameters and absolute photometry are then derived from grids of isochrones and is converted to apparent magnitudes via bolometric corrections, distance modulus and extinction.

The work here aims at verifying TRILEGAL's representation of Galactic populations by comparing the TRILEGAL output in terms of stellar number densities to those of current observations such as 2MASS and UKIDSS due to their large sky coverage. Comparison regions were chosen to represent purely a Galactic population with as little contamination as possible from other objects and background galaxies. The regions of interest were taken at the symmetrical position across the Galactic plane to the Magellanic Clouds to represent as similar region as possible using the same galactic longitude (l) but at opposite galactic latitude (-b).

Target areas were then chosen and the stellar number densities in these regions were compared for the observations and the model output. Due to TRILEGAL being a model creating a synthetic population it can overestimate or underestimate the number of objects in any given field with respect to the observations as they include errors and incompleteness. However, the main issues addressed initially are the fact that TRILEGAL does not model background galaxies, which are found in large numbers for NIR surveys such as 2MASS, UKIDSS and VMC, and that TRILEGAL does not represent well the CMD space of a region as seen in Fig. 4.22 even though it accurately represents the number count within a chosen region (in this case the ratio excludes background galaxies red of the bold line chosen at $J - K = 1.0$ to remove background objects from observations). This is an illustration of the problem encountered after TRILEGAL has been run for selected 2MASS and UKIDSS fields in l and b.

4.4.1 Exploring the accuracy of TRILEGAL

In order to assess how well the TRILEGAL code represents the Galactic population, regions were identified in the NIR CMD that contain a purely Galactic

population, and were measured to assess how well TRILEGAL represents these populations. For this work a number of small spatial regions of 10 deg^2 were chosen at various longitude values at the same Galactic latitude as the Clouds, and the opposite position across the Galactic plane (292° and +39°). The b values were also varied within a small range to assess whether there was a change in accuracy along Galactic latitude.

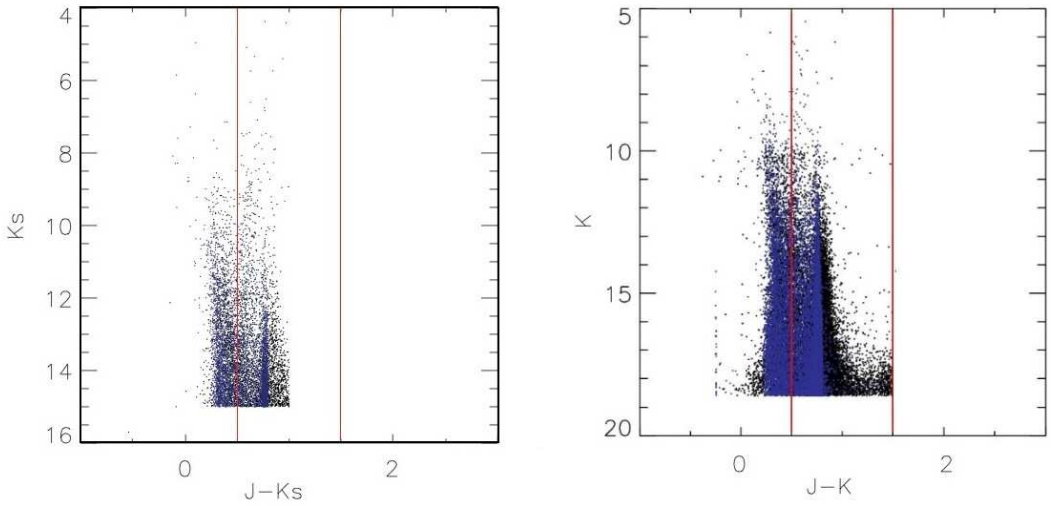

Figure 4.22: Near-IR CMD of TRILEGAL (blue) and observations (black) for 2MASS (left) and UKIDSS (right) showing the separation in foreground sequences ($J - K = 0.5$) and background ($J - K = 1.0$) objects (red lines).

These regions were downloaded from the public catalogues of 2MASS and UKIDSS, and were filtered using flags as described in Chapter 3. The TRILEGAL 1.6 web-interface was used to retrieve the same synthetic data for comparison. The co-ordinates of the region of interest were entered into the TRILEGAL web interface with the area required equivalent to the observational data. The photometric system required was chosen, with the required limiting magnitude of the wavebands used to be consistent with observations. The IMF used is the Chabrier lognormal Chabrier (2001) with binary fraction of 0.3, and default values of extinction, solar position, thick disc, thin disc, halo and bulge components (Girardi et al., 2005).

Colours were calculated from the TRILEGAL output magnitudes and CMDs were

created to compare the observational data with TRILEGAL simulations. For 2MASS and UKIDSS, CMDs were created in $J-K$ vs K, which were sub-divided to isolate the Galactic dwarf (A) and giant (B) populations at $J-K=0.5$, along with the background for observations (C) at $J-K=1.0$ (Fig. 4.22). In order to test the variation of objects from TRILEGAL compared to observations, the ratio of the number of objects in TRILEGAL and observations was calculated ($\frac{N_{tri}}{N_{obs}}$) for regions A and B and plotted as a function of Galactic longitude and latitude. The variation of TRILEGAL objects across the Galaxy followed a normal distribution, confirming that TRILEGAL well represents the Galactic population. These regions were then binned in colour and brightness with bins of 0.1 and 0.5 mag respectively to compare the ratio of objects per bin in CMD space.

It appeared that the TRILEGAL population synthesis well represented the population on the left side of the 2MASS and UKIDSS CMD in terms of both numbers and positions, however the redder objects of the Galactic foreground population were represented well in terms of numbers, but they were not in terms of colours. It appears that the TRILEGAL representation of redder objects does not allow for enough of a spread in colour to accurately represent these populations. The photometric errors from the observations do not account for the large difference in colour spread of TRILEGAL opposed to the observations at a $J-K$ colour of ~ 0.8. This is especially concerning for the work in this thesis on removing Galactic foreground objects as all of the removal methods make use of colours of objects in a foreground population. It is interesting that the region of the CMD that TRILEGAL does not well represent the observations, is the same region that causes problems when removing the Galactic foreground from the VMC catalogue. From the above analysis, the decision was made not to proceed with TRILEGAL as a method of removing Galactic foreground objects. The primary reason is that although TRILEGAL represents the number of objects in a Galactic field well, the colours of objects reproduced by TRILEGAL are not accurate enough to carry out a foreground removal that is based heavily on colours of objects in

the Galaxy in comparison to Magellanic objects. The observational methods of removing the Galactic foreground described above are satisfactory for this work as the removal from most catalogues includes a foreground region from the catalogue itself, and even in the case of the VMC catalogue, at the start of the investigation into TRILEGAL, there was not sufficient UKIDSS data publicly available to use as foreground for the VMC catalogue however, since the start of this work this is no longer the case. As such it was felt that the observational data available provides a more accurate removal process. It should also be noted that work is being carried out to increase the accuracy of TRILEGAL in terms of reproducing stellar colours and that this may be an accurate tool in removing Galactic foreground from any catalogue, in any direction in the future.

It is possible that the same redder Galactic foreground objects are affecting the accuracy of all methods of removing the Galactic foreground in this work. A thorough investigation should take place to discover a way to remove the excess Galactic K and M dwarfs from a clean Magellanic sample. This will be a very interesting project in the future as without removing the entire foreground population accurately (without over-compensation) the full extent of the lower density Magellanic regions will not be known.

4.5 Summary

A number of different processes have been carried out in order to remove Galactic foreground objects in the direction of the Magellanic Bridge and Stream. These different methods, applied to different catalogues are a crucial part of the process of analysing the Magellanic Bridge and Stream populations due to their low stellar densities. It is important to perform thorough foreground removal towards these regions to gain some confidence that the remaining candidate objects truly belong to the Magellanic Clouds System. There is a consistency between the results in all three foreground removal methods. Although there are more objects recovered

from the statistical cleaning, followed by the probability method and colour-cut method this is due to the robustness of each method which are proportional to the objects recovered after the removal is applied.

The work done on the removal from the 2MASS catalogue in the direction of the Magellanic Bridge proves successful as it recovers brighter objects within the Bridge. The removal process appears to become more difficult at fainter magnitudes due to the population of Galactic K and M dwarfs which are harder to remove from the Magellanic populations. It may not be a coincidence that the same objects cause a problem when applying the TRILEGAL population synthesis as a method of removal. These Galactic K and M dwarfs vary periodically across Galactic latitude which makes them somewhat difficult to model within the accuracy required when looking at such low density regions such as the Stream. It also seems that the Stream tiles do not follow the same trend in terms of the redder objects at fainter magnitudes with more objects at less red colours and less objects at the redder end of the VMC CMDs. More work needs to be done on the topic of these foreground objects so that it becomes possible to utilise the full extent of the VMC Magellanic populations especially in regions like the Bridge and Stream which are dominated by Galactic foreground. It may be possible to use other removal methods such as spectroscopic observations, or proper motions to separate Magellanic Cloud objects from Galactic foreground objects in the redder region of the $(J - K_{\rm s})$ vs $K_{\rm s}$ CMD which can be studied using the public VMC survey data.

Table. 4.4 summarises the objects remaining from each catalogue in the direction of the Bridge and Stream which will be analysed in the following Chapters.

The remaining candidate Magellanic Bridge and Stream objects in Table. 4.4 will be analysed in terms of stellar populations and densities using various tools such as CMDs, isochrones and density maps in an attempt to characterise these new populations presented here.

Table 4.4: Magellanic candidates after foreground removal

Catalogue and region	Foreground method applied	Sources remaining
VMC Stream 1_1	UKIDSS opposite probability	365
2MASS-DENIS Bridge	2MASS-DENIS local colour-cuts	365
SuperCOSMOS Bridge	SuperCOSMOS local colour-cuts	267
2MASS Bridge	2MASS opposite colour-cuts	2499
VMC Bridge 2_3	VMC 2_1 probability	1963
VMC Bridge 2_4	VMC 2_1 probability	2780
VMC Bridge 2_8	VMC 2_1 probability	6666
VMC Bridge 3_5	VMC 2_1 probability	4554
VMC Bridge 3_7	VMC 2_1 probability	3177
VMC Bridge 2_3	UKIDSS opposite probability	2448
VMC Bridge 2_4	UKIDSS opposite probability	2479
VMC Bridge 2_8	UKIDSS opposite probability	3402
VMC Bridge 3_5	UKIDSS opposite probability	2914
VMC Bridge 3_7	UKIDSS opposite probability	2337
VMC Bridge 2_3	VMC 2_1 statistical final	3436
VMC Bridge 2_4	VMC 2_1 statistical final	1530
VMC Bridge 2_8	VMC 2_1 statistical final	1332
VMC Bridge 3_5	VMC 2_1 statistical final	943
VMC Bridge 3_7	VMC 2_1 statistical final	1084

Chapter 5

A study into the Magellanic Bridge from public surveys

This chapter gives a comprehensive overview of the Magellanic Bridge in terms of stellar densities and populations from public catalogues prior to the availability of VMC catalogues in the direction of the Bridge. The types of objects expected from observations of the Bridge are described in Chapter 2, ranging from young blue objects, to an older population of red giants. The catalogues of 2MASS, 2MASS-DENIS, SuperCOSMOS and WISE data were created as described in Chapter 3, with foreground removal methods applied as in Chapter 4. This chapter uses various techniques to explore the known younger population in the Bridge, the possible existence of an older Bridge population and the density and distributions of the stellar Bridge populations, as well as the extension of the Magellanic Bridge.

5.1 Stellar densities within the Magellanic Bridge

In order to investigate the density of the stellar population within the central Bridge ($30 - 60$ deg in RA, to avoid too large LMC and SMC contamination), stellar density maps were created from the catalogues of 2MASS and SuperCOSMOS prior to the removal of a Galactic foreground population (Fig. 5.1) to look into different stellar densities. Since a mostly structureless, smooth spatial dis-

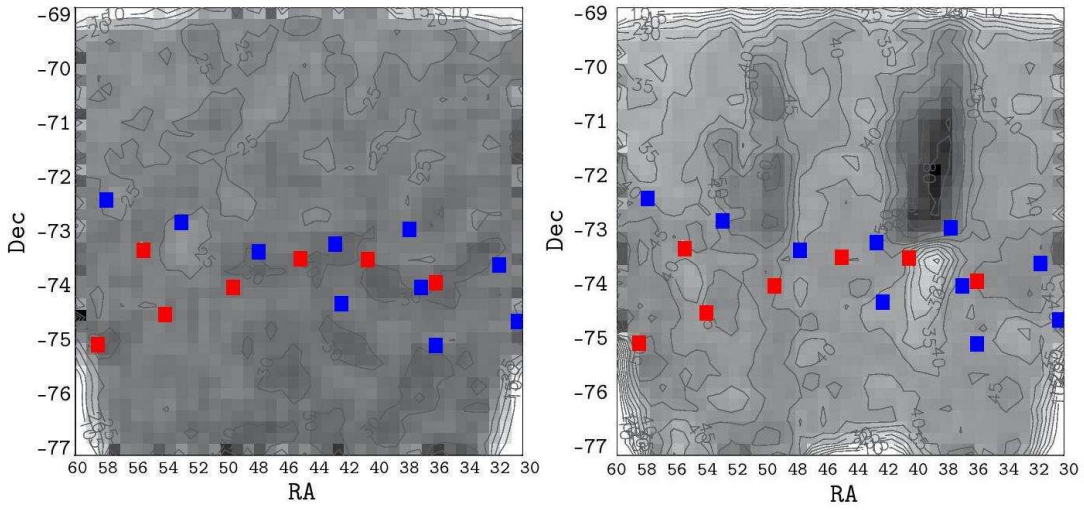

Figure 5.1: Stellar density maps of the Magellanic Bridge from the 2MASS (left) and SuperCOSMOS (right) catalogues, with bin size of 0.2×0.2 deg^2. The rectangles represent the centres (not to scale) of VMC observation tiles (1.5×1 deg^2), red) (Cioni et al., 2011), and fields observed by Harris (2007) ($36' \times 36'$, blue). North is at the top and east is to the right with the LMC to the outer left and SMC to outer the right. The region of interest here is approximately 14 kpc across.

tribution of foreground stars and background galaxies can be expected across the Magellanic Clouds, any structure found should reflect the Bridge population.

The positions of the stars in the 2MASS and SuperCOSMOS catalogues were converted into cartesians, and then binned, with smoothed number density maps created with bin size dependent on the total number of stars present. Bins were optimised at $\Delta\alpha = \Delta\delta = 0.2$ as this was the bin size that produced the clearest contours on the density maps with an average of 8 and 41 objects in each bin for the 2MASS and SuperCOSMOS catalogues respectively.

Regions previously observed by other authors were placed (not to scale) on top of the maps. The most significant observations in this region were those by Harris (2007) observing tiles of $36' \times 36'$ in regions across the Bridge (see Fig. 5.1). The position of the VMC tiles ($\sim 1.5 \times 1$ deg^2) is also indicated on the maps (not to scale) to give an idea of the range that VMC covers in comparison to previous observations. The exact location of the VMC tiles were decided according to the results from this section, with tiles placed at higher declinations than initially planned with the expectation to observe different stellar populations outside of

the main HI ridge.

It can be seen from the 2MASS density map of the Bridge (Fig. 5.1), that the stellar distribution is not even. The Harris tiles follow the HI ridge line within the Bridge and the stellar populations are distributed along it, but also in other regions. The SuperCOSMOS map (Fig. 5.1) shows an apparent increase in star numbers in the northern part of the Bridge just outside the regions observed by Harris. One would expect to find a greater number of young blue objects in the SuperCOSMOS catalogue compared to the redder objects in the 2MASS catalogues. Therefore the greater number of objects in the northern part of the Bridge in SuperCOSMOS opposed to 2MASS indicates the possibility of a denser younger population in the north of the Bridge. It also appears from the 2MASS density map that the number of objects increases towards the south, this could indicate a possible difference in young and older populations from the north to the south. The steep drops near the limits of the figures are artificial due to a lack of data.

In order to confirm that the observed stellar density fluctuations in the Bridge are truly a feature of the Bridge and not from the Galactic foreground population a study into the Galactic foreground was carried out. As described in Chapter 4, the foreground removal was carried out using an opposite foreground region in 2MASS and SuperCOSMOS, with the application of the colour-cut removal procedure. Density maps were then recreated in these catalogues without contamination of Galactic foreground objects. Density maps were also created of the foreground regions to determine whether these fields are uniform.

It can be seen from the stellar density maps of the foreground field for 2MASS and SuperCOSMOS (Fig. 5.2) that in each case, with the same binning as the Bridge regions, the stellar density across the foreground region is not entirely smooth. In the SuperCOSMOS map there is a visible gap due to the photographic plates used to obtain the photometry. It cannot be confirmed by eye whether some of the features seen within the Bridge, are true Bridge over densities. In

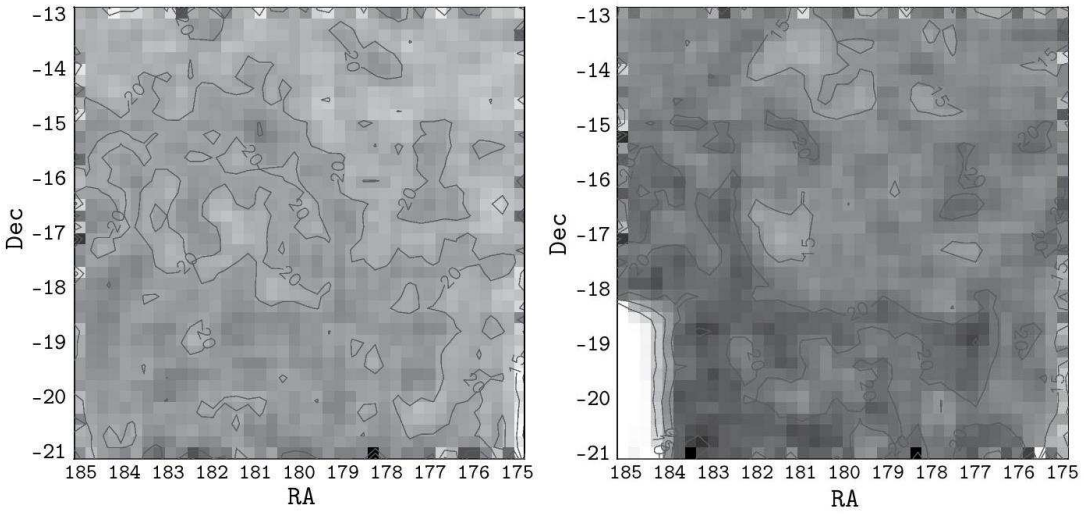

Figure 5.2: Stellar density maps of the Galactic foreground field from the 2MASS (left) and SuperCOSMOS (right) catalogues, with bin size of 0.2×0.2 deg^2. Contour levels are at: 10, 15 and 20 stars. North is at the top and east is to the right. The region of interest here is approximately 14 kpc across.

order to clarify whether true Bridge structure remains, a statistical removal of the Galactic foreground was applied as described in Chapter 4. The objects remaining in each catalogue after the probability foreground removal were then analysed to seek density fluctuations that are genuinely Bridge features and not an effect of the Galactic foreground population. Fig. 5.3 shows the stellar densities within the Bridge weighted by the probability of objects belonging to the Bridge. By multiplying the density maps with the probability of an object in a given bin belonging to the Bridge, the stellar densities after foreground removal can be seen. In the cases of 2MASS it appears as though the candidate Bridge population is smooth, but that the SuperCOSMOS catalogue shows density variations. Due to the less reliable SuperCOSMOS data, the two over-dense regions seen here cannot be confirmed yet as true Bridge features. The SuperCOSMOS data were taken from photographic plates and do not cover the entire Bridge region uniformly and have higher photometric errors than the other catalogues used here. A further study into the younger Bridge population is required to draw a firm conclusion.

Figure 5.4 shows the number of Bridge candidate stars (multiplied by their probability) from 2MASS and SuperCOSMOS, after the removal of Galactic fore-

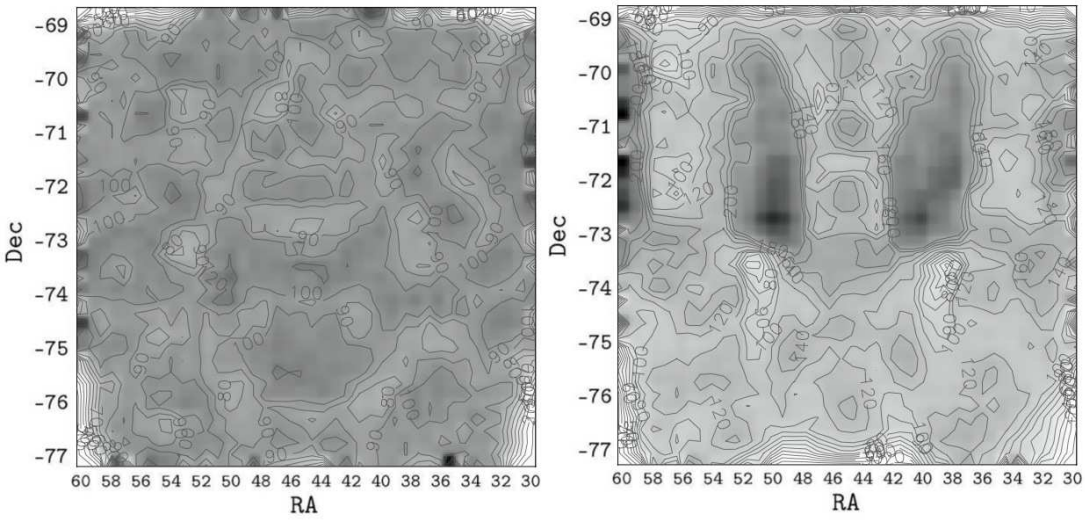

Figure 5.3: Stellar density maps of the Magellanic Bridge from the 2MASS (left) and SuperCOSMOS (right) catalogues after the statistical removal of the Galactic foreground multiplied by the probability of a star belonging to the Bridge, with bin size of 0.2×0.2 deg^2. North is at the top and east is to the right with the LMC to the outer left and SMC to the outer right. The region of interest here is approximately 14 kpc across.

ground objects, across bins of declination. It can be seen here that the number of objects are not constant across the declination range of the Bridge. The highest density of blue objects is not along the main concentration of HI gas around which Harris (2007) carried out his observations of Bridge objects. This work shows a peak in stellar density of blue objects in the northern part of the Bridge decreasing towards the south. Harris does however state that due to ram pressure from the Magellanic Clouds passing the MW, tidally stripped stars can be displaced from the main gas concentration, indicating that perhaps there has been movement in the position of the main concentration of HI gas.

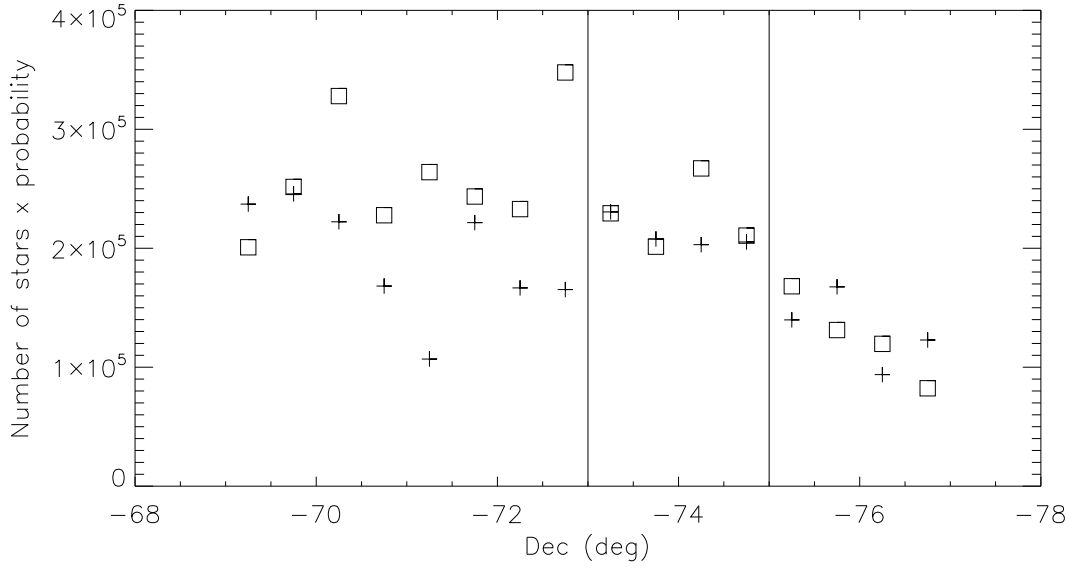

Figure 5.4: Number of stars in bins of declination for the central Magellanic Bridge ($\alpha = 30° - 60°$) in the SuperCOSMOS (crosses) and 2MASS catalogues (squares, scaled by a factor of 3) after the statistical removal of Galactic foreground objects. The Bridge is binned over all RA with a bin size of 0.5° in Dec. Vertical lines represent the range of declination of Harris (2007) observations. Error bars are included but are smaller than the symbols.

5.2 The younger population within the Magellanic Bridge

This section confirms and expands on the previously observed younger population within the Magellanic Bridge region. The SuperCOSMOS catalogue is used in this work as it is the only large scale public optical survey available in the direction of the Magellanic System. SuperCOSMOS has larger photometric errors than more recent surveys however, in this work SuperCOSMOS can make a contribution to our knowledge of the younger Bridge population. The remaining 274 objects in the SuperCOSMOS catalogue after the colour-cut removal of Galactic foreground (Chapter 4) were cross-matched with the SIMBAD database and were characterised in α and δ (Fig. 5.5). It can be seen here that the known LMC and SMC populations from the database are confined to each side of the Bridge in the SuperCOSMOS catalogue, with known blue Bridge objects spreading across

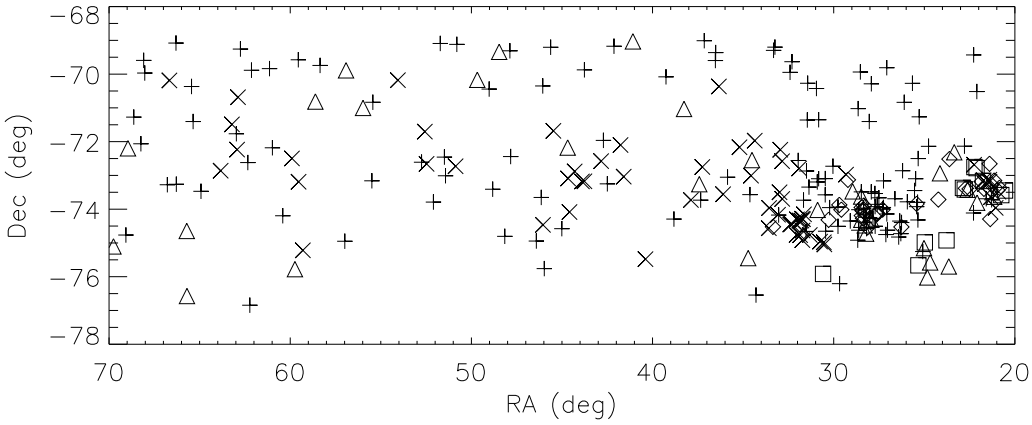

Figure 5.5: The spatial distribution of the different populations present within the Magellanic Bridge from the SuperCOSMOS blue catalogue after the removal of Galactic foreground and background galaxies. The different symbols represent: known SuperCOSMOS Bridge objects (crosses), known SMC sources (diamonds), known Magellanic Cloud halo sources (squares), other known sources (triangles) and new sources (pluses).

the entire region. Objects categorised as other, such as IR and X-ray sources are evenly distributed within the Bridge. The objects of interest here are the unknown objects, which in both 2MASS and SuperCOSMOS catalogues, make up the majority of the populations and are spread across the Bridge.

Figure 5.6 shows two CMDs comparing the population within a field of the Bridge (α = 2:00:00, $\delta = -75$:30:00) to an offset field (α = 3:26:00, $\delta = -59$:53:0) of the same size ($2^\circ \times 2^\circ$). The panel with the Bridge field also includes the remaining blue objects in the northern part of the Bridge in the SuperCOSMOS catalogue after the removal of galactic foreground for comparison, with isochrones (Girardi et al., 2000) over-plotted representing objects with SMC metallicity (Z = 0.004) at an average Cloud distance of 55 kpc for a range of ages. The isochrones were downloaded from the web interface CMD 2.5 input form with PARSEC v1.1, with a range of ages, for the required photometric system, with the Chabrier lognormal IMF, with extinction values for the Bridge region from Schlegel et al. (1998)[10]. The output magnitude values were then converted to a Magellanic Cloud distance via the distance modulus equation with colours calculated. It

[10]http://stev.oapd.inaf.it/cgi-bin/cmd

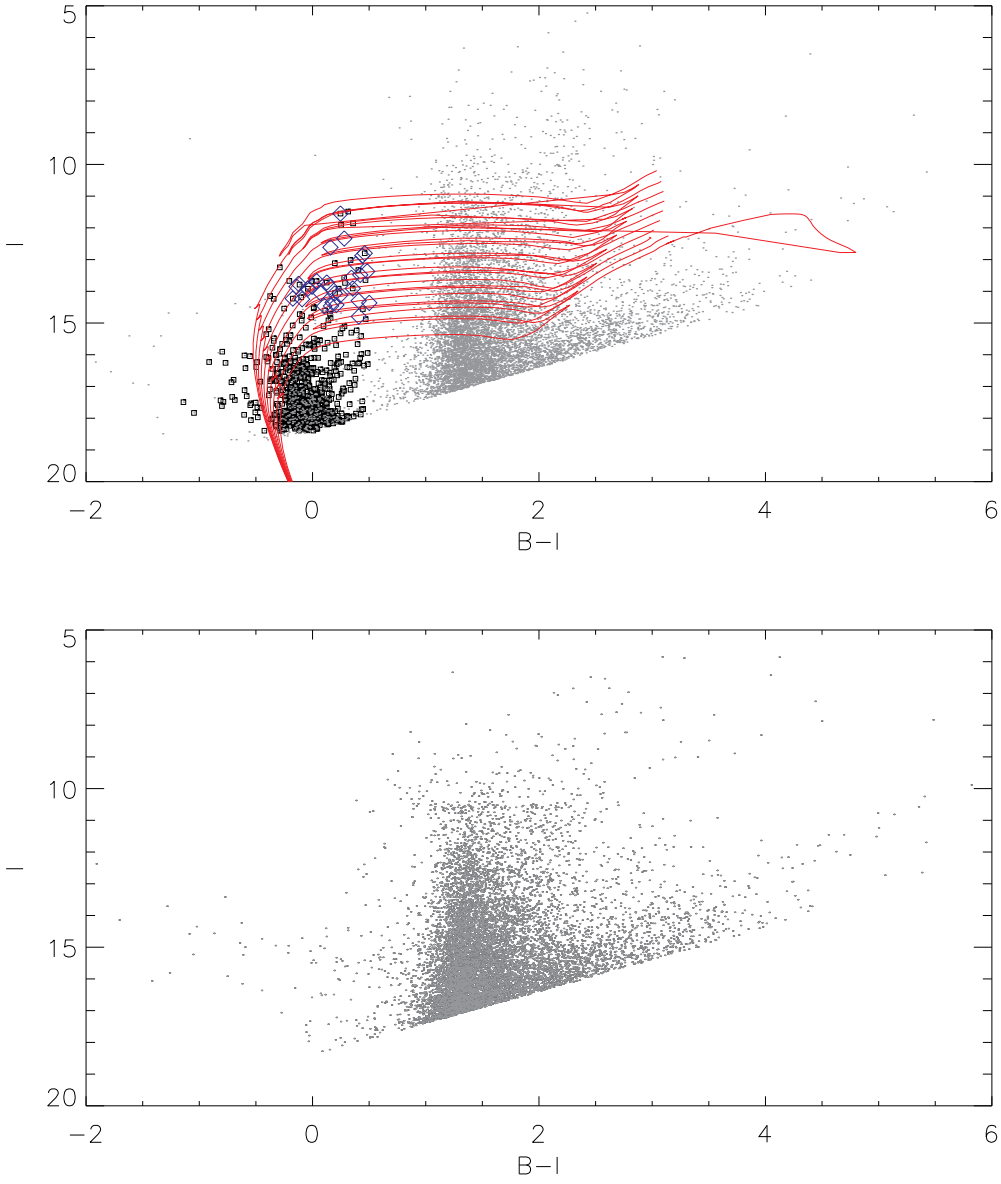

Figure 5.6: CMD, top is $(B-I)$ vs I of the blue objects of the Magellanic Bridge from SuperCOSMOS from one of the Bridge fields (α = 2:00:00, $\delta = -75$:30:00) chosen in Chapter 4 prior to the removal of the galactic foreground population. Also shown are known (squares), and unknown (diamonds) blue objects in the northern part of the Bridge which remained after the removal of galactic foreground objects. Overlaid onto these populations are Padova isochrones (red lines) for stars at the estimated distance of the Magellanic Bridge (55 kpc) with SMC metallicity (Z = 0.004) at a range of ages from log(age/yr) of 7.2 − 8.1 (top to bottom) with age steps of 0.1. Bottom is $(B-I)$ vs I of an offset field (α = 3:26:00, $\delta = -59$:53:0) chosen in Chapter 4 for comparison to the Bridge population.

can be seen from this figure that the remaining blue northern objects are truly plausible Bridge B stars and not a manifestation of the foreground population or background galaxies. The blue objects with known classification are all on their MS phase or beyond. This result confirms the methods used here to find a remaining blue Bridge population outside of the regions studied by Harris (2007) and Demers and Battinelli (1998) who concentrated their studies along the H ridge-line at the central Bridge declination.

Table 5.1 shows a breakdown of the objects as identified by SIMBAD within the Magellanic Bridge for the blue (SuperCOSMOS) objects after the colour-cut removal of Galactic foreground and background contamination. It should be noted that the objects identified as background Galaxies here were consequently removed from the final sample.

Table 5.1: Blue populations identified within the Magellanic Bridge from SIMBAD. [1] Irwin et al. (1990), [2] Cannon and Pickering (1918), [3] Hog et al. (1998), [4] Skrutskie et al. (2006), [5] Holmberg et al. (1974), [6] Abraham et al. (1995), [7] Westerlund and Glaspey (1971), [8] Demers and Irwin (1991).

Object	No. within SuperCOSMOS	Reference
Bridge star	63	[1]
SMC star	30	[1] [7]
LMC star	0	[1]
Magellanic Cloud object	11	[1] [8]
Background Galaxy	3	[4] [5]
Other known object	20	[2] [3] [6]
Unknown	129	

5.3 An older population in the Magellanic Bridge

5.3.1 Data

The aim of this work is to establish source catalogues in the region of the Magellanic Bridge to search for an older stellar component, prior to the analysis of

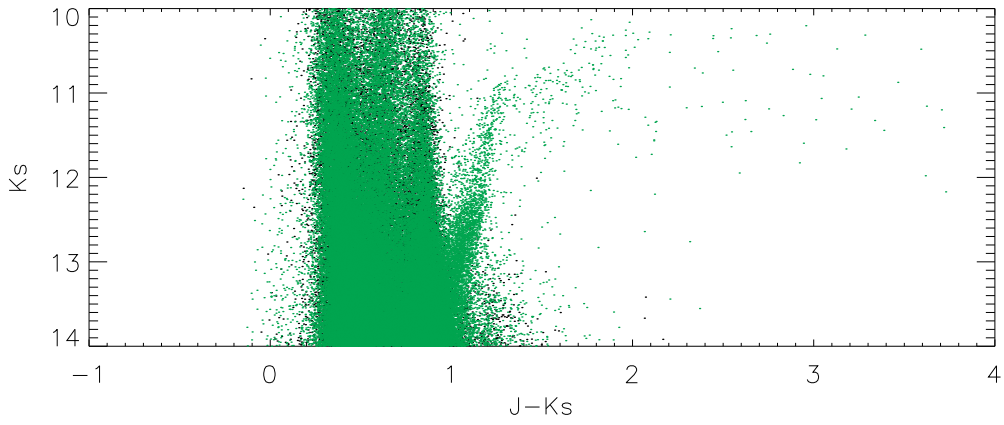

Figure 5.7: CMD, $(J - K_s)$ vs K_s of the Magellanic Bridge in 2MASS before the removal of Galactic foreground objects (black), and also the chosen Galactic foreground field (green) prior to the removal of foreground objects.

observations using the VISTA telescope (Emerson et al., 2004) as part of the VMC survey (Cioni et al., 2011). As such, the main source of data used in this work is NIR photometry from 2MASS. WISE data are also used for comparison. As described in Chapter 3, the Bridge area was chosen from previous definitions of the Bridge coverage by Kerr and de Vaucouleurs (1955), McGee and Newton (1981) and Harris (2007). This corresponds to an area between the LMC and SMC from 70° to 20° in right ascension (α) and from −69° to −77° in declination (δ).

5.3.2 Galactic foreground removal

The foreground removal for both 2MASS and WISE in this case uses the opposite foreground field for removal as described in Chapter 4 which is possible as both surveys cover the entire sky. The two approaches applied here to remove the Galactic contamination from the Bridge sample were the probability and colour-cut methods.

The CMDs chosen for the removal here were $(J - K_s)$ vs K_s in 2MASS, and the WISE removal was based on the shorter wavelengths $(W1 - W2)$ vs $W2$ as these bands are more likely to reveal a stellar population in the direction of the Bridge, and have magnitude limits comparable to 2MASS or slightly fainter. Bin

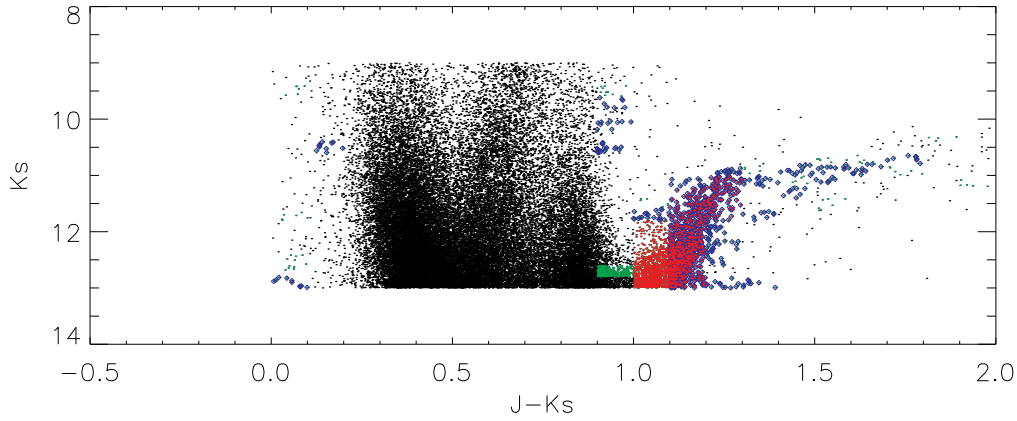

Figure 5.8: CMD, $(J - K_s)$ vs K_s of the Magellanic Bridge in 2MASS before the removal of Galactic foreground objects (black), and also after the application of the probability removal method, keeping only objects with probabilities of $0.75 - 0.85$ (green), $0.85 - 0.95$ (blue) and 0.95 and over (red).

sizes used in the removal and methods are described in Chapter 4.

2MASS

The probability method applied to the 2MASS catalogue confirms an over density of likely Bridge candidates, with 2515 Bridge objects remaining (Fig. 5.8) that are likely to belong to the Bridge given the position on the CMD (Sect. 3.1.2).

Figure 5.9 shows the two colour diagram $(H - K_s)$ vs $(J - H)$ with the application of a cut at $(J - H) > 0.78$ to remove the Galactic objects from the 2MASS Bridge catalogue. This colour selection criteria for 2MASS was applied to the Bridge catalogue and from this colour-cut removal, 2499 Bridge candidates remain.

WISE

The same methods of Galactic foreground removal were applied to the WISE catalogues as in 2MASS. As described in Chapter 4, there were no WISE Bridge candidate objects remaining after the removal of Galactic foreground contamination due to the absence of a separation between the foreground and Bridge objects in CMD space in the WISE catalogue (Fig. 5.11). A further study could be car-

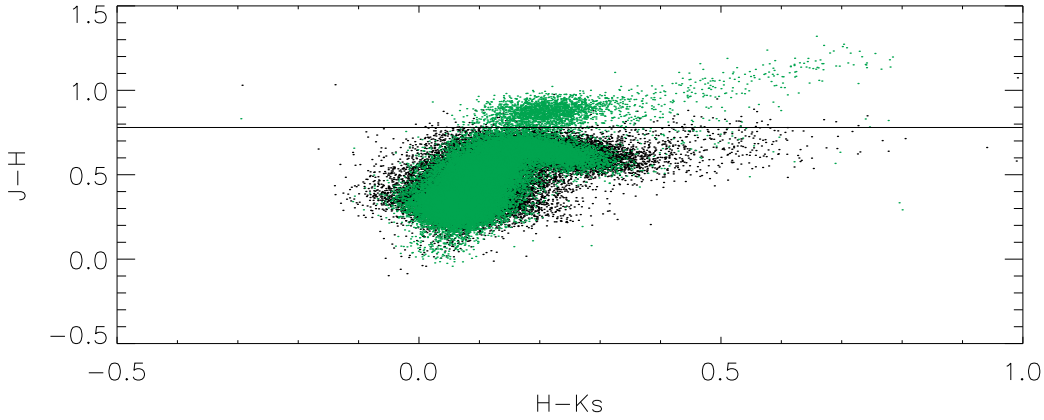

Figure 5.9: Two colour diagram, $(H - K_s)$ vs $(J - H)$ of the 2MASS Galactic foreground field (black) and the Magellanic Bridge (green), in order to apply a colour-cut method of removing the foreground objects. A line at $(J - H) > 0.78$ is shown to indicate the selection criteria that an object belongs to the Magellanic Bridge and not the Galactic foreground.

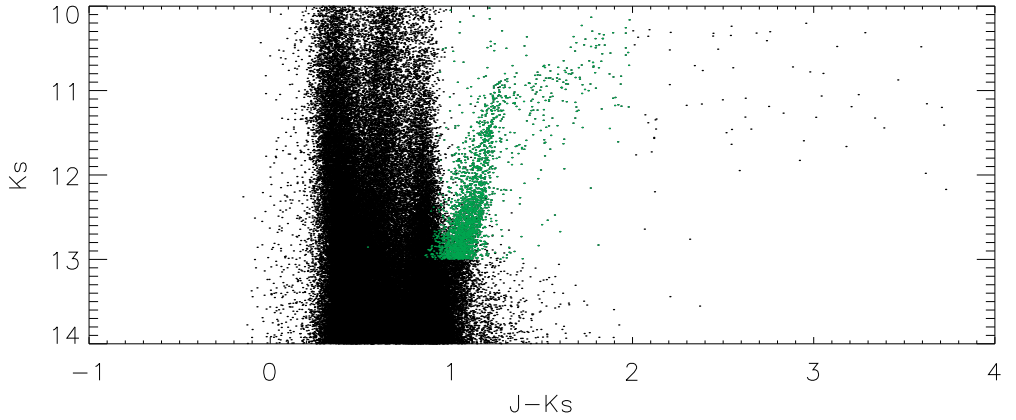

Figure 5.10: CMD, $(J - K_s)$ vs K_s of the Magellanic Bridge in 2MASS before the removal of Galactic foreground objects (black), and also after the application of the color-cut removal method (green).

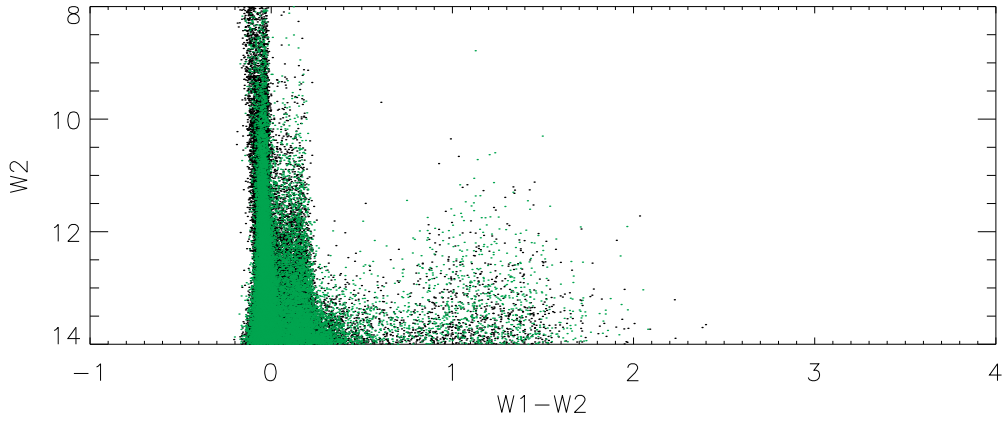

Figure 5.11: CMD, $(W1-W2)$ vs $W2$ of the Magellanic Bridge in WISE (black), and the Galactic foreground field (green).

ried out to try and separate a Bridge population from the Galactic objects in the future.

5.3.3 Older stellar populations within the Bridge

This work attempts to identify and characterise an older population within the Magellanic Bridge. The results are shown in the form of CMDs showing the different stellar populations making use of work by Nikolaev and Weinberg (2000).

2MASS

In order to characterise the stellar populations within the Bridge from 2MASS, a CMD was created in $(J-K_{\rm s})$ vs $K_{\rm s}$ with the application of boxes from Nikolaev and Weinberg (2000). These boxes were created to characterise the population of the LMC, and have been adapted here for the Magellanic Bridge using the distance modulus at an average Bridge distance of 55 kpc between the LMC (Walker, 2012) and SMC (Graczyk et al., 2012). The boxes were then overlaid onto the observed CMD of the Bridge.

There are twelve regions identified marked from A through L and several techniques were applied by Nikolaev and Weinberg to identify the populations in each region. The LMC populations were identified based on the NIR photometry

of known populations from the literature. The authors also performed a preliminary isochrone analysis, where they matched the features of the CMD with Girardi et al. (2000) isochrones, to derive the ages of populations and draw evolutionary connections among the CMD regions. The regions of the CMD present in an outer region of the LMC, and the Bridge population from the 2MASS catalogue prior to the Galactic foreground removal are presented in Fig. 5.12. The characterisation of the central Bridge population after the removal of Galactic foreground (Fig. 5.13), are primarily E, F, and J, with a small contribution from L and I. Even considering photometric uncertainties in magnitudes and colour, the stellar populations still fit well into the boxes characterising the different types of stars.

A summary of the types of stars found in the regions according to Nikolaev and Weinberg:

Region E covers the upper RGB and includes the tip of the RGB. The tip of the RGB is defined by the ignition of the degenerate helium burning core in old (low mass) stars, the helium flash (Renzini and Fusi Pecci, 1988). Stars, after ignition, evolve rapidly to the HB. Region F contains primarily oxygen-rich AGB stars of intermediate age that are the descendants of stars in region E. Some fraction of region F stars are long-period variables and reddened supergiants. Region J sources are primarily carbon rich thermally pulsing (TP)-AGB stars. These stars are descendants of oxygen-rich TP-AGBs in regions F and G. Region K contains extremely red objects identified as obscured AGB carbon-rich stars, as well as some dusty oxygen-rich AGB stars. Their large $(J - K_{\rm s})$ colours are due to dust in their circumstellar envelopes. The population in region I is younger, with an age of approximately 500 Myr. A significant contributor to the source density in this region are K- and M-type supergiants.

From the above population analysis, it can be seen that the youngest populations remaining within the Bridge after the removal of Galactic foreground are a very small number of K and M supergiants with an age of $\sim$ 500 Myr. There is

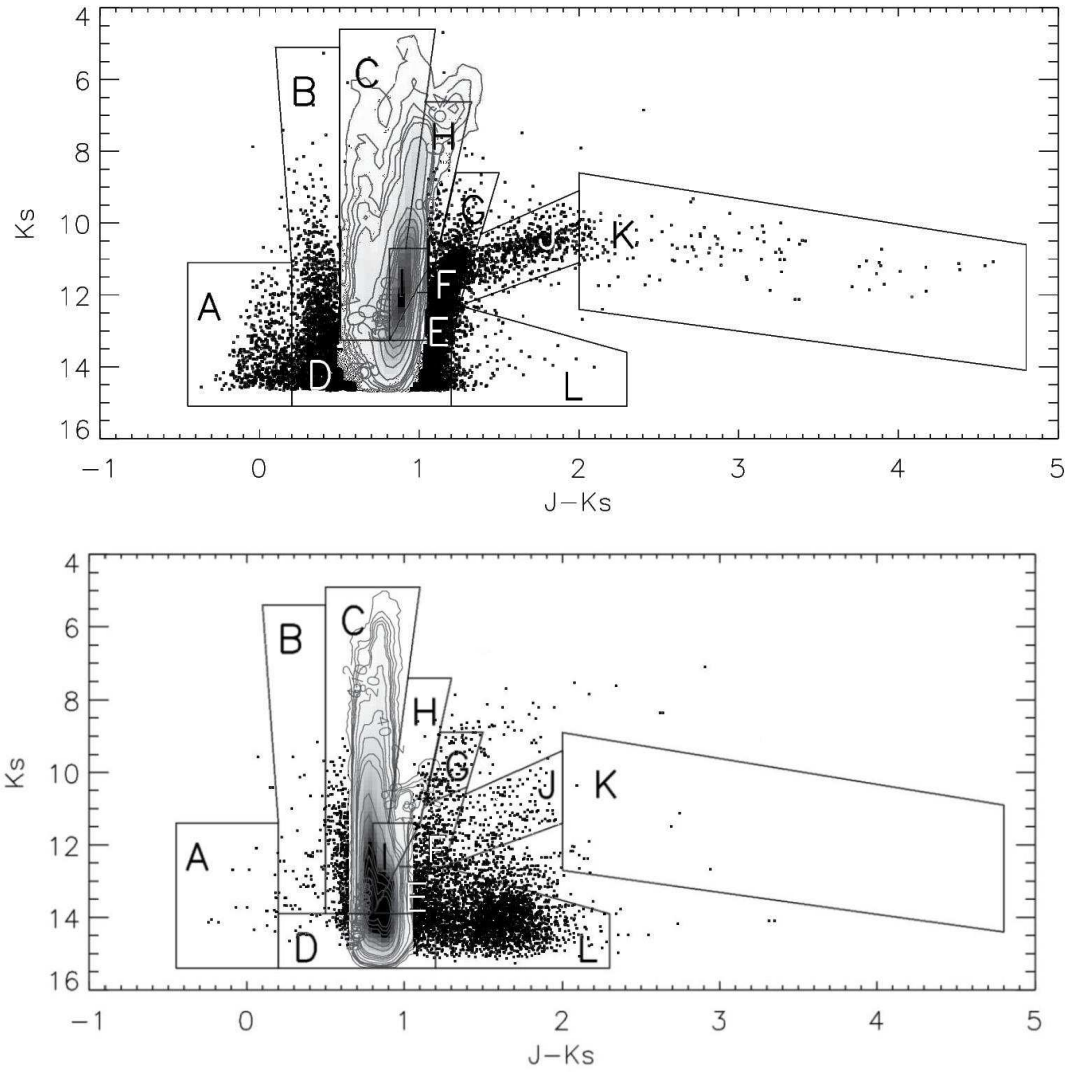

Figure 5.12: Hess diagram, $(J - K_s)$ vs K_s, of the LMC (top), and Magellanic Bridge (bottom) from the 2MASS catalogue. Boxes overlaid on the plot are taken from Nikolaev and Weinberg (2000) and foreground stars have not been removed from the catalogues. Here for the Bridge, the boxes have been shifted by 0.25 mag in K_s. Contour levels are at: 10, 20, 30, 40, 50 and 60 stars.

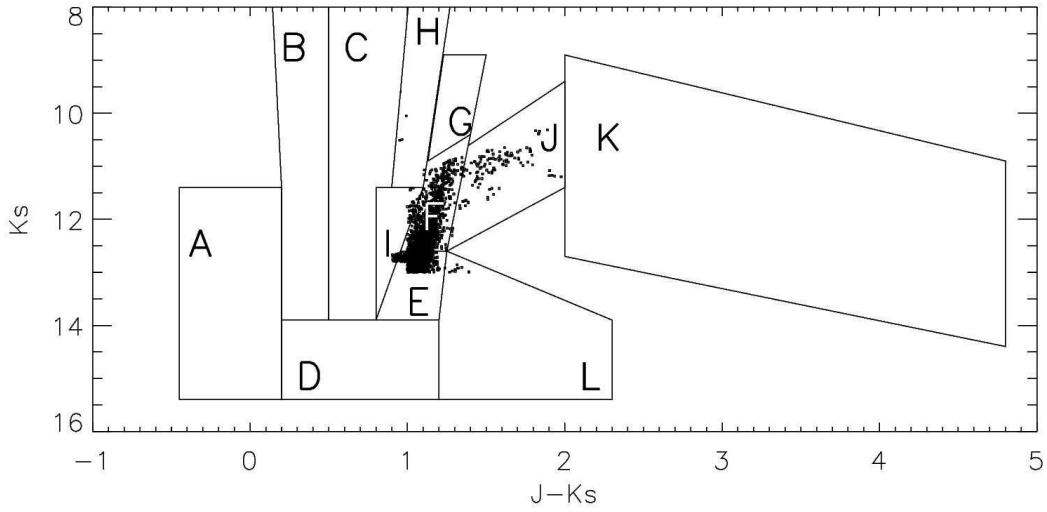

Figure 5.13: CMD, $(J - K_s)$ vs K_s of Bridge stars from 2MASS observations after the removal of Galactic foreground stars. The boxes overlaid on the plot are taken from Nikolaev and Weinberg (2000). The boxes have been shifted by 0.25 mag for the Bridge to account for the distance difference.

also a negligible contamination of brighter objects in box H which represents K- and M-type giants. These objects are still expected to be older than the assumed age of the Bridge implying that the red objects here are all older than the postulated Bridge age of ~ 200 Myr. The majority of Bridge candidates remaining fall into the boxes representing an old/intermediate population of RGB and AGB stars with ages of ~ 400 Myr and older.

SIMBAD objects within the Bridge

The remaining objects in the 2MASS catalogue after the colour-cut removal of Galactic foreground, were cross-matched to the SIMBAD database and were characterised in α and δ (Fig. 5.14). Objects here belong to the centre most 30° to 60° of the Bridge to remove contamination from the LMC and SMC to isolate a true inter-Cloud population.

It can be seen from the lower panel of Fig. 5.14 that the unknown, central Bridge candidate population is contained within boxes E, F and I representing an older Bridge population. Table 5.2 shows a breakdown of the objects as identified

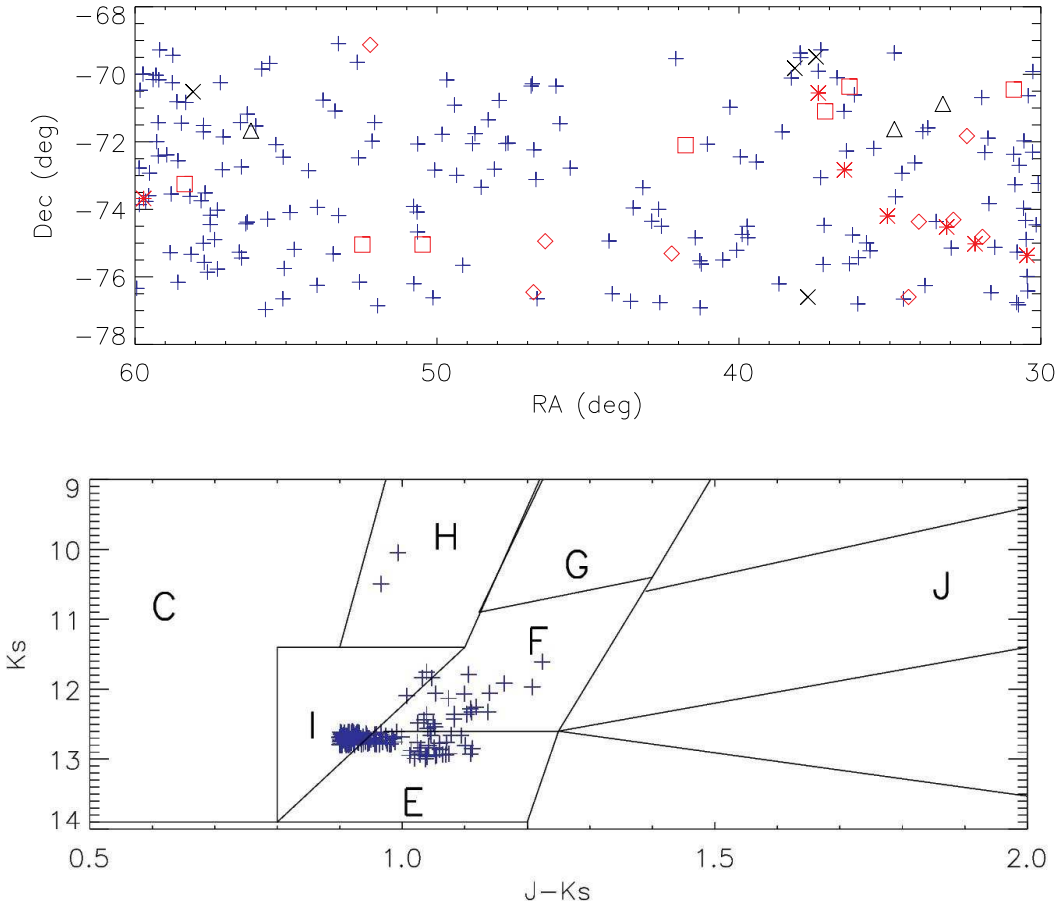

Figure 5.14: The spatial distribution (top) of the different populations present within the central Magellanic Bridge (30° to 60°) from the 2MASS catalogue after the removal of Galactic foreground. The different symbols represent: background galaxies (crosses), known SMC sources (red stars), known Bridge objects (red squares), known Magellanic Cloud halo sources (red diamonds), other known sources (triangles) and new previously unpublished sources (blue pluses) from SIMBAD. The $(J - K_s)$ vs (K_s) CMD of unpublished sources (blue pluses from top panel) is also presented (bottom), with boxes overlaid as in Fig. 5.12.

by SIMBAD within the central Magellanic Bridge after the removal of Galactic foreground and background contamination. It should be noted that the objects occupying region J from Fig. 5.13 are removed when focusing on the central Bridge, indicating that these dustier AGB stars are confined to the outer LMC and SMC regions. From the SIMBAD search, objects belonging to the SMC have been recovered, along with a small number of previously observed younger Bridge objects. A small number of objects remaining were background galaxies which have been removed from the final sample. The majority of objects have an unknown origin, and are strong candidates for an older Bridge population.

Table 5.2: Different populations identified within the Magellanic Bridge from SIMBAD. [1] Irwin et al. (1990), [2] Cannon and Pickering (1918), [3] Hog et al. (1998), [4] Skrutskie et al. (2006), [5] Holmberg et al. (1974), [6] Abraham et al. (1995), [7] Westerlund and Glaspey (1971), [8] Demers and Irwin (1991).

Object	No. within 2MASS Bridge catalogue	Reference
Bridge star	7	[1]
SMC star	7	[1] [7]
Magellanic Cloud object	9	[1] [8]
Background Galaxy	4	[4] [5]
Other known object	5	[2] [3] [6]
Unknown	202	

5.4 What is the extent of the Magellanic Bridge?

The density maps produced in Sect. 5.1 do not show a definite end to the Magellanic Bridge region. In order to further investigate whether the Bridge does have a northern and southern limit as well as the width limits set by the LMC and SMC on either side, data covering a greater range in declination were downloaded from 2MASS. The new region covers the same RA as previously ($\alpha = 20^\circ - 70^\circ$) but was extended to $\delta = -60^\circ$ northwards and $\delta = -85^\circ$ southwards (Fig. 5.15). Catalogue flags were used as described in Chapter 3, with the removal of the Galactic foreground population using the colour-cut removal method. Figure 5.15 shows

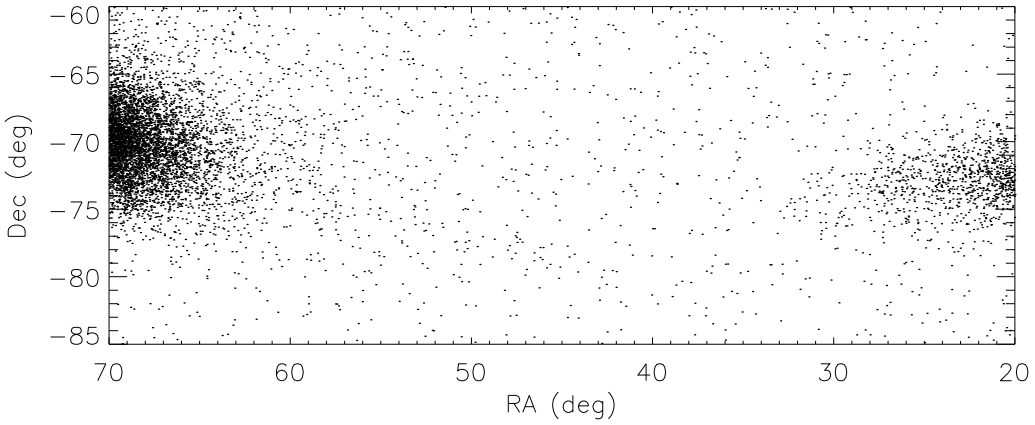

Figure 5.15: Map of the extended Magellanic Bridge from the 2MASS catalogue after the removal of the Galactic foreground population using the colour-cut method. North is at the top and east to the left.

the remaining objects in the outer LMC and SMC with the stellar density decreasing radially outwards and without a clear end to their population. It should be noted that this is the case for the stellar population as the HI gas follows a somewhat different path with a main ridge along the southern part (Harris, 2007). Assuming an accurate foreground removal process and that the remaining objects in each catalogue are genuinely within the Magellanic System, the outer stars of the Bridge in Fig. 5.15 either are true Bridge stars or are loose member of the LMC or SMC which can be confirmed with follow up spectroscopic observations.

5.5 Summary

The density maps of the Bridge region all display a structured distribution of stars. The SuperCOSMOS map shows that for the central region of the Bridge, the population has a differing pattern in the northern and southern parts.
An interesting finding here is of the stellar distributions of blue and red objects within the Bridge. Firstly a new red population has been identified after the Galactic foreground removal. Also an analysis of the blue objects within the Bridge yields a very interesting result that indeed there is a young population which extends further northward than previously observed and also that the den-

sity of the blue objects is higher in the northern Bridge than in the south and not mostly concentrated along the HI ridge as suggested by Harris (2007). This implies that ram pressure may have played a role in the Magellanic system as it has moved through the MW halo displacing the gas within the Bridge. The north-south divide observed here, agrees with the work of Muller et al. (2004) who showed that the Magellanic Bridge comprises two distinct arms of gas making up the northern and southern parts. His results on the gas are confirmed here from stellar density maps supporting the hypothesis that the Bridge is not formed of a single filamentary feature.

Harris (2007) created an infrared CMD of a 35 deg^2 region of the central part of the Magellanic Bridge and a region of the outer Bridge towards the LMC. He found that in the outer region of the Bridge there was an abundance of RGB and AGB stars associated with the LMC but in the central region there were hardly any of these populations. The work here uses a method of Galactic foreground removal using colour-cuts, and finds a population within the Bridge including RGB and AGB stars within the Galactic foreground subtracted stellar Bridge population. The ages of the 2MASS RGB and AGB populations identified here could range from $\sim$ 400 Myr to 5 Gyr for redder, lower-luminosity stars (Frogel and Blanco, 1990). This indicates the presence of a population older than the age of the Bridge that is likely to have been drawn in tidally at the time of the Bridge forming event. An alternative explanation could be that the Bridge is older than previously estimated. Olsen et al. (2011) have identified a population of SMC objects within the LMC. These objects have lower metallicity than the LMC but are consistent with SMC giants which supports the theory of tidal interaction. With the discoveries of LMC and SMC objects reaching these great distances, and the work presented here, it is possible that there is not actually a bridge between the two Clouds, but that each Cloud has a large halo that overlaps with the other. Metallicity measurements of Bridge objects will constrain their membership to either the LMC or SMC and will determine whether the Bridge objects belonging to each Cloud

overlap or are separated.

Other recent studies (Chen et al., 2010a) have used mid-IR Spitzer IRAC and MIPS observations to detect a number of YSOs in the Magellanic Bridge, mostly nearby high HI density regions. They have also studied how star formation has proceeded and estimated the star formation efficiency in the Bridge by looking for Herbig Ae/Be stars using known catalogues of blue stars and stellar clusters. If the new populations in this work are genuine Bridge members they will contribute to the present knowledge of star formation within this region. More recently, soon after the publication of this work, Noël et al. (2013) published photometric work on an older population in the Magellanic Bridge. They present stellar populations in two fields in the Bridge and find that $\sim 28\%$ of the stars are of intermediate age and support the model that the Bridge was stripped from the SMC.

The Magellanic Bridge is one tidal Bridge between two irregular galaxies. Bekki (2008) investigated a Bridge that formed tidally between the outer halos of M31 and M33 made only from HI gas with no stars associated to it. Its origin is also under debate and it could be in-fact a tidal stream like the Magellanic Stream containing no or a very small stellar component. Smith et al. (2010) have used the GALEX ultraviolet telescope to study various tidal features including bridges, spiral arms and tails of gas in the Interacting Galaxy Survey. There are many tidal features in existence, some with and some without stars within the gas in galaxies out to distances of 50 kpc (Pakzad et al., 2004). A more detailed study is required to determine a model to distinguish a tidal bridge from a stream, spiral arm or tail and a study into the conditions that form these features will give more information to the likely presence of stars within them. The Magellanic Bridge has a known stellar population, however in the Magellanic Stream no stars have been detected within the HI gas. Perhaps unless drawn in at formation as indicated here, tidal features do not contain a stellar population until an event occurs that is strong enough to trigger star formation within the tidal feature in an environment with a high enough gas density. Further observations of tidal systems, including

the Magellanic Clouds with VISTA, are needed to give us a better picture of the interactions that form these features and star formation within.

Chapter 6

The Magellanic Bridge with VISTA

This chapter builds upon the previous work carried out in the direction of the Magellanic Bridge with public catalogues in Chapter. 5. A young, and an older population from Bagheri et al. (2013) and Noël et al. (2013) have been identified in the Magellanic Bridge, which can be further studied with the VMC survey catalogues which reach fainter magnitudes than the work in this thesis so far. The main aims of working with the VMC catalogues are to identify the young and older populations in the Bridge, and to classify these populations further in terms of ages, which will aid in piecing together the picture of how the Bridge formed and past interactions between the Magellanic Clouds. Populations that are identified here after the removal of Galactic foreground objects, will be analysed using a number of different tools such as CMDs, two-colour diagrams and the application of isochrones.

6.1 Data

At the time of carrying out the work for this thesis, there were five available VMC tiles from the VSA data release v20121128, partially completed in the direction of the Bridge. It should be noted that in the weeks prior to the submission of this

thesis, it was realised that a zero point issue occurred in the VMC data release used here. The offset introduced by this problem is of the order of 0.02 mag. This problem was realised too late to change the work done here, but taking into account an offset of 0.02 mag, it should not have too great an effect on the analysis here and as the issue is consistent with the Stream tiles from this data release, will not effect the foreground removal. The Bridge tiles used here were tiles 2_3, 2_4, 2_8, 3_5 and 3_7 (Fig. 3.9) with focus on tiles 2_3 and 2_8 as these are the most complete tiles. Table 6.1 shows the completion of each Bridge tile in the data released analysed in this chapter, with each tile completed up to 11 epochs in total with 1 hour exposures each, and two epochs with a 30 second exposure time to reach the nominal survey depth (Cioni et al., 2011). Some tiles have completed observations however, the completed tile may not be available in the combined catalogue release as the data reduction is still in process. The tiles have been cleaned using the methods outlined in Chapter 3 leaving catalogues which will undergo Galactic foreground removal. The K_s magnitude was cut at the faint end at 20 mag for the catalogues of the Bridge tiles, to reduce errors from photometric uncertainties and any problems due to completion. The photometric errors in the VMC data are small in comparison to 2MASS with errors better than 0.1 mag.

Table 6.1: VMC Magellanic Bridge tile completion to date

Bridge tile	Observations available in the VSA
2_3	up to epoch 10
2_4	up to epoch 5
2_8	up to epoch 8
3_5	up to epoch 5
3_7	up to epoch 7

6.2 Galactic foreground removal

Each of the methods applied to the Bridge to remove the Galactic foreground population are outlined in Chapter 4. For this work, the most successful method

of removing Galactic objects from the Bridge is with the use of the one-by-one statistical removal, opposed to making specific cuts in colour and magnitude, due to the large number of objects in the VMC survey. This method makes use of the different colours and magnitudes in the VMC catalogue and also make use of a foreground field chosen to cover the same area as the Bridge tiles, that can be removed from the Bridge. The one-by-one statistical method is preferred here over the colour-cut method as there are expected to be mixed regions in CMD space of both Magellanic Bridge and MW objects, which will be separated best with the statistical method.

As there is not an offset tile in the VMC survey, the foreground field that is most like the Bridge in terms of location and reddening effects is this Stream tile, which will represent an upper limit on the Galactic foreground accounting for a very small number of possible Magellanic objects present in the tile. Chapter 8, will present a study to reveal a potential stellar population in the Magellanic Stream from the VMC tiles. The results from this work indicated that there was no significant Magellanic Cloud population in the Stream tile 2_1 from any of the catalogues analysed. If Magellanic Cloud stars exist in the Stream tiles their numbers must be very small. The Stream tile 1_1 contained a potential younger population and for this reason tile 1_1 was not chosen to represent the Bridge foreground.

The Magellanic Stream tile was used as an offset field to the Bridge tiles for both the probability removal and the statistical removal as this field makes full use of the full VMC magnitude depth. The decision was taken not to analyse the Bridge tiles using UKIDSS as a foreground region as the UKIDSS data are too shallow to make a large difference from the findings with the 2MASS catalogue. As described in Chapter 4, the removal of Galactic foreground objects was performed most accurately using the statistical one-by-one removal and for this reason the objects analysed in the Bridge in this chapter are the Bridge candidates recovered from the statistical method only.

As described in Chapter 4, the removal of Galactic foreground objects is compromised by the presence of Galactic dwarfs remaining in the cleaned sample at redder $(J - K_s)$ and $(Y - K_s)$ colours. In the absence of a more thorough investigation into the metallicity effects on these remaining Galactic objects, this chapter will carry out a thorough analysis of the objects in the cleaned Bridge tiles with $(J - K_s) < 0.65$.

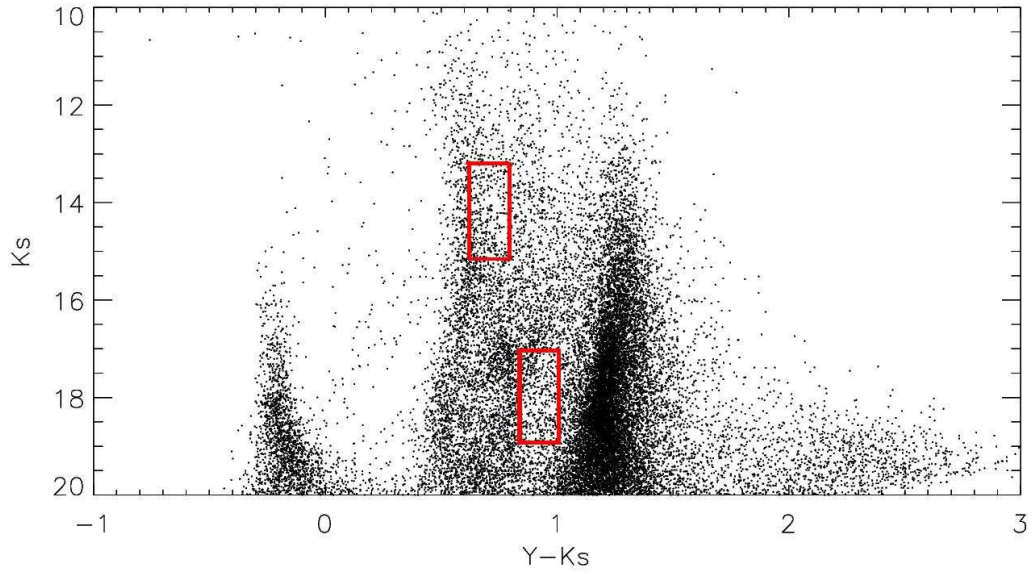

Figure 6.1: CMD, $(Y - K_s)$ vs K_s of the Bridge tile 2_3 to illustrate the regions chosen to compare the number of objects in the different tiles (red boxes). The selected regions are at $(Y-K_s) = 0.6-0.8$, $K_s = 13-15$ and $(Y-K_s) = 0.8-1.0$, $K_s = 17-19$.

To confirm the reliability of the remaining objects, two regions were chosen from the $(Y - K_s)$ vs K_s CMD (Fig. 6.1), and the number of objects in these regions were compared in the foreground region 2_1, and the Bridge tiles 2_3 and 2_8 before and after foreground removal. These regions were chosen as they do not cover areas of the CMD with a large number of Bridge candidates and include regions with foreground populations. The number of objects in each region in the cleaned tiles 2_3 and 2_8 were assumed to be remaining foreground objects and were divided by the number of objects in each region in the foreground field. The worst case ratio was between the cleaned tile 2_8 and the foreground for the right hand box giving a ratio of 0.38. This means that there remains up to 38%

remaining foreground contamination in the cleaned Bridge tiles (Table 6.2) after the statistical removal. This is a worst case scenario and it should be noted that due to the distance gradient across the CMD from closer objects on the blue side, to further objects on the red side, this effect is greater towards the red side of the CMD.

Table 6.2: Magellanic Bridge objects

Bridge tile	No. of sources	Poisson error	No. after statistical removal
2_3	11,389	107	3436
2_4	8,888	94	1530
2_8	8,195	91	1442
3_5	7,203	85	943
3_7	8,178	90	1084

Table 6.2 shows the number of objects in each Bridge tile before and after the statistical foreground removal for objects with $(J - K_s) < 0.65$, as well as the Poisson error on the total number of objects in each tile in this colour range, showing that the recovered objects are well above statistical uncertainty.

6.3 Results

This section investigates the younger and intermediate age Bridge candidates in each of the VMC tiles in terms of the stellar populations and densities. Tiles 2_4, 3_5 and 3_7 contain candidate Bridge objects similar to those in 2_3 and 2_8 from the SMC towards the LMC however, as these tiles are less complete than 2_3 and 2_8 they will not be analysed here. The next VMC data release will see more observations completed in these tiles and thus they will be analysed as part of the ongoing VMC study of the Bridge along with other tiles as they become available.

6.3.1 Stellar populations

Figs. 6.3 and 6.2 show the objects remaining in the Bridge tiles 2_3 and 2_8 after the statistical foreground removal with the total objects in each tile, and also the Bridge candidates with Padova isochrones (Girardi et al., 2000) with a range of different ages to aid in characterising the populations. The inclusion of the Padova isochrones confirms that the candidate Bridge objects of various ages, lie within the stellar tracks at the distance and mean metallicity of the Magellanic Clouds. Tile 2_3 and 2_8 are the available tiles that cover the regions closest to the SMC and LMC respectively and are also the most complete tiles. By comparing these two tiles we can better understand the populations that may have been drawn into the Bridge from each Cloud. Due to the published distance gradient between the LMC and SMC (Grondin et al., 1991), isochrones are overlaid at a distance of 55 kpc for tile 2_3 with SMC metallicity (Maeder and Meynet, 2001), and 50 kpc for tile 2_8 with mean LMC metallicity (Ventura et al., 2005). As the Bridge is thought to have formed primarily from the SMC, a VMC tile in the direction of the SMC, outside of the centre is used for a comparison to the Bridge populations.

Figure 6.2 shows that tile 2_8 contains a population of Bridge candidates at $(J - K_{\rm s}) \sim 0.5$. It can be seen from Fig. 6.3 that tile 2_3 contains a young blue population as well as an older redder population. There are also some objects between these two distinct populations forming a connection between young blue stars and red giants. There is a younger candidate Bridge population in the tile closest to the SMC (2_3) in a region that coincides with the extended SMC wing, whereas the tile closest to the LMC (2_8) does not appear to contain a notable younger population, however there are a small number of blue stars present. For the purpose of analysing the Bridge populations, the bluer population in tile 2_3 will be analysed separately from the redder populations in both tiles.

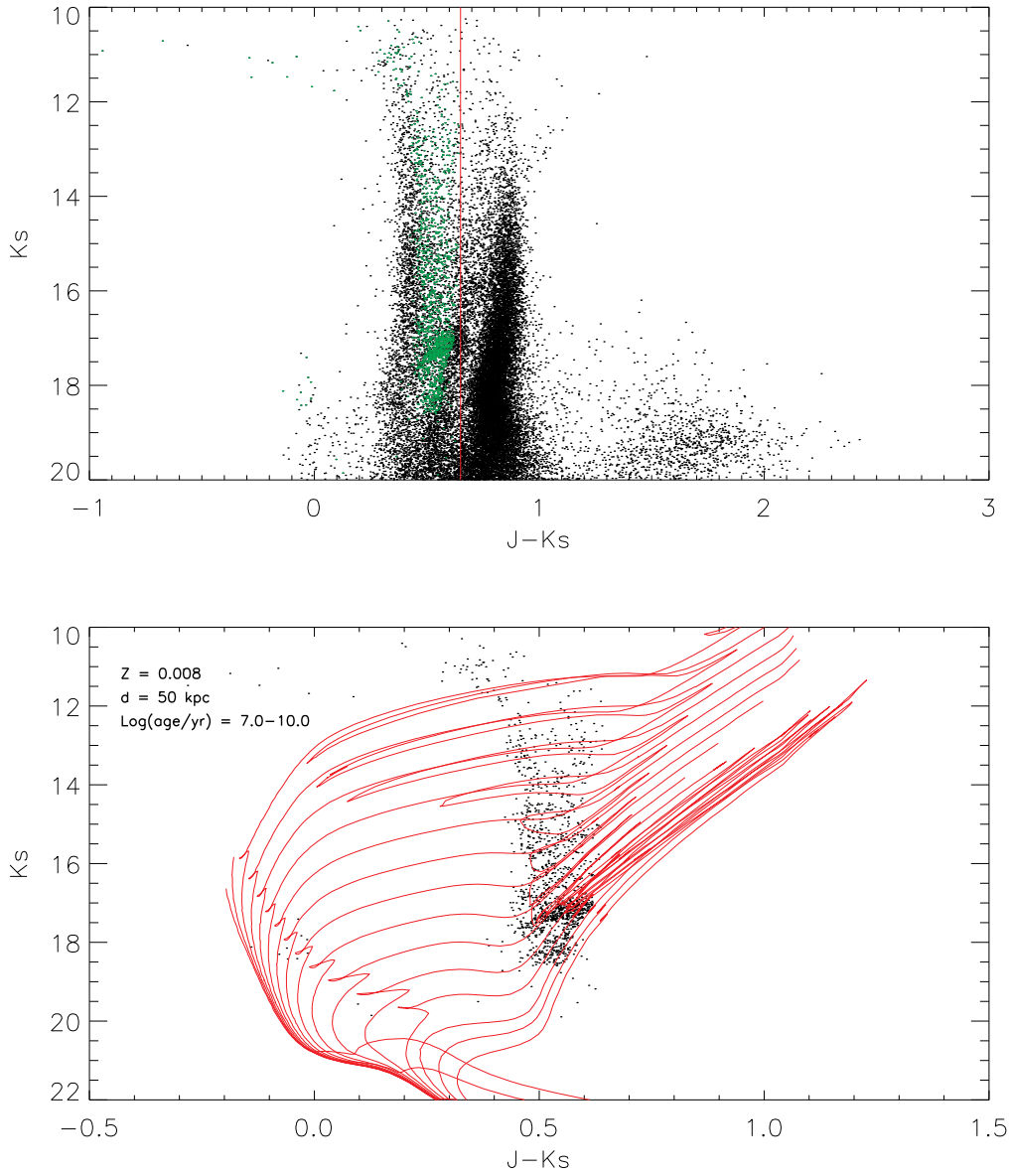

Figure 6.2: CMD, $(J - K_s)$ vs K_s of the Bridge tile 2_8, after the removal of the Galactic foreground population (green) using the statistical method (top), from the VMC catalogues with the VMC Stream tile 2_1 representing the foreground population (black) in the direction of the Magellanic Clouds. Bottom is the cleaned Bridge candidates with Padova isochrones of ages (top to bottom) log(age/yr)$= 7.0 - 10.0$ in steps of 0.2.

Blue objects in the Bridge

Figure 6.4 shows the ages of the bluer population within the Magellanic Bridge which range from $\sim$ 10 Myr to $\sim$ 1.5 Gyr. The objects in this region of the CMD populate the MS region with numbers dropping sharply after the stars finish their

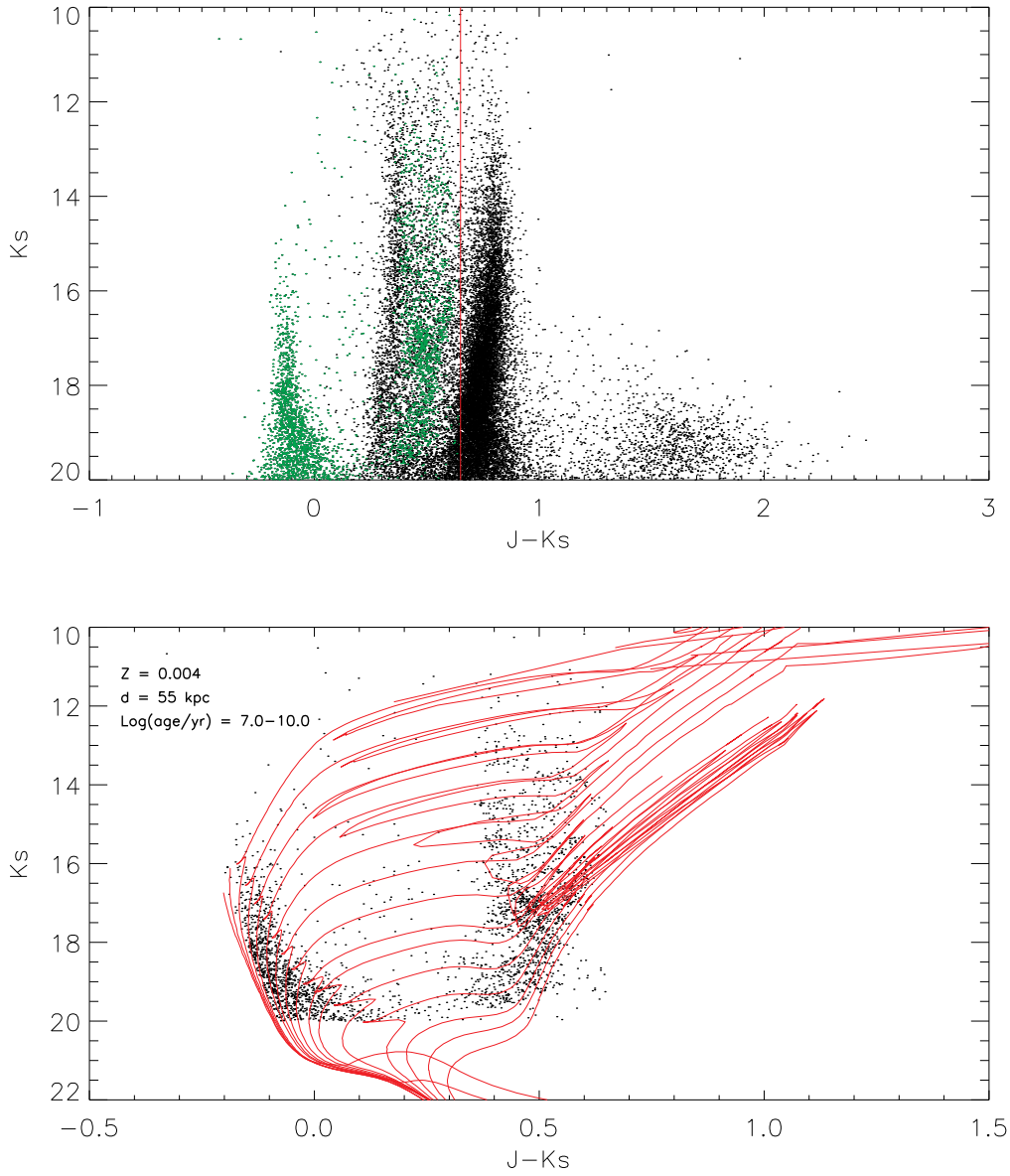

Figure 6.3: CMD, $(J - K_s)$ vs K_s of the Bridge tile 2_3, after the removal of the Galactic foreground population (green) using the statistical method (top), from the VMC catalogues with the VMC Stream tile 2_1 representing the foreground population (black) in the direction of the Magellanic Clouds. Bottom is the cleaned Bridge candidates with Padova isochrones of ages (top to bottom) log(age/yr)$= 7.0 - 10.0$ in steps of 0.2.

core hydrogen burning phase. In order to further characterise these objects, they were split into two categories, those objects that are younger or approximately equal to the estimated age of the Bridge ($0 - 500$ Myr), and assumed to have formed in-situ, and objects that have ages older than the Bridge age (500 Myr to 1.5Gyr), which are assumed to have been drawn into the Bridge tidally at

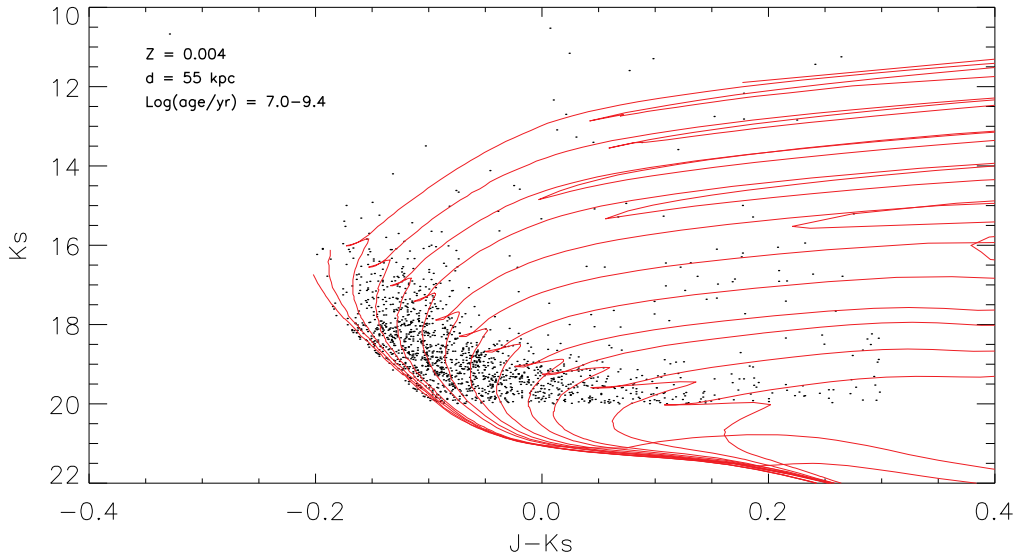

Figure 6.4: CMD, $(J - K_s)$ vs K_s of the Bridge tile 2_3, after the removal of the Galactic foreground population (green) using the statistical method (top), from the VMC catalogues with the VMC Stream tile 2_1 representing the foreground population (black) in the direction of the Magellanic Clouds. Overlaid are Padova isochrones of ages (top to bottom) log(age/yr)$= 7.0 - 9.4$ in steps of 0.2.

formation. For this work the separation was chosen to be at 500 Myr as the age of the Bridge is estimated as $\sim$ 200 Myr (Bekki, 2007), while the second close encounter between the Clouds (starburst event) that could possibly have formed the Bridge was at 500 Myr ago (Harris and Zaritsky, 2009). Therefore an assumed maximum Bridge age of 500 Myr here is satisfactory to separate the younger and older populations within the Bridge. It should be noted that due to the cut in the K_s magnitude at 20 mag, only a fraction of the objects with ages of 500 Myr to 1.5 Gyr will be included.

Red objects in the Bridge

Both tiles 2_3 and 2_8 have a redder population with ages from $\sim$ 60 Myr to $\sim$ 10 Gyr as shown in Fig. 6.5. As well as the older ages of objects in the Bridge, by eye the red clump can be seen, where stars go through their core helium burning phase on the RGB. The region of the red clump was isolated and the number of objects in this region were compared for both Bridge tiles and also for the cleaned

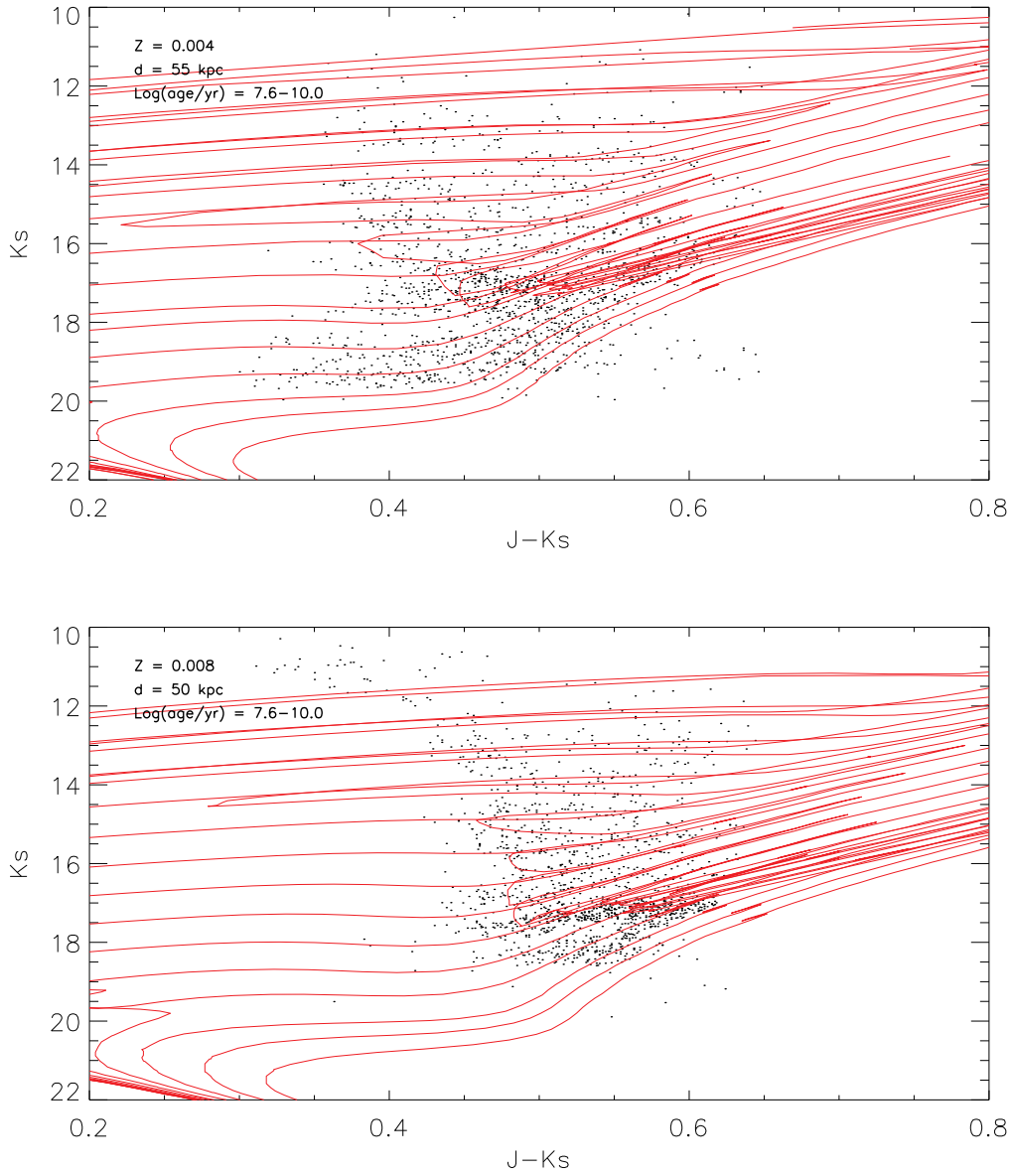

Figure 6.5: CMD, $(J - K_s)$ vs K_s of the Bridge tile 2_3 (top) and 2_8 (bottom), after the removal of the Galactic foreground population (green) using the statistical method (top), from the VMC catalogues with the VMC Stream tile 2_1 representing the foreground population (black) in the direction of the Magellanic Clouds. Overlaid are Padova isochrones of ages (top to bottom) log(age/yr)= $7.6 - 10.0$ in steps of 0.2.

SMC tile 3_3. The objects in the red clump region of the CMD (Fig. 6.6) make up 66% of the total cleaned SMC population for $(J - K_s) < 0.65$, with 63% and 27% respectively for tiles 2_8 and 2_3.

The lower percentage of red clump stars in the tile 2_3 is due to the larger number of younger blue objects in this region, which have likely formed in-situ

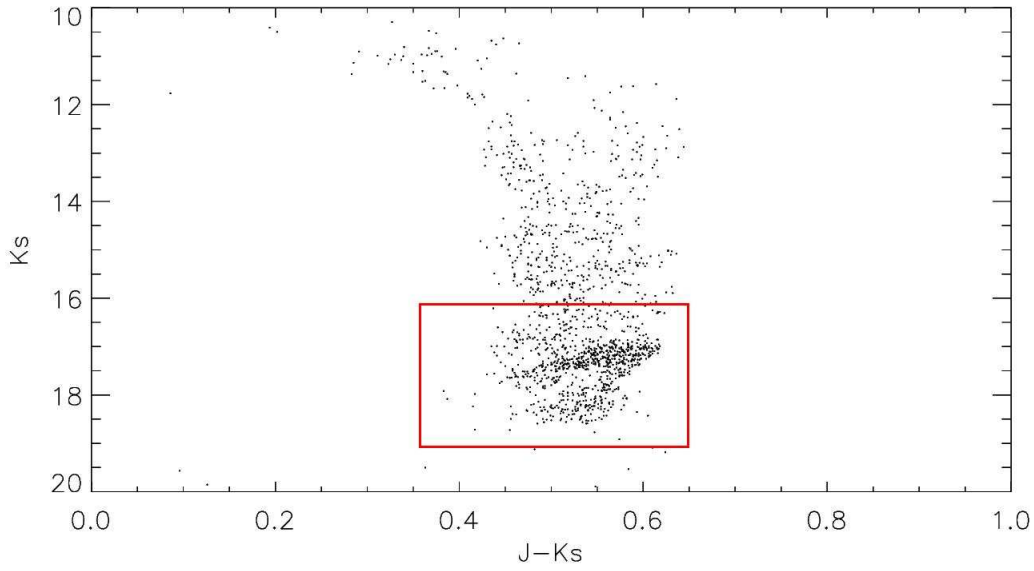

Figure 6.6: CMD, $(J - K_s)$ vs K_s of the Bridge tile 2_8 to illustrate the region chosen to represent the red clump to compare the number of objects in the different tiles (red boxes). The selected regions are at $(J-K_s) = 0.35-0.65$, $K_s = 16-19$.

from the gas within the Bridge. The SMC tile 3_3 and Bridge tile 2_8 have a larger contribution of objects from this redder region of the CMD representing an older population with ages of $\sim$ 700 Myr to $\sim$ 10 Gyr from the isochrones. This result is expected from the SMC which has a known older population however, this is a new result for the Bridge showing that on the side closer to the LMC (tile 2_8), there exists an older population which make up the majority of objects in this region. These objects did not form in-situ in the Bridge and due to their older ages of up to $\sim$ 10 Gyr must have been drawn in tidally from the Clouds. The fact that these objects reside close to the LMC indicates that they are possibly LMC stars that have been drawn into the Bridge, or belong to an extended LMC halo. The work in Chapter 7 will address this question.

It is also possible from the identification of the red clump in the Bridge tiles, to estimate rough distances to Magellanic Cloud stars in each tile using the distance modulus equation: M - m =5logd - 5 (Kinman, 1958). Where M is the absolute magnitude of the red clump stars, m is the apparent magnitude from the VMC observations and d is the distance to the Bridge tiles. Using an absolute K_s

band magnitude of ~ -1.6 from Laney et al. (2012) who determine red clump magnitudes for the LMC in the 2MASS system, with an apparent magnitude of 17.2 and 16.9 for the Bridge tiles 2_8 and 2_3 respectively, the distances are approximately 50 kpc and 58 kpc. Even this very rough calculation (without the consideration of extinction and metallicity effects), results in a distance gradient between the LMC and SMC side of the Bridge with the SMC being further away.

6.3.2 Stellar densities within the Bridge

The stellar densities in this section represent the different populations described above in the Bridge tiles 2_3 and 2_8 after the removal of Galactic foreground objects. The stellar populations have been divided into the bluer ($(J-K_{\rm s}) < 0.30$) and redder ($(J-K_{\rm s}) = 0.30-0.65$) objects (Chapter 4), and further categorised in ages of < 500 Myr and > 500 Myr to represent objects that are likely to have formed in-situ and drawn into the Bridge tidally.

The youngest blue objects are most dense closest to the SMC where the density of gas is highest. The older objects have the highest density close to the SMC, yet the overall distribution is more diffuse. Diffuse stellar populations will remain diffuse, however star formation is triggered in the densest regions of gas clouds, therefore newly formed stars can populate more concentrated regions than the initial gas distribution. In both cases the younger and older populations have the highest density close to the SMC, which is expected in a scenario with the Bridge being formed tidally from the SMC with the tidal force from the LMC still effecting the SMC at present.

In the Bridge tile 2_8, the regions of highest stellar density in both the younger and older populations are co-located. There is a higher density of younger, redder objects to the left of the image which represents the region of the tile closest to the LMC. These younger objects could have formed from a higher density of gas from the LMC in this region that is drawn in from the tidal forces from the SMC. It is also possible that due to the nature of the stellar density in this region, there is a

clustering of younger objects which formed in-situ. A similar effect is observed in the Bridge tile 2_3 close by the SMC, with the presence of a higher density to the right side close by the SMC. It is interesting here though that the highest density of the younger objects in this tile do not lie at the very far right by the SMC, but lie more centrally in the tile. These objects also display some clustering and are likely to have formed in-situ. It should be noted that there is likely to be some foreground contamination remaining in the redder objects.

6.4 Summary

After the removal of Galactic foreground objects in the direction of the five Bridge VMC tiles, the main results are that there are clearly candidate Bridge objects remaining in each tile above statistical uncertainty and that these candidate objects reside in two main populations, as in Chapter 5. The Bridge candidates contain a younger population within the age of the Bridge ($\sim 200-500$ Myr), that are likely to have formed in-situ in regions of the Bridge closest to the SMC in locations of higher density gas. The number of younger bluer objects in the Bridge tiles is greater towards the SMC and decreases towards the LMC. This complements the higher density of gas on the SMC side of the Bridge (Hindman et al., 1963b), which supports that the Bridge is formed primarily from the SMC in the tidal formation. These results support that the Bridge was formed tidally from the SMC, by the existence of tidally drawn in objects older than the Bridge on the SMC side that diminish towards the LMC. The younger objects have a higher density as they are likely to have formed in-situ from the gas within the Bridge which is more dense in the SMC wing and on the outer LMC. In order to fully compare the stellar densities of the younger objects from this work with the work in Chapter 5, the full coverage of VMC tiles should be analysed.

The red population observed in the Bridge tiles here confirms the work in the previous Chapter that there is an older population within the Bridge. The popu-

lation in the mid region of the $(J - K_s)$ vs K_s CMD which have ages up to ~ 3 Gyr, are likely to have been drawn into the Bridge from the Magellanic Clouds at formation, assuming the age of the Bridge is $\sim 200 - 500$ Myr. These results are consistent with the original discovery of the older Bridge population from Chapter 5 that there is an older Bridge population with ages up to a few billion years. Figure 6.7 shows the cleaned 2MASS stellar density map from Fig. 5.3 with the VMC tiles 2_3 and 2_8 overlaid. It is also possible that the Bridge is older than previously assumed, proposed in Putman et al. (2003) who state that the Stream appears to have a component that formed from the Bridge, therefore the Bridge must be older than the Stream.

The identification of the red clump in the Bridge here is also an important observation as the red clump is a well defined distance indicator (Cole, 1998), and different positions of the red clump stars in different VMC Bridge tile leads to different distances within the Bridge. In this case, using the red clump stars in the Bridge tiles 2_3 and 2_8 at either side of the Bridge, shows that there is a distance gradient between the LMC and SMC sides with the SMC side of the Bridge being further away as in the study of the Bridge in Grondin et al. (1991). Models of the interaction history of the Magellanic Clouds (Harris and Zaritsky, 2009) suggest that the Clouds have had two close encounters with each other at 2 Gyr and 500 Myr. Previous work suggests that the Stream was formed in the first encounter and the Bridge was formed in the most recent encounter (Diaz and Bekki, 2011). This work supports that Bridge was formed from the second close encounter, and that objects older than ~ 500 Myr were drawn into the Bridge tidally at formation, with the younger objects being formed not from a one off starburst event, but continuously from when the Bridge was formed.
In the Bridge, close to the LMC, the existence of an older population with ages up to ~ 10 Gyr indicates that these objects must have been drawn in from the Clouds at the formation of the Bridge. The fact that these objects reside close to the LMC indicated that they are possibly LMC stars that have been drawn

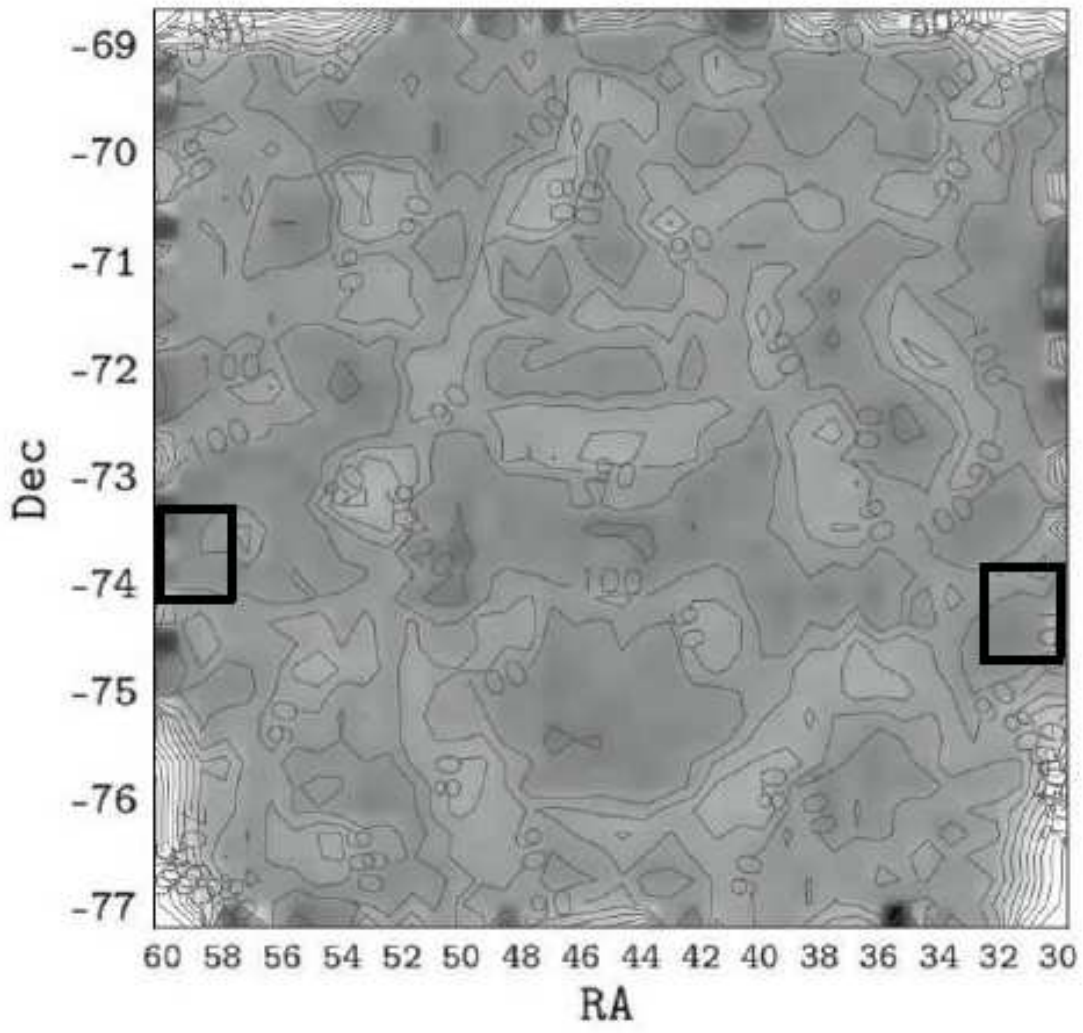

Figure 6.7: Stellar density map of the Magellanic Bridge from the 2MASS catalogue after the statistical removal of the Galactic foreground multiplied by the probability of a star belonging to the Bridge, with bin size of 0.2×0.2 deg^2. North is at the top and east is to the right with the LMC to the outer left and SMC to the outer right with the VMC tiles 2_3 (right) and 2_8 (left) overlaid. The region of interest here is approximately 14 kpc across.

into the Bridge tidally, or that the LMC halo extends further into the inter-Cloud region. The work in Chapter 7 looking at metallicities and radial velocities of Bridge red giants will confirm whether objects in the Bridge have a contribution from the LMC as well as the SMC, and to what extent in RA do LMC objects exist in the Bridge.

The spatial distribution of objects within the Bridge indicates that the number of stars is highest in the regions closest to the LMC and SMC where the density

of gas is highest. Particularly for the case of younger objects in the Bridge tile 2_3, the stellar density is much higher in the region closest to the SMC. In all cases it does appear that the older objects are less locally confined and are likely to be present in the Bridge from tidal interactions between the Clouds. It is also interesting that there appears to be a difference in the stellar densities of the younger objects in the Bridge between the redder and bluer objects. It will be of interest to study the spatial distribution of Magellanic Bridge candidates when all of the VMC tiles are more complete in order to gain a better understanding of the spatial variation of Bridge objects.

Future work will include the analysis of objects redder than $(J - K_{\rm s}) = 0.65$ with a full study of the Galactic foreground population in order to make a reliable separation between Bridge candidates and foreground objects. As other Bridge tiles become complete they will also be analysed to gain a fuller understanding of how the Bridge stellar populations change across the width of the Bridge from LMC to SMC. This will tie into the results from Chapter 7 which confirms the metallicities and radial velocities of a range of red giants across the width of the Bridge.

Chapter 7

A spectroscopic follow up of Magellanic Bridge objects

The work presented in Chapter 5 (Bagheri et al., 2013), provides the first large scale study of the Magellanic Bridge using NIR and optical photometry confirming a larger young population than previously observed and the first large scale identification of an older population. New spectroscopically derived abundances and RVs of these objects using CaII triplet (CaT) spectra (8498.03 Å, 8542.09 Å, and 8662.14 Å) will not only verify Bridge membership of these candidates but will also confirm their origin from either the LMC or SMC. This will have major implications for the formation of the Bridge and the relationship between the LMC and SMC.

No systematic spectroscopic study has been carried out to date covering the CaT lines for central Magellanic Bridge objects. A proposal was submitted to ESO (PI Bagheri), to obtain spectroscopic follow up observations of 34 candidate Bridge objects (Chapter 5) to yield spectroscopically derived abundances and velocities. The objects were chosen from a larger sample as bright stars that cover the entire Bridge region. 34 objects were chosen as this was the highest number of objects that could be observed within two nights to improve the chance of our proposal being accepted. Medium resolution spectra should yield RVs of Bridge

members with enough accuracy to determine a possible north-south divide and an investigation of the metallicity distribution within the Bridge should allow for an estimate of the age-metallicity relation. Similar work on the SMC and LMC aid in exploring the importance of metallicity in different contexts including star formation, and stellar and galactic evolution. However, the Bridge is a much lower density environment and is the product of a tidal interaction meaning that this work will complement and improve upon our understanding of the above in this unique case of a local low density star forming region and will be a proxy for tidal Bridges formed in more distant galaxies, as well as constraining the interaction history of the Magellanic Clouds and Milky Way.

7.1 Observations

The target objects in this chapter were selected from the analysis in Chapter 5 with candidate objects from the 2MASS catalogue following the colour-cut removal method and CMD analysis of stellar populations. This analysis yielded $\sim$ 200 unknown red objects in the Bridge region and 34 of these objects were chosen for spectroscopic follow up observations. The spectroscopic targets cover the whole of the Bridge concentrating on previously unexplored northern regions in addition to the south which, prior to the submission of the observation proposal, was only known to contain young objects (Fig. 7.1).

The observations were carried out using the FORS2 instrument at the VLT, which was considered to be the most suitable instrument for this type of study with sufficiently high resolution spectroscopy for a number of target objects covering the CaT lines required. Using the ESO exposure time calculator version 3.2.7 for FORS2 for the required setup gave a S/N of 90 at the central wavelength for an integration time of 900 sec which is greater than other instruments using the same exposure time with comparable resolution. These capabilities for the requested number of objects allowed the collect a statistically significant sample of spectra

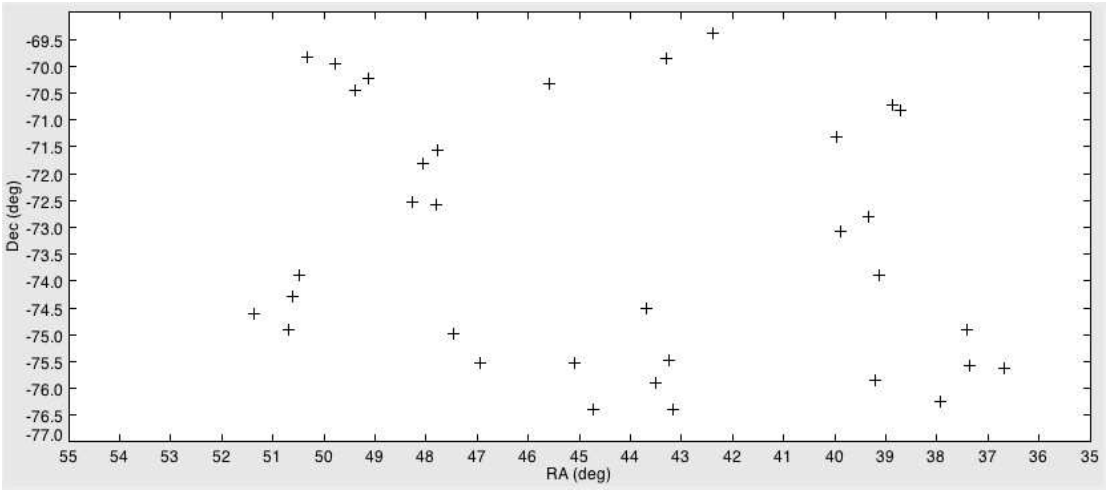

Figure 7.1: The spatial distribution of the 34 Bridge candidate objects chosen for the follow up spectroscopic study.

(within a reasonable observation time requested) with uncertainties in measurements accurate enough to determine the membership of different objects within the Bridge with RV measurements which will be achievable with FORS2. FORS2 has also been used in the past for similar work from Grocholski et al. (2006) and Parisi et al. (2010a) yielding successful results with reasonable uncertainties.

Previous work by Grocholski et al. (2006) and Parisi et al. (2010a) obtain a peak S/N of $70-90$ for their observations of objects within our brightness range, which leads to RVs with statistical errors of $5-7.5$ km/s, and metallicity measurements with accuracies better than 0.15 dex. Our objects are $15.5-16.5$mag in I band and with LSS and MIT setup in standard resolution with 2×2 high readout mode and GRIS 1028z(OG590) with 14 days from a new moon, this gives a S/N of 90 at the central wavelength for the faintest objects ($I = 16.5$). The requested seeing of these observations was $1.0''$ as the targets are in an un-crowded field. Exposure times ranged from $500-1100$ seconds for the brightest and faintest objects respectively.

The spectroscopic observations of the Bridge targets were successfully carried out between July and August 2012. Each object was observed at least twice by the VLT staff as well as calibration exposures, bias frames and flat fields. The science time of this proposal was scheduled in service mode for a total of 15h with

observations carried out from the 22nd July to 6th August 2012. The 34 Bridge candidate objects were named BRG1−34 with two exposures taken of each object, that were combined to create the final spectra for analysis.

7.2 Reduction method

The reduction process contains a number of steps, including the correction of the science images for bias, flat-field and cosmic rays, followed by the extraction of the one dimensional spectra along with the arc spectra and the flux calibration. The first step in the data reduction process was to obtain the dark, flat, bias and arc files from the ESO archives. The darks were taken over an exposure time of 30 mins and are used to test the CCD quality, the bias was checked to see if there were any variations across the nights of the observations, the flat-fields were used to correct for sensitivity variations of the CCD and the arc spectrum for a lamp with helium, argon and neon gas is extracted to identify spectral lines in the target spectra and carry out the wavelength calibration.

The flats and arcs are downloaded for the same grism as the target observations, and are downloaded for nights at the start and end periods of the target observations to check for variations. The bias, dark and flat frames were combined with the IRAF tasks *zerocombine, darkcombine* and *flatcombine* with the default parameters. The IRAF package *imstat* was used to look at the average counts (mean and mode) in the bias and darks for a number of nights. The difference in counts were very small ($1-2$ counts difference in average between dark and bias), and the average counts in the overscan region were the same for the bias and dark. Cosmic rays were rejected for the CCD exposures from the dark frames using the task *cosmicrays* which can discriminate between cosmic rays and poorly sampled point sources.

The IRAF package *ccdproc* used in the reduction process, requires file headings to contain the parameter IMAGETYP in order to carry out the reduction procedure

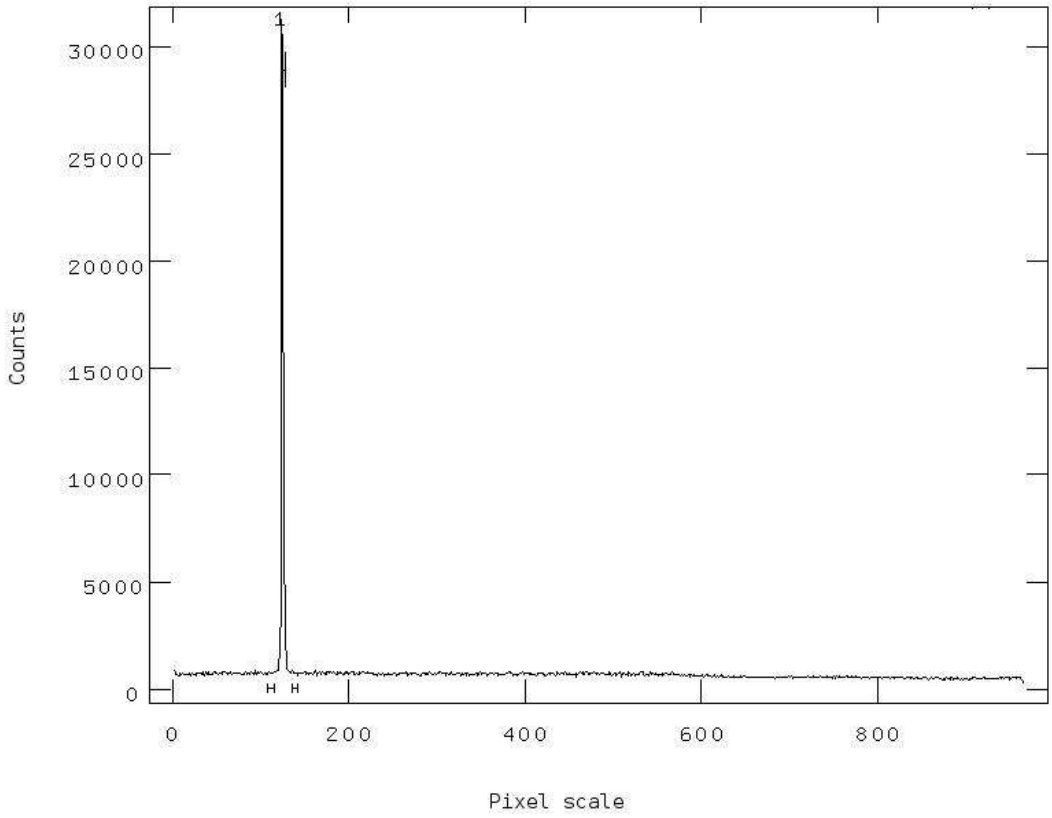

Figure 7.2: Typical output of the first stage of the *apall* task showing a cut along the spatial axis with the target object (large spike) and the background regions (two bars at the base of the object).

with image types of dark (for darks), other (for arcs), flat (for flats), zero (for bias) and object (for the target observations). These headings were added using the *ccdhedit* task in IRAF. The *epar ccdproc* command was used to include the names of the files required for *ccdproc* to trim the target images and subtract the overscan and remove the bias.

After the corrections were applied to the target images, the spectra were then extracted. A plot was produced (Fig. 7.2) using the task *implot*, of a number of slices perpendicular to the dispersion axis to ensure that the cleaning of the image was successful and that the object was visible and well above the background counts.

The target object and suitable background regions, were also identified here in pixel coordinates. The IRAF task *apall* in the *ctioslit* package was used to do the

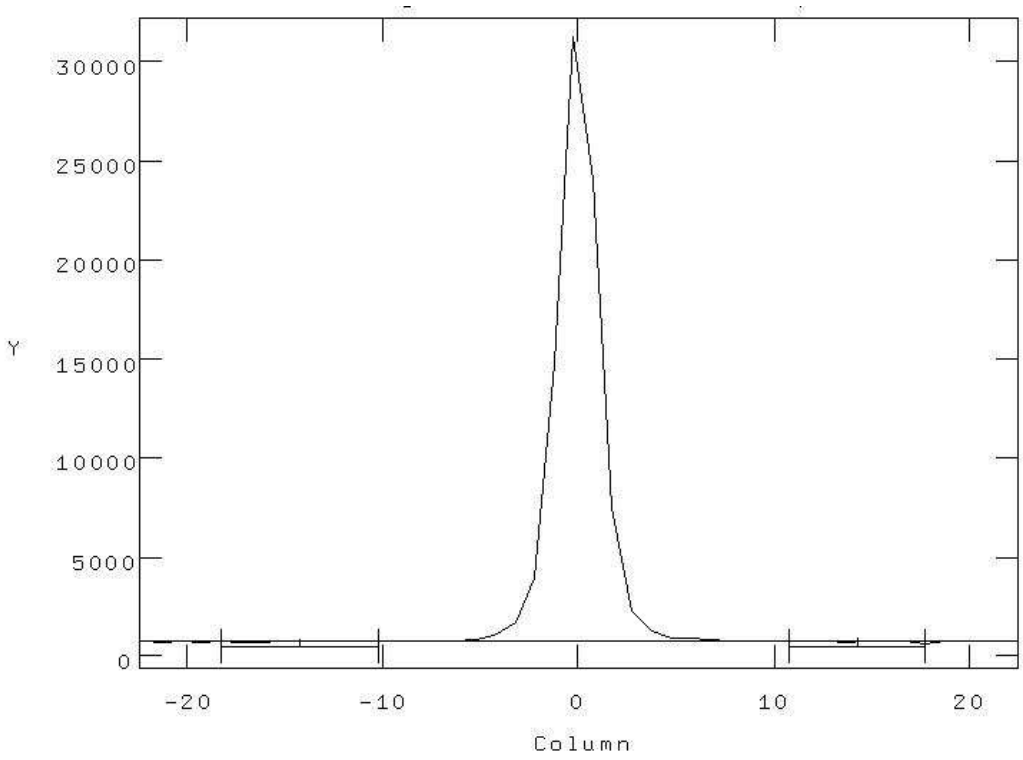

Figure 7.3: An example of the determination of suitable background regions (bars to the left and right of the base of the spike) to use in the IRAF task *apall*.

extraction of the spectra all in one procedure. The *apall* task locates the aperture, the target object and background regions (Fig. 7.3) and performs the extraction of the spectrum using a set of parameters that can be adjusted interactively by the user.

An example of an extracted spectrum for one of the Magellanic Bridge candidates is shown in Fig. 7.4. Of the 34 Bridge candidate objects, all of the extractions appeared to be successful apart from $BRG5$ and $BRG11$ which required the target object to be chosen manually as there were either two stars visible on the CCD or cosmic ray effects. The task *apall* was then carried out for the arc spectra, assigning each arc a reference Bridge object in order to ensure that the arc and object spectra are extracted from the same region. There were two types of extraction to choose between, average extraction and optimum extraction. The optimum extraction fits a profile to the cross-dispersion flux distribution and extracts the flux per bin, using weights which are derived from the fitted profile and

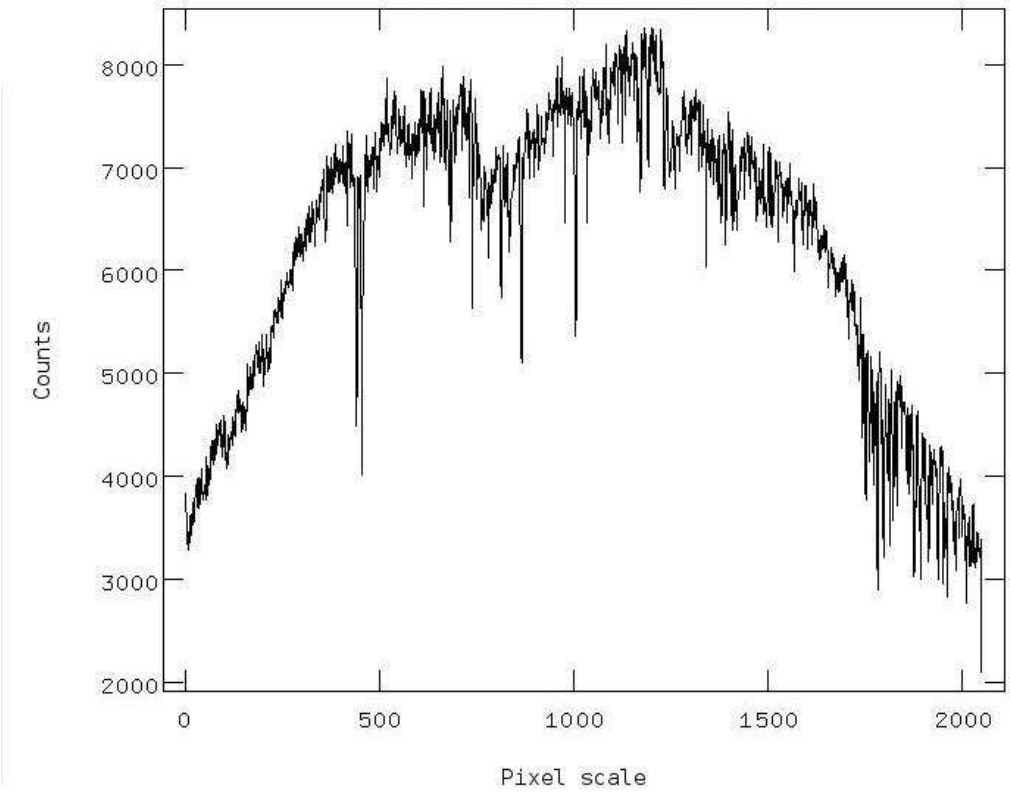

Figure 7.4: An extracted stellar spectrum as a product of the task *apall* of a Bridge candidate object.

the average extraction extracts the flux without weights and does not have a cosmic ray rejection. The optimum extraction was chosen because it minimises the noise in the extracted spectrum. However, if the spectrum is traced incorrectly, it can lead to systematic errors, therefore both extraction methods were applied and the resulting spectra were compared to verify that the optimum extraction provided the best result.

After the extraction of the stellar spectra, the FORS2 calibration spectrum was extracted from the arc lamp (Fig. 7.5) for the grism used in the Bridge observations in order to determine the dispersion solution. Spectral lines were identified in the calibration spectrum using the IRAF task *identify* which enabled the identification of all the spectral lines present in the FORS2 arc lamp (He, Ar and Ne). This process was carried out for one of the arc spectra and the dispersion solution was then used as an initial solution for the remaining arcs using the task

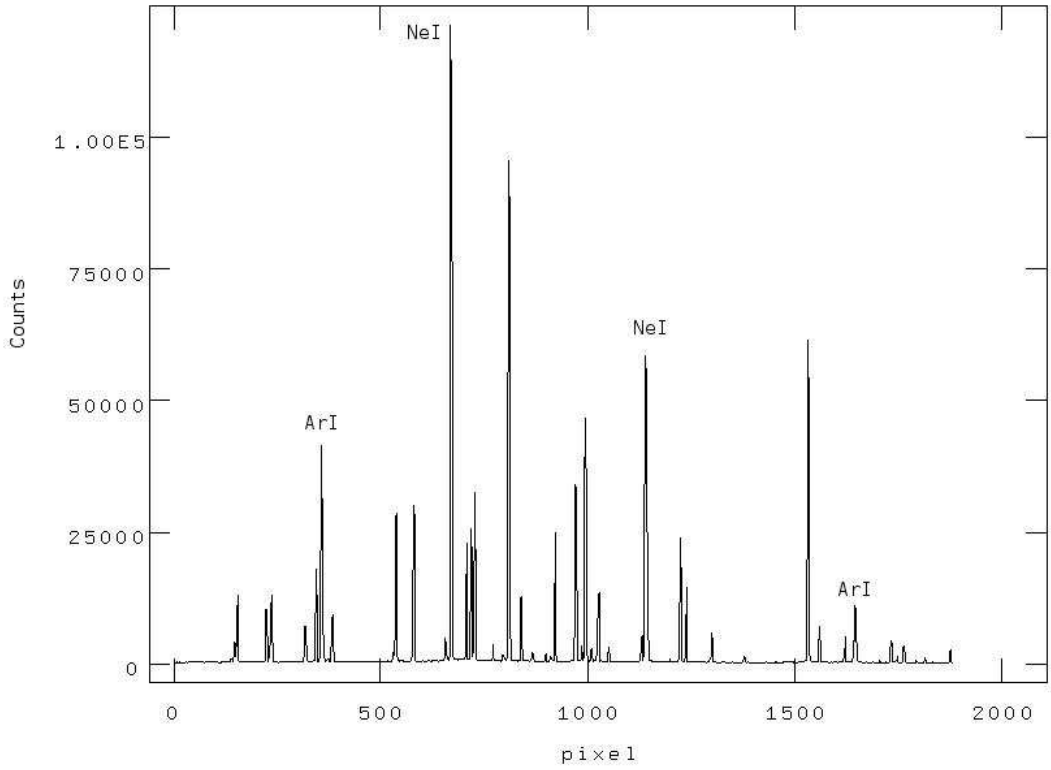

Figure 7.5: The calibration spectrum for FORS2 to be applied to the target Bridge objects. Labelled are four emission lines used in the identification of the spectral lines here from the IRAF task *identify*.

reidentify, with the dispersion solution for each of the Bridge objects assigned via the file headers.

The next stage was to apply the dispersion solution to the program objects to set the wavelength scale using the task *dispcor* and setting the wavelength range for the spectra. After the application of the dispersion solution and an airmass correction, the flux calibration was carried out using standard stars. In the case of the candidate Bridge objects, the most suitable standard star was $EG21$ (spectral type DA) from the ESO standard star catalogue, with a corresponding entry in the IRAF database. The task *standard* was executed, it integrated the target objects over the relevant band passes and divides by the exposure time, giving a listing of the observed counts with each bandpass with the standard star fluxes. After running the task *standard*, the next step was to fit the sensitivity function as a function of wavelength feeding the output from *standard* into the task *sensfunc*,

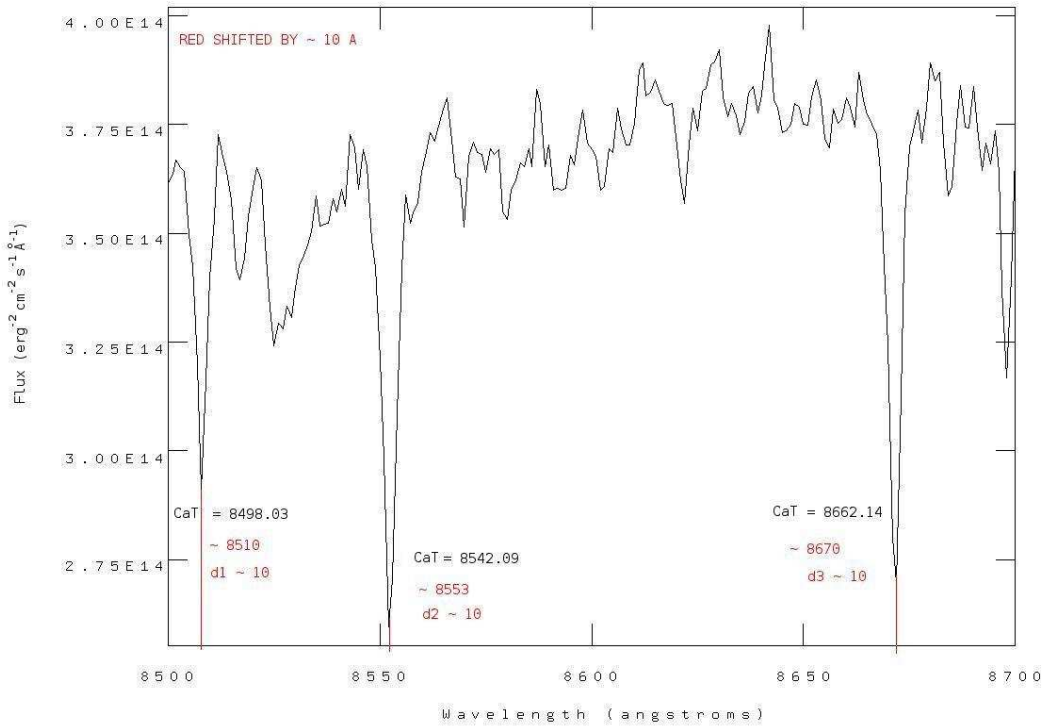

Figure 7.6: A closeup of the spectrum of a candidate Bridge star (BRG1) after the final flux calibration. The CaT lines are indicated and their laboratory wavelengths given. Comparison with the measured wavelengths indicates a red shift by ~ 10 Å.

which calculates the response function. The sensitivity function is then applied to the target objects via the task *calibrate* which performs the final flux calibration, resulting in the final spectra of the target objects, which were then combined for each object using the task *scombine* (Fig. 7.6).

7.3 Analysis

Before the determination of RVs was carried out, all of the calibrated spectra were quality checked by eye as shown in Fig. 7.6, focussing on the CaT region to ensure that the flux calibration was successful and that no anomalies were present. The CaT lines were of interest as they are strong in red giant stars and they are a useful tool in spectral analysis as the three lines can be used together to improve statistics. The RVs of the candidate Bridge objects were obtained using the IRAF

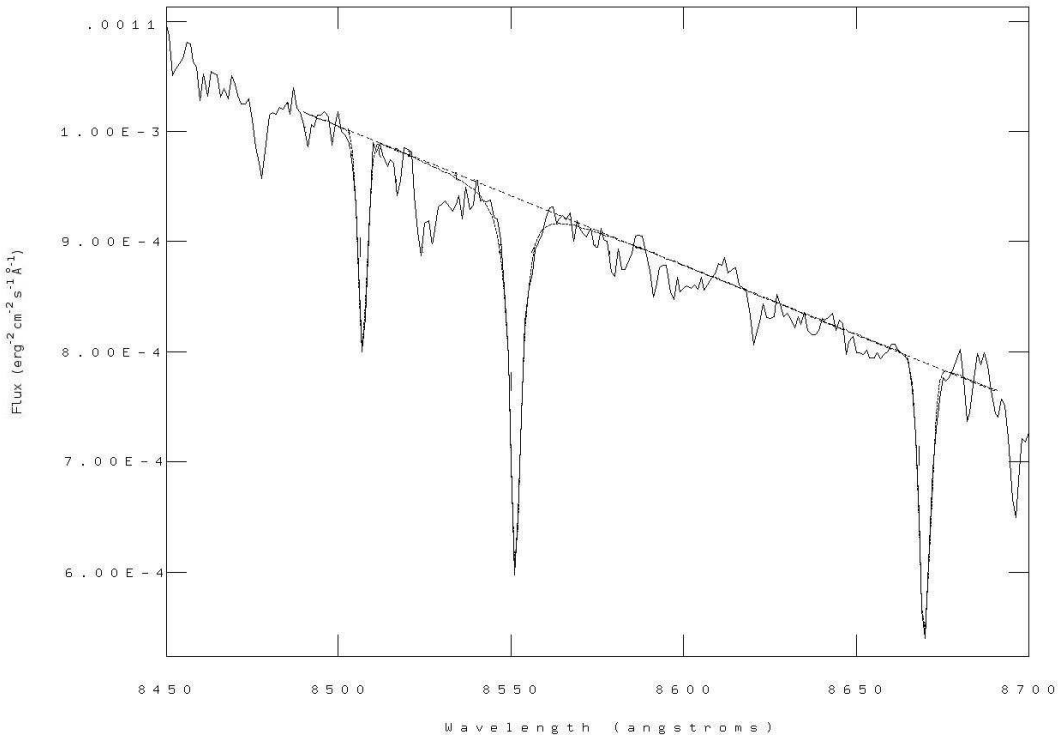

Figure 7.7: An example of the IRAF task *splot* used to fit a Gaussian to the CaT lines in the Bridge spectra giving the central wavelengths and EWs for each object.

task *splot* by performing a polynomial fit to the continuum and a Gaussian fit to each of the three CaT lines. This task gives the central wavelength of each of the CaT lines, as well as the equivalent widths (EWs) and fluxes (Fig. 7.7). The Gaussian fits were performed three times per object to reduce the errors from manually fitting the continuum and allowing an estimate of the uncertainties.

The average RVs (for the CaT) were then calculated for each object using the Doppler shift between the central wavelength of each line from a laboratory in air, and the values measured for the Bridge candidates. Heliocentric corrections to the RVs were applied using the IRAF task *bcvcorr* to produce final values for each object. It should be noted that due to the location of these objects, the difference between heliocentric and Galactocentric velocities is negligible. Errors on the RV were determined by calculating the spread in values across the objects with a resulting scatter for individual lines of $\sigma \approx 21$ km s^{-1}. The final RV for each star is computed from an average over all three lines and thus the error is

$\sigma_{mean}/\sqrt{3} = 11.9$ km s^{-1}. The errors are slightly higher than the value initially aimed at, but the accuracy is still sufficient to assess the membership of each candidate as done by Grocholski et al. (2006). A cross correlation with templates would make use of a larger number of lines and improve accuracy. However, this would require high resolution spectra templates with well known RVs which were not available in this study. Figures 7.9 to 7.12 show the CaT lines for the Bridge objects. It can be seen for the more metal rich objects in Fig. 7.11 that the CaT lines are stronger than the very metal poor stars in the lower panel of Fig. 7.12, where the CaT lines can not be located without focusing on a smaller wavelength range.

Once the RVs had been calculated, the EWs of the three CaT lines were combined linearly for each star to obtain the line strength index (ΣW) for each object (Appendix D). For each line the error was estimated from the spread of the three measurements, averaged over the whole sample. Derived values are $\sigma_{line1} = 0.17$, $\sigma_{line2} = 0.33$, $\sigma_{line3} = 0.23$. The error of the ΣW is estimated as $\sigma_{\Sigma W} = \sigma_1 + \sigma_2 + \sigma_3 = 0.67$ Å. A straight sum is used because the mean error source is from the continuum placement, which means that the measurements are not statistically independent. There is a well known linear relationship between a red giant star's absolute magnitude and ΣW (Armandroff and Da Costa, 1991), with larger ΣW values higher up the RGB for a given metallicity.

To remove the effect of luminosity on ΣW a reduced EW W' is calculated. Parisi et al. (2010a) adopted the relationship $W' = \Sigma W + \beta(V - V_{HB})$ where V_{HB} is the absolute V band magnitude of a HB/red clump star and V is the absolute V band magnitude of the target objects. β (Åmag^{-1}) is the gradient in the V_{HB} vs W' graph, or alternatively it can be calculated from the equation, when a sample of objects with a known metallicity is studied (Fig. 7.8). A conversion from the IR photometry available in this work to V band magnitudes would have introduced larger errors in the process and the decision was taken to recalibrate the relation for the I band. The errors in $I - I_{HB}$ are the photometric errors

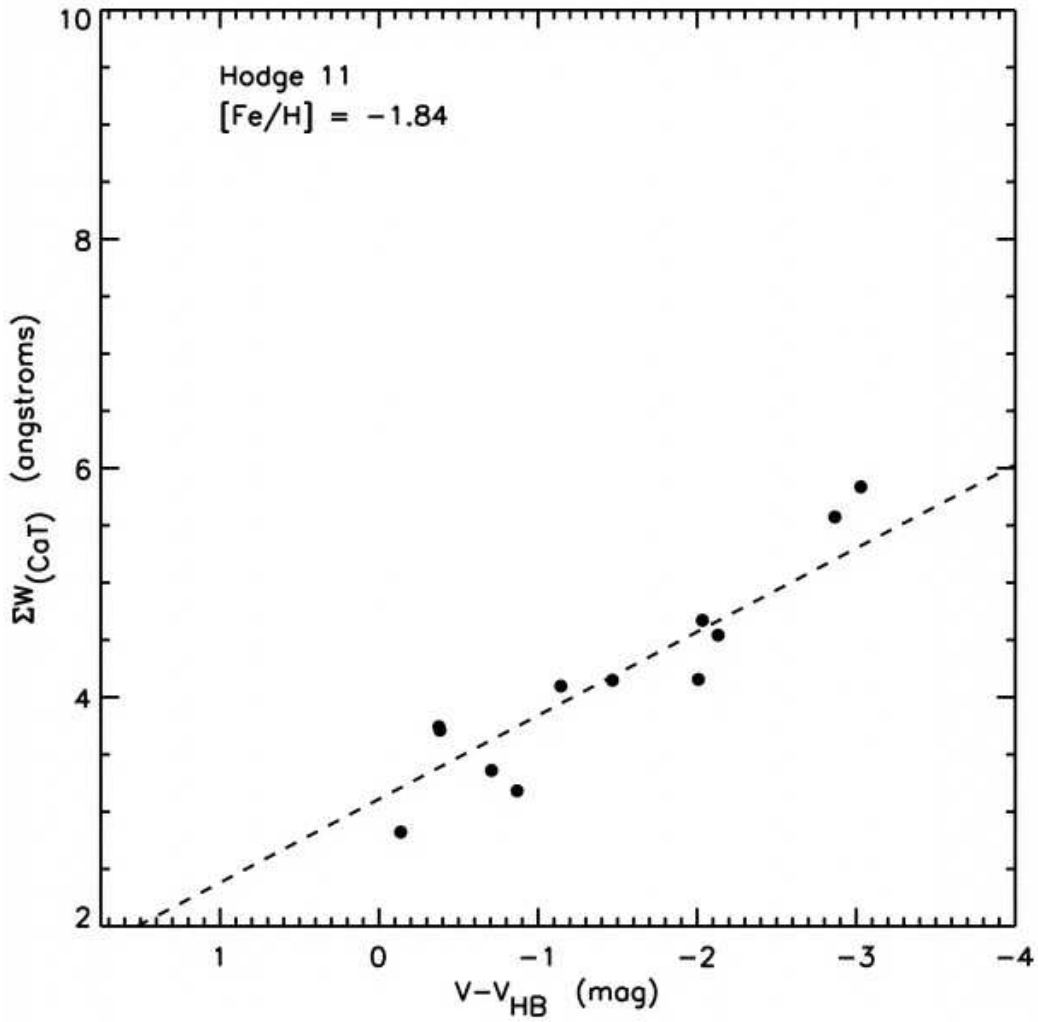

Figure 7.8: Summed EWs vs brightness above the HB from Grocholski et al. (2006, Fig. 6). The dashed line represents an isoabundance line at the mean metallicity of $[Fe/H] = -1.84$, with a slope of $\beta = 0.73$.

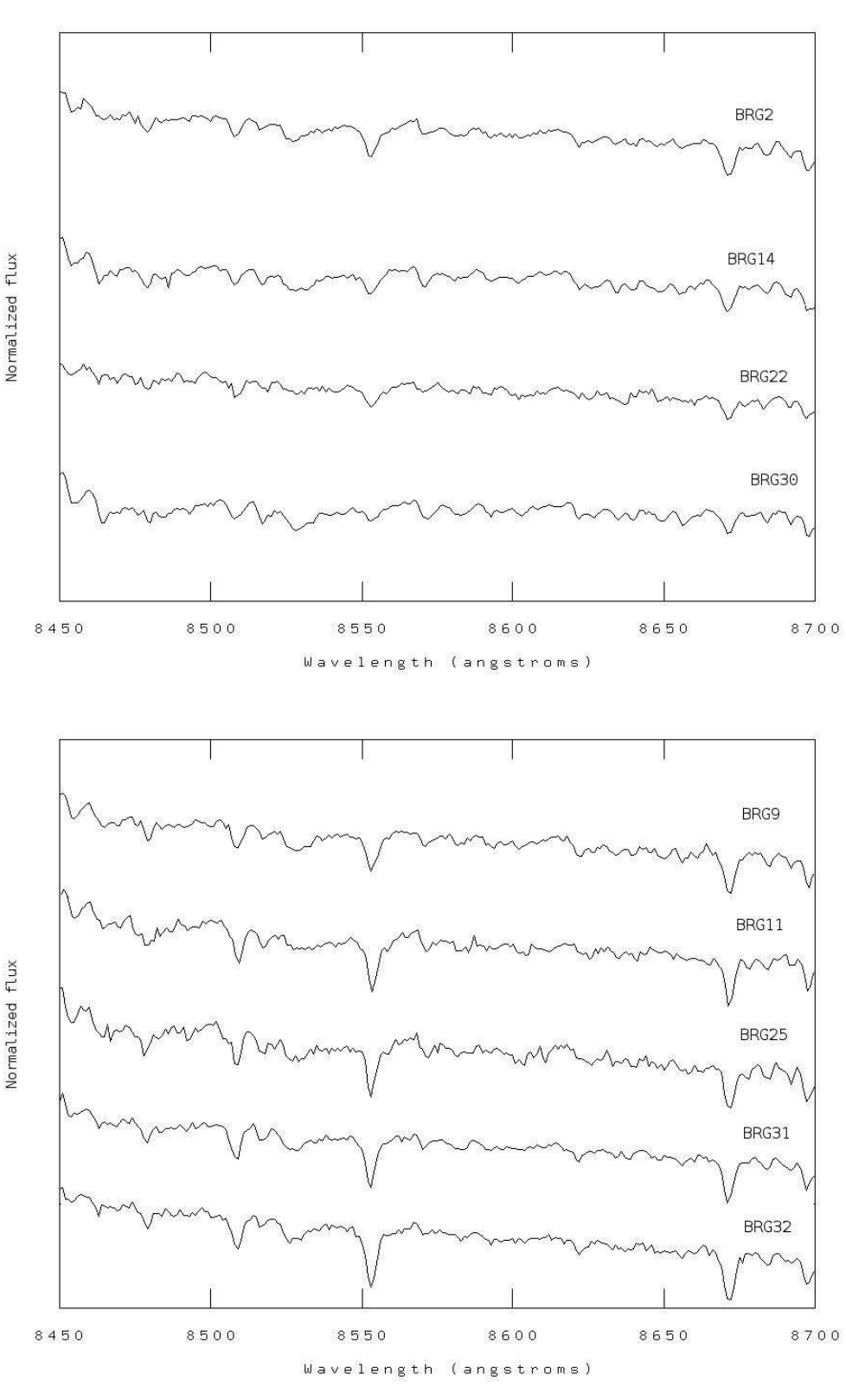

Figure 7.9: A closeup of the CaT lines for Bridge objects BRG2, BRG14, BRG22 and BRG30 (top) and BRG9, BRG11, BRG25, BRG31 and BRG32 (bottom). Each figure is shown on the same wavelength scale with flux values normalized to represent the different CaT line strenghts of different objects.

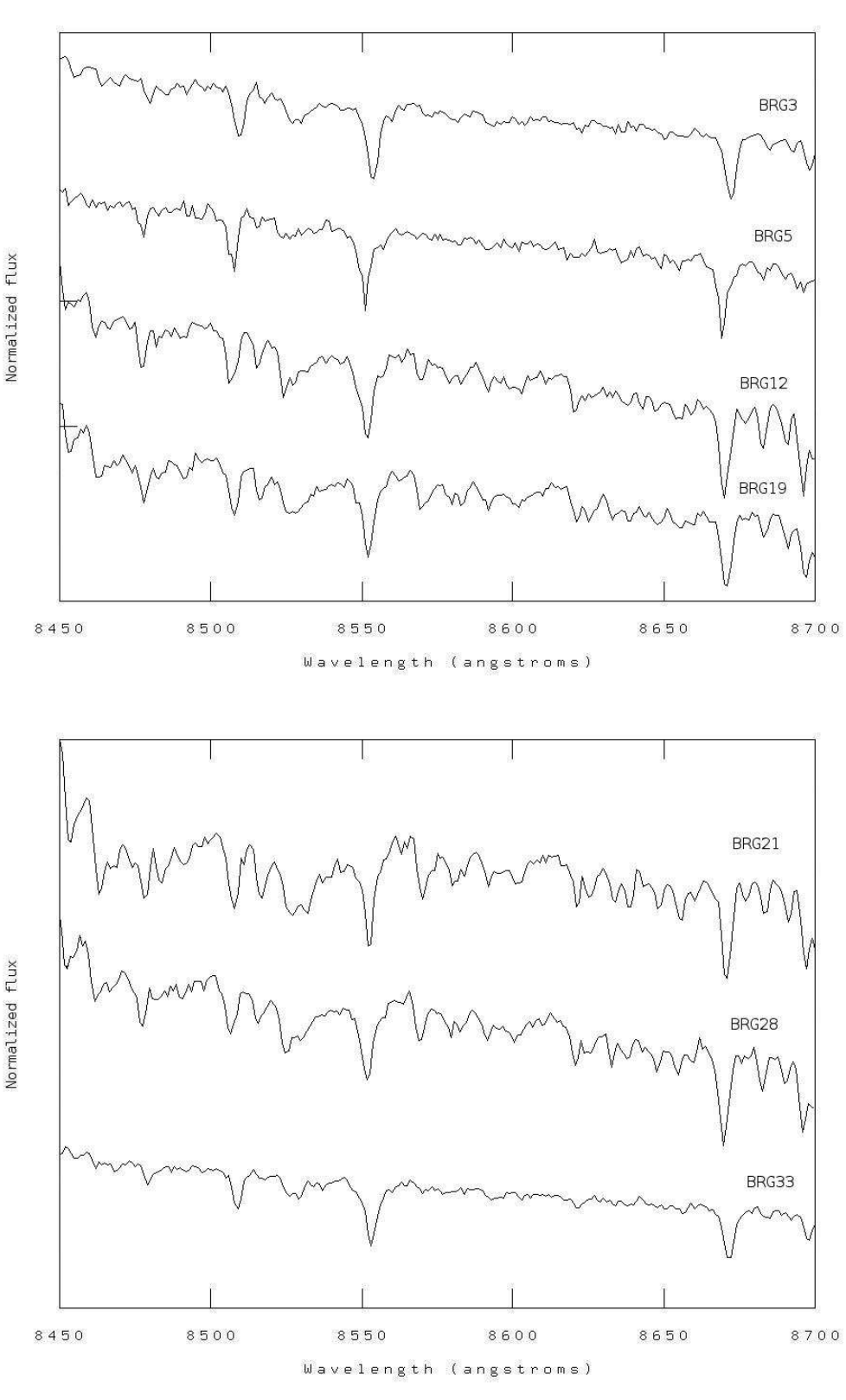

Figure 7.10: A closeup of the CaT lines for Bridge objects BRG3, BRG5, BRG12 and BRG19 (top) and BRG21, BRG28 and BRG33 (bottom). Each figure is shown on the same wavelength scale with flux values normalized to represent the different CaT line strenghts of different objects.

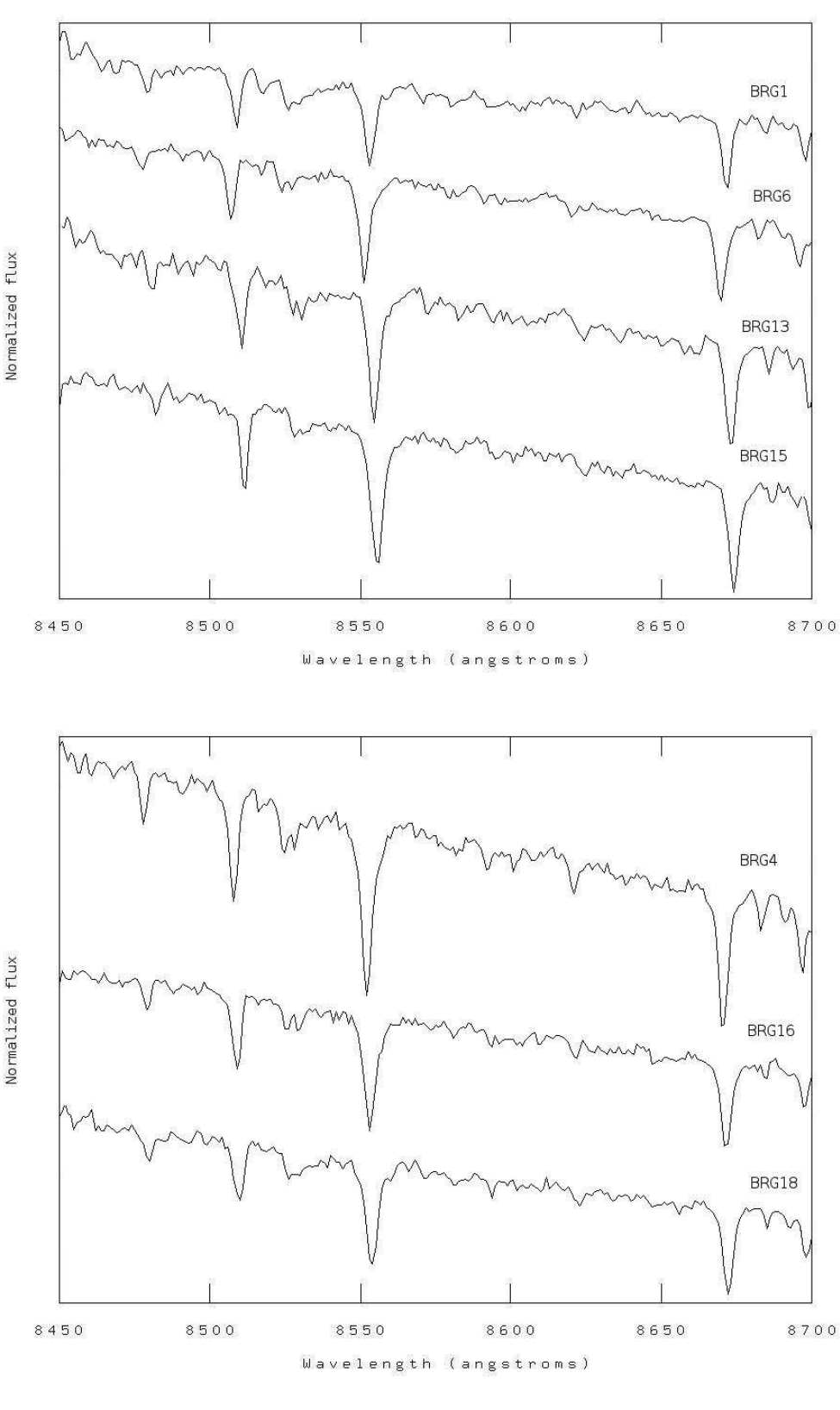

Figure 7.11: A closeup of the CaT lines for Bridge objects BRG1, BRG6, BRG13 and BRG15 (top) and BRG4, BRG16 and BRG18 (bottom). Each figure is shown on the same wavelength scale with flux values normalized to represent the different CaT line strenghts of different objects.

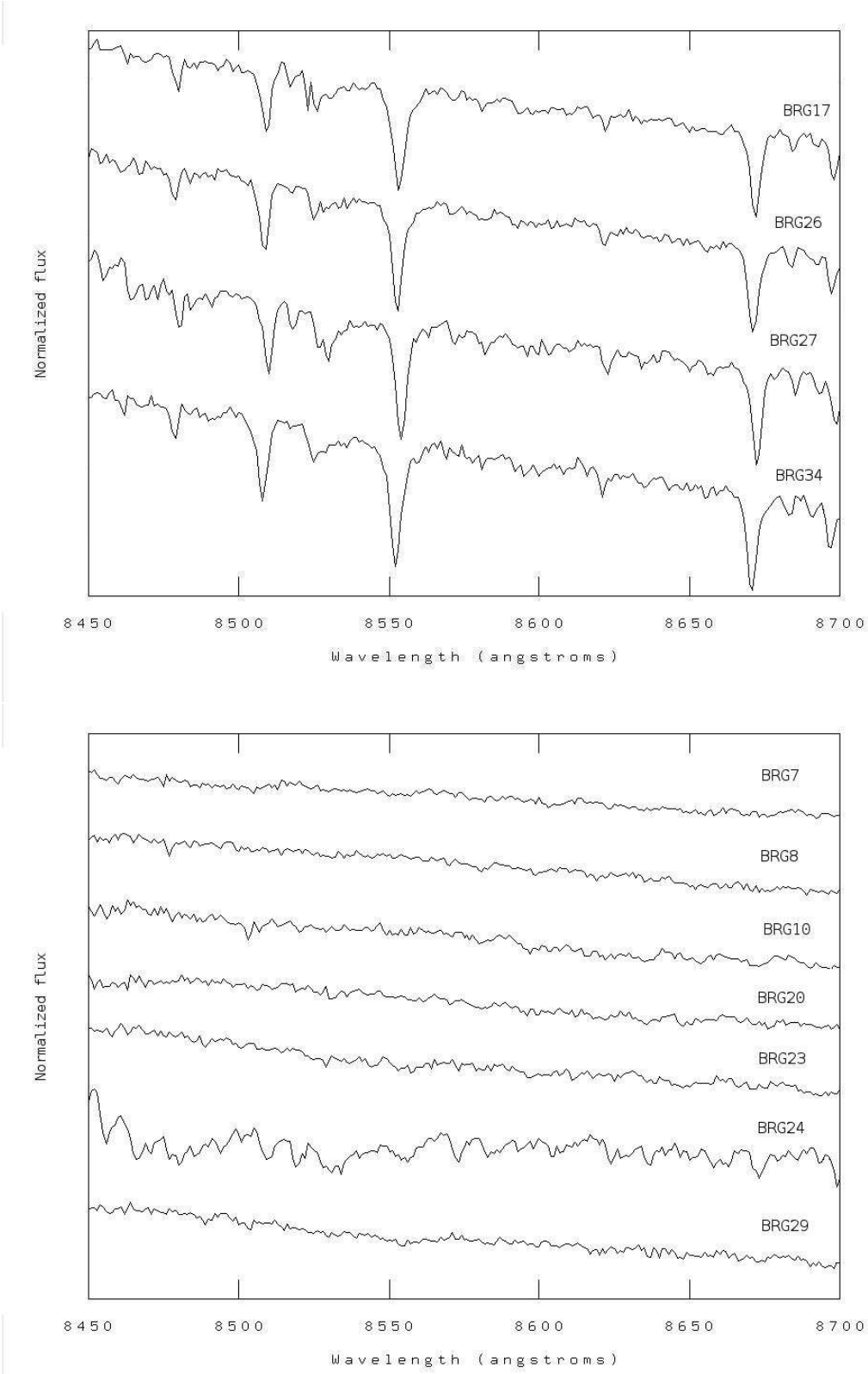

Figure 7.12: A closeup of the CaT lines for Bridge objects BRG17, BRG26, BRG27 and BRG34 (top) and the very metal poor objects BRG7, BRG8, BRG10, BRG20, BRG23, BRG24 and BRG29 (bottom). Each figure is shown on the same wavelength scale with flux values normalized to represent the different CaT line strenghts of different objects.

added in quadrature and are less than 0.1 mag for each object.

Following Parisi et al. (2010a) a value of β was calculated as the gradient of the isoabundance line (chosen to lie at [Fe/H] = -1.0 corresponding to the mean SMC value) in the $I - I_{HB}$ vs ΣW graph, as this is how the value of β was chosen for $V - V_{HB}$ (Fig. 7.8). The SMC value was chosen as it is generally accepted that the Bridge formed primarily from the SMC (Chapter 2). To check how the β value depends on the adopted metallicity, the value of β was recalculated using the LMC metallicity from Grocholski et al. (2006). The results for beta showed that $\beta_{SMC} = 0.83$ and $\beta_{LMC} = 0.73$ however, once metallicity values were obtained for the Bridge objects, it became clear that the large spread of metallicities calculated, meant that the SMC value for β was not the most suitable value to use, as the SMC metallicity range is much smaller than the Bridge here. The Bridge β value was calculated by performing a linear regression with metallicity as a free parameter for different ranges of ΣW as a with objects grouped by their metallicity. From this analysis, the values of beta were calculated to be 0.09, 0.48, 0.68, 0.87 and 1.07 for [Fe/H] values of < -2.0, -2.0 to -1.5, -1.5 to -1.0, -1.0 to -0.5 and > -0.5 dex respectively with errors of ± 0.62, ± 0.13, ± 0.30, ± 0.35 and ± 0.24.

Once the values of W' had been calculated for each object, the calculation of the metallicity was carried out using the equation [Fe/H] = $(-2.966 \pm 0.032) + (0.362 \pm 0.014)W'$ (Parisi et al., 2010a). The error on [Fe/H] was calculated at each step of the process of determining the final values incorporating the errors from ΣW, β and $I - I_{HB}$ into the final equation for [Fe/H], with a combined error of 0.6, 0.2, 0.3, 0.4 and 0.2 dex for metallicity bins of < -2.0, -2.0 to -1.5, -1.5 to -1.0, -1.0 to -0.5 and > -0.5 dex respectively, which is dominated by the errors in the EWs. It should be noted that this process has been carried out using just the two strongest CaT lines and yields very similar results.

7.4 Results

The values for the RVs and metallicities of each of the 34 Bridge objects are presented in Table 7.1. The average RV for the objects is 351 km s^{-1} with the range from $\sim 300-395$ km s^{-1} and [Fe/H] $= -0.30$ to -1.92 dex with an average of [Fe/H] $= -0.98$ dex (without the very metal poor stars). The LMC mean metallicity and range of RV values are -0.48 dex (Rolleston et al., 2002) and $\sim 200-300$ km s^{-1} (van der Marel et al., 2002) respectively, with a global mean metallicity of -1.0 dex (Parisi et al., 2010b) and RV range of $\sim 150-200$ km s^{-1} (De Propris et al., 2010) for the SMC. The majority of MW stars have RV values of up to ~ 100 km s^{-1} (Bilir et al., 2012), with few halo stars having higher values. The first conclusion that can be drawn from the results is that all of the candidate Bridge objects are very likely to be Magellanic Cloud members due to their high RV values. Each star was also given a rough spectral class using the standard stellar spectra from Danks and Dennefeld (1994) which revealed that the objects are late K-type objects.

7.4.1 Radial velocities

Assigning a membership for each of the Bridge objects to either the LMC or SMC proves somewhat difficult here as the RV values are higher than expected for the SMC and most are also higher than the LMC values (Fig. 7.13), even though the Bridge is thought to have been formed from gas and stars drawn in from the SMC. The data reduction method and flux calibration were checked to ensure that no mistake had been made in the process of obtaining the RV values for the candidate Bridge objects.

It is possible that the Bridge stars have been drawn into the Bridge tidally from the SMC towards the LMC, and that the tidal force on the objects has caused the RV to increase. A simple calculation was carried out, assuming that the angular distance between the outer regions of the Clouds is $\sim 10^{\circ}$ (Chapter 2), to estimate

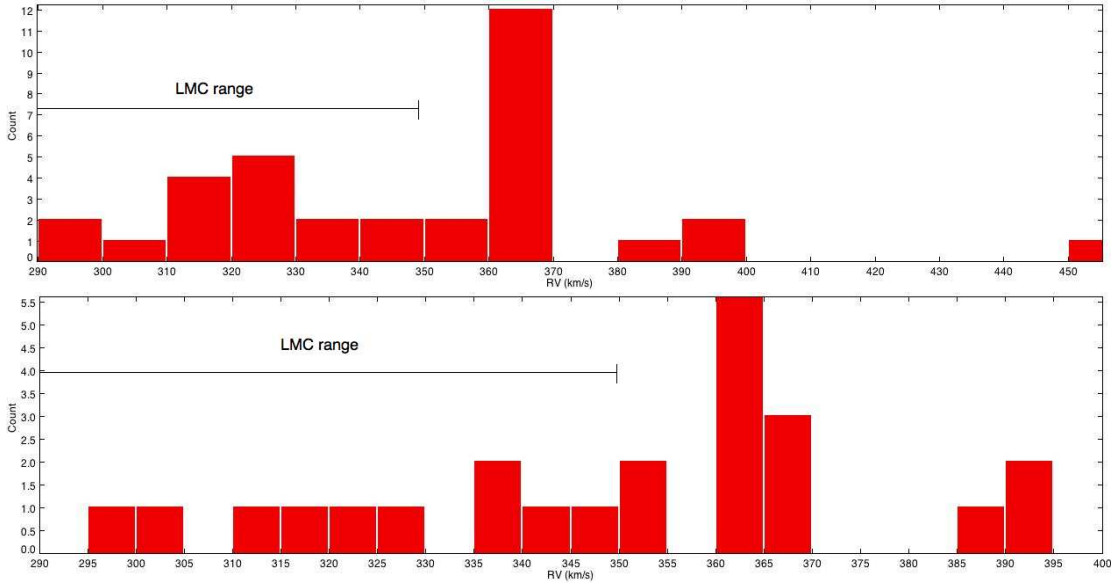

Figure 7.13: Histograms showing the range of values of RVs for the whole sample (top) and without the very metal poor stars (bottom) for the Magellanic Bridge objects.

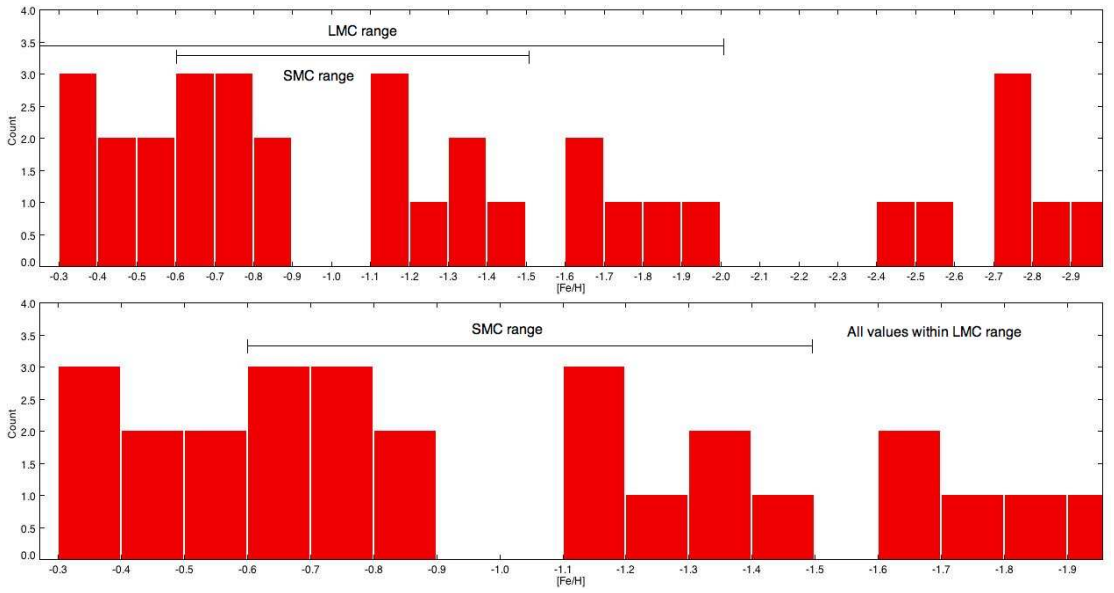

Figure 7.14: Histograms showing the range of values of [Fe/H] for the whole sample (top) and without the very metal poor stars (bottom) for the Magellanic Bridge objects.

the differential velocity required for a star to be drawn from the outer SMC to the outer LMC over the timescale of the estimated age of the Bridge (250 Myr) with an average distance of the Magellanic Clouds of 55 kpc. The results show that the maximum increase in velocity required is ~ 40 km s^{-1} for a star to migrate from the SMC to the outer LMC. Although this is an estimate of the radial velocity, it gives an indication of the amount of acceleration stars have experienced. Based on this calculation, it is possible that approximately half of the stars in the Bridge here, could have had SMC RV values prior to the tidal interaction between the Clouds. If we consider the errors calculated on the RV values, it is also possible that the error of ± 12 km s^{-1} are effecting the final RV values and this combining these two factors, some RV values could be over-estimated by ~ 50 km s^{-1}. If this is the case, half of the Bridge objects have RV values that place them outside of the MW in the Magellanic Clouds, within the LMC RV range. There are ongoing studies (North et al., 2009) of the depth of the SMC which is thought to be up to ~ 66 kpc away at the far side, which could also have an effect on the objects stripped to form the Bridge, if the SMC was disrupted tidally by the LMC enough to tear it into two parts Mathewson (1985), this process could have also had an effect on the RVs of outer SMC objects which then migrated into the Bridge.The lack of available RV standards for Bridge red giants means that it is not possible to confirm that these values are correct.

7.4.2 Metallicities

It can be seem from Fig. 7.14 that three distinct metallicity regimes appear to exist in the Bridge within the range of the Magellanic Clouds, which is not reflected in the RV values. The values of [Fe/H] for the LMC have a greater range than those of the SMC so it is difficult to confirm which Cloud the objects belong to.

The average [Fe/H] for the Bridge stars without the very metal poor stars, is -1.05 dex which corresponds to that of the SMC as determined by Parisi et al.

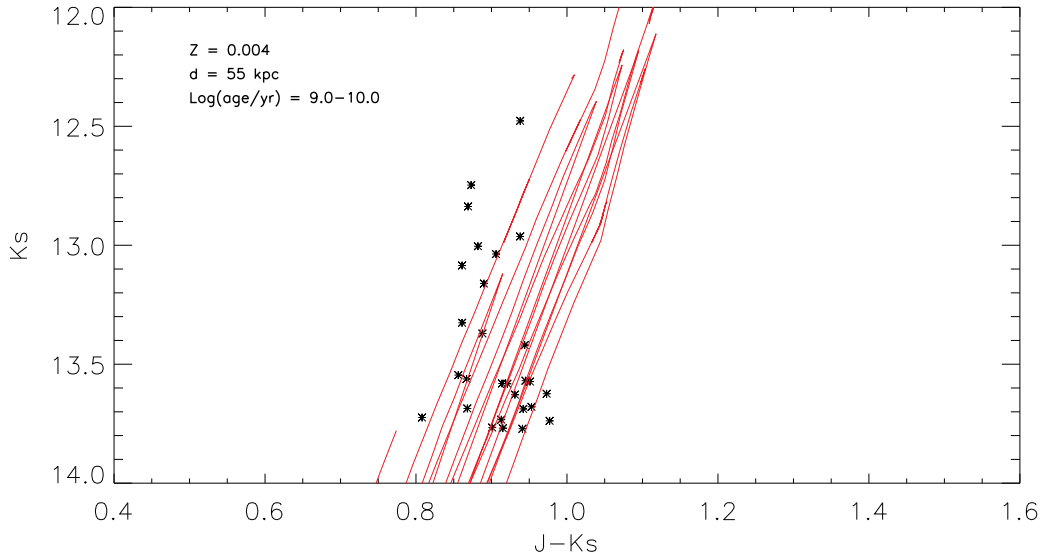

Figure 7.15: $(J - K_s)$ vs K_s CMD of the final Bridge target objects with Padova isochrones overlaid to show the ages of the Bridge objects.

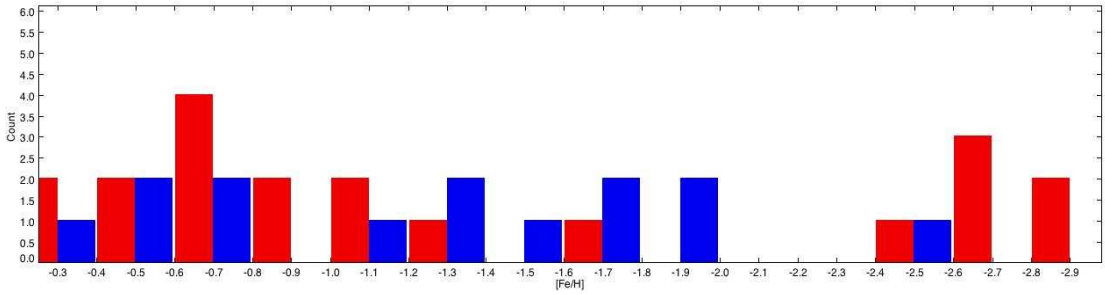

Figure 7.16: A histogram showing the different metallicity values for Bridge objects older (red) and younger (blue) than 3 Gyr.

(2010b). However, the lowest SMC values in that study reach just -1.5 dex and the Bridge values go down to ~ -2.0 dex and below (for the extremely metal poor objects), which corresponds to the lower LMC values (Grocholski et al., 2006). It is also possible however that the metallicity of the Bridge stars is lower than the SMC as these objects would have been stripped from the outer regions of the SMC where lower metallicity objects are likely to reside. Figure 7.15 shows a comparison of the Bridge objects with isochrones, indicating that their ages range from 1 Gyr to 10 Gyr, i.e. that the objects are all older than the most recent tidal interaction between the Clouds.

Fig. 7.16 shows the metallicity histogram for the Bridge objects which have

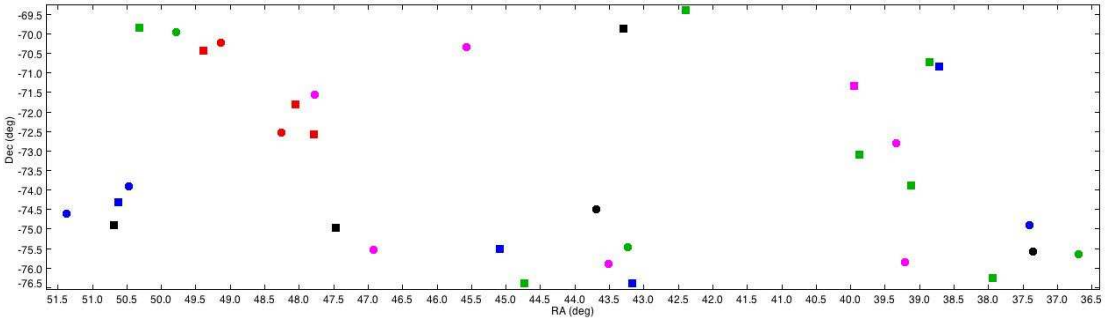

Figure 7.17: The spatial distribution of the Bridge objects categorised into [Fe/H] ranges of −2.0 or poorer (pink), −2.0 to −1.5 (red), −1.5 to −1.0 (blue), −1.0 to −0.5 (green) and −0.5 or greater (black), with RV ranges of $290 - 350$ km s^{-1} (circles) and 350+ km s^{-1} (squares). The SMC is to the right and LMC to the left.

been split into a younger and older sample, representing the mid-point between the isochrones in Fig. 7.15, and also this is the rough age of the first encounter between the Clouds. It can be seen from Fig. 7.16 that the objects younger than ~ 3 Gyr generally have lower metallicities. It is possible that these objects were formed from metal poor gas within the Bridge drawn in from the first encounter between the Clouds. The objects in the centre of Fig. 7.16 are likely to have formed in the SMC as they represent SMC metallicity values, with the objects on either side of this range (and some within) likely to belong to the LMC. The older, more metal poor objects on the right hand side of Fig. 7.16 could be LMC halo objects that have been drawn into the Bridge. It is assumed that the LMC has a stronger tidal force on the SMC, however it is also possible that LMC stars have been drawn into the Bridge. All of the metallicity values presented here are within the Magellanic Cloud range, apart from the few very metal poor objects. The stars presented here have a wide range of metallicities for both young and old objects, indicating that they could have formed within the Bridge gas or from the Clouds.

7.4.3 Membership

The spatial distribution of objects can be studied in terms of their [Fe/H] and RV as presented in Fig. 7.17. It can be seen here that there does not appear to

be a pattern in the spatial distribution of the Bridge objects in terms of [Fe/H] and RV between the Clouds. The red objects with [Fe/H] = −2.0 to −1.5 dex appear to reside on the LMC side of the Bridge which is expected as these values correspond to the LMC values. The pink objects represent the very metal poor stars and these objects are concentrated in the more central region of the Bridge and possibly have formed from metal poor gas drawn into the Bridge in the first encounter between the Clouds. Most of the objects on the SMC side of the Bridge have [Fe/H] values between −1.5 to −0.5 dex which corresponds to the values for SMC stars.

7.4.4 Very metal poor objects

Of the 34 objects, 6 appear to have much lower [Fe/H] values that also lie outside of the range for the Magellanic Clouds ($BRG7$, $BRG8$, $BRG10$, $BRG20$, $BRG23$, $BRG24$ and BRG29. The RV and metallicity values of these objects were determined by fitting the CaT lines in *splot* individually, opposed to the rest of the objects with the CaT lines fitted simultaneously, due to the inability to locate the CaT from the spectra of these objects without refining the spectral range of *splot* to cover one line at a time. The spectra of these objects can be classified as late-K type stars as with the other objects, although with less absorption lines. These objects have magnitudes within the range of the sample, and are not the faintest objects, indicating that they are metal poor opposed to having noisy spectra. In this case the RVs and EWs were obtained as above. The upper limits obtained for [Fe/H] for these objects range from −2.93 dex to −2.48 dex which are much lower than the lower limit for the LMC values. These values lie outside the range of [Fe/H] = −2.2 to −0.5 used by Carretta and Gratton (1997) to calibrate the ΣW / [Fe/H] relation and should be taken with caution. Since the curve of the growth implies that these lines are becoming more sensitive to metallicity for the metal poorest stars, they may not be as metal poor as indicated by the upper limits given in Table 7.1. However, it is safe to assume that their [Fe/H] values are

well below −2.0. Improved estimates would require a detailed model atmosphere analysis. Each of these objects has a RV value that is consistent with belonging to the Magellanic Clouds. It is possible that due to the lower S/N of these objects that they may not be reliable. A visual inspection of some of these objects in the VMC catalogue does indicate however that they appear to be of stellar origin.

Table 7.1: Magellanic Bridge candidates with RV and [Fe/H] values

Bridge candidate	[Fe/H]	$\sigma_{Fe/H}$	RV (km s^{-1})
BRG1	−0.6	0.4	364
BRG2	−1.2	0.3	361
BRG3	−0.3	0.2	366
BRG4	−0.6	0.4	317
BRG5	−0.4	0.2	300
BRG6	−0.8	0.4	323
BRG7	−2.6	0.6	329
BRG8	−2.8	0.6	312
BRG9	−1.4	0.3	364
BRG10	−2.4	0.6	293
BRG11	−0.4	0.2	340
BRG12	−1.5	0.2	304
BRG13	−1.2	0.3	395
BRG14	−1.1	0.3	349
BRG15	−0.3	0.2	452
BRG16	−0.5	0.4	366
BRG17	−0.6	0.4	368
BRG18	−0.9	0.4	388
BRG19	−1.2	0.3	327
BRG20	−2.9	0.6	318
BRG21	−1.8	0.2	339
BRG22	−1.9	0.2	360
BRG23	−2.8	0.6	362
BRG24	−2.5	0.6	351
BRG25	−1.6	0.2	362
BRG26	−0.8	0.4	351
BRG27	−1.4	0.3	395
BRG28	−1.7	0.2	313
BRG29	−2.8	0.6	324
BRG30	−1.7	0.2	361
BRG31	−0.8	0.4	350
BRG32	−0.7	0.4	362
BRG33	−0.6	0.4	362
BRG34	−0.6	0.4	343

7.5 Summary

Out of 34 candidate Bridge objects observed with FORS2, all of the objects can be confirmed to belong to the Magellanic Cloud System as they have RV values that do not correspond to MW objects and their spectra indicate that they are K-type objects which rules out that they could be background galaxies. This confirms that the strict selection criteria described in Chapter 4 produced a very clean sample of Magellanic Cloud objects. The five objects with very low metallicities should be studied in more detail as it is possible that they are stars that lie within the outer halo of the LMC with very low metallicities, as they have RV values consistent with the LMC values. It is thought that the Bridge was formed from the SMC tidally during one of two close encounters between the Clouds (Chapter. 2). The results of the spectroscopic work do not indicate that the Bridge objects here belong to the SMC as they have a broader range of [Fe/H] values (which does however have a mean value corresponding to the SMC), and higher RV values than would be expected from an SMC star. This does not necessarily rule out SMC origin of these objects however, as it is possible that the tidal force on these objects has caused an increase in their RVs as they have migrated from the SMC towards the LMC.

There are also other possible Bridge formation scenarios that could explain the higher RV values calculated in this work. It is possible that a larger portion of gas and stars were drawn into the Bridge from the LMC than previously considered. This work has confirmed that all of the candidate Bridge objects analysed here belong to the Magellanic Cloud System. However, these objects are just 34 of ~ 200 unknown candidate older Bridge objects presented in Chapter 5, with many more objects of various ages presented in Chapter 6. Future work could be carried out in determining the extent that the continuum of the spectra influences the EWs of the CaT lines. A study of the this effect on the metallicity could include deriving abundances based on one or two of the CaT lines. It is possible that some AGB stars are included in the Bridge sample which are strongly affected by molecular

absorption that may influence one or more CaT lines. A full spectroscopic study is required of Magellanic Bridge objects in order to quantify the effect of the tidal interaction between the LMC and SMC and to confirm membership of the Bridge objects to either Cloud.

Chapter 8

The Magellanic Stream

This chapter focuses on the search for a stellar population within the Magellanic Stream in the direction of the two VMC observing tiles. The existence of a stellar counterpart to the gaseous Magellanic Stream will aid in the production of accurate models to describe the formation of the Stream and in turn, the past interaction history of the LMC and SMC with each other and also the Milky Way. To date, the Magellanic Stream has no observed stellar population. If the Stream was formed from a tidal interaction between the Magellanic Clouds and the Galaxy, some form of stellar population would be expected. If there remains no detection of stars in the Stream after deeper observations, this may imply a different formation mechanism of the Stream which should be investigated.

The detection of a young population in the Magellanic Stream would give an insight, in terms of the membership of these stars, to the creation of the Stream in terms of where the Stream material originated from. However, the detection of an older population in the Stream would likely have stronger implications as it could indicate the presence of tidal forces in the creation of the Stream, and would constrain the process of Stream formation as well as the origin. The confirmation that the Stream does not contain a stellar component would also be an important result, especially from the analysis of the deeper VMC survey, as a non-detection would aid in constraining the Stream formation mechanism.

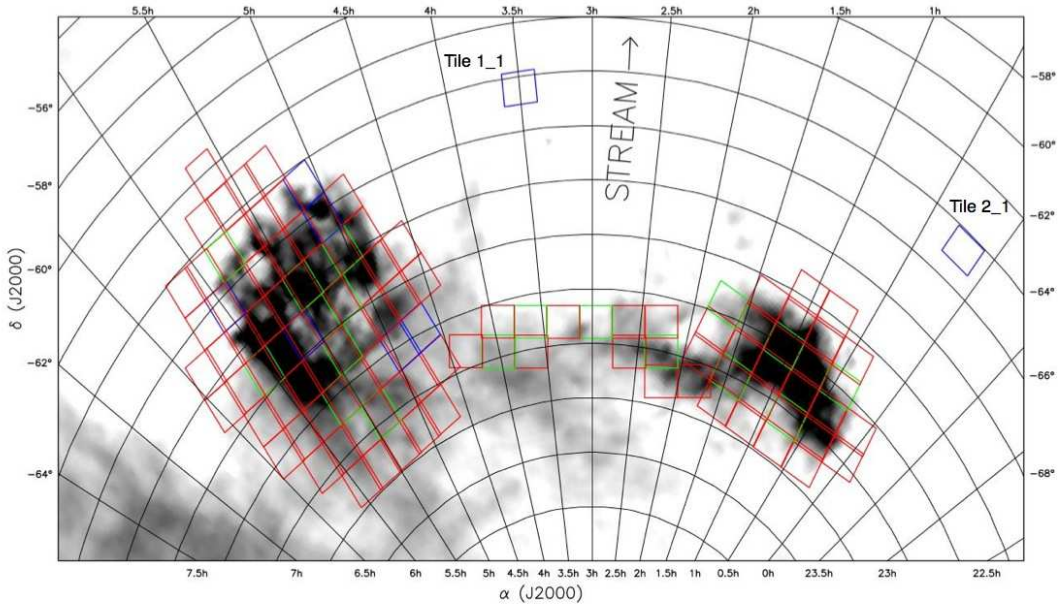

Figure 8.1: Fig. 2 from Cioni et al. (2011) of the VMC observing tiles in the direction of the Magellanic Clouds overlaid on the HI distribution (McClure-Griffiths et al., 2009). The two Stream tiles can be seen above the SMC (top right) and the Magellanic Bridge (top centre). See Cioni et al. (2011) for an explanation of the different tile colours.Note that this figure includes only the gas covering the Clouds.

8.1 Catalogues

The aim of this work is to establish source catalogues in the region of the Magellanic Stream from the VMC and SuperCOSMOS surveys (Chapter 3) to search for the existence of a candidate Stream stellar population.

From previous studies of the Magellanic System with e.g. HST, DENIS, 2MASS, the global picture of the system is still incomplete. This work makes use of the VMC survey catalogues as they are the deepest NIR catalogues available and supersede 2MASS and DENIS. The filters chosen for the VMC survey will allow various CMDs and colour-colour diagrams to be created and will enable a good characterisation of populations within the Magellanic Clouds. Combining the VMC survey with wide spectroscopic and optical photometric surveys, will increase our understanding of the Magellanic System.

The VMC survey observed two tiles in the Stream (Table 8.1) in all three VMC photometric bands (Fig. 8.1). The data for the Stream regions were downloaded

from the VSA, with different flags applied to clean the catalogues as described in Chapter 3. The VMC tiles in this work were from the VSA data release v20121128, completed in the direction of the Stream.

Table 8.1: Number of stellar objects in each cleaned Stream tile catalogue

Tile	Central co-ordinates	VMC sources	SuperCOSMOS sources
1_1	$03:30:03.40, -64:25:24.88$	$\sim 65,000$	$\sim 28,000$
2_1	$00:11:59.42, -64:39:30.96$	$\sim 75,000$	$\sim 35,000$

In order to carry out a complete search for a stellar population within the Stream, the SuperCOSMOS survey was also studied in the direction of the two VMC tiles to give a comparison, and to be able to analyse catalogues over a larger range of photometric bands as it is possible that there may exist a young or older population within the Stream. Initially these catalogues were created in the direction of the two VMC tiles in order to perform a comparison to the VMC catalogue. The Magellanic Stream is a very large feature ($> 100°$), and it is therefore necessary to use a wide area survey to observe the entire Stream. As this work is the first of this kind, this study is limited to a search for a Stream stellar component in the two tile regions available from the VMC survey. If successful, subsequent work will include the search for stars in other regions of the Stream based on the predictions of various models.

8.1.1 Foreground stars

As discussed in Chapter 4, when observing low density regions such as the Magellanic Stream, the contribution from Galactic foreground stars can not be neglected as they will account for the vast majority of objects observed. This work makes use of the probability foreground removal method for the SuperCOSMOS and VMC catalogues in the direction of the two Stream tiles.

In each catalogue, a CMD was chosen to carry out the Galactic foreground removal by binning objects in colour and magnitude bins of $(B - I)$ vs I in SuperCOSMOS (Fig. 8.3), and $(Y - K_s)$ vs K_s in VMC and UKIDSS to make use

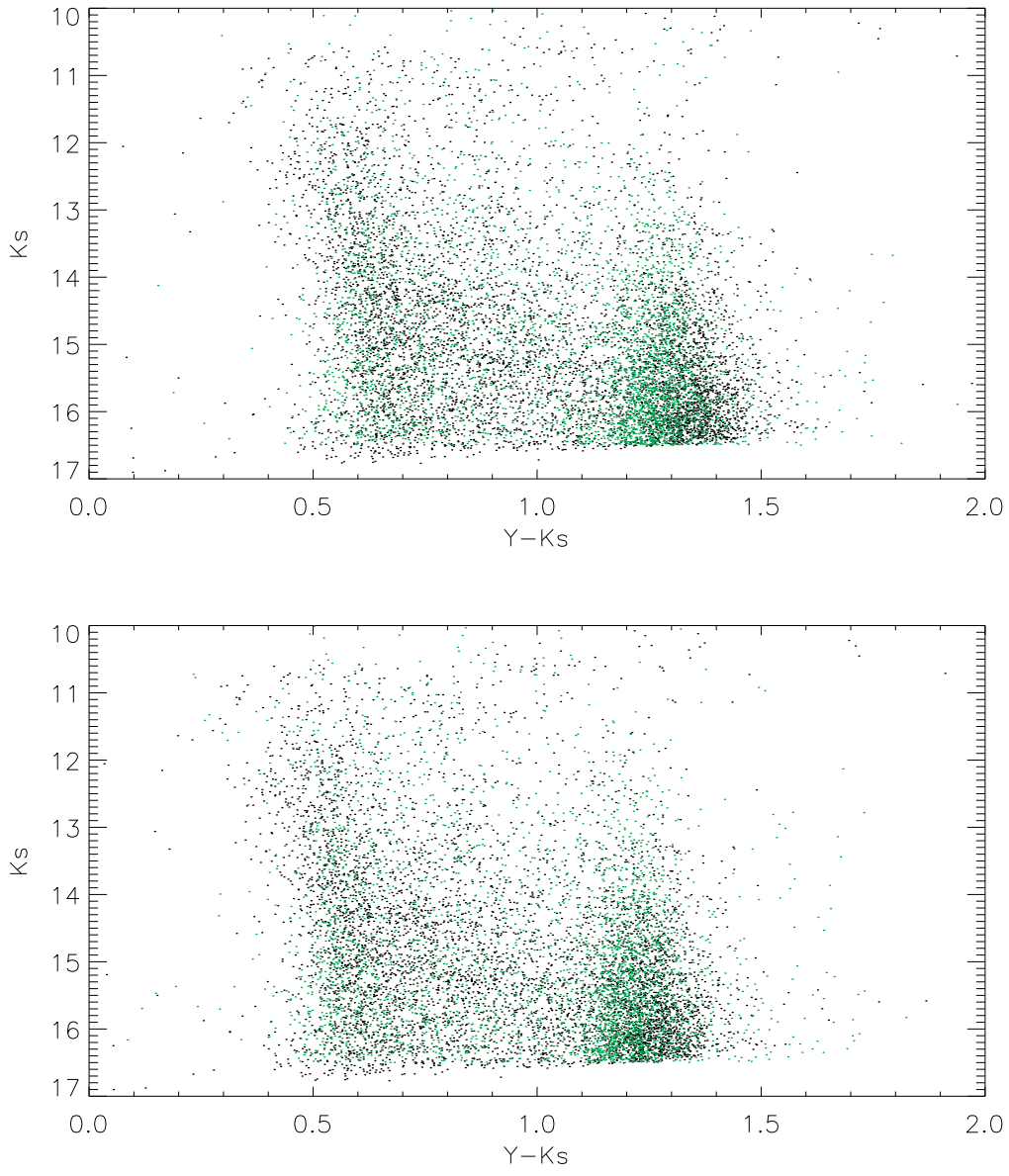

Figure 8.2: CMD, $(Y - K_s)$ vs K_s of the Magellanic Stream tiles 1_1 (top) and 2_1 (bottom), from the VMC catalogue before the removal of Galactic foreground objects (green), and also the chosen Galactic foreground field from UKIDSS (black) prior to the removal of foreground objects.

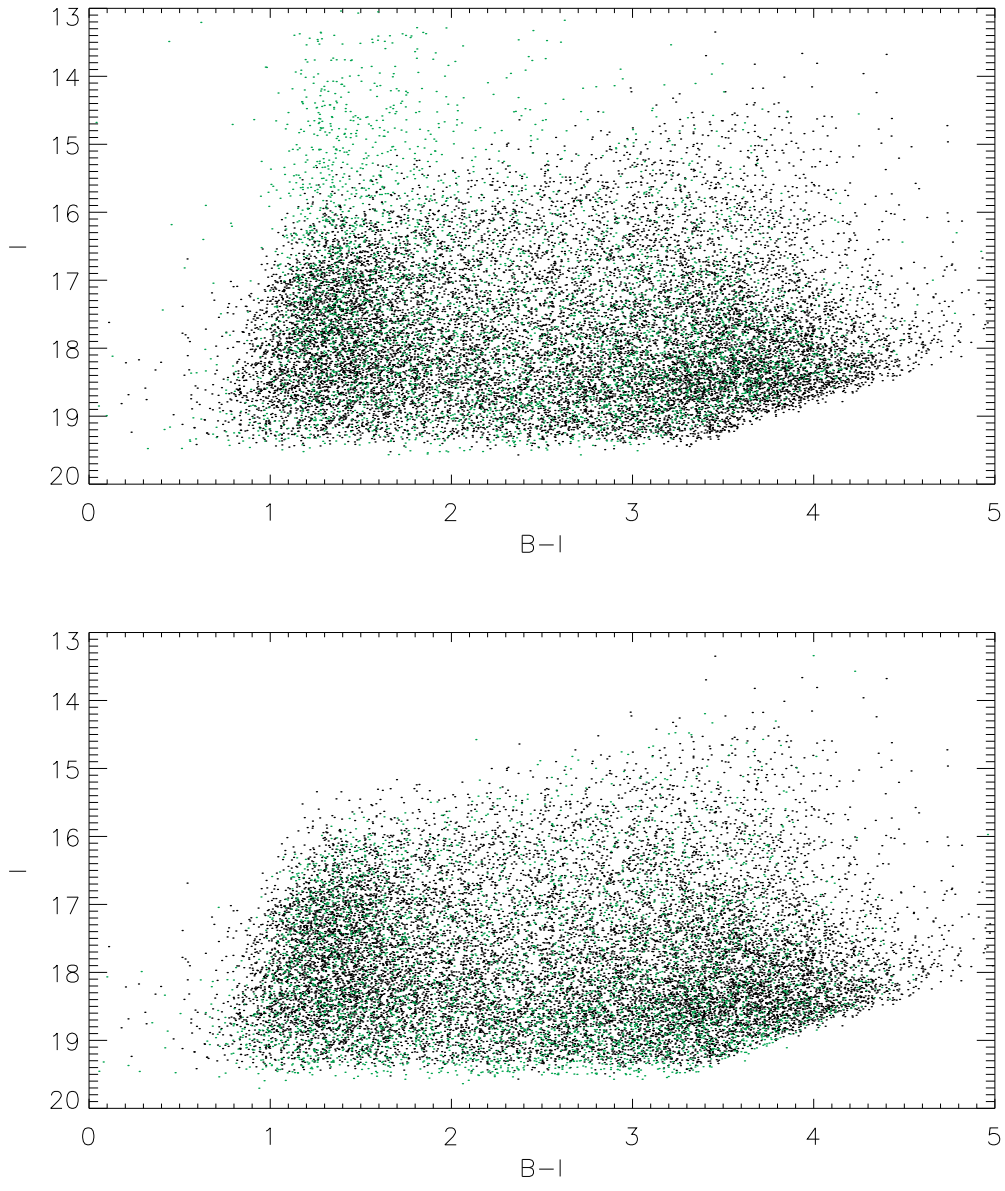

Figure 8.3: CMD, $(B - I)$ vs I of the Magellanic Stream tiles 1_1 (top) and 2_1 (bottom), in SuperCOSMOS before the removal of Galactic foreground objects (green), and also the chosen Galactic foreground field (black) prior to the removal of foreground objects.

of the largest population separations. The bin sizes were chosen to be 0.1×0.5 in colour and magnitude in all cases as this bin size is large enough to contain a reasonable number of objects in each bin (up to 1000 in this case), but small enough to have enough bins with different probabilities to optimise accuracy. Table 8.2 shows the number of objects remaining in each catalogue for the Stream tiles after the removal of foreground objects.

Table 8.2: Stream candidates after foreground removal

Tile	Catalogue	No. of sources remaining (P> 0.75)
1_1	SuperCOSMOS	365
1_1	VMC	0
2_1	SuperCOSMOS	4
2_1	VMC	0

After the Galactic foreground removal was applied to the VMC catalogue using UKIDSS for the two Stream tiles, no Stream stellar candidates remained above statistical errors. For now it appears that there are no candidate redder objects in the Magellanic Stream. The use of UKIDSS in the removal of Galactic foreground in the direction of the Stream from the VMC catalogue does not allow an analysis of the full depth of the VMC catalogue. As no Stream population has been identified to date and this study could hold very important results, an attempt should be made to apply foreground removal to the VMC catalogue using the full VMC depth. Although the population synthesis of TRILEGAL was not accurate enough in this case to be applied to the VMC catalogue, it is possible to use data from other VISTA surveys to use as an offset field for the Stream. The application of other Galactic foreground removal method from the VMC Stream catalogue is explored further below.

The SuperCOSMOS catalogue left just 4 objects in tile 2_1, but a population of 365 candidates in tile 1_1 indicating the presence of a potential stellar counterpart to the Stream. It should be noted that only very few blue, young MS stars candidates are found (Fig. 8.4). The Poisson error on the total number of objects,

$\sqrt{N} = 255$ for the tile 1_1 catalogue, confirming that the candidates here are above statistical uncertainty. It should be noted that all of the objects remaining after the SuperCOSMOS removal occupy the same region of CMD space and due to the lower accuracy of SuperCOSMOS, this will be investigated further in the next section.

8.2 Results

The below describes the analysis of potential Stream candidate objects after the removal of the Galactic foreground population with an estimate of the types of populations present.

8.2.1 SuperCOSMOS

After the removal of the Galactic foreground from the Stream region, there were 365 and 4 objects remaining from the probability (Fig. 8.4) method in tiles 1_1 and 2_1 respectively. It should also be noted that the number of objects remaining in the direction of tile 2_1 after the probability method is below the statistical error on the number of objects in total ($\sqrt{N}$) and are therefore discarded.

The remaining Stream candidates were then plotted alongside a set of Padova isochrones (Girardi et al., 2000) with a distance of 55 kpc and Z = 0.004, to represent the region that tile 1_1 lies in above the Magellanic Bridge (Fig. 8.5). The ages of the best fitting isochrones were $\log(\text{age/yr}) = 7.8 - 8.1$. This would correspond to a young population of stars with ages of $\sim 60 - 125$ Myr. However, longer lived blue MS stars corresponding to this age are not seen in Fig. 8.5.

The remaining objects were also entered into the SIMBAD database and none are known published objects. Most of the candidates lie in a region on the CMD, which is not occupied by any objects in the foreground field (Fig. 8.3). To confirm whether the separation between the objects in the foreground and tile 1_1 is real, the SuperCOSMOS foreground field was compared to other foreground regions to

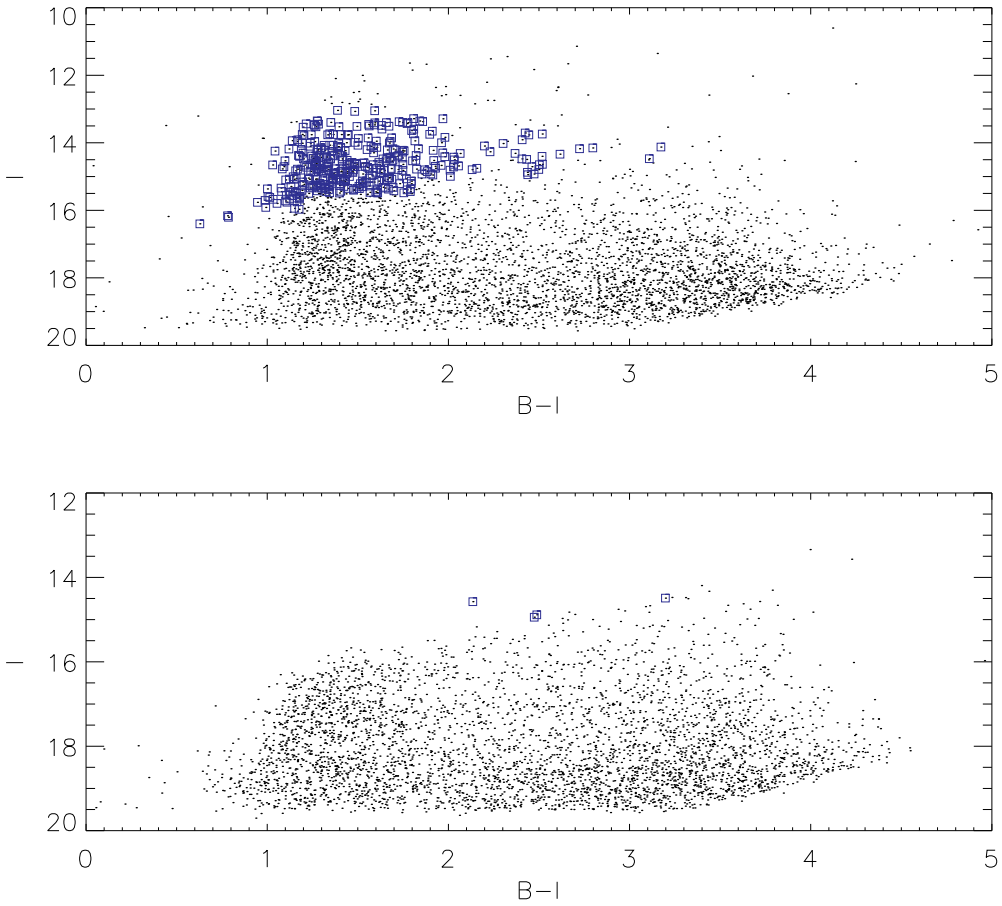

Figure 8.4: CMD, $(B - I)$ vs I of the Stream tile 1_1 (top) and tile 2_1 (bottom) objects from the SuperCOSMOS catalogue, prior to the removal of the Galactic foreground (black) and after the probability method of removal (blue).

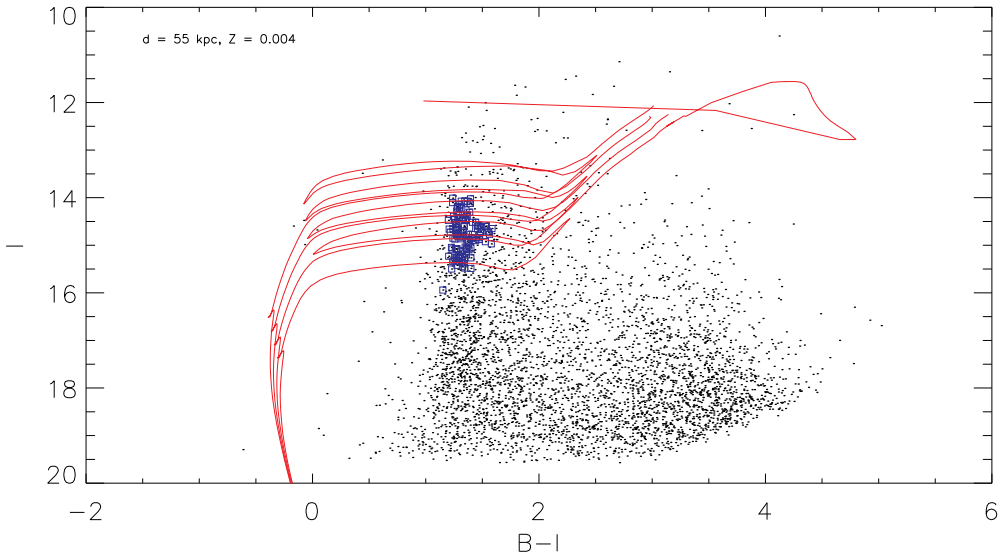

Figure 8.5: CMD, $(B - I)$ vs I of the Stream tile 1_1 prior to the foreground removal (black), with identified Stream candidates (blue), and Padova isochrones (red lines) for stars at the estimated distance of the Magellanic Bridge (55 kpc) with SMC metallicity (Z = 0.004) with a range of ages (log(age/yr) $7.8 - 8.1$).

determine whether the foreground chosen truly represents the Galactic foreground in SuperCOSMOS within normal fluctuations (Fig. 8.6).

The new foreground regions to be examined were chosen to cover the same area as the VMC tiles (and the original foreground field), to calibrate the SuperCOSMOS offset in order to gain confidence in the SuperCOSMOS removal process in the direction of the Stream. The new offset fields lie opposite the Magellanic Clouds across the Galactic plane and again lie at the opposite Galactic latitude (+39°), at two different Galactic longitudes ($\sim 270°$ and $\sim 290°$) sampling the nature of the Galactic foreground in this opposite region. Flags were used as described in Chapter 3 and cuts were applied at $I = 18.5$ to reduce photometric errors. CMDs were created in $(B - I)$ vs I for these new offset regions (Fig. 8.6) which were compared to the original foreground region used, to confirm whether or not the original field accurately represents the SuperCOSMOS foreground, and could be used in this analysis of Magellanic Stream candidates.

It appears in Fig. 8.6 that both of the extra offset fields represent a similar population to the original field used in the foreground removal. The region

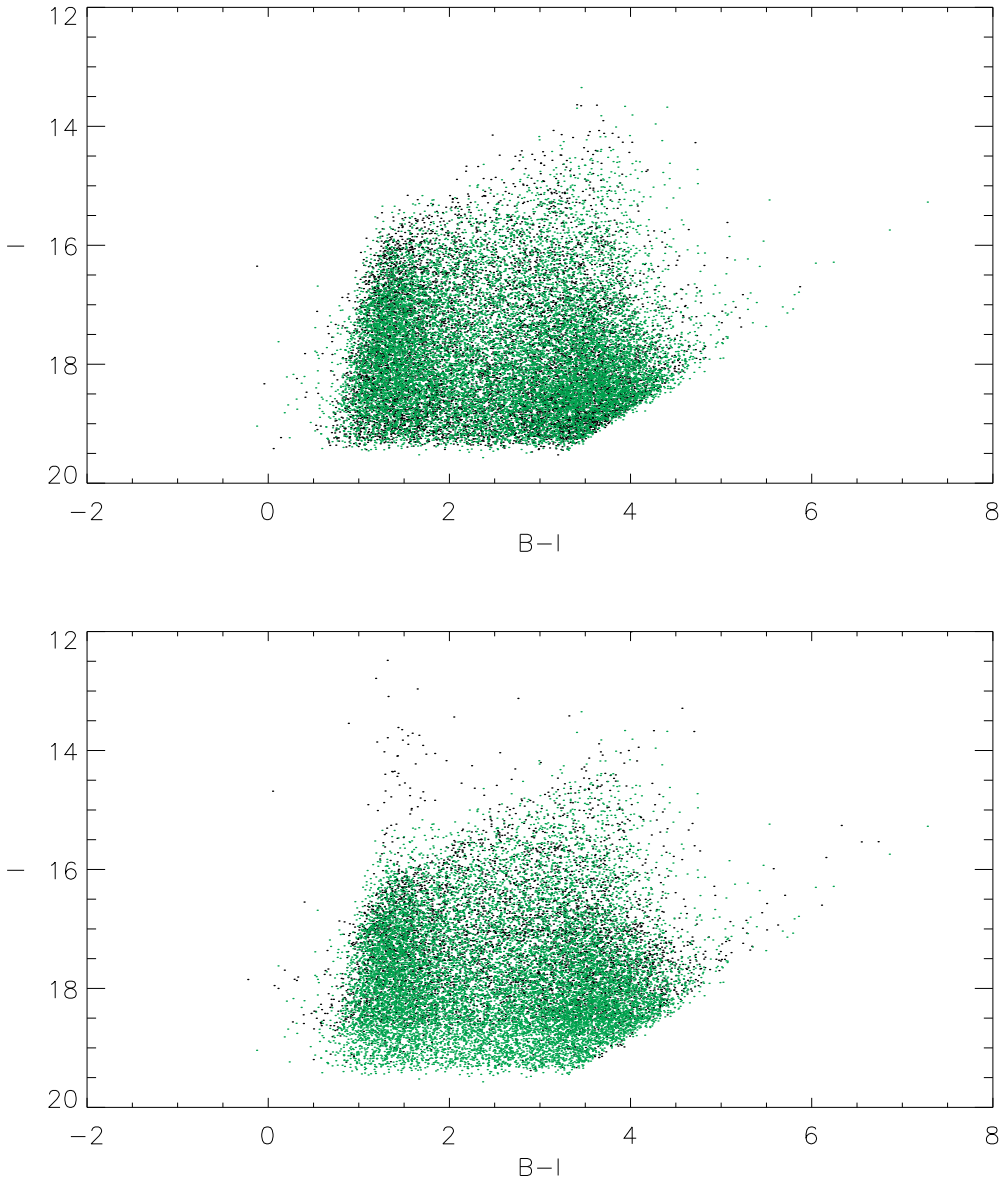

Figure 8.6: CMD, $(B - I)$ vs I of two further offset fields at $l =\sim 270°$ and $l =\sim 290°$ (black, top to bottom), with the same galactic latitude as the original field ($b = +39°$), compared to the original SuperCOSMOS foreground region (green) used in this work.

of interest is the brighter region at bluer colours that show a population in the Stream field 1_1 but not in the original foreground region. The analysis of further foreground regions at different Galactic longitudes confirms that the foreground across this region is mostly uniform with the exception of small fluctuations as explored in Chapter 4 with UKIDSS. The region to the top left of the CMD does show some objects in the bottom panel of Fig. 8.6 although smaller numbers are present here than in the Stream tile 1_1. These objects do not appear to be part of the main foreground population and have magnitudes brighter than expected for background galaxies. Future work to investigate the nature of the foreground would provide more information on the nature of these objects.

For now, the candidate objects from the SuperCOSMOS catalogue are further studies in order to gain insights into the nature of these possible candidate Stream population, within the selected sample. The original candidates were cross matched against other catalogues, and a search in other regions of the Stream was carried out. After cross-matching the 365 SuperCOSMOS Stream candidates to other public catalogues, 180, 179 and 177 of the objects were present in 2MASS, VMC and WISE respectively with 177 of the same objects present in every catalogue. The magnitudes of these objects were presented in CMDs to determine whether they could really be Stream objects.

Figures 8.7 and 8.8 are very interesting as the inclusion of all four catalogues provides different information about these potential Stream candidates. The candidate objects appear to be bright in SuperCOSMOS I band and the 2MASS and VMC $K_{\rm s}$ bands. The objects lie within the expected stellar populations in WISE (but not in a region that would support warm dusty AGB objects) and although one might argue that they are mixed within the foreground population in SuperCOSMOS and 2MASS, they appear to represent a different sequence in the VMC catalogue indicating that they could be candidate Stream objects. Figure 8.9 shows the distribution of the cross-matched Stream candidates from 2MASS, VMC and WISE in RA and Dec. It can be seen here that the objects are evenly

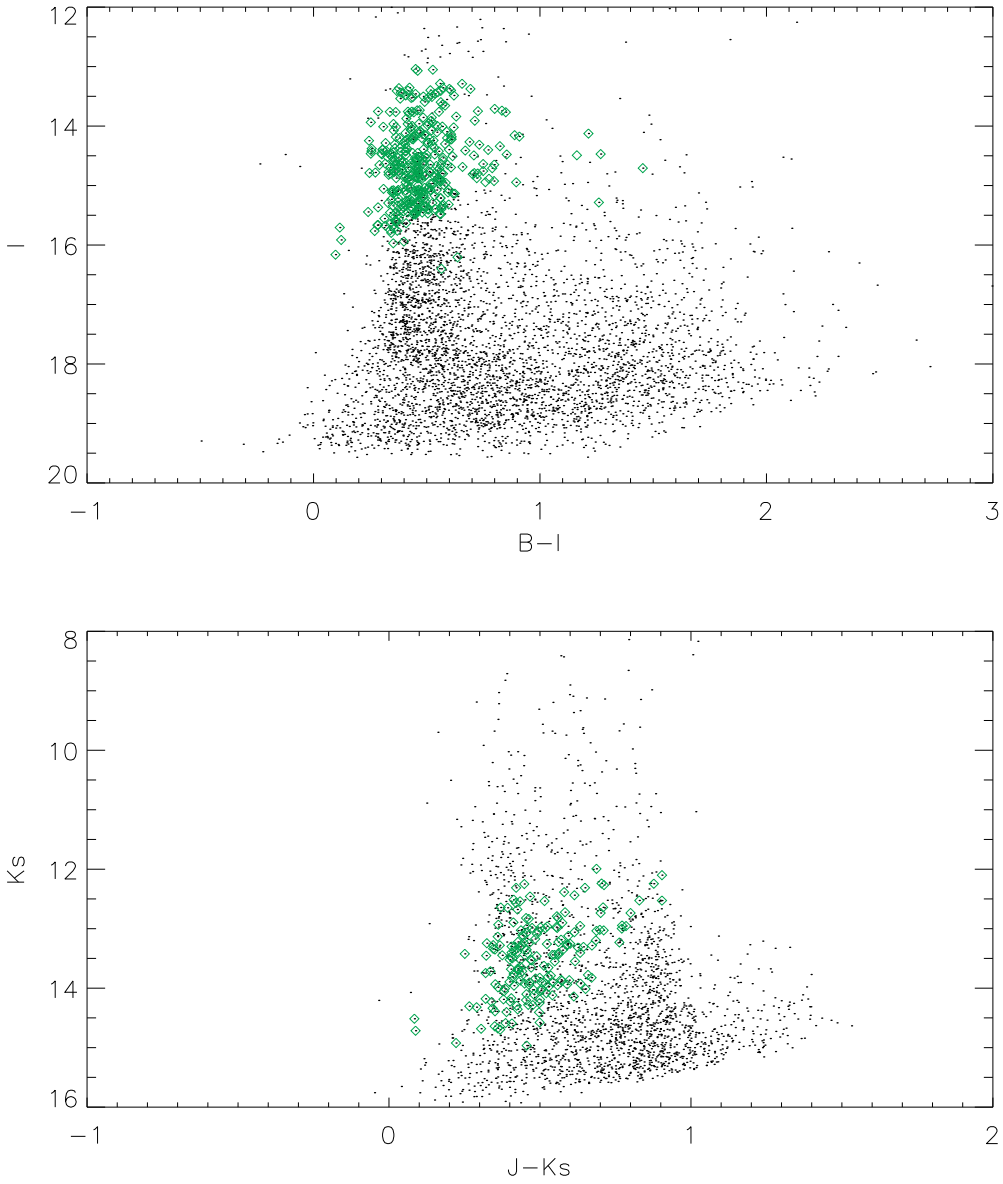

Figure 8.7: Different CMDs, of the 177 Stream candidates (green) present in SuperCOSMOS (top) and 2MASS (bottom) overlaid on the respective full catalogues in the direction of the Stream tile 1_1 (black). The CMDs were chosen to represent the best separation of populations in each catalogue showing the full magnitude depths.

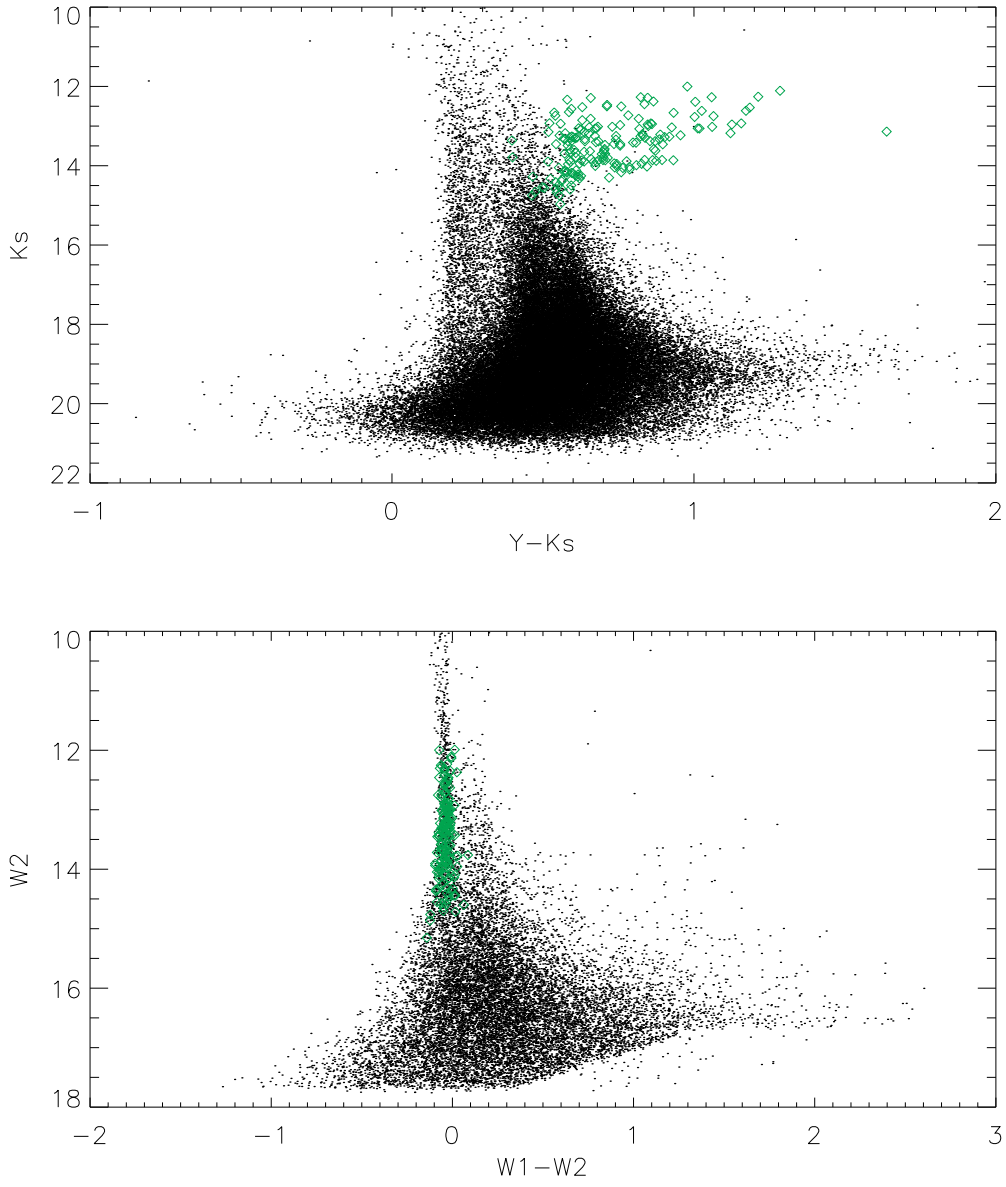

Figure 8.8: Different CMDs, of the 177 Stream candidates (green) present in the VMC catalogue (top) and WISE (bottom) overlaid on the respective full catalogues in the direction of the Stream tile 1_1 (black). The CMDs were chosen to represent the best separation of populations in each catalogue showing the full magnitude depths.

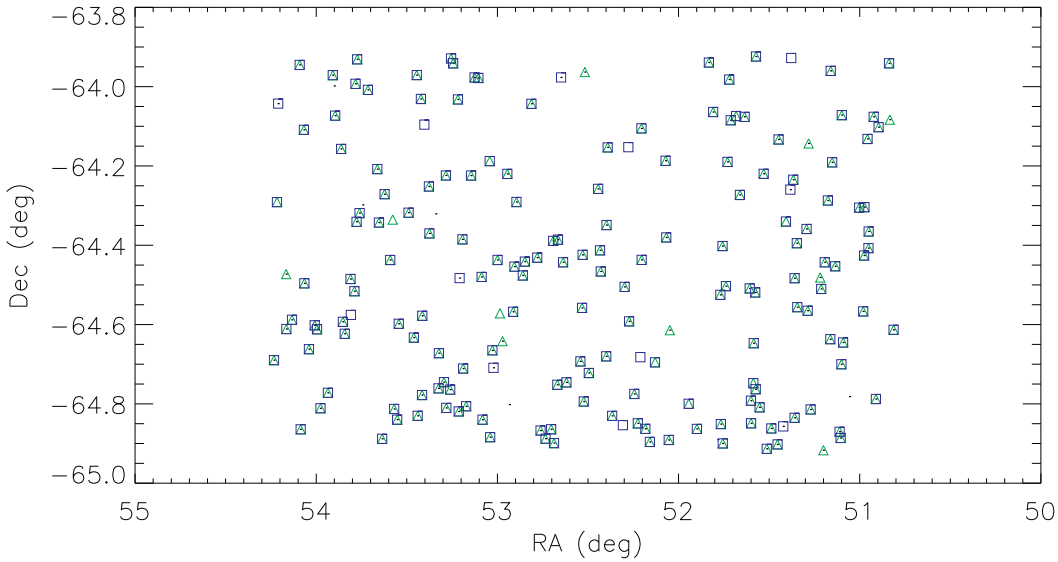

Figure 8.9: The spatial distribution of the SuperCOSMOS stellar candidates within the Stream tile 1_1 after the removal of Galactic foreground cross-matched with 2MASS (black dots), WISE (blue squares) and the VMC catalogue (green triangles).

distributed across the tile which rules out the possibility of a Galactic cluster in the direction of the tile.

It is possible that all of the objects in the SuperCOSMOS CMD covering a small colour and magnitude range, is due to the remaining objects, not present in other catalogues, being non-astronomical features that dominate this region of the CMD. These objects are bright in infrared bands which, with their young postulated ages, could indicate that they are dusty young objects. Upon inspection of a number of these objects in the VMC images, it is possible that they are of a stellar nature. For now it is not possible to confirm whether these are true Stream candidates and follow up spectroscopic observations are required to place these objects at a distance consistent with the Magellanic Clouds.

8.2.2 Analysis of the VMC catalogue

After the application of the removal of the Galactic foreground population using UKIDSS in the direction of the Stream with the probability removal, no ob-

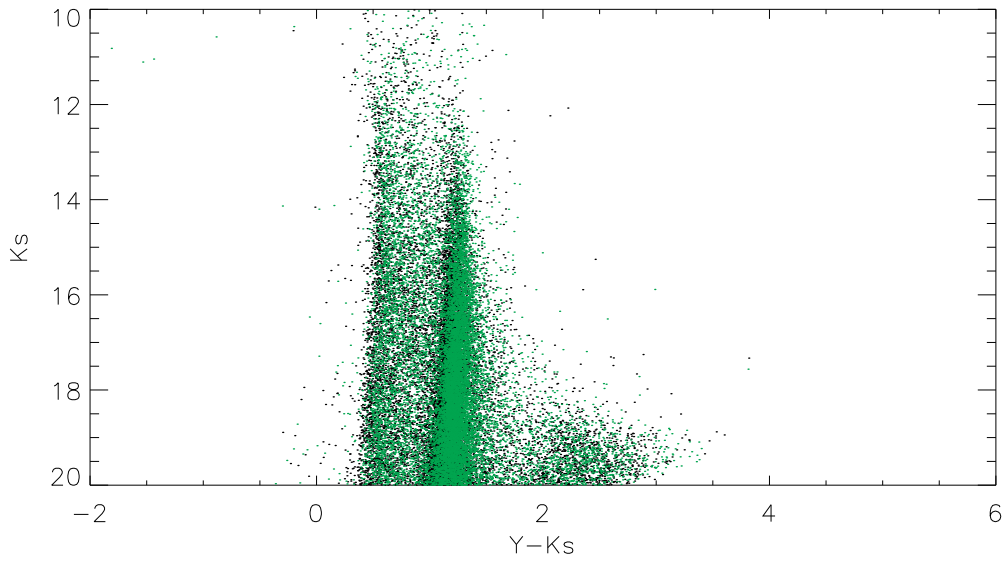

Figure 8.10: CMD, $(Y - K_s)$ vs K_s of the Stream tiles 2_1 (black) and 1_1 (green).

jects remained above statistical uncertainty. If the objects in the SuperCOSMOS cross-match above are real candidate Stream objects then they should have been revealed in the VMC catalogue after the removal of the Galactic foreground. As the VMC survey is the deepest NIR survey to date covering the Magellanic System, further work should be done to confirm a lack of a stellar population in the Stream. The foreground process was re-applied in the direction of the Magellanic Stream tile 1_1 using the statistical removal object-by-object. This removal method is more thorough and accurate enough to reveal even a very small number of Stream objects. Instead of using the UKIDSS catalogue for this more robust removal, the other Stream tile 2_1 was used as this will represent an upper limit of possible Stream candidates.

The statistical one-by-one foreground removal method was applied to the Stream tile 1_1 using tile 2_1 as the foreground field and vice versa. It can be seen from Fig. 8.10 that there is very little if any separation in the populations of the two Stream tiles as seen by eye. After applying the one-by-one statistical removal of each tile in turn as the foreground and target field, the number of objects remaining after the cleaning were too similar to the number of objects without a

match to confirm any candidate Stream objects with this method. Applying the statistical removal to each Stream tile using the UKIDSS foreground field produced the same result as before that there is not a candidate Stream population in the VMC catalogue after the removal of Galactic foreground objects. As stated above it is possible to use a foreground field that covers the same magnitude depth as the VMC survey to confirm this result more accurately.

8.3 Summary

A candidate Stream population is presented here from work with the SuperCOSMOS catalogue, and if confirmed by spectral follow up, are likely to be objects that formed from the gas within the Stream $\sim 50 - 125$ Myr ago. From the above analysis of the SuperCOSMOS Stream candidates, it appears that they are bright in all of the available photometric bands. These objects could be older than the isochrones appear, or they could be young objects with a large amount of dust around them which leads to brighter NIR magnitudes as well as bright optical magnitudes. Although the position of these objects in the WISE CMD does not support this. These objects appear to be inconsistent with a population of normal young objects as there are no young MS stars present, however they are also inconsistent with a normal foreground population. Due to limited time, these objects will be investigated further after the submission of this thesis. The future work will involve creating SEDs of these objects to try and classify them and give more accurate ages. If there is a high level of confidence that some of these objects could be Stream candidates after further rigorous analysis, a proposal will be submitted for a spectroscopic follow up observation.

The confirmation of a younger population in the Stream ties into work by many authors as this population can help in constraining models. In an overview of the Magellanic Stream, Mathewson (2012) discusses the discovery of the Stream and the different potential formation mechanisms. The author describes how previous

observations of the Magellanic Clouds led to a Stream age of 0.3 Gyr however, the more recent observations of the true extent of the Stream lead to a new Stream age of 1.5 Gyr. Mathewson states that we are no closer to understanding the formation of the Stream than ~ 40 years ago when it was first discovered. Finding an explanation for the formation mechanism of the Stream and estimating a time of formation has proven to be a difficult task. Over the past years, observations of the Stream have improved, and to date the estimated length of the Stream is somewhere around 140° (Nidever et al., 2010). Due to the hyperbolic orbit of the Clouds, the longer the Stream is, the older it has to be to explain its extent. If this is accurate then the young ages of the candidate Stream objects presented here indicate that the objects were formed in-situ and that perhaps tidal forces were not involved in the Stream creation.

The production of the Stream from the Bridge by ram pressure alone can be ruled out with the discovery of an older stellar component of the Stream, this is also the case if the Stream age is younger than presented. If these candidate objects are much younger than the Stream age, then they are likely to have formed in-situ and ram pressure could remain the dominant formation mechanism of the Stream. The confirmation of the membership of these candidates will bring implications to the creation of the Magellanic Stream and also the history of the LMC-SMC interaction. If this candidate stellar population is confirmed, it will give us more information as to the processes occurring in these Stream regions as a base for work in other Stream locations. Radial velocity measurements from follow up spectral observations will confirm that these objects belong to the Magellanic System, but also metallicity measurements will identify the origin of the population to the LMC, SMC or Bridge which will also aid in constraining models of the interactions between the Clouds.

This is the first work to put forward candidates for a possible stellar counterpart to the Magellanic Stream and finds that the candidate Stream stars are present in tile 1_1 from the SuperCOSMOS catalogue with postulated ages of $\sim 50 - 125$

Myr. Tile 2_1 appears to contain no stellar population and can be used as an offset field when analysing other VMC tiles such as the Bridge tiles 4.

Confirmation of these candidates by spectroscopic follow up will have a great impact on our ability to model the Magellanic Clouds and will help constrain their past and present interactions with each other, and also with the Galaxy. If radial velocities and metallicities are confirmed for these objects, their origins can be placed to either the LMC, SMC or Bridge regions which will aid in our knowledge of the origin of Stream material. The next step in this kind of work will be to search for the existence of an older population in the Stream which are not likely to have formed in-situ. If an older population can be observed, it will imply that tidal forces were involved in the creation of the Stream. The knowledge of where the Stream material originated from and how it formed the Stream will complete another piece of the puzzle of the past, present and future of the Magellanic System.

With time permitting a search should be carried out in other regions of the Stream, especially those that are predicted to contain a stellar population or in regions with highest gas column density. This search should not be limited to SuperCOSMOS but must utilise all large area surveys that cover the whole, or parts of the Magellanic Stream in order to make a conclusive discovery of whether there is a younger or older Stream population in any region.

Chapter 9

Summary and Conclusions

This work has made use of a variety of large-scale photometric catalogues in the direction of the Magellanic Bridge and Stream covering a range of wave bands from the optical to the mid-IR. An extensive study has been carried out to ensure that the objects recovered as candidate Bridge and Stream stars are free from contamination from Galactic foreground objects and background galaxies. Methods of removing the Galactic foreground contamination range from large-scale colour and magnitude cuts made using the separation of Magellanic and Galactic objects, to more statistical approaches, which aim to remove contamination object by object. These different methods, applied to different catalogues are a crucial part of the process of analysing the Magellanic Bridge and Stream populations due to their low stellar densities. It is important to perform a thorough removal of foreground objects towards these regions to gain the highest level of confidence that the remaining Magellanic candidate objects truly belong to the Magellanic System. The candidate Magellanic Bridge and Stream stars after the removal of the Galactic contamination have been analysed using a variety of tools such as CMDs, two-colour diagrams, isochrone analysis and stellar density maps. These tools will allow the study of different populations such as the identification of RGB and AGB stars in the Bridge, metallicity and age determinations, and the investigation of spatial trends across the Bridge and within age ranges.

9.1 The Magellanic Bridge

The Bridge candidates are made up of a young and old population. The young population within the age of the Bridge ($\sim 200 - 500$ Myr), that is likely to have formed in-situ in regions of high density gas closest to the SMC. The number of young blue objects in the Bridge tiles is greater towards the SMC and decreases towards the LMC. This complements the higher density of gas on the SMC side of the Bridge (Hindman et al., 1963b), which supports that the Bridge is formed primarily from the SMC. The young objects are likely to have formed in-situ from the gas within the Bridge, which is denser in the SMC wing and on the outer LMC.

The red population observed in the Bridge in Chapters 5 and 6 confirms work by Bagheri et al. (2013) and Noël et al. (2013) that there is an old and intermediate age population within the Bridge. Populations in the work here, with ages up to 3 Gyr are likely to have been drawn into the Bridge from the Clouds at formation assuming the age of the Bridge is ($\sim 200 - 500$ Myr). The identification of the red clump in the Bridge here is also an important observation. The red clump is a well defined distance indicator (Cole, 1998) and different positions of red clump stars in different VMC Bridge tiles gives different distance estimates within the Bridge. In this case, using the red clump stars ($\sim 0.6 - 4$ Gyr) in the Bridge tiles 2_3 and 2_8 nearest to the SMC and LMC respectively, shows that there is a distance gradient between the LMC and SMC sides with the SMC side at a greater distance.

The spatial distribution of objects within the Bridge indicates that the number of stars is highest in the regions closest to the LMC and SMC where the density of gas is highest. Particularly for the case of young objects in the Bridge tile 2_3 the stellar density is much higher in the region closest to the SMC than elsewhere. In all cases it does appear that the older objects are less locally confined and are likely to be present in the Bridge from tidal interactions between the Clouds. It appears from this work that on a larger scale there is no clear end to the Bridge

population above and below the defined Bridge indicating that perhaps there is not a discrete population of Bridge objects between the Clouds, but that the Clouds may lie within smoother halos which overlap to form the Bridge that we see. If the Clouds have a common halo that consists of objects older than the Stream, it would support the Clouds being bound on their approach to the MW. Further studies of field stars between the Clouds will help in confirming whether this is the case.

Models of the interaction history of the Magellanic Clouds (Harris and Zaritsky, 2009) suggest that the Clouds have had two close encounters with each other at 500 Myr and 2 Gyr. Previous work suggests that the Stream was formed in the first encounter and the Bridge was formed in the most recent encounter (Diaz and Bekki, 2011). This work supports that the Bridge was formed from the second close encounter, and that the Bridge objects older than $\sim$ 500 Myr were drawn into the Bridge tidally at formation, with the younger objects being formed not from a one off starburst event, but continuously from when the Bridge was formed. The high RV values presented in the spectroscopic study indicates that the Bridge stars could have originated in the LMC as well as the SMC, also supporting the possibility of overlapping halos opposed to a discrete Bridge. A larger spectroscopic survey of Bridge candidates identified from the VMC will add to our current understanding of the distribution of stars in the Bridge in terms of RVs metallicities and membership to either Cloud.

The Magellanic Bridge is one tidal Bridge between two irregular galaxies. Bekki (2008) investigated a Bridge that formed tidally between the outer halos of M31 and M33 made only from HI gas with no stars associated to it. Its origin is also under debate and it could be in-fact a tidal stream like the Magellanic Stream containing no, or only a very small stellar component. Smith et al. (2010) have used the GALEX ultraviolet telescope to study various tidal features including bridges, spiral arms and tails of gas between interacting galaxy pairs. There are many tidal features in existence, some with and some without stars within the

gas in galaxies out to distances of 50 kpc (Pakzad et al., 2004). A more detailed study is required to determine a model to distinguish a tidal bridge from a stream, spiral arm or tail and a study into the conditions that form these features will give more information to the likely presence of stars within them. The Magellanic Bridge has had a known stellar population however, in the Magellanic Stream no stars have been detected within the HI gas. Perhaps unless drawn in at formation as indicated here, tidal features do not contain a stellar population until an event occurs that is strong enough to trigger star formation within the tidal feature in an environment with a high enough gas density. Further observations of tidal systems, including the Magellanic Clouds with VISTA, are needed to give us a better picture of the interactions that form these features and star formation within.

9.2 The Magellanic Stream

A candidate Stream population is presented here from work with the SuperCOSMOS catalogue. Comparison with isochrones indicates a rough age of $\sim 50 - 125$ Myr, which indicates that these objects have formed in-situ from the gas in the Stream. Further observations are required to confirm the nature of these objects however, from the above analysis of the SuperCOSMOS Stream candidates it appears that they are bright in all of the available photometric bands. These objects could be older than the isochrones appear, or they could be young objects with a large amount of dust around them, which leads to brighter NIR magnitudes however, WISE photometry does not confirm the existence of hot dust. Due to limited time, these objects will be investigated further after the submission of this thesis. The future work will involve creating SEDs of these objects to try and classify them and give more accurate ages. If there is a high level of confidence that these objects could be Stream candidates after further rigorous analysis, a proposal will be submitted for a spectroscopic follow up observation.

The confirmation of a young population in the Stream ties into work by many authors as this population can help in constraining dynamical models. In an overview of the Magellanic Stream, Mathewson (2012) discusses the discovery of the Stream and the different potential formation mechanisms. The author describes how previous observations of the Magellanic Clouds led to a Stream age of 0.3 Gyr however, the more recent observations of the true extent of the Stream lead to a new Stream age of 1.5 Gyr. Mathewson states that we are no closer to understanding the formation of the Stream than 40 years ago when it was first discovered. Finding an explanation for the formation mechanism of the Stream and estimating a time of formation has proven to be a difficult task. Over the past years, observations of the Stream have improved, and to date the estimated length of the Stream is somewhere around 140° (Nidever et al., 2010). Due to the hyperbolic orbit of the Clouds, the longer the Stream is, the older it has to be to explain its extent.

9.3 Future work

With the wealth of data from the ongoing VMC survey, the next step in this work is to analyse all of the Bridge tiles once they have been observed to their full depth. By studying the tiles across the whole Bridge we will be able to gain a better understanding of how the stellar populations vary from the LMC to SMC. Further spectroscopic follow up observations can be carried out for the young and old populations to learn about their metallicities and membership to either LMC or SMC. A deeper study of the Galactic foreground population is required to make full use of the observations available in the directions of the Bridge and Stream, including a study of the variations in numbers and metallicity of foreground objects, and also the reddening across the region of the Clouds. Data may already be available in these areas of interest which would be a good starting point. The calibration of TRILEGAL using the above information will be highly beneficial

as TRILEGAL is a powerful tool in simulating the entire Galaxy in any direction, for any catalogue and will be of great use when studying low stellar density target regions.

A successful search for the existence of an older population in the Stream which are not likely to have formed in-situ will rule out the production of the Stream from the Bridge by ram pressure alone. If Stream objects are much younger than the Stream age, then ram pressure could remain the dominant formation mechanism of the Stream. Radial velocity measurements from follow up spectral observations will confirm that these objects belong to the Magellanic System, but also metallicity measurements will identify the origin of the population to the LMC, SMC or Bridge which will also aid in constraining models of the interactions between the Clouds. With time permitting a search should be carried out in other regions of the Stream, especially those that are predicted to contain a stellar population or in regions with highest gas column densities. This search should not be limited to SuperCOSMOS but must utilise all large area surveys that cover the whole, or parts of the Magellanic Stream in order to make a conclusive discovery of whether there is a young or old Stream population in any region.

Future observations with instruments such as GAIA will observe proper motions of objects to place them within this system and further contribute to our understanding. It is an exciting time to study the Magellanic Clouds, Bridge and Stream due to the wealth of photometric and spectroscopic observations we have to date, with more data arriving continually. With the many groups of Astronomers working on model simulations of the interactions of the LMC and SMC with each other, and with the MW, aided by the ongoing observations, it will not be long until we have a clear idea of how these two dwarf irregular galaxies came into contact with each other and also in the vicinity of the MW. A combination of studies including gas, stellar populations and dynamics are required in order to fully understand the tidal features of the Magellanic System. The LMC and SMC within our neighbourhood, are prime targets to improve our understanding of interactions between

galaxies and the behaviour of gas and stars in a low metallicity, and in the case of the Bridge, low density environments. By studying the Magellanic Clouds we can better understand the processes that occur in the MW and extrapolate these findings to other astronomical systems.

Bibliography

Abraham, P., Dobashi, K., Mizuno, A., and Fukui, Y. (1995). Molecular material and young stellar objects in the L 1188 dark cloud complex. *A&A*, 300:525.

Armandroff, T. E. and Da Costa, G. S. (1991). Metallicities for old stellar systems from Ca II triplet strengths in member giants. *AJ*, 101:1329–1337.

Bagheri, G., Cioni, M.-R. L., and Napiwotzki, R. (2013). The detection of an older population in the Magellanic Bridge. *A&A*, 551:A78.

Barger, K. A. and Haffner, L. M. (2011). Ionized Gas in the Magellanic Bridge: A First Look at New Observations with WHAM. In *American Astronomical Society Meeting Abstracts 217*, volume 217 of *American Astronomical Society Meeting Abstracts*, page 251.34.

Bekki, K. (2007). Triggered star formation in the Magellanic Clouds. In Elmegreen, B. G. and Palous, J., editors, *IAU Symposium*, volume 237 of *IAU Symposium*, pages 373–377.

Bekki, K. (2008). Formation of a giant HI bridge between M31 and M33 from their tidal interaction. *MNRAS*, 390:L24–L28.

Besla, G., Hernquist, L., and Loeb, A. (2012). The Origin of the Microlensing Events Observed Towards the LMC and the Stellar Counterpart of the Magellanic Stream. *ArXiv e-prints*.

Besla, G., Hernquist, L., and Loeb, A. (2013). The origin of the microlensing events observed towards the LMC and the stellar counterpart of the Magellanic stream. *MNRAS*, 428:2342–2365.

Besla, G., Kallivayalil, N., Hernquist, L., van der Marel, R. P., Cox, T. J., and Kereš, D. (2010). Simulations of the Magellanic Stream in a First Infall Scenario. *ApJ*, 721:L97–L101.

Bessell, M. S. and Brett, J. M. (1988). JHKLM photometry - Standard systems, passbands, and intrinsic colors. *PASP*, 100:1134–1151.

Bica, E. L. D. and Schmitt, H. R. (1995). A Revised and Extended Catalog of Magellanic System Clusters, Associations, and Emission Nebulae. I. Small Magellanic Cloud and Bridge. *ApJS*, 101:41.

Bilir, S., Karaali, S., Ak, S., Önal, Ö., Dağtekin, N. D., Yontan, T., Gilmore, G., and Seabroke, G. M. (2012). Local stellar kinematics from RAVE data - III. Radial and vertical metallicity gradients based on red clump stars. *MNRAS*, 421:3362–3374.

Braine, J., Duc, P.-A., Lisenfeld, U., Charmandaris, V., Vallejo, O., Leon, S., and Brinks, E. (2001). Abundant molecular gas in tidal dwarf galaxies: On-going galaxy formation. *A&A*, 378:51–69.

Bressan, A., Marigo, P., Girardi, L., Salasnich, B., Dal Cero, C., Rubele, S., and Nanni, A. (2012). PARSEC: stellar tracks and isochrones with the PAdova and TRieste Stellar Evolution Code. *MNRAS*, 427:127–145.

Byrd, G. and Salo, H. (1994). Tidal bridges, tails and spiral arms in M51's multiple encounter history. In *Bulletin of the American Astronomical Society*, volume 26 of *Bulletin of the American Astronomical Society*, page 917.

Cannon, A. J. and Pickering, E. C. (1918). The Henry Draper catalogue 0h, 1h, 2h, and 3h. *Annals of Harvard College Observatory*, 91:1–290.

Carretta, E. and Gratton, R. G. (1997). Abundances for globular cluster giants. I. Homogeneous metallicities for 24 clusters. *A&AS*, 121:95–112.

Castellani, V., Degl'Innocenti, S., Marconi, M., Prada Moroni, P. G., and Sestito, P. (2003). Stellar evolutionary models for Magellanic Clouds. *A&A*, 404:645–653.

Chabrier, G. (2001). The Galactic Disk Mass Budget. I. Stellar Mass Function and Density. *ApJ*, 554:1274–1281.

Chen, C.-H. R., Indebetouw, R., Chu, Y.-H., Gruendl, R. A., Testor, G., Heitsch, F., Seale, J. P., Meixner, M., and Sewilo, M. (2010a). Spitzer View of Young Massive Stars in the Large Magellanic Cloud H II Complexes. II. N 159. *ApJ*, 721:1206–1232.

Chen, C. H. R., Indebetouw, R., Gordon, K. D., Solan, G. C., and SAGE-SMC Team (2010b). Massive Star Formation in the Magellanic Bridge. In *American Astronomical Society Meeting Abstracts 215*, volume 42 of *Bulletin of the American Astronomical Society*, page 369.02.

Christodoulou, D. M., Tohline, J. E., and Keenan, F. P. (1997). Star-forming Processes Far from the Galactic Disk: Inoperative or Indolent Where Operative. *ApJ*, 486:810.

Cioni, M.-R., Clementini, G., Girardi, L., Guandalini, R., Gullieuszik, M., Miszalski, B., Moretti, M.-I., Ripepi, V., Rubele, S., Bagheri, G., Bekki, K., Cross, N., de Blok, E., de Grijs, R., Emerson, J., Evans, C., Gibson, B., Gonzales-Solares, E., Groenewegen, M., Irwin, M., Ivanov, V., Lewis, J., Marconi, M., Marquette, J.-B., Mastropietro, C., Moore, B., Napiwotzki, R., Naylor, T., Oliveira, J., Read, M., Sutorius, E., van Loon, J., Wilkinson, M., and Wood, P. (2011). The VISTA Near-infrared YJKs Public Survey of the Magellanic Clouds System (VMC). *The Messenger*, 144:25–31.

Cioni, M.-R., Loup, C., Habing, H. J., Fouqué, P., Bertin, E., Deul, E., Egret, D., Alard, C., de Batz, B., Borsenberger, J., Dennefeld, M., Epchtein, N., Forveille, T., Garzón, F., Hron, J., Kimeswenger, S., Lacombe, F., Le Bertre, T., Mamon, G. A., Omont, A., Paturel, G., Persi, P., Robin, A., Rouan, D., Simon, G., Tiphène, D., Vauglin, I., and Wagner, S. (2000). The DENIS Point Source Catalogue towards the Magellanic Clouds. *A&AS*, 144:235–245.

Cole, A. A. (1998). Age, Metallicity, and the Distance to the Magellanic Clouds from Red Clump Stars. *ApJ*, 500:L137.

Cross, N. J. G., Collins, R. S., Mann, R. G., Read, M. A., Sutorius, E. T. W., Blake, R. P., Holliman, M., Hambly, N. C., Emerson, J. P., Lawrence, A., and Noddle, K. T. (2012). The VISTA Science Archive. *A&A*, 548:A119.

Danks, A. C. and Dennefeld, M. (1994). An atlas of southern MK standards from 5800 to 10200 A. *PASP*, 106:382–396.

De Propris, R., Rich, R. M., Mallery, R. C., and Howard, C. D. (2010). A Radial Velocity and Calcium Triplet Abundance Survey of Field Small Magellanic Cloud Giants. *ApJ*, 714:L249–L253.

Demers, S. and Irwin, M. J. (1991). Catalogue of blue stars between the Magellanic Clouds. *A&AS*, 91:171–182.

Diaz, J. and Bekki, K. (2011). Constraining the orbital history of the Magellanic Clouds: a new bound scenario suggested by the tidal origin of the Magellanic Stream. *MNRAS*, 413:2015–2020.

Diaz, J. D. and Bekki, K. (2012). The Tidal Origin of the Magellanic Stream and the Possibility of a Stellar Counterpart. *ApJ*, 750:36.

Emerson, J. P. and Sutherland, W. J. (2010). VISTA: status and performance. In *Society of Photo-Optical Instrumentation Engineers (SPIE) Conference Se-*

ries, volume 7733 of *Society of Photo-Optical Instrumentation Engineers (SPIE) Conference Series*.

Emerson, J. P., Sutherland, W. J., McPherson, A. M., Craig, S. C., Dalton, G. B., and Ward, A. K. (2004). The Visible & Infrared Survey Telescope for Astronomy. *The Messenger*, 117:27–32.

Epchtein, N. (1994). DENIS: A Deep Near-Infrared Southern Sky Survey. *Experimental Astronomy*, 3:73–76.

For, B.-Q., Staveley-Smith, L., and McClure-Griffiths, N. M. (2013). Galactic All-Sky Survey High-velocity Clouds in the Region of the Magellanic Leading Arm. *ApJ*, 764:74.

Frogel, J. A. and Blanco, V. M. (1990). The Large Magellanic Cloud Bar West field. *ApJ*, 365:168–179.

Gardiner, L. T. and Hatzidimitriou, D. (1992). Stellar populations and the large-scale structure of the Small Magellanic Cloud. IV - Age distribution studies of the outer regions. *MNRAS*, 257:195–224.

Gibson, B. K., Giroux, M. L., Penton, S. V., Putman, M. E., Stocke, J. T., and Shull, J. M. (2000). Metal Abundances in the Magellanic Stream. *AJ*, 120:1830–1840.

Girardi, L., Bertelli, G., Bressan, A., Chiosi, C., Groenewegen, M. A. T., Marigo, P., Salasnich, B., and Weiss, A. (2002). Theoretical isochrones in several photometric systems. I. Johnson-Cousins-Glass, HST/WFPC2, HST/NICMOS, Washington, and ESO Imaging Survey filter sets. *A&A*, 391:195–212.

Girardi, L., Bressan, A., Bertelli, G., and Chiosi, C. (2000). Evolutionary tracks and isochrones for low- and intermediate-mass stars: From 0.15 to 7 M_{sun}, and from Z=0.0004 to 0.03. *A&AS*, 141:371–383.

Girardi, L., Groenewegen, M. A. T., Hatziminaoglou, E., and da Costa, L. (2005). Star counts in the Galaxy. Simulating from very deep to very shallow photometric surveys with the TRILEGAL code. *A&A*, 436:895–915.

Gordon, K. D., Clayton, G. C., Misselt, K. A., Landolt, A. U., and Wolff, M. J. (2003). A Quantitative Comparison of the Small Magellanic Cloud, Large Magellanic Cloud, and Milky Way Ultraviolet to Near-Infrared Extinction Curves. *ApJ*, 594:279–293.

Graczyk, D., Pietrzyński, G., Thompson, I. B., Gieren, W., Pilecki, B., Udalski, A., Soszyński, I., Kołaczkowski, Z., Kudritzki, R.-P., Bresolin, F., Konorski, P., Mennickent, R., Minniti, D., Storm, J., Nardetto, N., and Karczmarek, P. (2012). The Araucaria Project: An Accurate Distance to the Late-type Double-lined Eclipsing Binary OGLE SMC113.3 4007 in the Small Magellanic Cloud. *ApJ*, 750:144.

Grocholski, A. J., Cole, A. A., Sarajedini, A., Geisler, D., and Smith, V. V. (2006). Ca II Triplet Spectroscopy of Large Magellanic Cloud Red Giants. I. Abundances and Velocities for a Sample of Populous Clusters. *AJ*, 132:1630–1644.

Grondin, L. and Demers, S. (1993). Recent Star Formation Between the Magellanic Clouds. In D. D. Sasselov, editor, *Luminous High-Latitude Stars*, volume 45 of *Astronomical Society of the Pacific Conference Series*, pages 380–+.

Grondin, L., Demers, S., and Kunkel, W. E. (1992). Young stars between the Magellanic Clouds. III - Overall properties of associations: A shallow mass function. *AJ*, 103:1234–1251.

Grondin, L., Demers, S., Kunkel, W. E., and Irwin, M. J. (1991). String of Young Clusters Linking the Magellanic Clouds. In R. Haynes & D. Milne, editor, *The Magellanic Clouds*, volume 148 of *IAU Symposium*, pages 478–+.

Guhathakurta, P. and Reitzel, D. B. (1998). Local Group Suburbia: Red Giants in M31's Outer Spheroid and a Search for Stars in the Magellanic Stream. In D. Zaritsky, editor, *Galactic Halos*, volume 136 of *Astronomical Society of the Pacific Conference Series*, pages 22–+.

Hambly, N. C., Dufton, P. L., Keenan, F. P., Rolleston, W. R. J., Howarth, I. D., and Irwin, M. J. (1994). High-resolution spectroscopy of two young stars between the Magellanic Clouds. *A&A*, 285:716–722.

Hambly, N. C., MacGillivray, H. T., Read, M. A., Tritton, S. B., Thomson, E. B., Kelly, B. D., Morgan, D. H., Smith, R. E., Driver, S. P., Williamson, J., Parker, Q. A., Hawkins, M. R. S., Williams, P. M., and Lawrence, A. (2001). The SuperCOSMOS Sky Survey - I. Introduction and description. *MNRAS*, 326:1279–1294.

Harris, J. (2007). The Magellanic Bridge: The Nearest Purely Tidal Stellar Population. *ApJ*, 658:345–357.

Harris, J. and Zaritsky, D. (2009). The Star Formation History of the Large Magellanic Cloud. *AJ*, 138:1243–1260.

Hewett, P. C., Warren, S. J., Leggett, S. K., and Hodgkin, S. T. (2006). The UKIRT Infrared Deep Sky Survey ZY JHK photometric system: passbands and synthetic colours. *MNRAS*, 367:454–468.

Hindman, J. V., Kerr, F. J., and McGee, R. X. (1963a). A Low Resolution Hydrogen-line Survey of the Magellanic System. II. Interpretation of Results. *Australian Journal of Physics*, 16:570–+.

Hindman, J. V., McGee, R. X., Carter, A. W. L., Holmes, E. C. J., and Beard, M. (1963b). A Low Resolution Hydrogen-line Survey of the Magellanic System. I. Observations and Digital Reduction Procedures. *Australian Journal of Physics*, 16:552–+.

Hog, E., Kuzmin, A., Bastian, U., Fabricius, C., Kuimov, K., Lindegren, L., Makarov, V. V., and Roeser, S. (1998). The TYCHO Reference Catalogue. *A&A*, 335:L65–L68.

Holmberg, E. B., Lauberts, A., Schuster, H.-E., and West, R. M. (1974). The ESO/Uppsala survey of the ESO (B) atlas of the southern sky. I. *A&AS*, 18:463–489.

Irwin, M. J. (1991). Optical Surveys of the Magellanic Bridge, Stream and Outer Halos. In Haynes, R. and Milne, D., editors, *The Magellanic Clouds*, volume 148 of *IAU Symposium*, page 453.

Irwin, M. J., Demers, S., and Kunkel, W. E. (1990). A blue stellar link between the Magellanic Clouds. *AJ*, 99:191–200.

Jones, B. F., Klemola, A. R., and Lin, D. N. C. (1994). Proper motion of the Large Magellanic Cloud and the mass of the galaxy. 1: Observational results. *AJ*, 107:1333–1337.

Kallivayalil, N., van der Marel, R. P., Alcock, C., Axelrod, T., Cook, K. H., Drake, A. J., and Geha, M. (2006). The Proper Motion of the Large Magellanic Cloud Using HST. *ApJ*, 638:772–785.

Kallivayalil, N., van der Marel, R. P., Besla, G., Anderson, J., and Alcock, C. (2013). Third-epoch Magellanic Cloud Proper Motions. I. Hubble Space Telescope/WFC3 Data and Orbit Implications. *ApJ*, 764:161.

Kennicutt, Jr., R. C. (1989). The star formation law in galactic disks. *ApJ*, 344:685–703.

Kerr, F. J. and de Vaucouleurs, G. (1955). Rotation and Other Motions of the Magellanic Clouds from Radio Observations. *Australian Journal of Physics*, 8:508–+.

Kinman, T. D. (1958). A Revision of the Distance Moduli of the Galactic Globular Clusters [erratum: 1958MNSSA..17...55K]. *Monthly Notes of the Astronomical Society of South Africa*, 17:19.

Kobulnicky, H. A. and Dickey, J. M. (1999). Detection of Cold Atomic Clouds in the Magellanic Bridge. *AJ*, 117:908–919.

Laney, C. D., Joner, M. D., and Pietrzyński, G. (2012). A new Large Magellanic Cloud K-band distance from precision measurements of nearby red clump stars. *MNRAS*, 419:1637–1641.

Larson, R. B. (2006). Understanding the Stellar Initial Mass Function. In *Revista Mexicana de Astronomia y Astrofisica Conference Series*, volume 26 of *Revista Mexicana de Astronomia y Astrofisica Conference Series*, pages 55–59.

Maeder, A. and Meynet, G. (2001). Stellar evolution with rotation. VII. . Low metallicity models and the blue to red supergiant ratio in the SMC. *A&A*, 373:555–571.

Mastropietro, C., Moore, B., Mayer, L., Stadel, J., and Wadsley, J. (2004). On the Formation of the Magellanic Stream. In F. Prada, D. Martinez Delgado, & T. J. Mahoney, editor, *Satellites and Tidal Streams*, volume 327 of *Astronomical Society of the Pacific Conference Series*, pages 234–+.

Mathewson, D. (2012). Discovery of the Magellanic Stream. *Journal of Astronomical History and Heritage*, 15:100–104.

Mathewson, D. S. (1985). The Magellanic system. *Proceedings of the Astronomical Society of Australia*, 6:104–109.

Mathewson, D. S., Cleary, M. N., and Murray, J. D. (1974). The Magellanic Stream. In J. R. Shakeshaft, editor, *The Formation and Dynamics of Galaxies*, volume 58 of *IAU Symposium*, pages 367–+.

Mathewson, D. S., Wayte, S. R., Ford, V. L., and Ruan, K. (1987). The 'high velocity cloud' origin of the Magellanic system. *Proceedings of the Astronomical Society of Australia*, 7:19–25.

Matthews, D., Staveley-Smith, L., Dyson, P., and Muller, E. (2009). Cool Gas in the Magellanic Stream. *ApJ*, 691:L115–L118.

McClure-Griffiths, N. M., Madsen, G. J., Gaensler, B. M., McConnell, D., and Schnitzeler, D. H. F. M. (2010). Measurement of a Magnetic Field in a Leading Arm High-velocity Cloud. *ApJ*, 725:275–281.

McClure-Griffiths, N. M., Pisano, D. J., Calabretta, M. R., Ford, H. A., Lockman, F. J., Staveley-Smith, L., Kalberla, P. M. W., Bailin, J., Dedes, L., Janowiecki, S., Gibson, B. K., Murphy, T., Nakanishi, H., and Newton-McGee, K. (2009). Gass: The Parkes Galactic All-Sky Survey. I. Survey Description, Goals, and Initial Data Release. *ApJS*, 181:398–412.

McGee, R. X. and Newton, L. M. (1981). H I in the Small Magellanic Cloud re-examined. *Proceedings of the Astronomical Society of Australia*, 4:189–195.

Mizuno, N., Muller, E., Maeda, H., Kawamura, A., Minamidani, T., Onishi, T., Mizuno, A., and Fukui, Y. (2006). Detection of Molecular Clouds in the Magellanic Bridge: Candidate Star Formation Sites in a Nearby Low-Metallicity System. *ApJ*, 643:L107–L110.

Moore, B. and Davis, M. (1994). The Origin of the Magellanic Stream. *MNRAS*, 270:209–+.

Muller, E. and Bekki, K. (2007). The origin of large-scale HI structures in the Magellanic Bridge. *MNRAS*, 381:L11–L15.

Muller, E. and Parker, Q. A. (2007). Hα Emission from the Magellanic Bridge. *PASA*, 24:69–76.

Muller, E., Stanimirović, S., Rosolowsky, E., and Staveley-Smith, L. (2004). A Statistical Investigation of H I in the Magellanic Bridge. *ApJ*, 616:845–856.

Muller, E., Staveley-Smith, L., Zealey, W., and Stanimirović, S. (2003). High-resolution HI observations of the Western Magellanic Bridge. *MNRAS*, 339:105–124.

Murai, T. and Fujimoto, M. (1980). The Magellanic Stream and the Galaxy with a Massive Halo. *PASJ*, 32:581–+.

Nidever, D. L., Majewski, S. R., Butler Burton, W., and Nigra, L. (2010). The 200deg Long Magellanic Stream System. *ApJ*, 723:1618–1631.

Nikolaev, S. and Weinberg, M. D. (2000). Stellar Populations in the Large Magellanic Cloud from 2MASS. *ApJ*, 542:804–818.

Noël, N. E. D., Conn, B. C., Carrera, R., Read, J. I., Rix, H.-W., and Dolphin, A. (2013). The MAGellanic Inter-Cloud Project (MAGIC). I. Evidence for Intermediate-age Stellar Populations in between the Magellanic Clouds. *ApJ*, 768:109.

Noel, N. E. D., Gallart, C., Costa, E., and Mendez, R. (2005). SMC: Stellar Populations through deep CMDs. *ArXiv Astrophysics e-prints*.

North, P. L., Gauderon, R., and Royer, F. (2009). New distance and depth estimates from observations of eclipsing binaries in the SMC. In Van Loon, J. T. and Oliveira, J. M., editors, *IAU Symposium*, volume 256 of *IAU Symposium*, pages 57–62.

Olsen, K. A. G., Zaritsky, D., Blum, R. D., Boyer, M. L., and Gordon, K. D. (2011). A Population of Accreted SMC Stars in the LMC. *ArXiv e-prints*.

Pakzad, S. L., Majewski, S. R., Frinchaboy, P. M., Hummels, C. B., Ivezic, Z., Johnston, K. V., Law, D. R., Patterson, R. J., Prada, F., and Skrutskie, M. F. (2004). Tidal Streams in the Outer Galactic Halo: Pieces of a 500-degree Long

Trailing Sagittarius Tidal Tail? In *American Astronomical Society Meeting Abstracts*, volume 36 of *Bulletin of the American Astronomical Society*, page 142.05.

Parisi, M. C., Geisler, D., Grocholski, A. J., Clariá, J. J., and Sarajedini, A. (2010a). Ca II Triplet Spectroscopy of Small Magellanic Cloud Red Giants. II. Abundances for a Sample of Field Stars. *AJ*, 139:1168–1177.

Parisi, M. C., Grocholski, A., Geisler, D., Sarajedini, A., and Clariá, J. J. (2010b). Metallicity analysis of an SMC cluster sample using Caii-triplet spectroscopy. In de Grijs, R. and Lépine, J. R. D., editors, *IAU Symposium*, volume 266 of *IAU Symposium*, pages 483–486.

Pietrinferni, A., Cassisi, S., Salaris, M., and Castelli, F. (2004). A Large Stellar Evolution Database for Population Synthesis Studies. I. Scaled Solar Models and Isochrones. *ApJ*, 612:168–190.

Putman, M. E., de Heij, V., Staveley-Smith, L., Braun, R., Freeman, K. C., Gibson, B. K., Burton, W. B., Barnes, D. G., Banks, G. D., Bhathal, R., de Blok, W. J. G., Boyce, P. J., Disney, M. J., Drinkwater, M. J., Ekers, R. D., Henning, P. A., Jerjen, H., Kilborn, V. A., Knezek, P. M., Koribalski, B., Malin, D. F., Marquarding, M., Minchin, R. F., Mould, J. R., Oosterloo, T., Price, R. M., Ryder, S. D., Sadler, E. M., Stewart, I., Stootman, F., Webster, R. L., and Wright, A. E. (2002). HIPASS High-Velocity Clouds: Properties of the Compact and Extended Populations. *AJ*, 123:873–891.

Putman, M. E. and Gibson, B. K. (1999). Early Results from the Parkes Multibeam High-Velocity Cloud Survey. In B. K. Gibson & M. E. Putman, editor, *Stromlo Workshop on High-Velocity Clouds*, volume 166 of *Astronomical Society of the Pacific Conference Series*, pages 276–+.

Putman, M. E., Gibson, B. K., and Staveley-Smith, L. (1999). New HI Features of the Magellanic System. In Chu, Y.-H., Suntzeff, N., Hesser, J., and

Bohlender, D., editors, *New Views of the Magellanic Clouds*, volume 190 of *IAU Symposium*, page 51.

Putman, M. E., Staveley-Smith, L., Freeman, K. C., Gibson, B. K., and Barnes, D. G. (2003). The Magellanic Stream, High-Velocity Clouds, and the Sculptor Group. *ApJ*, 586:170–194.

Renzini, A. and Fusi Pecci, F. (1988). Tests of evolutionary sequences using color-magnitude diagrams of globular clusters. *ARA&A*, 26:199–244.

Rolleston, W. R. J., Trundle, C., and Dufton, P. L. (2002). The present-day chemical composition of the LMC. *A&A*, 396:53–64.

Ruzicka, A., Theis, C., and Palouš, J. (2011). Rotation of the Milky Way and the Formation of the Magellanic Stream. In Koleva, M., Prugniel, P., and Vauglin, I., editors, *EAS Publications Series*, volume 48 of *EAS Publications Series*, pages 337–343.

Schlegel, D. J., Finkbeiner, D. P., and Davis, M. (1998). Maps of Dust Infrared Emission for Use in Estimation of Reddening and Cosmic Microwave Background Radiation Foregrounds. *ApJ*, 500:525–+.

Shu, F. H. (1992). Book-Review - the Physics of Astrophysics - V.2 - Gas Dynamics. *Science*, 256:253–+.

Skrutskie, M. F., Cutri, R. M., Stiening, R., Weinberg, M. D., Schneider, S., Carpenter, J. M., Beichman, C., Capps, R., Chester, T., Elias, J., Huchra, J., Liebert, J., Lonsdale, C., Monet, D. G., Price, S., Seitzer, P., Jarrett, T., Kirkpatrick, J. D., Gizis, J. E., Howard, E., Evans, T., Fowler, J., Fullmer, L., Hurt, R., Light, R., Kopan, E. L., Marsh, K. A., McCallon, H. L., Tam, R., Van Dyk, S., and Wheelock, S. (2006). The Two Micron All Sky Survey (2MASS). *AJ*, 131:1163–1183.

Smith, B. J., Giroux, M. L., Struck, C., Hancock, M., and Hurlock, S. (2010). Tidal Dwarf Galaxies, Accretion Tails, and 'Beads on a String' in the 'Spirals, Bridges, and Tails' Interacting Galaxy Survey. In Smith, B., Higdon, J., Higdon, S., and Bastian, N., editors, *Galaxy Wars: Stellar Populations and Star Formation in Interacting Galaxies*, volume 423 of *Astronomical Society of the Pacific Conference Series*, page 257.

Smith, B. J., Struck, C., Hancock, M., Appleton, P., Reach, W., and Charmandaris, V. (2006). The Spitzer Spirals, Bridges, and Tails Interacting Galaxy Survey. *ArXiv Astrophysics e-prints*.

Sofue, Y. (1994). Fate of the Magellanic Stream. *PASJ*, 46:431–440.

Stanimirović, S., Dickey, J. M., Krčo, M., and Brooks, A. M. (2002). The Small-Scale Structure of the Magellanic Stream. *ApJ*, 576:773–789.

Stanimirovic, S., Gallagher, III, J. S., and Nigra, L. (2010). The Small-Scale Structure of the Magellanic Stream as a Foundation for Galaxy Evolution. *Serbian Astronomical Journal*, 180:1–10.

Stanimirović, S., Hoffman, S., Heiles, C., Douglas, K. A., Putman, M., and Peek, J. E. G. (2008). The Many Streams of the Magellanic Stream. *ApJ*, 680:276–286.

Staveley-Smith, L., Sault, R. J., Hatzidimitriou, D., Kesteven, M. J., and McConnell, D. (1997). An HI aperture synthesis mosaic of the Small Magellanic Cloud. *MNRAS*, 289:225–252.

van der Marel, R. P., Alves, D. R., Hardy, E., and Suntzeff, N. B. (2002). New Understanding of Large Magellanic Cloud Structure, Dynamics, and Orbit from Carbon Star Kinematics. *AJ*, 124:2639–2663.

Ventura, P., Castellani, M., and Straka, C. W. (2005). Diffusive convective overshoot in core He-burning intermediate mass stars. I. The LMC metallicity. *A&A*, 440:623–636.

Vieira, K., Girard, T. M., van Altena, W. F., Zacharias, N., Casetti-Dinescu, D. I., Korchagin, V. I., Platais, I., Monet, D. G., López, C. E., Herrera, D., and Castillo, D. J. (2010). Proper-motion Study of the Magellanic Clouds Using SPM Material. *AJ*, 140:1934–1950.

Walker, A. R. (2012). The Large Magellanic Cloud and the distance scale. *Ap&SS*, 341:43–49.

Westerlund, B. E. and Glaspey, J. (1971). On the structure of the wing of the Small Magellanic Cloud. *A&A*, 10:1–7.

Wright, E. L., Eisenhardt, P. R. M., Mainzer, A. K., Ressler, M. E., Cutri, R. M., Jarrett, T., Kirkpatrick, J. D., Padgett, D., McMillan, R. S., Skrutskie, M., Stanford, S. A., Cohen, M., Walker, R. G., Mather, J. C., Leisawitz, D., Gautier, III, T. N., McLean, I., Benford, D., Lonsdale, C. J., Blain, A., Mendez, B., Irace, W. R., Duval, V., Liu, F., Royer, D., Heinrichsen, I., Howard, J., Shannon, M., Kendall, M., Walsh, A. L., Larsen, M., Cardon, J. G., Schick, S., Schwalm, M., Abid, M., Fabinsky, B., Naes, L., and Tsai, C.-W. (2010). The Wide-field Infrared Survey Explorer (WISE): Mission Description and Initial On-orbit Performance. *AJ*, 140:1868–1881.

Appendix A

Error vs magnitude for photometric bands

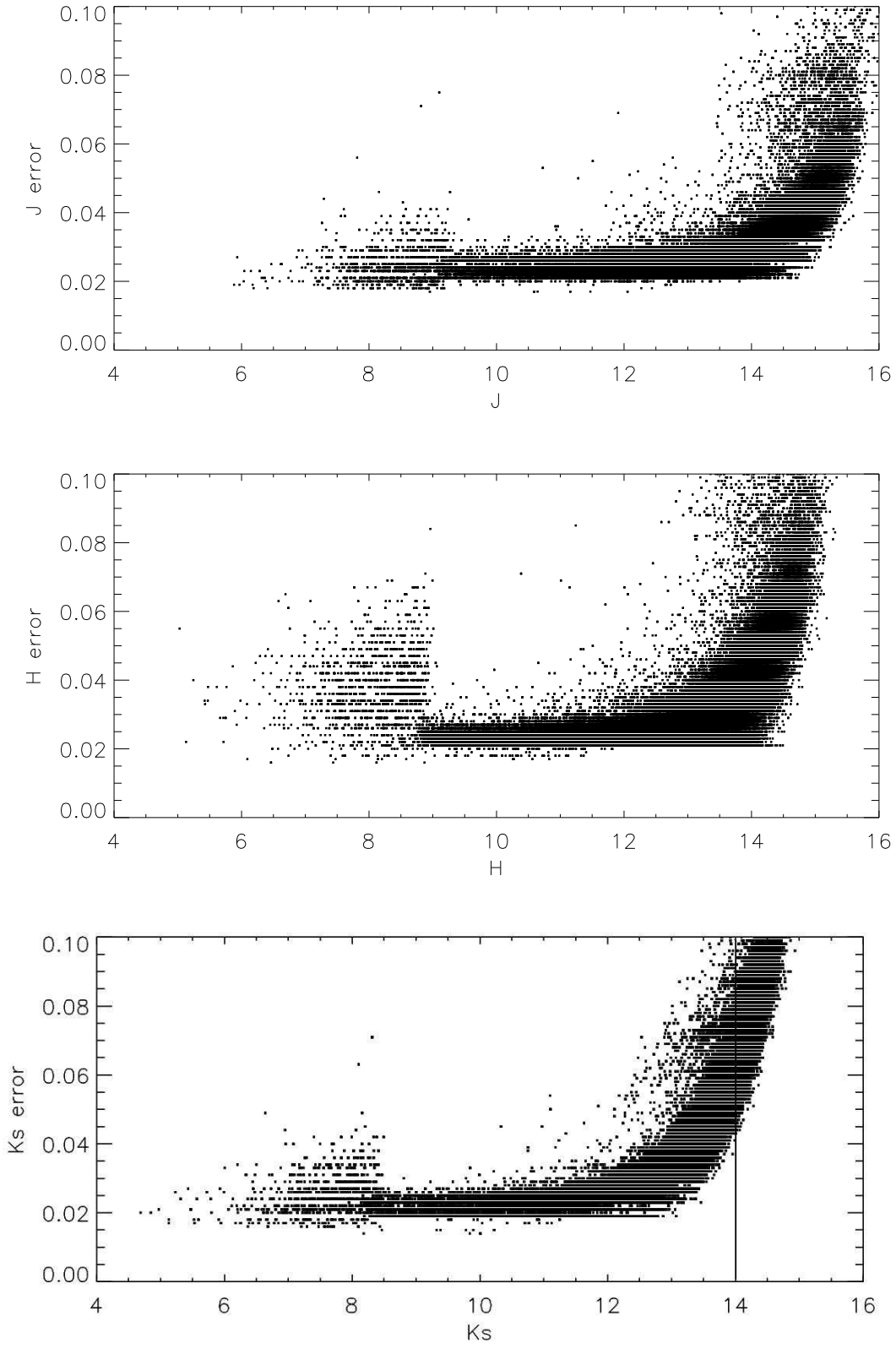

Figure A.1: A comparisson of magnitude versus error for the (top to bottom) 2MASS J, H, $K_{\rm s}$ bands.

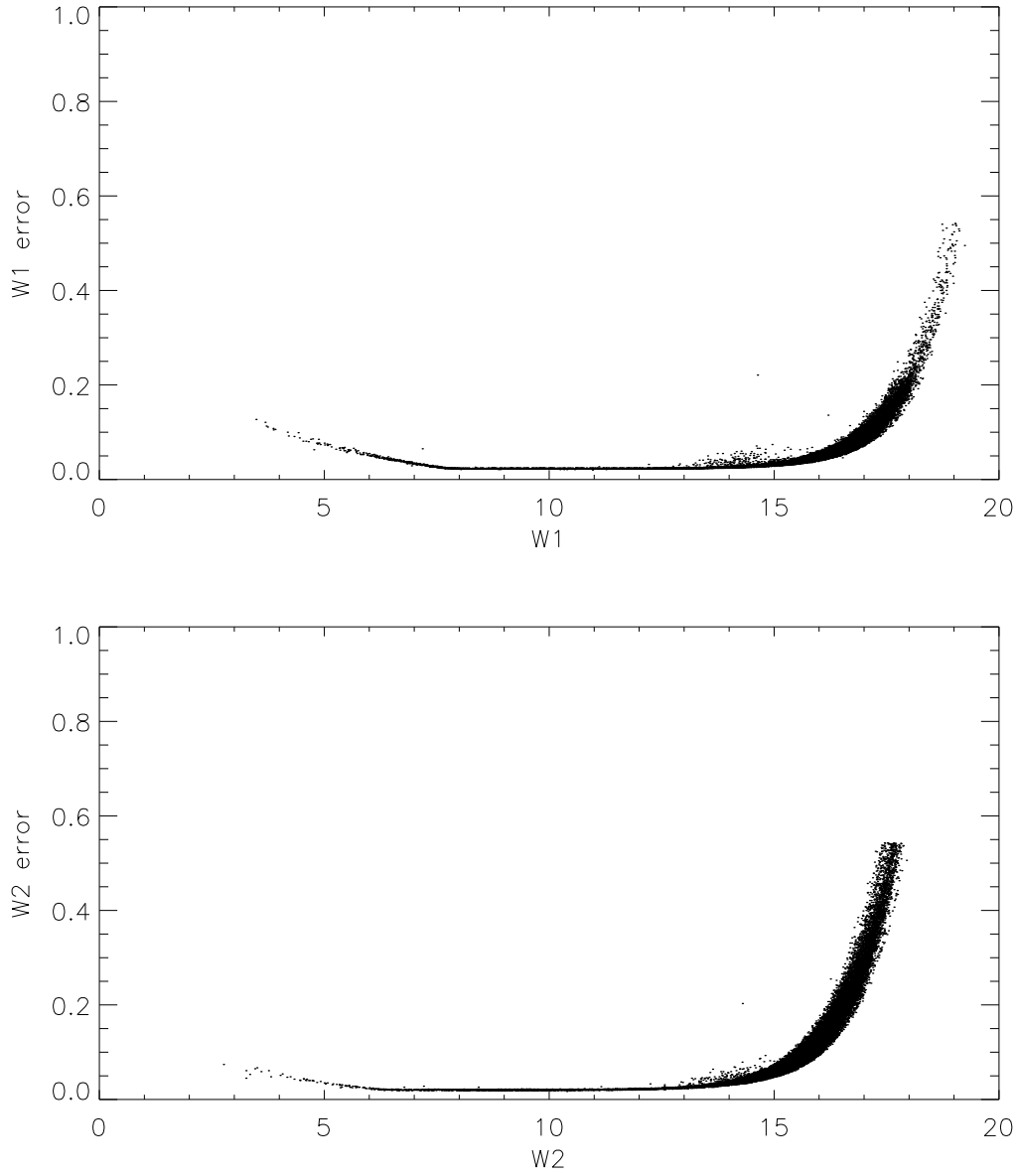

Figure A.2: A comparisson of magnitude versus error for the (top to bottom) WISE $W1$ and $W2$ bands.

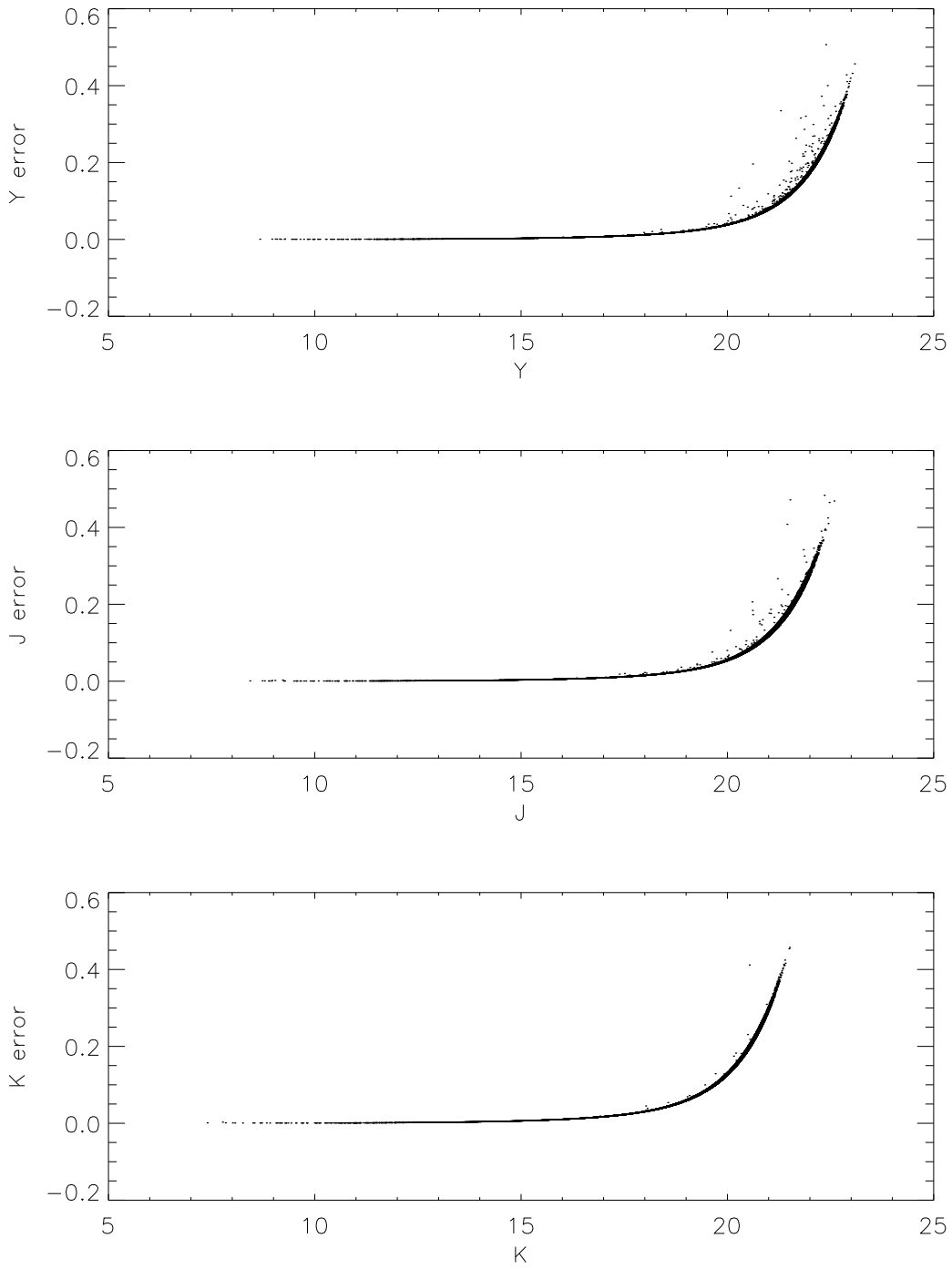

Figure A.3: A comparisson of magnitude versus error for the (top to bottom) VMC Y, J, $K_{\rm s}$ bands.

Appendix B

CMDs of the VMC Bridge for the Galactic foreground removal

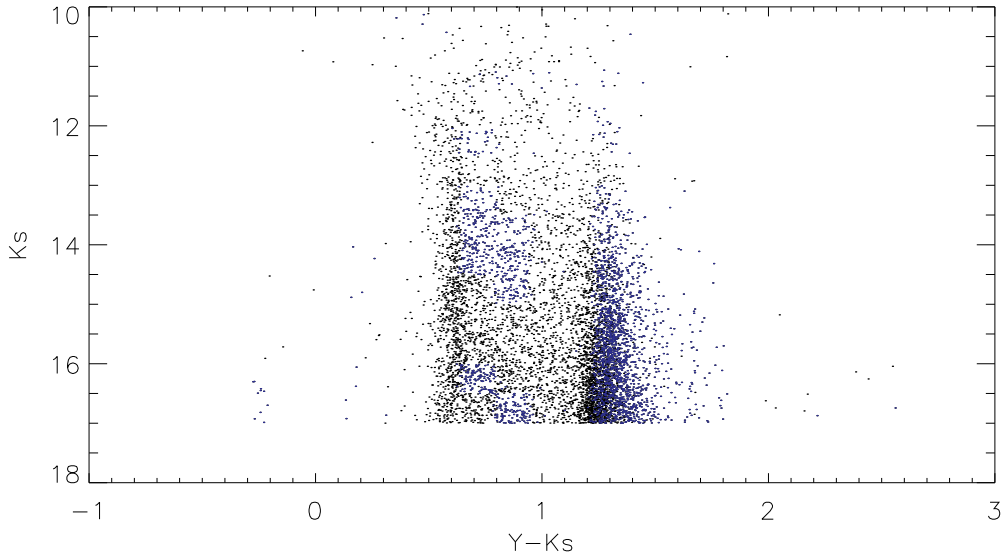

Figure B.1: CMD, $(Y - K_s)$ vs K_s of the Bridge tile 2_4, after the removal of the Galactic foreground population (blue) using the probability method, from the VMC catalogues with the UKIDSS field representing the foreground population (black) in the direction of the Magellanic Clouds.

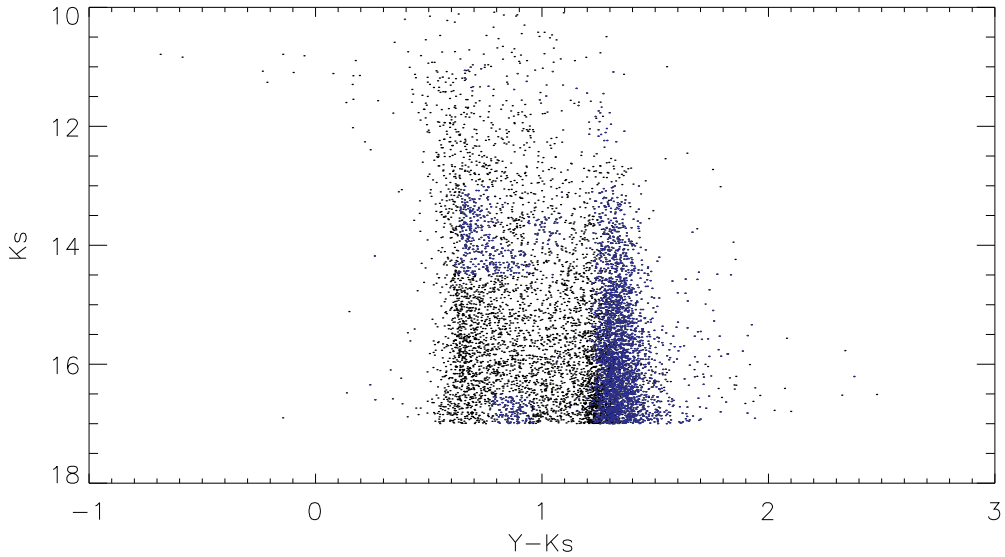

Figure B.2: CMD, $(Y - K_s)$ vs K_s of the Bridge tile 2_8, after the removal of the Galactic foreground population (blue) using the probability method, from the VMC catalogues with the UKIDSS field representing the foreground population (black) in the direction of the Magellanic Clouds.

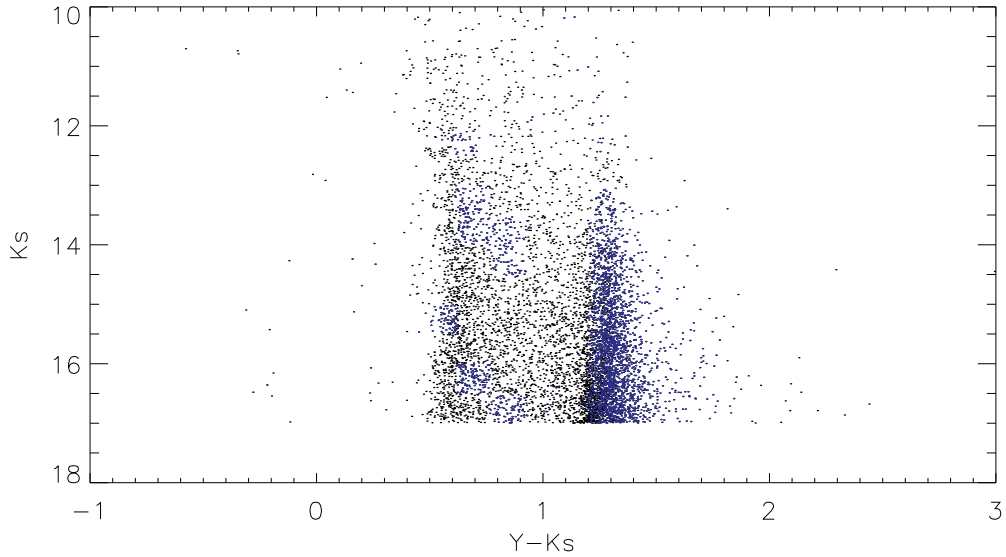

Figure B.3: CMD, $(Y - K_s)$ vs K_s of the Bridge tile 3_5, after the removal of the Galactic foreground population (blue) using the probability method, from the VMC catalogues with the UKIDSS field representing the foreground population (black) in the direction of the Magellanic Clouds.

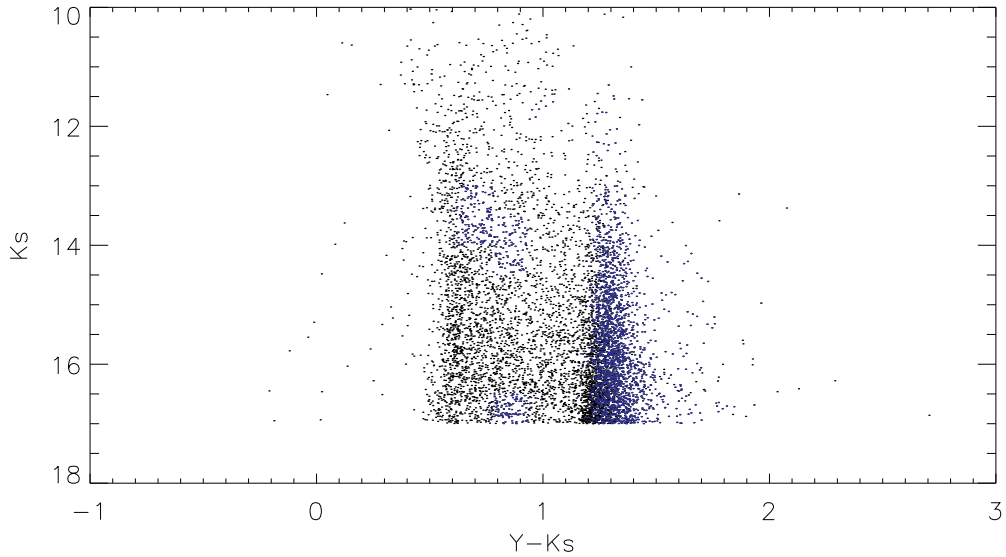

Figure B.4: CMD, $(Y - K_s)$ vs K_s of the Bridge tile 3_7, after the removal of the Galactic foreground population (blue) using the probability method, from the VMC catalogues with the UKIDSS field representing the foreground population (black) in the direction of the Magellanic Clouds.

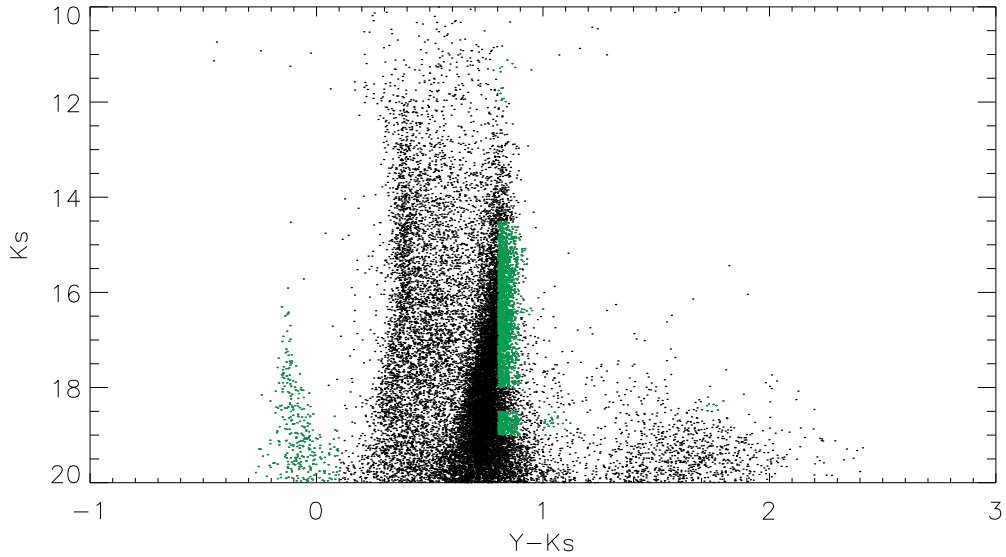

Figure B.5: CMD, $(J - K_s)$ vs K_s of the Bridge tile 2_4, after the removal of the Galactic foreground population (green) using the probability method, from the VMC catalogues with the VMC Stream tile 2_1 representing the foreground population (black) in the direction of the Magellanic Clouds.

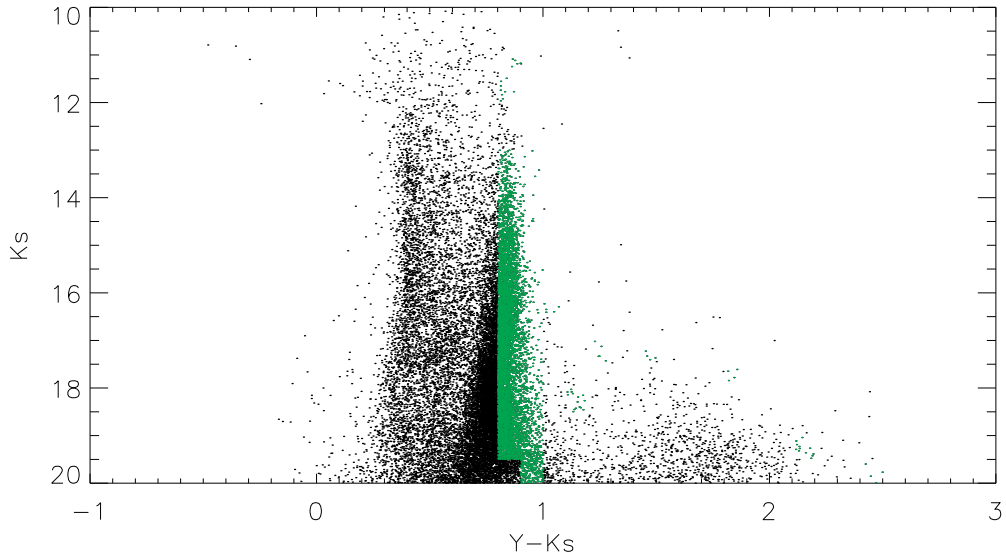

Figure B.6: CMD, $(J - K_s)$ vs K_s of the Bridge tile 2_8, after the removal of the Galactic foreground population (green) using the probability method, from the VMC catalogues with the VMC Stream tile 2_1 representing the foreground population (black) in the direction of the Magellanic Clouds.

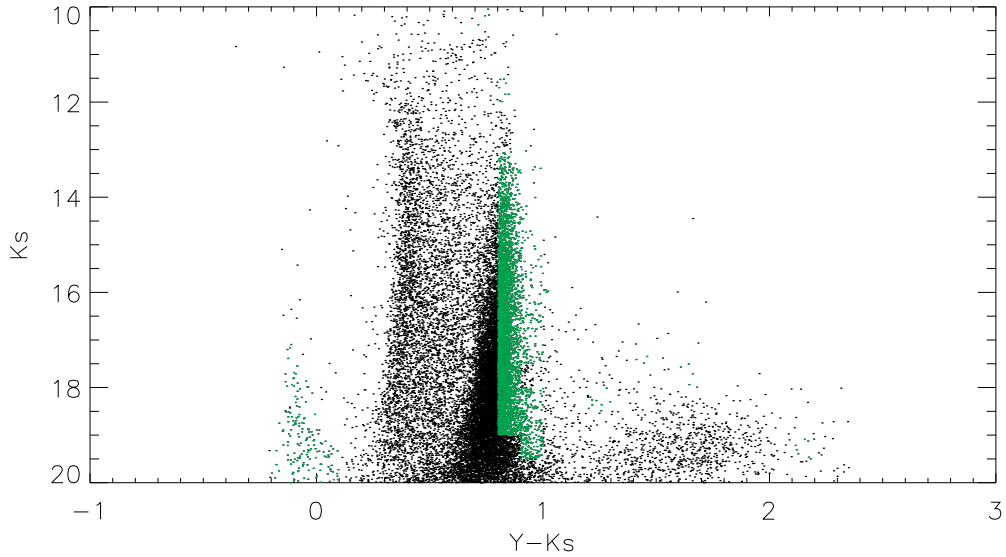

Figure B.7: CMD, $(J - K_s)$ vs K_s of the Bridge tile 3_5, after the removal of the Galactic foreground population (green) using the probability method, from the VMC catalogues with the VMC Stream tile 2_1 representing the foreground population (black) in the direction of the Magellanic Clouds.

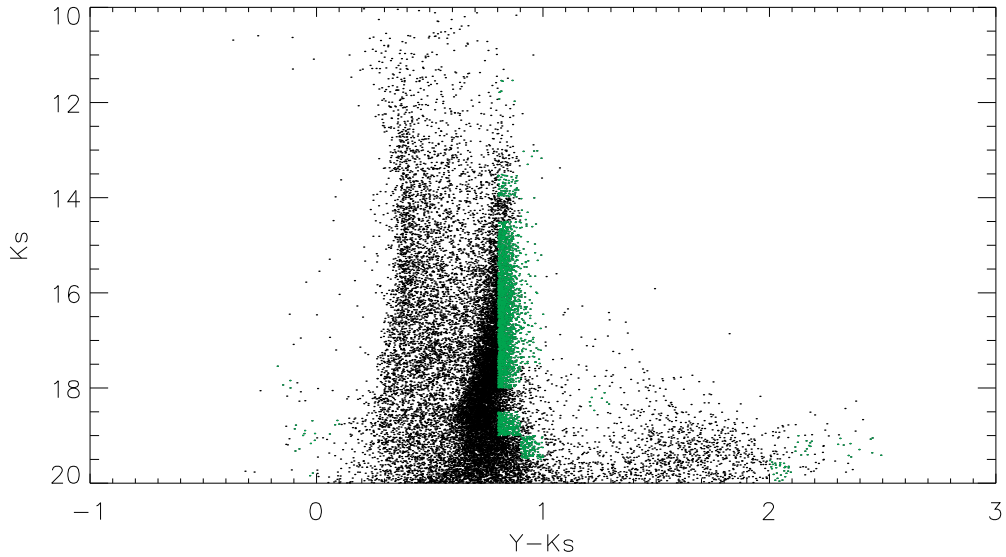

Figure B.8: CMD, $(J - K_s)$ vs K_s of the Bridge tile 3_7, after the removal of the Galactic foreground population (green) using the probability method, from the VMC catalogues with the VMC Stream tile 2_1 representing the foreground population (black) in the direction of the Magellanic Clouds.

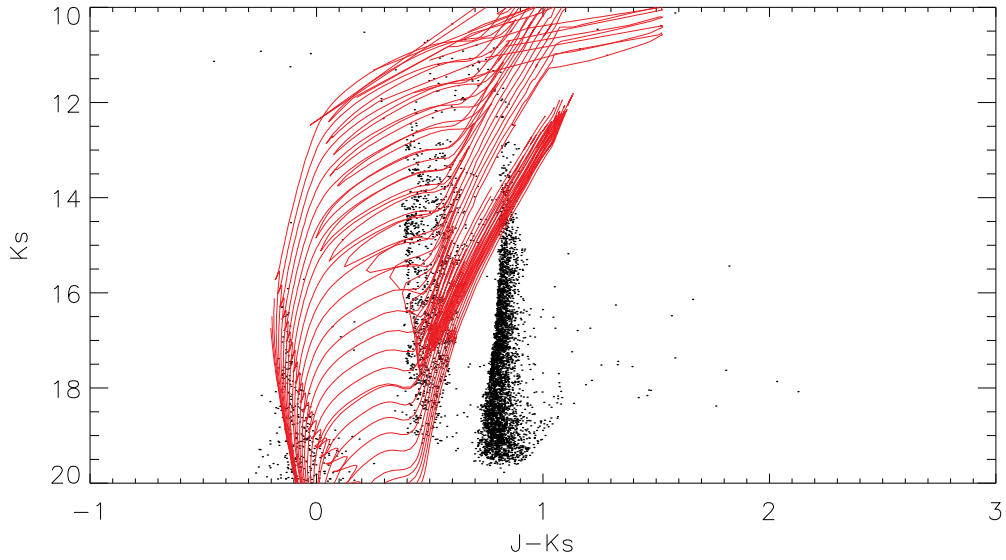

Figure B.9: CMD, $(J - K_s)$ vs K_s of the Bridge tile 2_4, after the removal of the Galactic foreground population using the statistical method, from the VMC catalogues with the VMC Stream tile 2_1 representing the foreground in the direction of the Magellanic Clouds. Overlaid are Padova isochrones (red) at a distance of 55 kpc and a metallicity of $z = 0.004$ and ages from 10 Myr to 10 Byr.

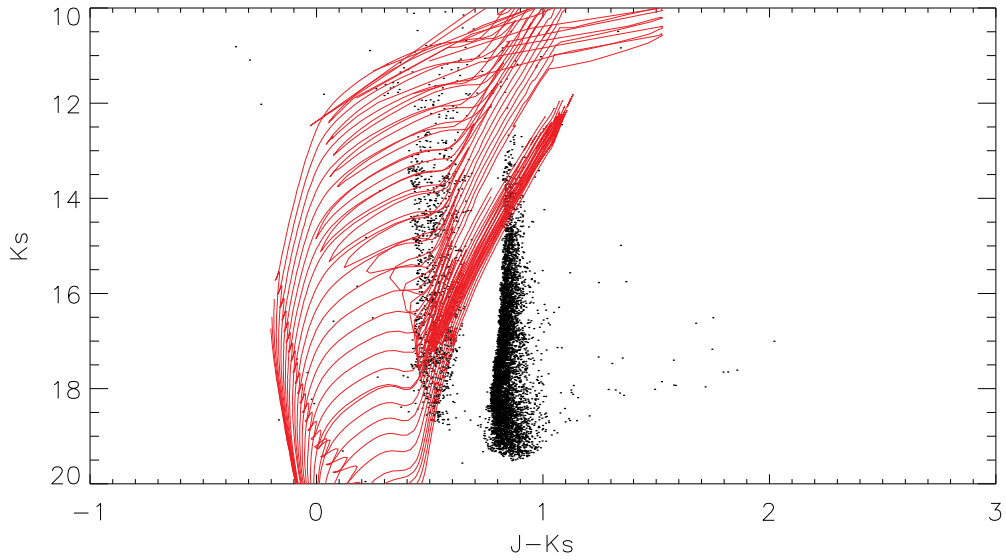

Figure B.10: CMD, $(J - K_s)$ vs K_s of the Bridge tile 2_8, after the removal of the Galactic foreground population using the statistical method, from the VMC catalogues with the VMC Stream tile 2_1 representing the foreground in the direction of the Magellanic Clouds. Overlaid are Padova isochrones (red) at a distance of 55 kpc and a metallicity of $z = 0.004$ and ages from 10 Myr to 10 Byr.

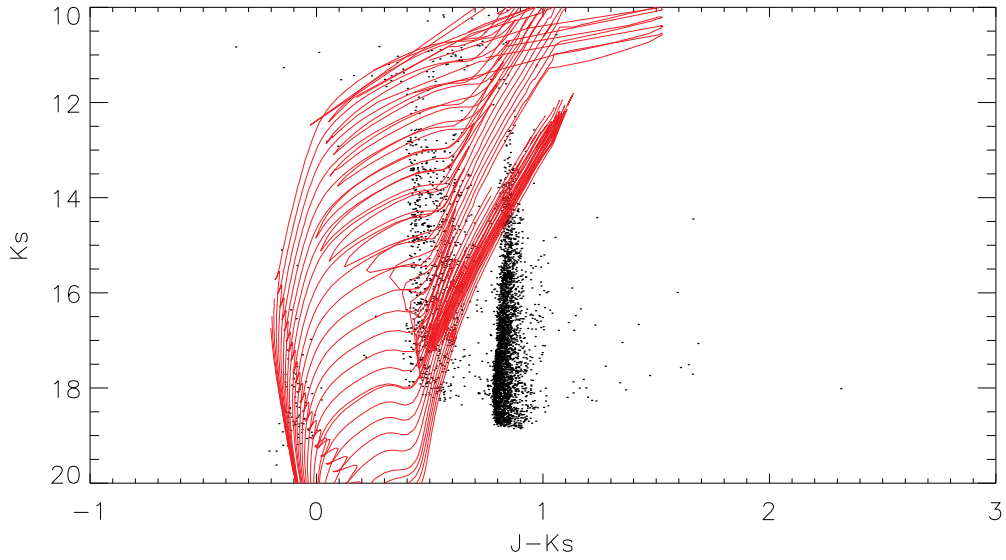

Figure B.11: CMD, $(J - K_s)$ vs K_s of the Bridge tile 3_5, after the removal of the Galactic foreground population using the statistical method, from the VMC catalogues with the VMC Stream tile 2_1 representing the foreground in the direction of the Magellanic Clouds. Overlaid are Padova isochrones (red) at a distance of 55 kpc and a metallicity of $z = 0.004$ and ages from 10 Myr to 10 Byr.

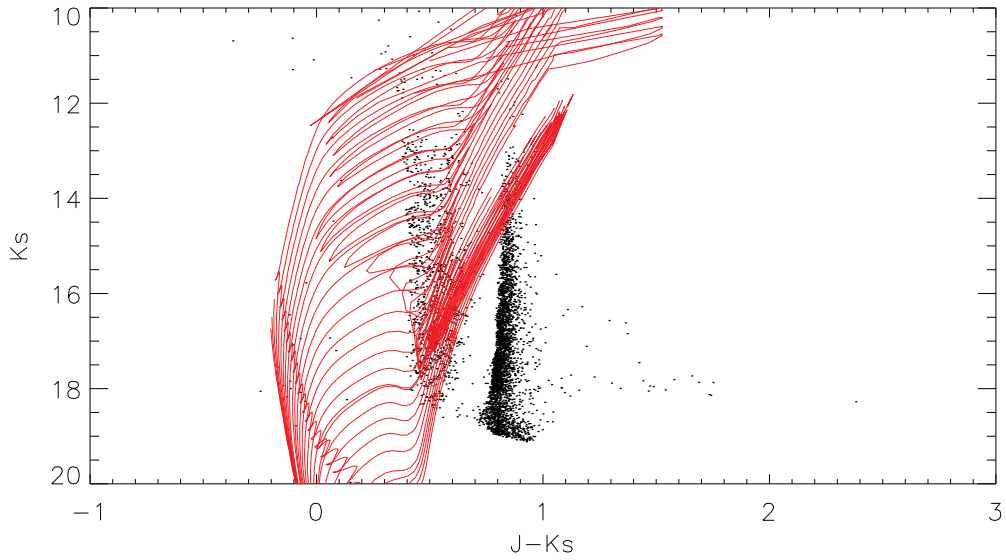

Figure B.12: CMD, $(J - K_s)$ vs K_s of the Bridge tile 3_7, after the removal of the Galactic foreground population using the statistical method, from the VMC catalogues with the VMC Stream tile 2_1 representing the foreground in the direction of the Magellanic Clouds. Overlaid are Padova isochrones (red) at a distance of 55 kpc and a metallicity of $z = 0.004$ and ages from 10 Myr to 10 Byr.

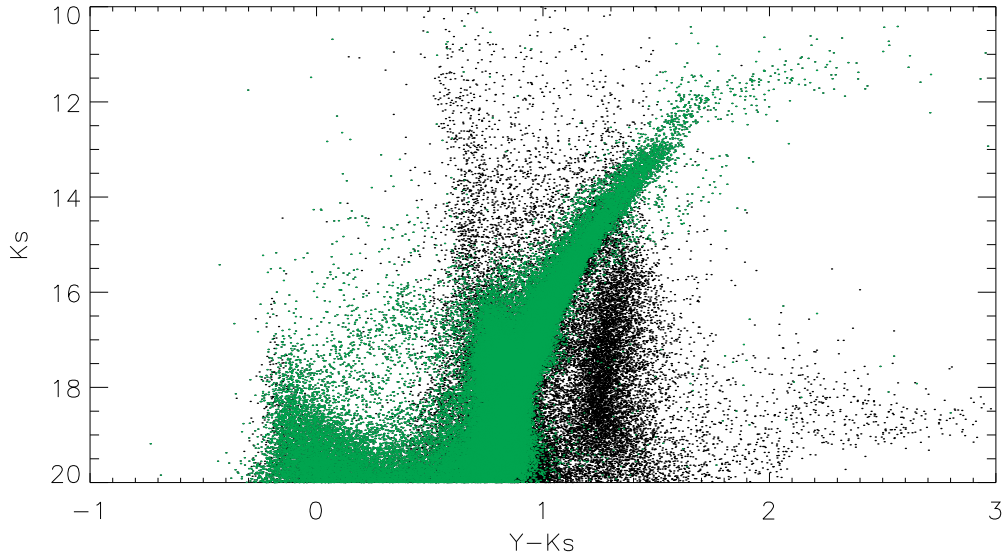

Figure B.13: CMD, $(Y - K_s)$ vs K_s of the SMC tile 3_3 (green) using the Bridge tiles (black) 2_4 as the Galactic foreground region using the statistical method, from the VMC catalogues.

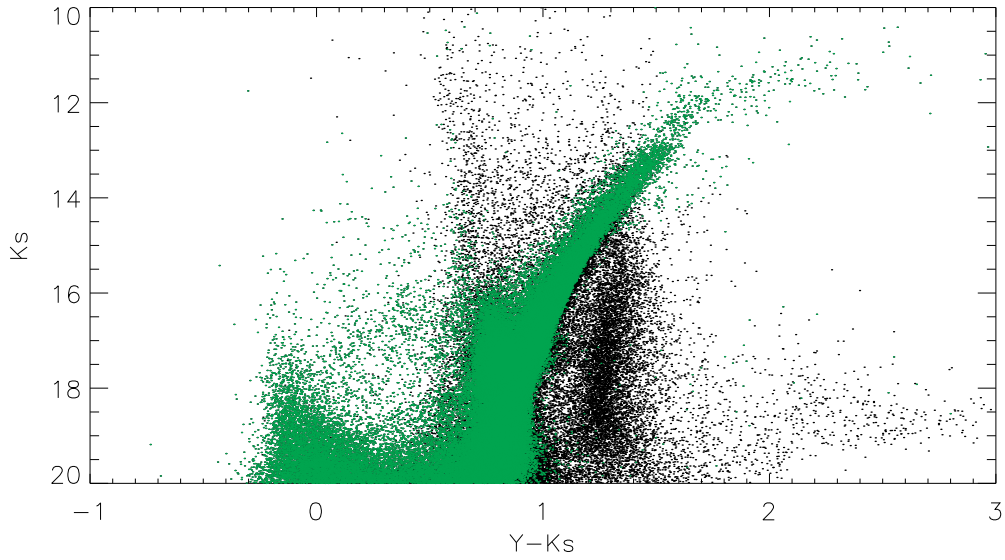

Figure B.14: CMD, $(Y - K_s)$ vs K_s of the SMC tile 3_3 (green) using the Bridge tiles (black) 2_8 as the Galactic foreground region using the statistical method, from the VMC catalogues.

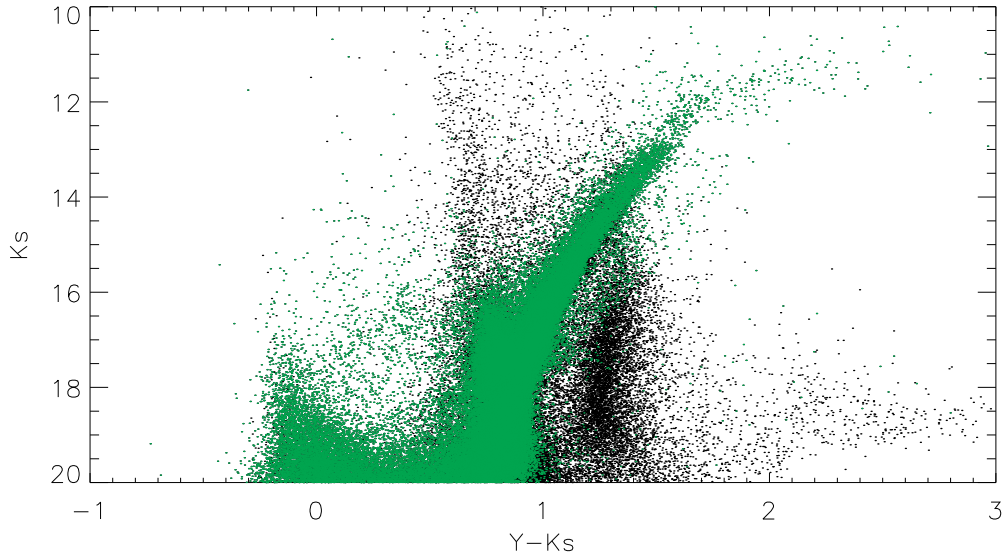

Figure B.15: CMD, $(Y - K_s)$ vs K_s of the SMC tile 3_3 (green) using the Bridge tiles (black) 3_5 as the Galactic foreground region using the statistical method, from the VMC catalogues.

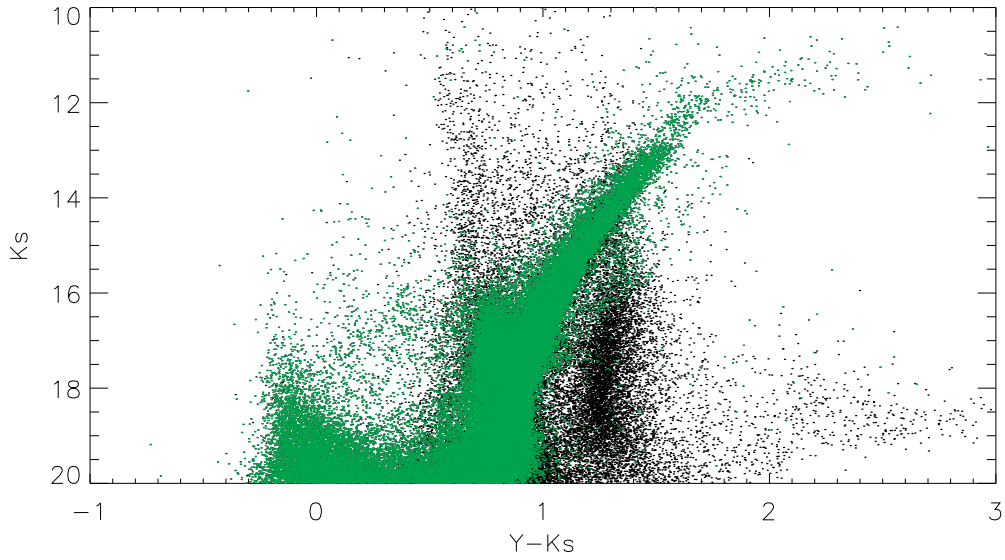

Figure B.16: CMD, $(Y - K_s)$ vs K_s of the SMC tile 3_3 (green) using the Bridge tiles (black) 3_7 as the Galactic foreground region using the statistical method, from the VMC catalogues.

Appendix C

Magellanic Bridge candidates from the VMC catalogue

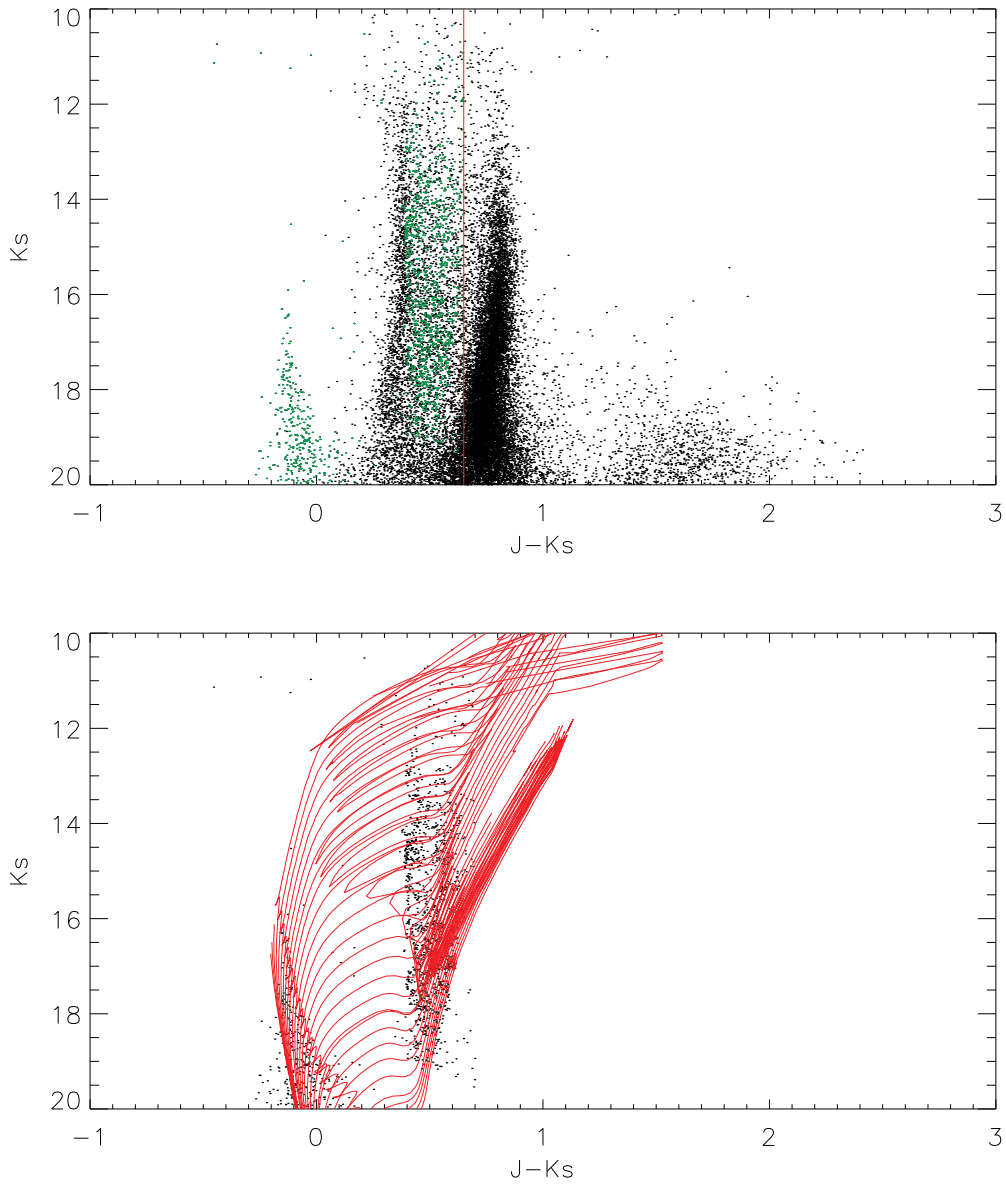

Figure C.1: CMD, $(J - K_s)$ vs K_s of the Bridge tile 2_4, after the removal of the Galactic foreground population (green) using the statistical method (top), from the VMC catalogues with the VMC Stream tile 2_1 representing the foreground population (black) in the direction of the Magellanic Clouds. Bottom is the cleaned Bridge candidates with Padova isochrones of ages (top to bottom) log(age/yr)=7.0 − 10.0 in steps of 0.1.

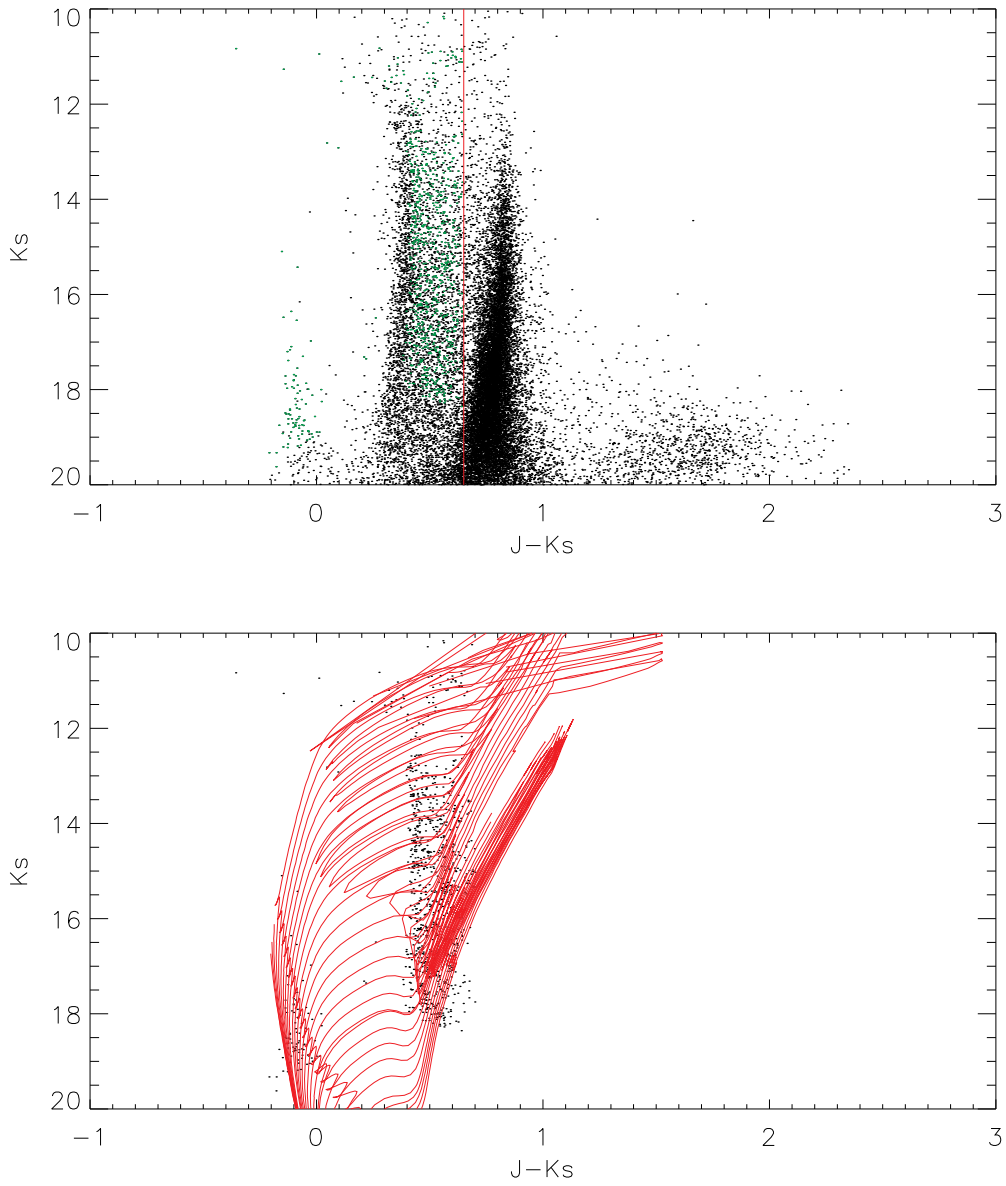

Figure C.2: CMD, $(J - K_s)$ vs K_s of the Bridge tile 3_5, after the removal of the Galactic foreground population (green) using the statistical method (top), from the VMC catalogues with the VMC Stream tile 2_1 representing the foreground population (black) in the direction of the Magellanic Clouds. Bottom is the cleaned Bridge candidates with Padova isochrones of ages (top to bottom) log(age/yr)=7.0 − 10.0 in steps of 0.1.

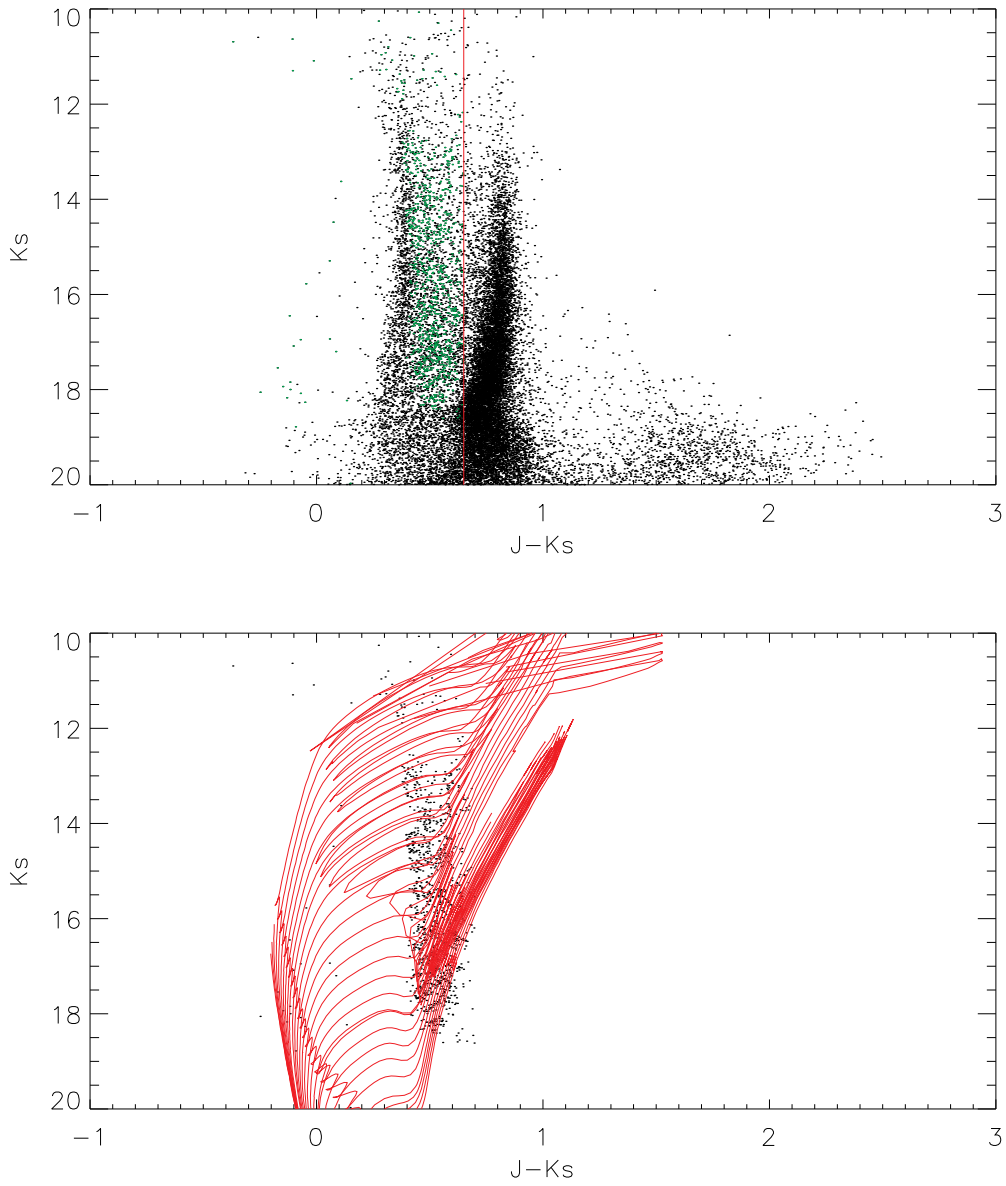

Figure C.3: CMD, $(J - K_s)$ vs K_s of the Bridge tile 3_7, after the removal of the Galactic foreground population (green) using the statistical method (top), from the VMC catalogues with the VMC Stream tile 2_1 representing the foreground population (black) in the direction of the Magellanic Clouds. Bottom is the cleaned Bridge candidates with Padova isochrones of ages (top to bottom) log(age/yr)=7.0 − 10.0 in steps of 0.1.

Appendix D

Bridge candidate Spectra

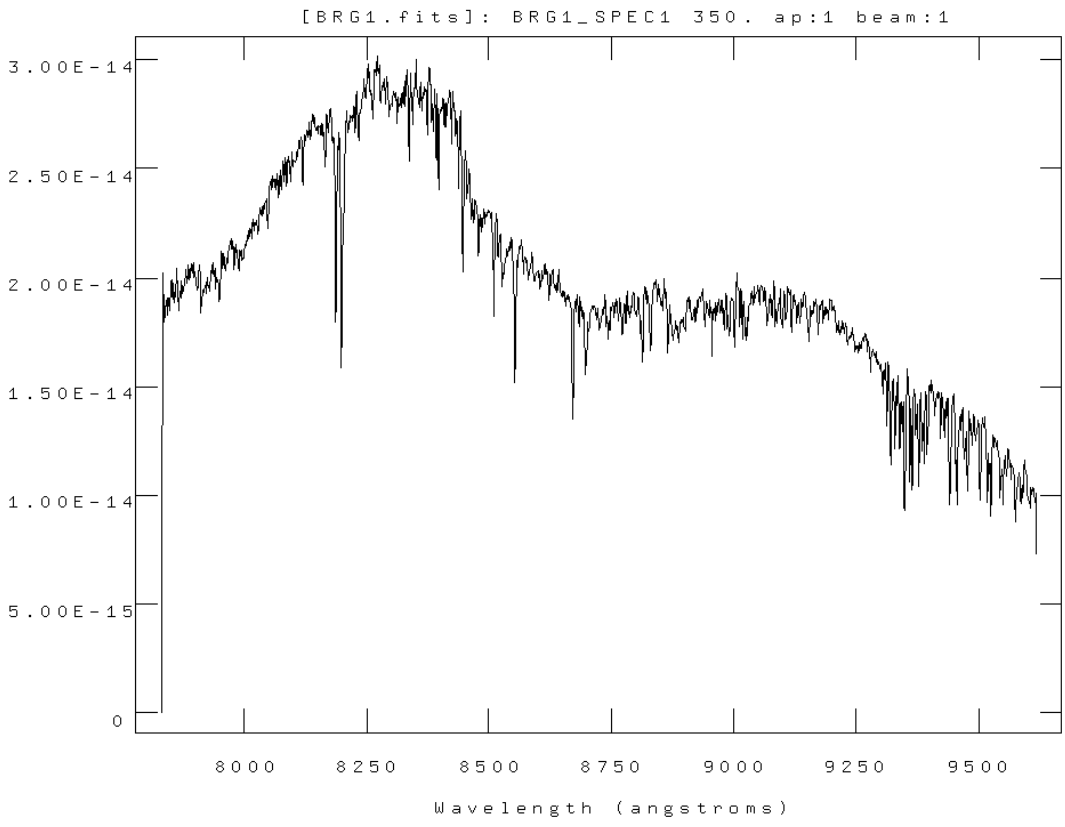

Figure D.1: The final flux calibrated spectrum of object BRG1 with flux in erg^{-2} cm^{-2} s^{-1} Å^{-1}.

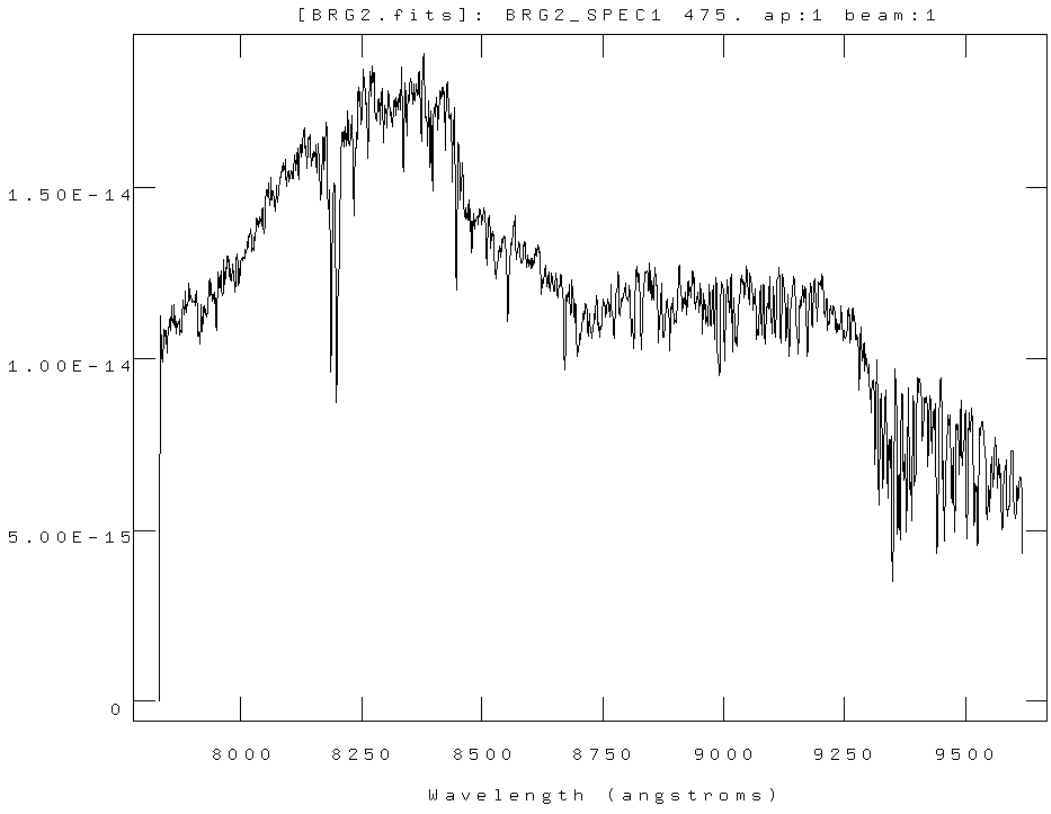

Figure D.2: The final flux calibrated spectrum of object BRG2 with flux in erg^{-2} cm^{-2} s^{-1} Å^{-1}.

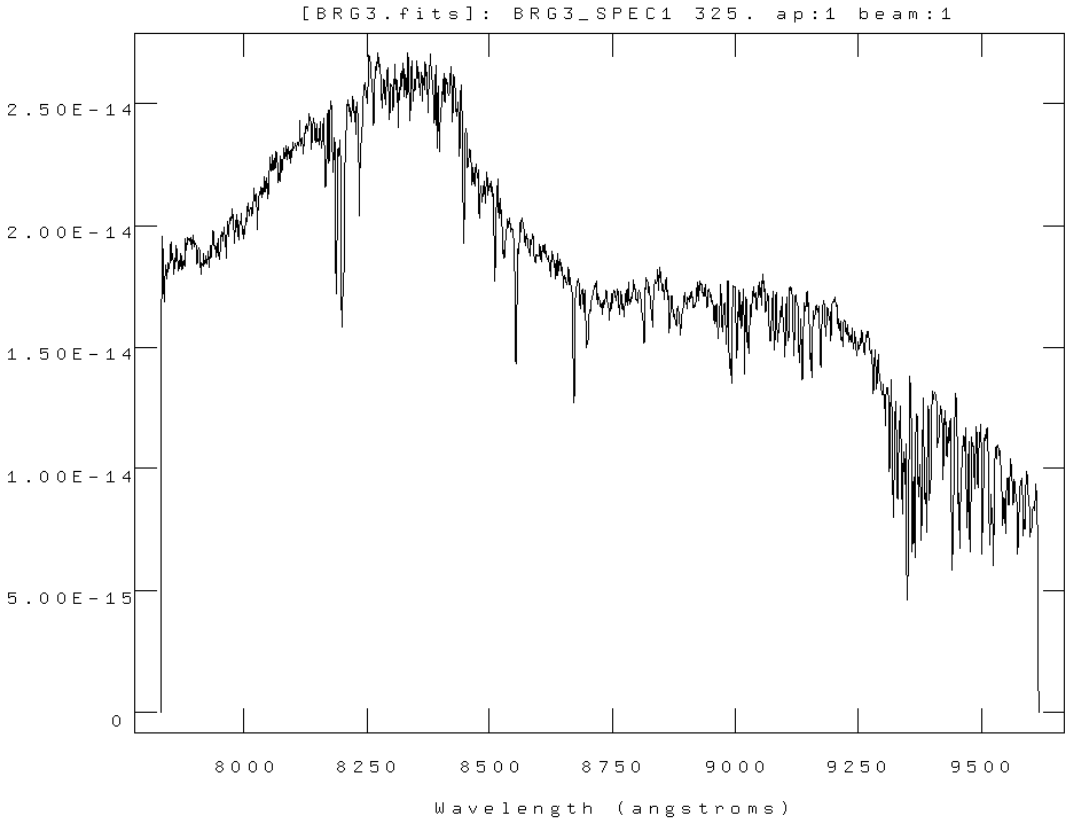

Figure D.3: The final flux calibrated spectrum of object BRG3 with flux in erg^{-2} cm^{-2} s^{-1} Å^{-1}.

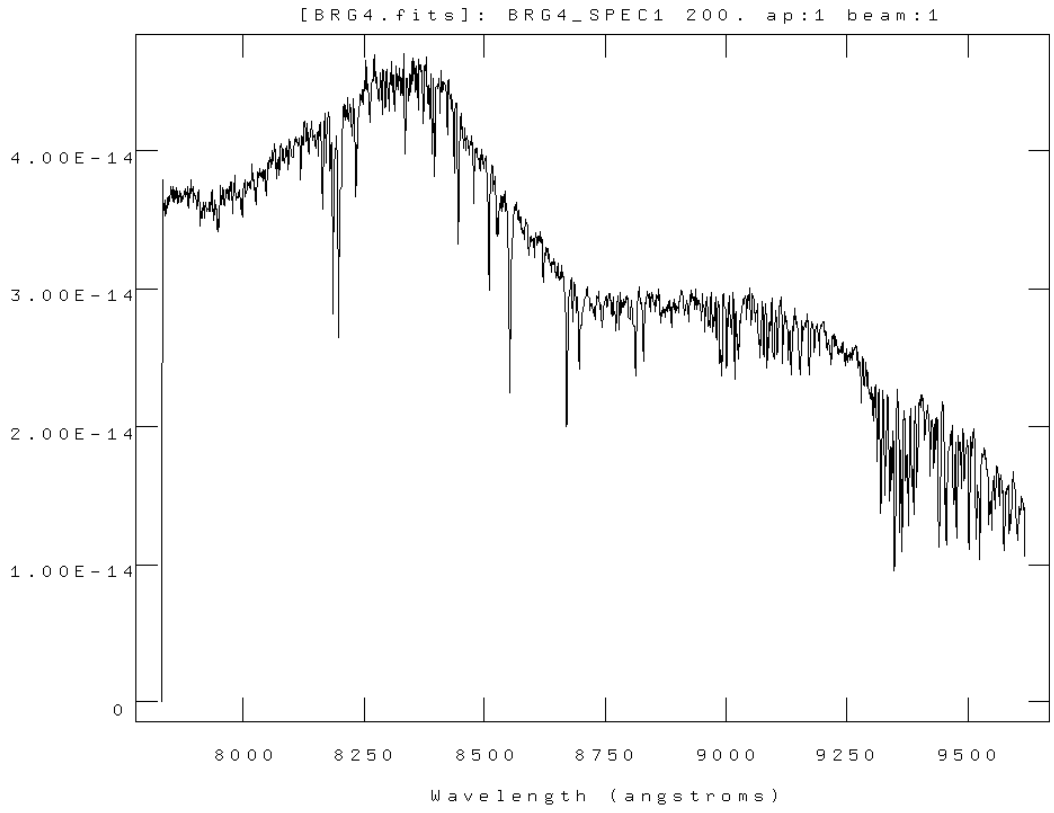

Figure D.4: The final flux calibrated spectrum of object BRG4 with flux in erg^{-2} cm^{-2} s^{-1} Å^{-1}.

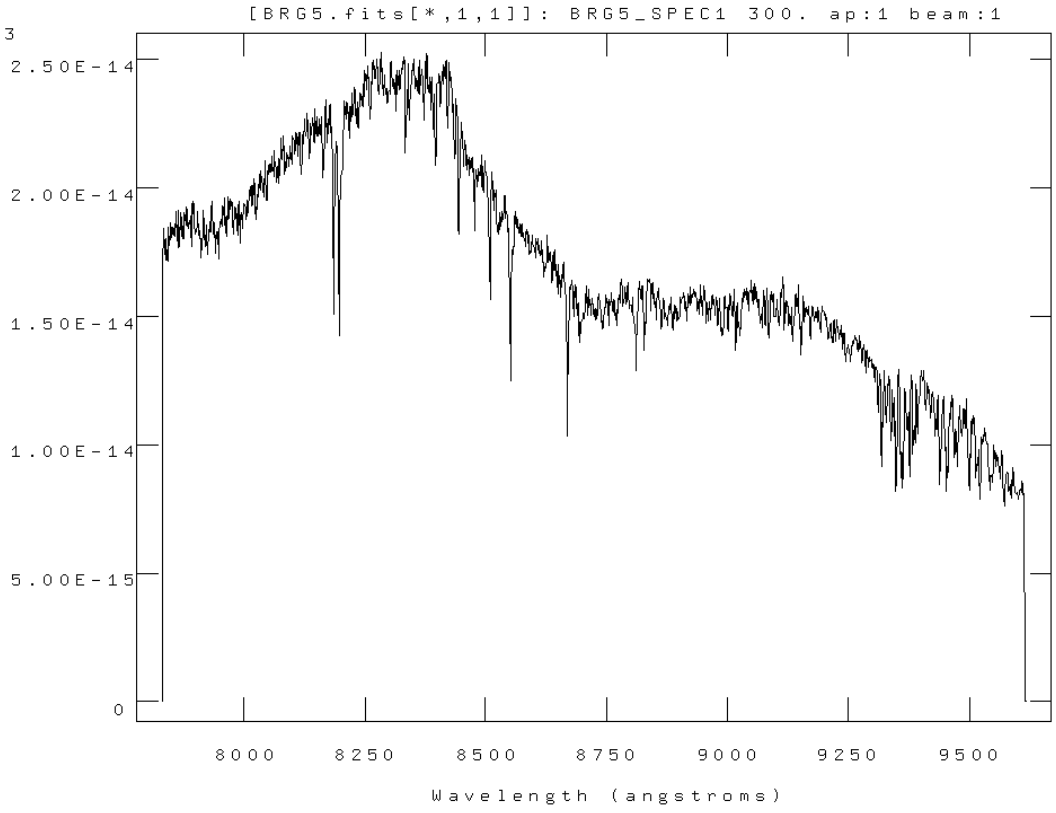

Figure D.5: The final flux calibrated spectrum of object BRG5 with flux in erg^{-2} cm^{-2} s^{-1} Å^{-1}.

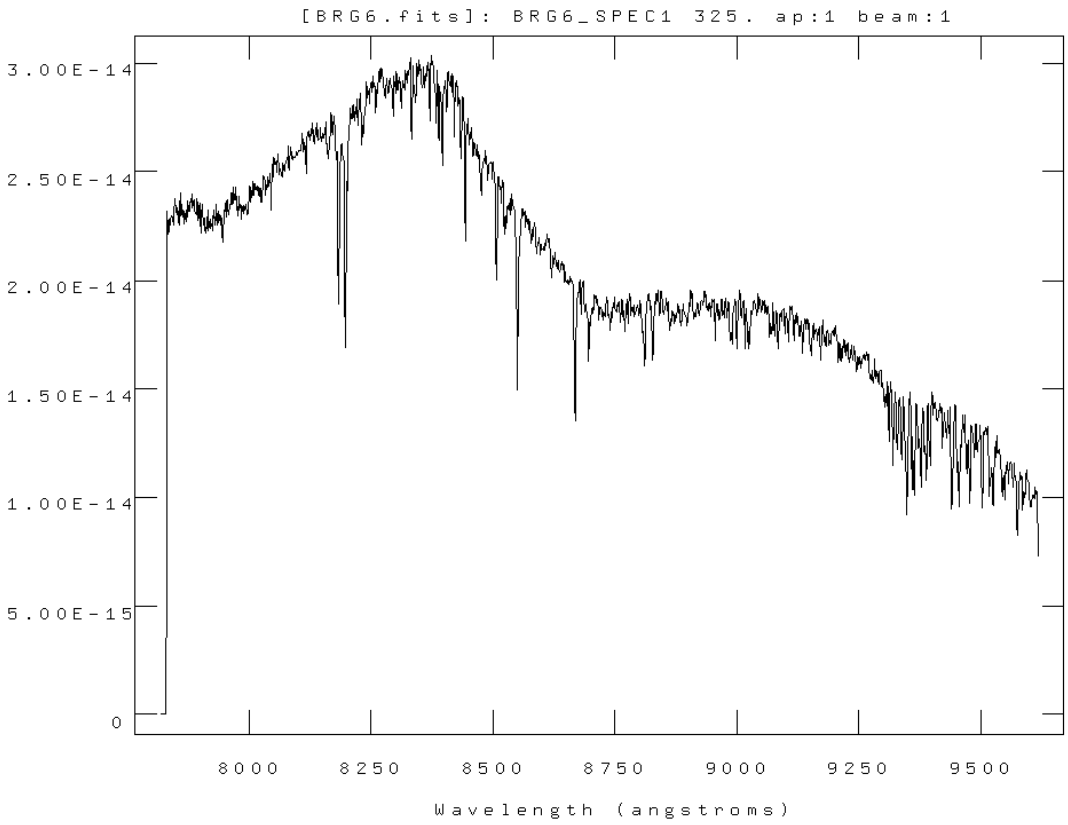

Figure D.6: The final flux calibrated spectrum of object BRG6 with flux in erg^{-2} cm^{-2} s^{-1} Å^{-1}.

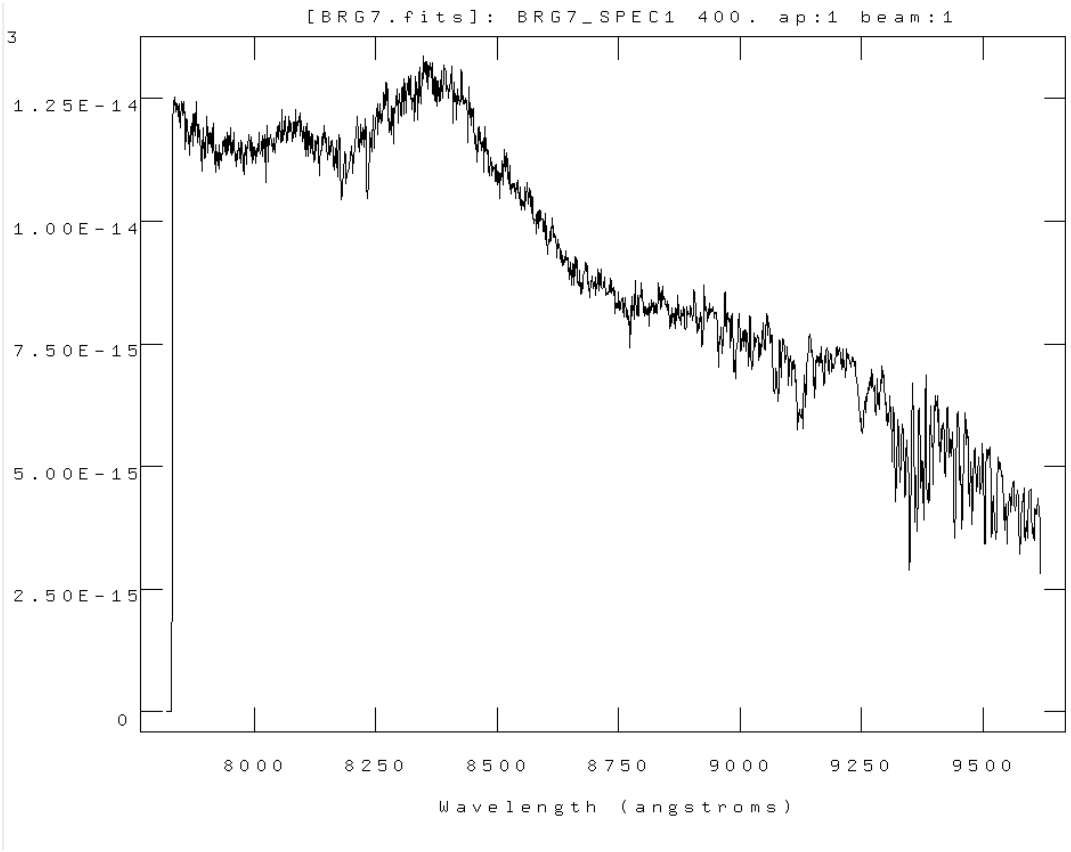

Figure D.7: The final flux calibrated spectrum of object BRG7 with flux in erg^{-2} cm^{-2} s^{-1} Å^{-1}.

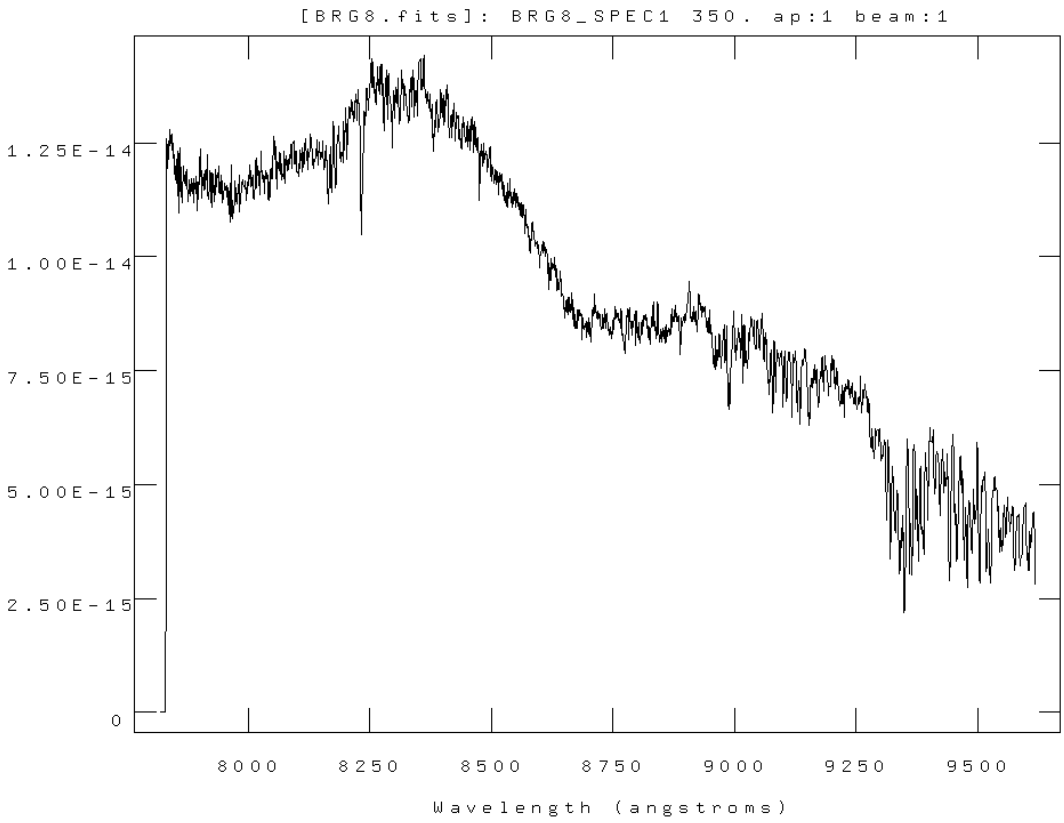

Figure D.8: The final flux calibrated spectrum of object BRG8 with flux in erg^{-2} cm^{-2} s^{-1} Å^{-1}.

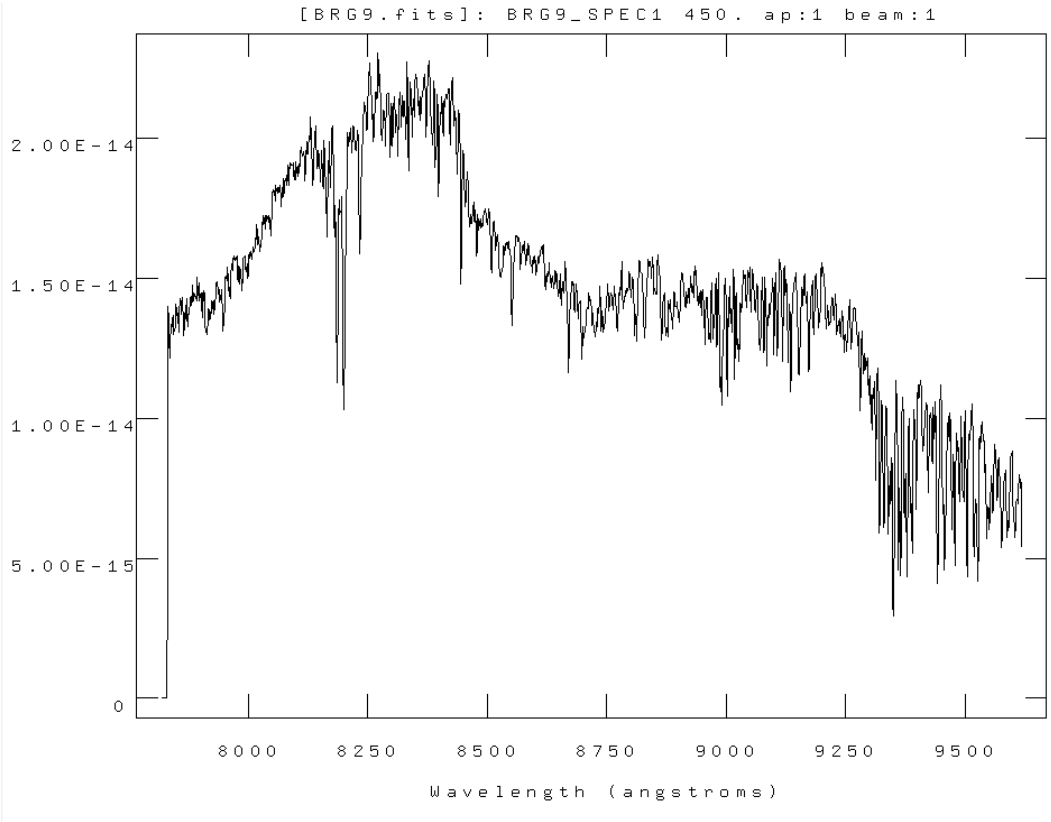

Figure D.9: The final flux calibrated spectrum of object BRG9 with flux in erg^{-2} cm^{-2} s^{-1} Å^{-1}.

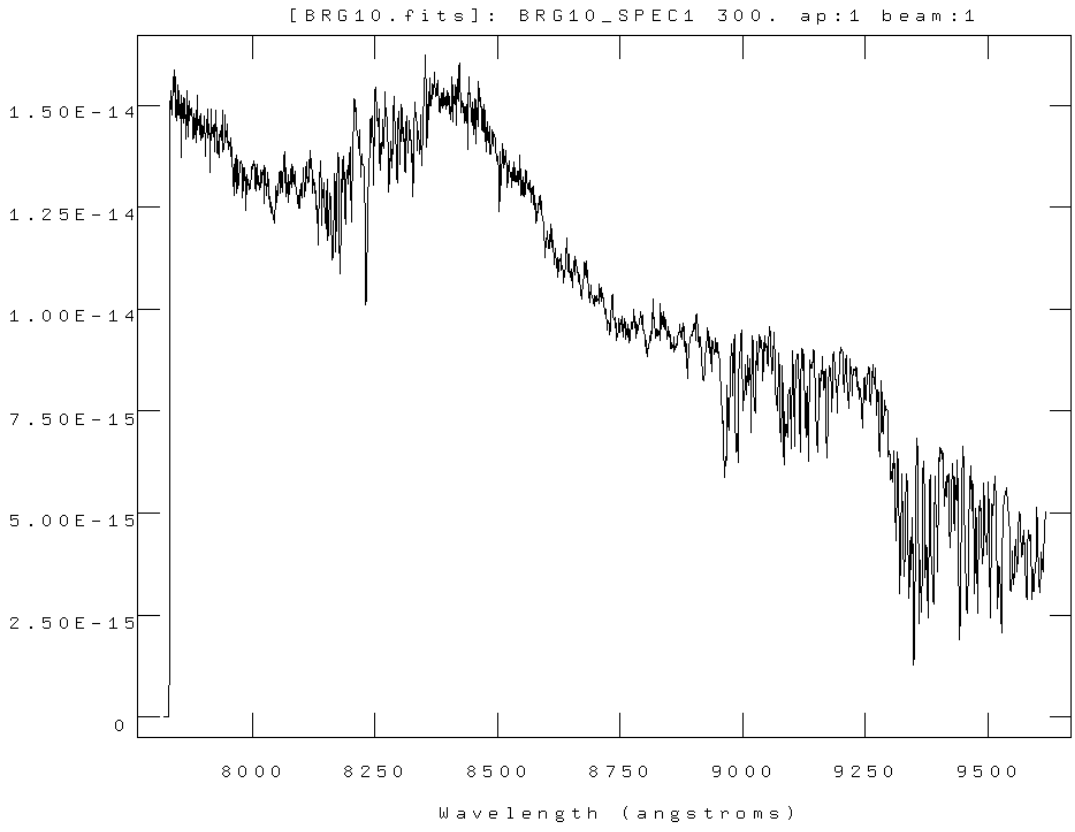

Figure D.10: The final flux calibrated spectrum of object BRG10 with flux in $\mathrm{erg}^{-2}\ \mathrm{cm}^{-2}\ \mathrm{s}^{-1}\ \mathrm{\AA}^{-1}$.

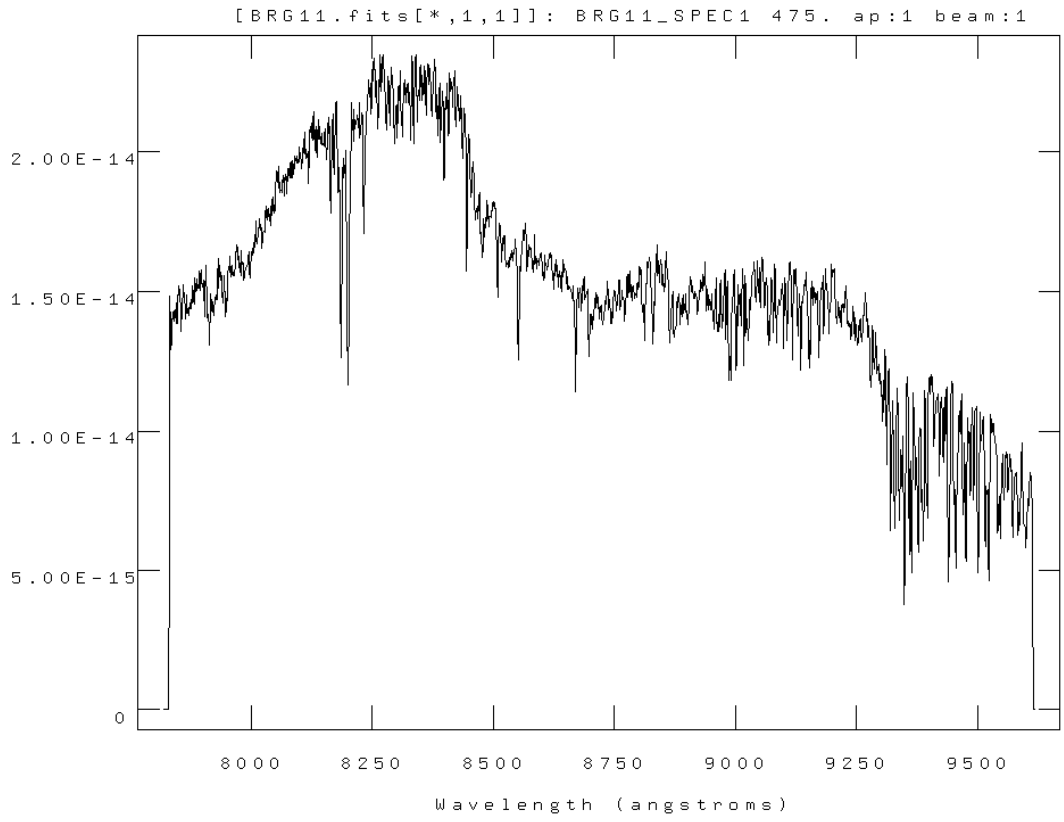

Figure D.11: The final flux calibrated spectrum of object BRG11 with flux in $\mathrm{erg}^{-2}\ \mathrm{cm}^{-2}\ \mathrm{s}^{-1}\ \mathrm{\AA}^{-1}$.

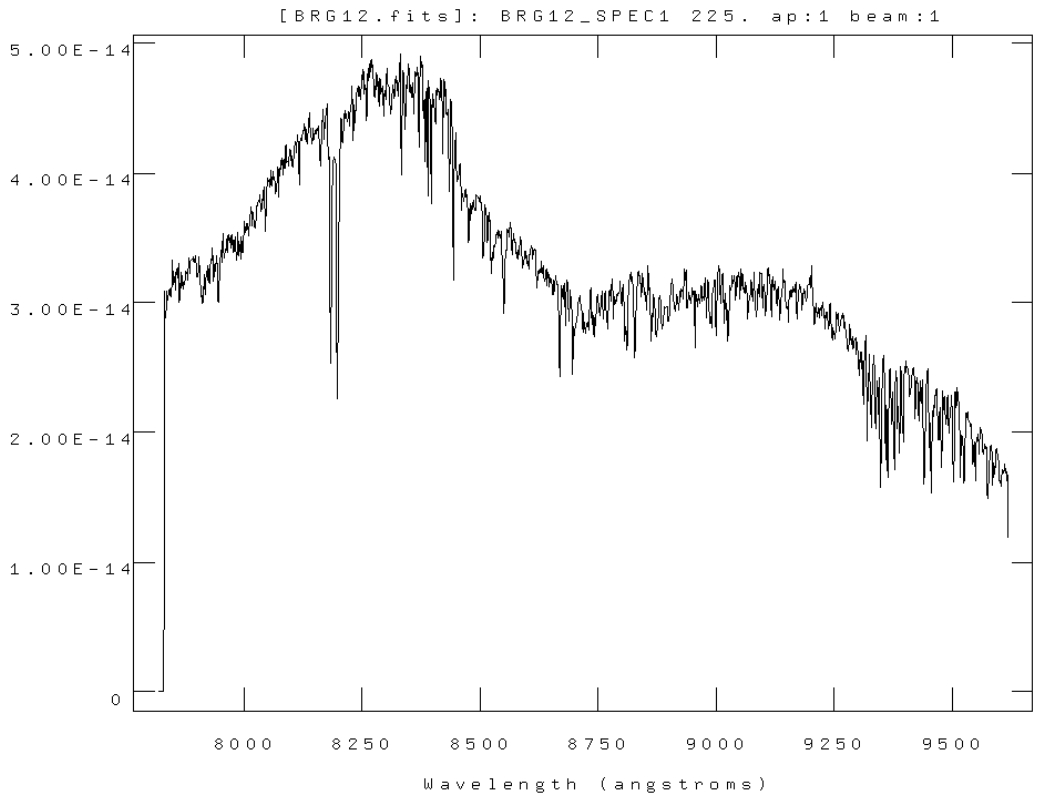

Figure D.12: The final flux calibrated spectrum of object BRG12 with flux in $\mathrm{erg}^{-2}\ \mathrm{cm}^{-2}\ \mathrm{s}^{-1}\ \text{Å}^{-1}$.

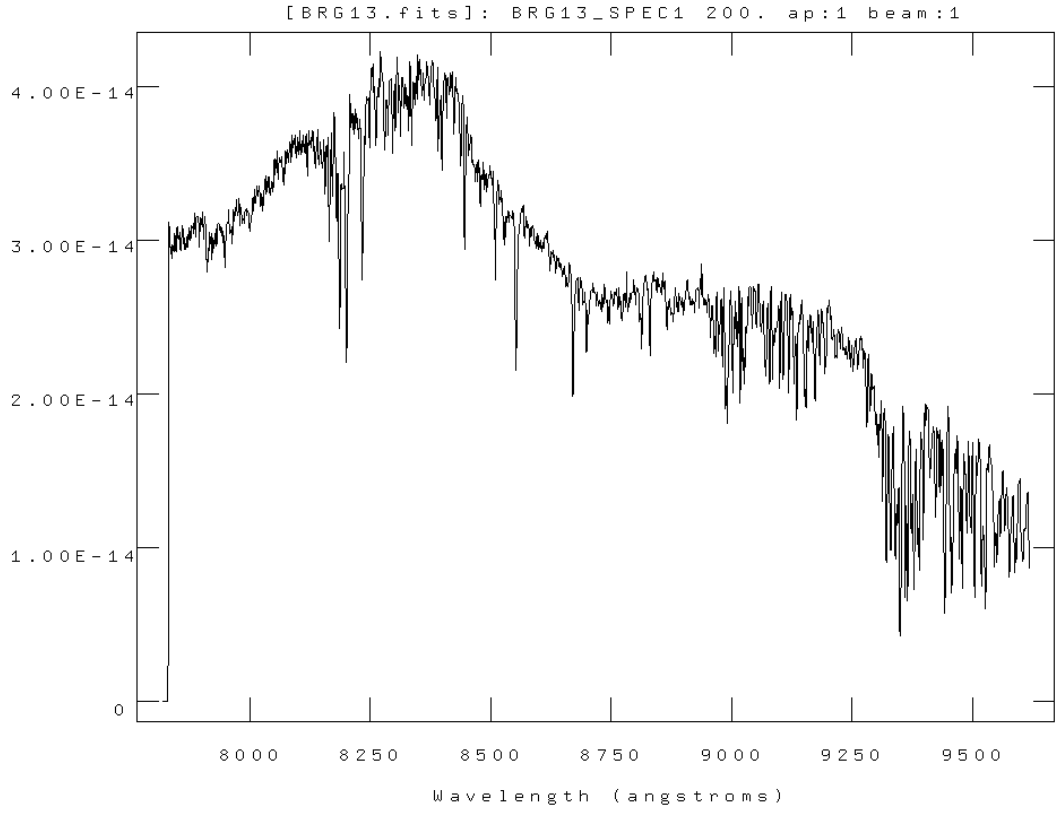

Figure D.13: The final flux calibrated spectrum of object BRG13 with flux in $\mathrm{erg}^{-2}\ \mathrm{cm}^{-2}\ \mathrm{s}^{-1}\ \mathrm{\AA}^{-1}$.

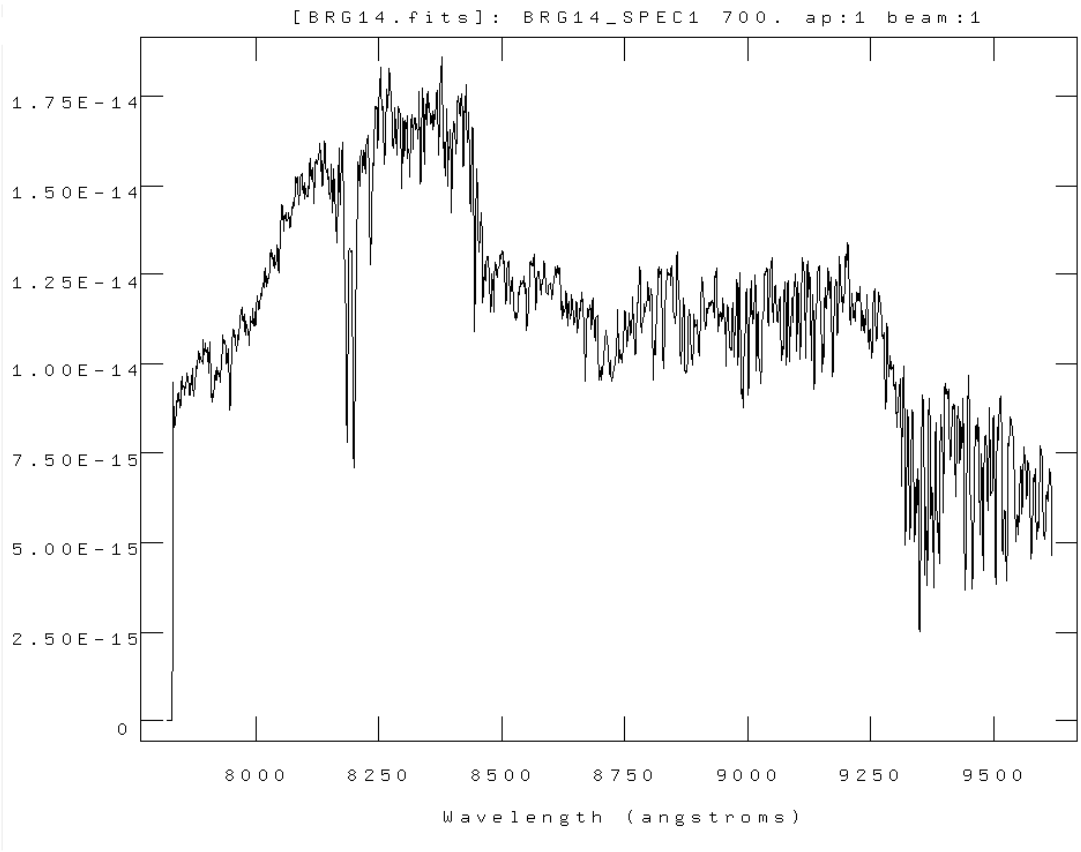

Figure D.14: The final flux calibrated spectrum of object BRG14 with flux in $\mathrm{erg}^{-2}\ \mathrm{cm}^{-2}\ \mathrm{s}^{-1}\ \text{Å}^{-1}$.

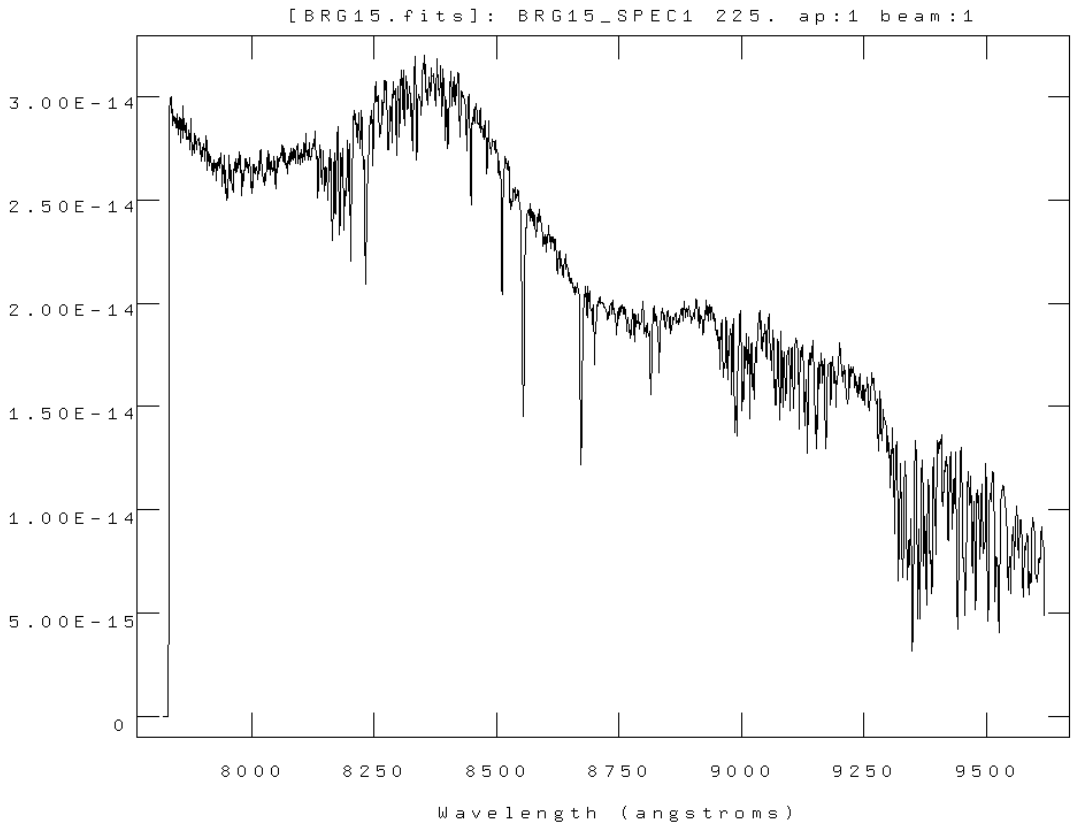

Figure D.15: The final flux calibrated spectrum of object BRG15 with flux in $\mathrm{erg}^{-2}\ \mathrm{cm}^{-2}\ \mathrm{s}^{-1}\ \mathrm{\AA}^{-1}$.

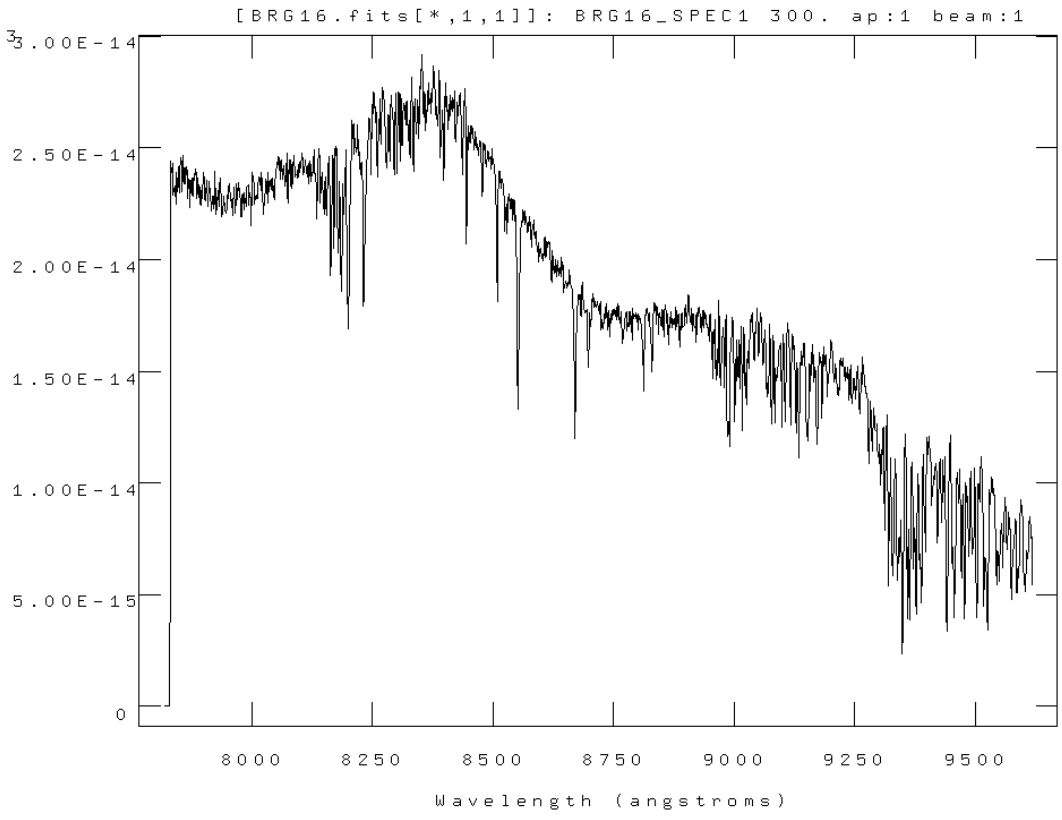

Figure D.16: The final flux calibrated spectrum of object BRG16 with flux in $\mathrm{erg}^{-2}\ \mathrm{cm}^{-2}\ \mathrm{s}^{-1}\ \mathrm{\AA}^{-1}$.

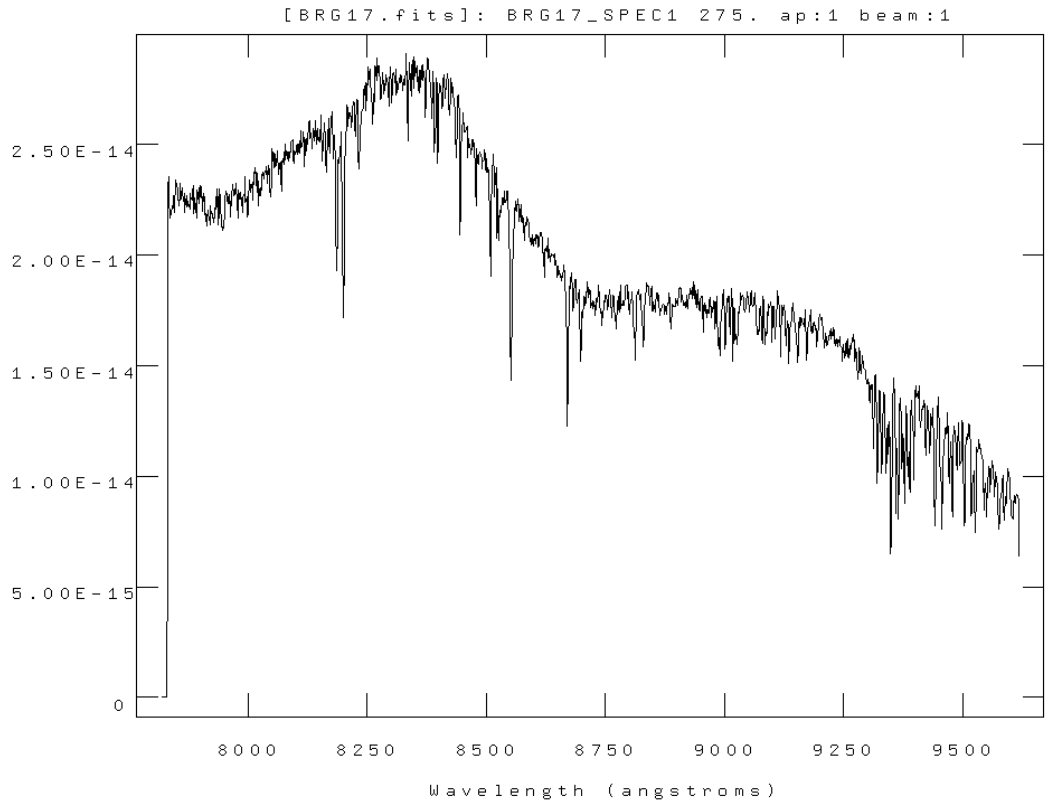

Figure D.17: The final flux calibrated spectrum of object BRG17 with flux in $\mathrm{erg}^{-2}\ \mathrm{cm}^{-2}\ \mathrm{s}^{-1}\ \text{Å}^{-1}$.

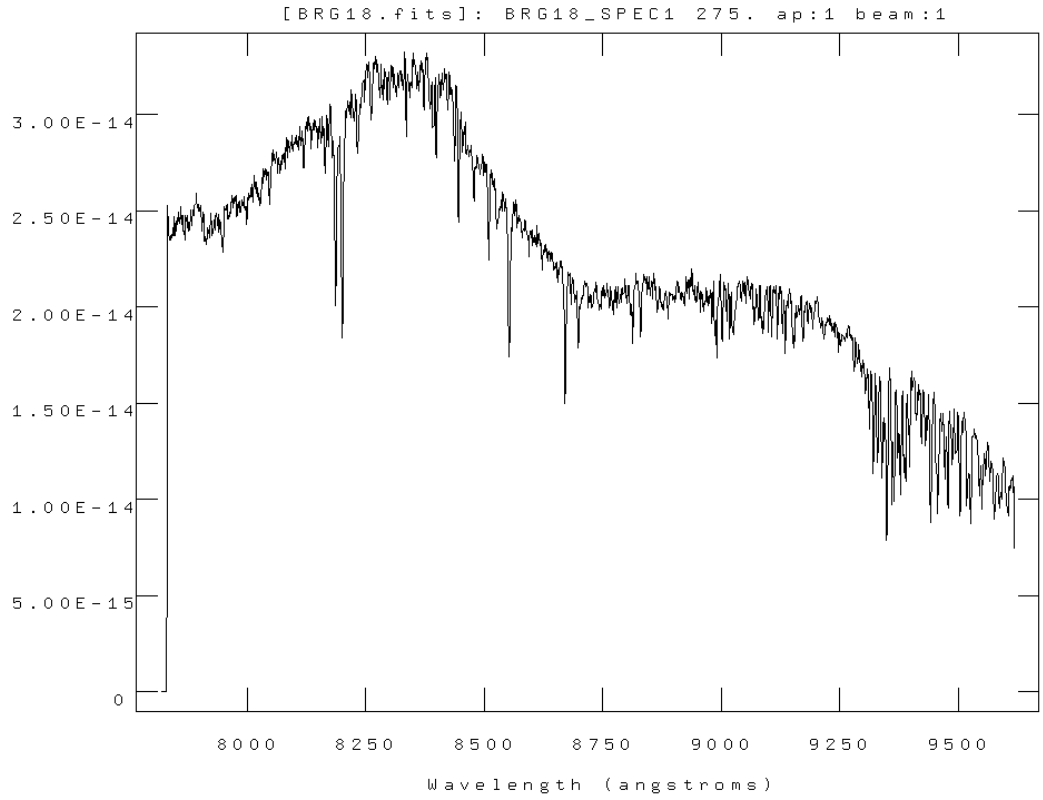

Figure D.18: The final flux calibrated spectrum of object BRG18 with flux in $\mathrm{erg}^{-2}\ \mathrm{cm}^{-2}\ \mathrm{s}^{-1}\ \text{Å}^{-1}$.

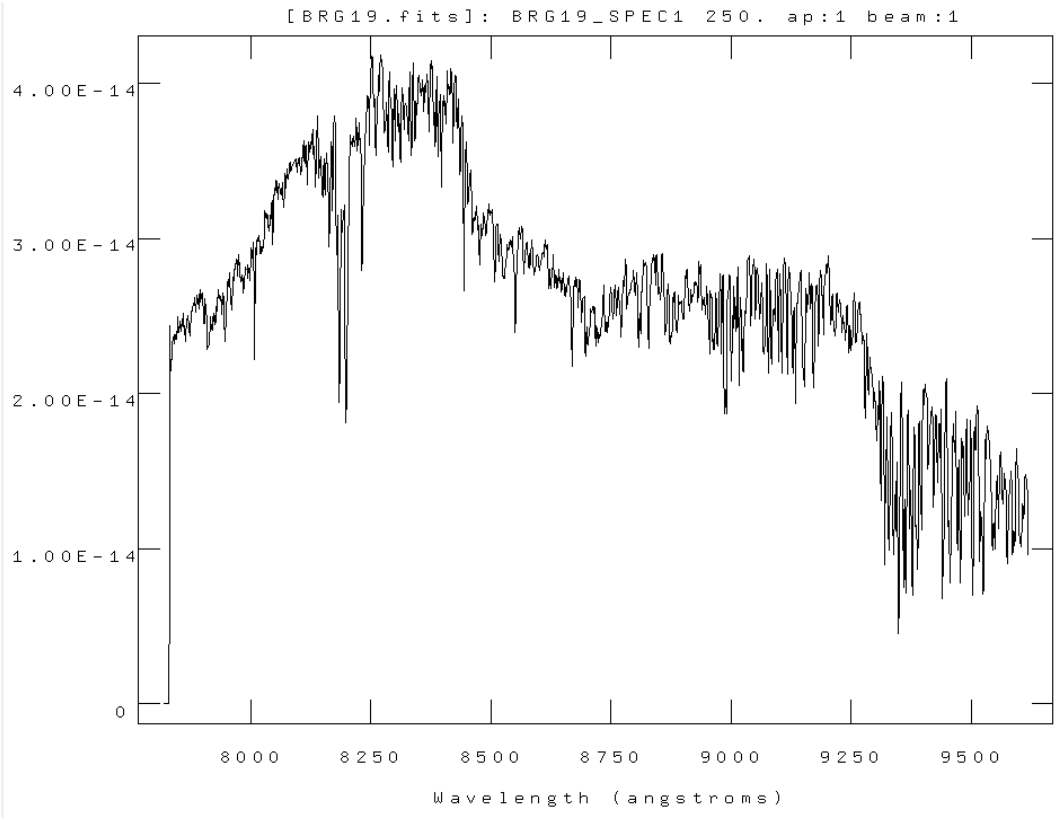

Figure D.19: The final flux calibrated spectrum of object BRG19 with flux in $\mathrm{erg}^{-2}\ \mathrm{cm}^{-2}\ \mathrm{s}^{-1}\ \mathrm{\AA}^{-1}$.

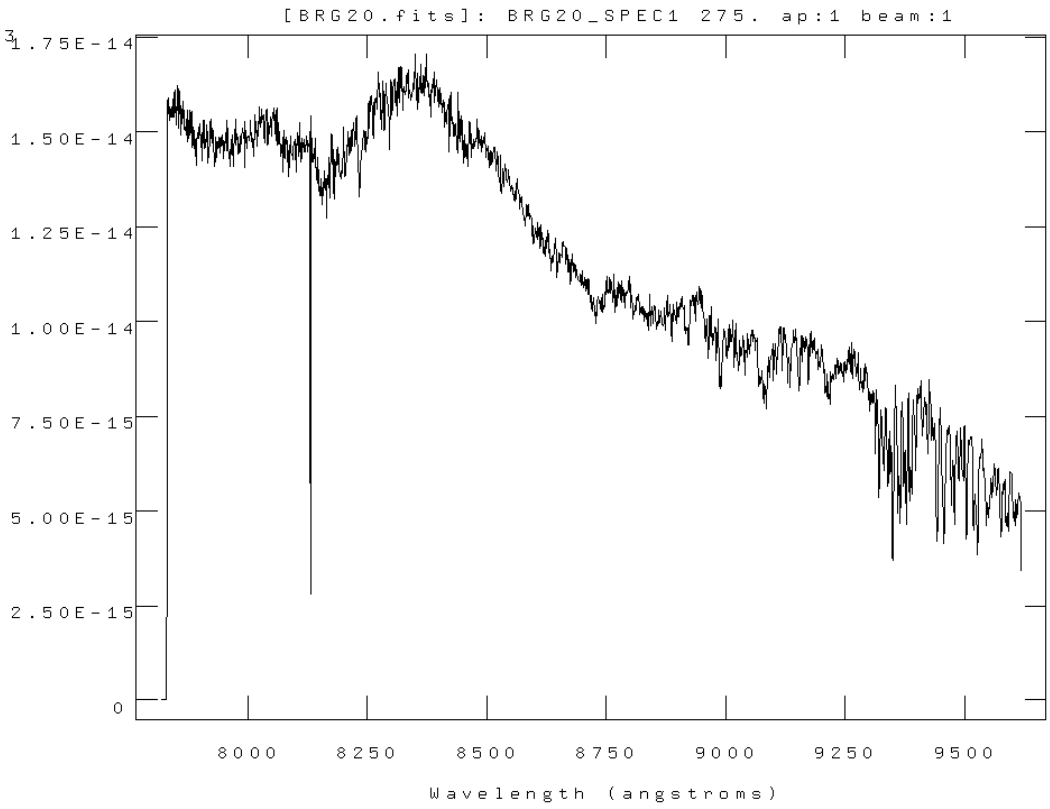

Figure D.20: The final flux calibrated spectrum of object BRG20 with flux in $\mathrm{erg}^{-2}\ \mathrm{cm}^{-2}\ \mathrm{s}^{-1}\ \mathrm{\AA}^{-1}$.

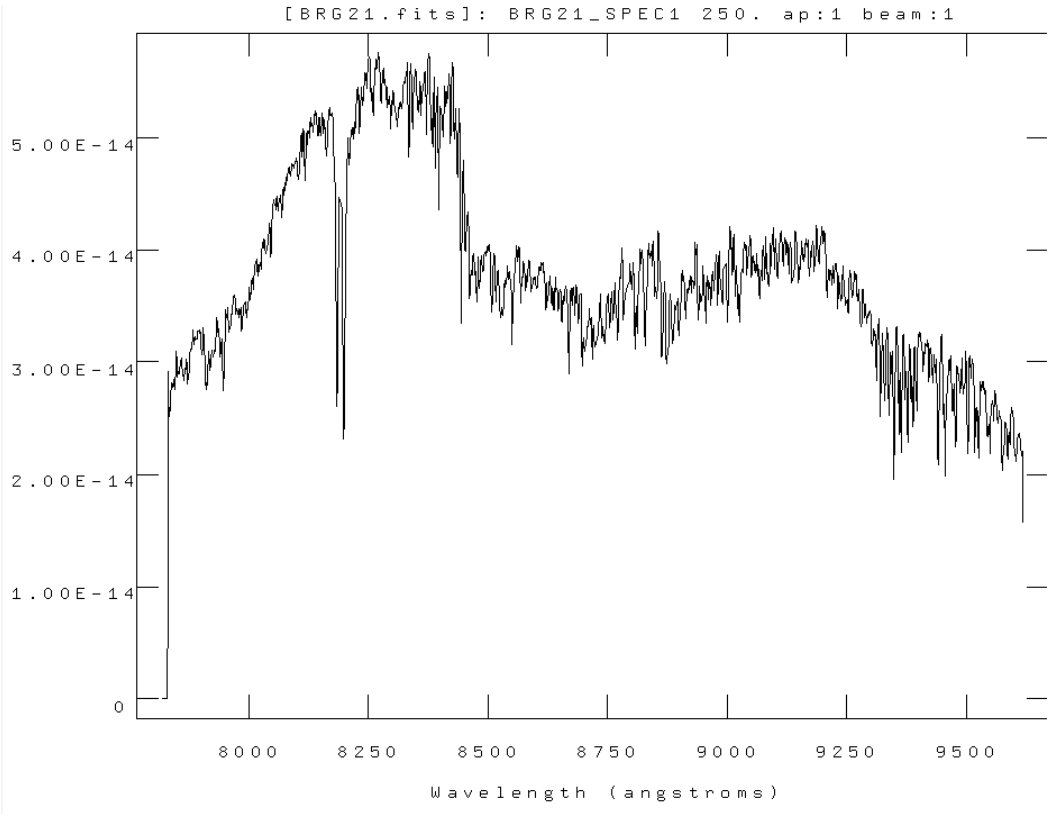

Figure D.21: The final flux calibrated spectrum of object BRG21 with flux in $\mathrm{erg}^{-2}\ \mathrm{cm}^{-2}\ \mathrm{s}^{-1}\ \mathrm{\AA}^{-1}$.

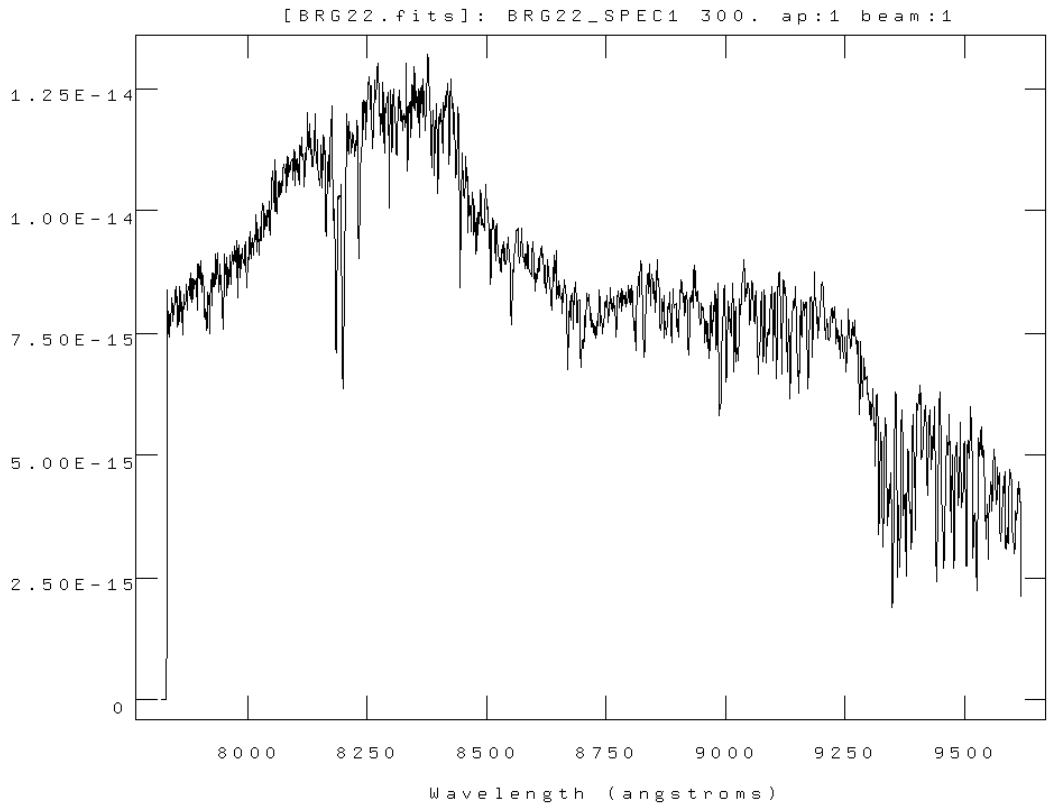

Figure D.22: The final flux calibrated spectrum of object BRG22 with flux in $\mathrm{erg}^{-2}\ \mathrm{cm}^{-2}\ \mathrm{s}^{-1}\ \mathrm{\AA}^{-1}$.

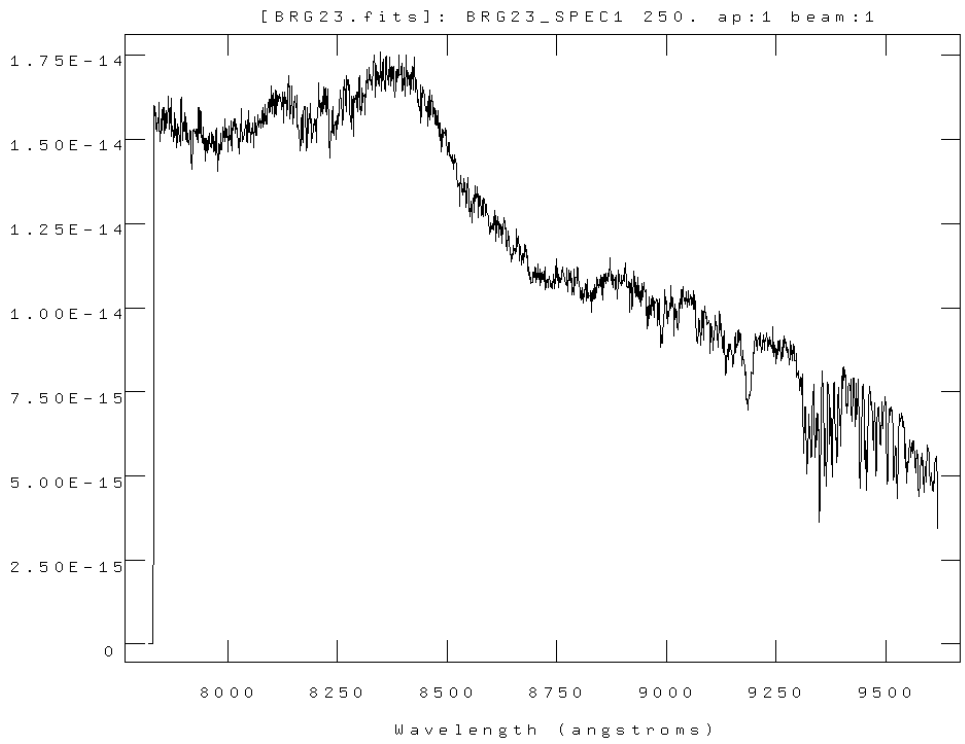

Figure D.23: The final flux calibrated spectrum of object BRG23 with flux in $\mathrm{erg}^{-2}\ \mathrm{cm}^{-2}\ \mathrm{s}^{-1}\ \mathrm{\AA}^{-1}$.

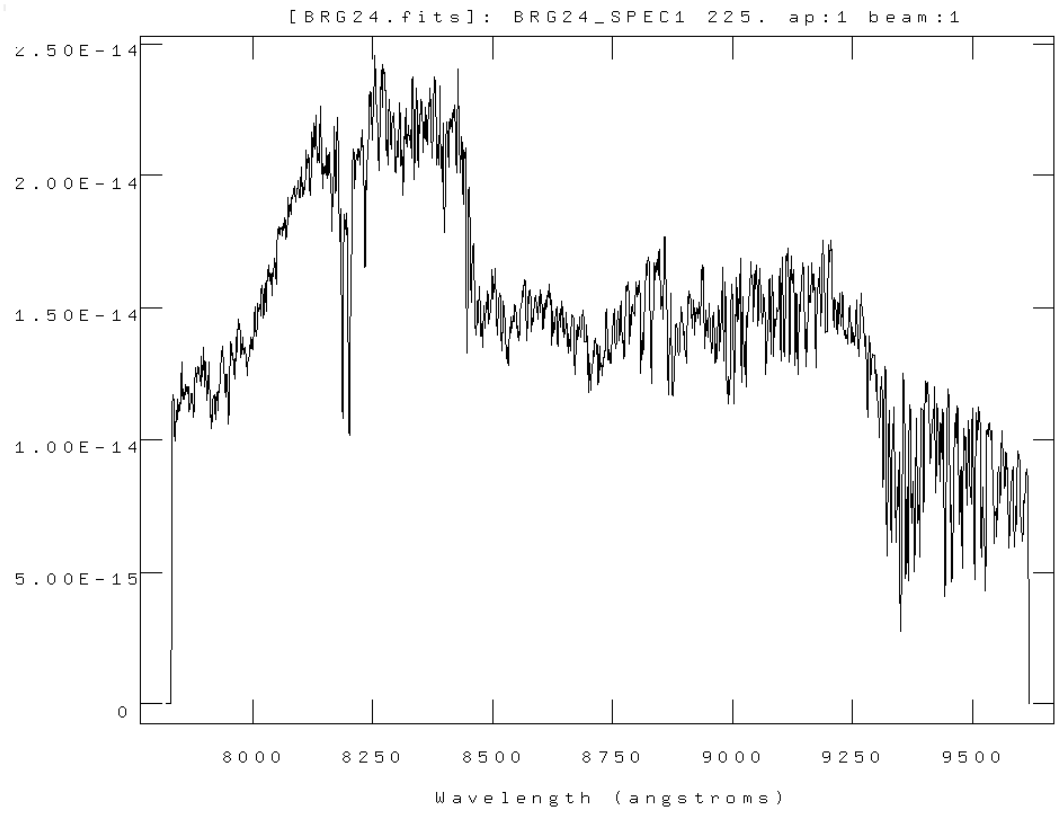

Figure D.24: The final flux calibrated spectrum of object BRG24 with flux in $\mathrm{erg}^{-2}\ \mathrm{cm}^{-2}\ \mathrm{s}^{-1}\ \text{Å}^{-1}$.

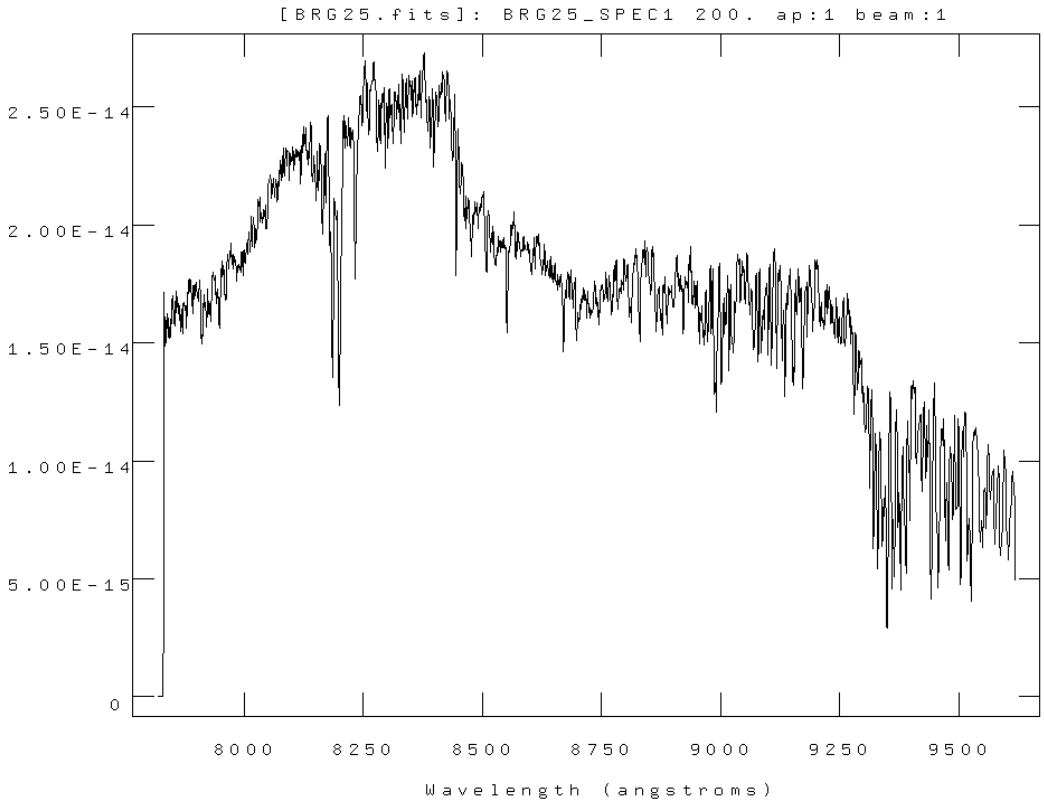

Figure D.25: The final flux calibrated spectrum of object BRG25 with flux in $\mathrm{erg}^{-2}\ \mathrm{cm}^{-2}\ \mathrm{s}^{-1}\ \mathrm{\AA}^{-1}$.

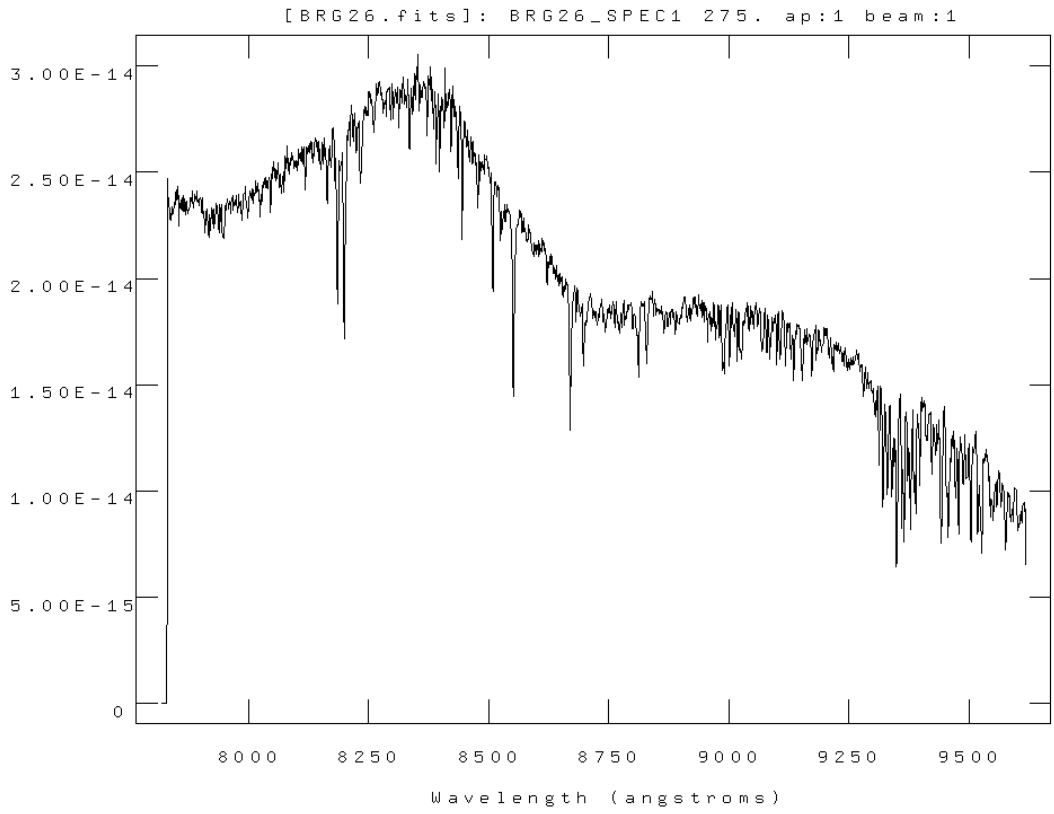

Figure D.26: The final flux calibrated spectrum of object BRG26 with flux in $\mathrm{erg}^{-2}\ \mathrm{cm}^{-2}\ \mathrm{s}^{-1}\ \mathrm{\AA}^{-1}$.

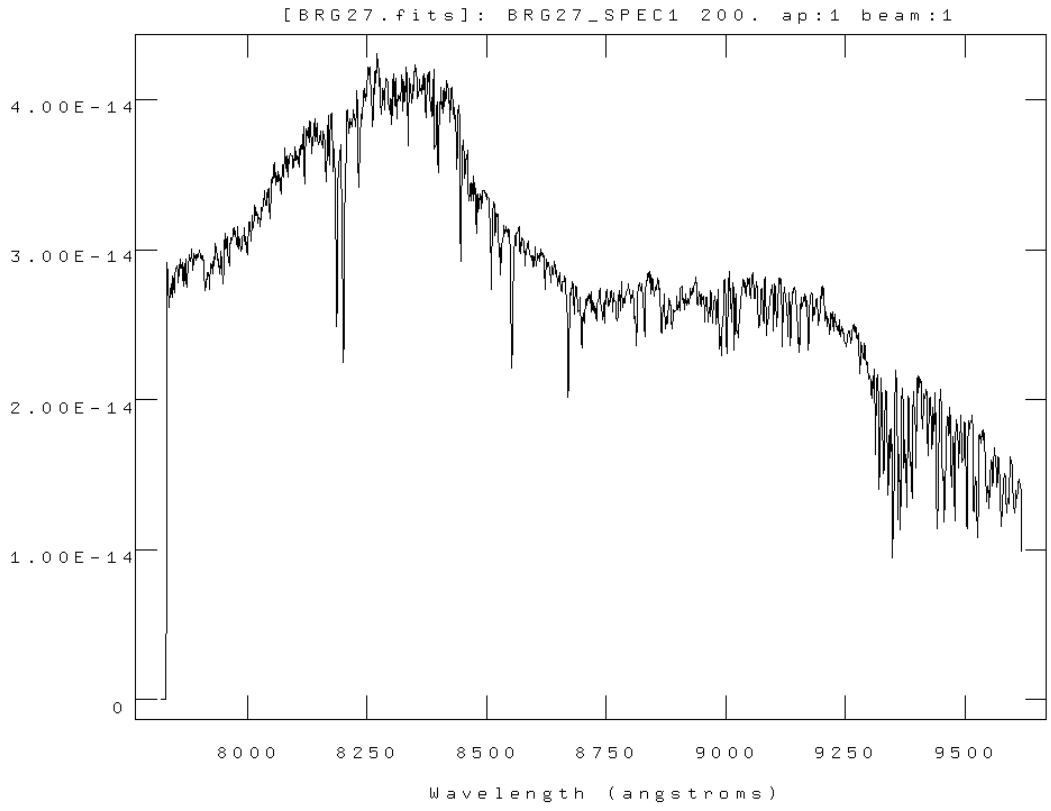

Figure D.27: The final flux calibrated spectrum of object BRG27 with flux in $\mathrm{erg}^{-2}\ \mathrm{cm}^{-2}\ \mathrm{s}^{-1}\ \mathrm{\AA}^{-1}$.

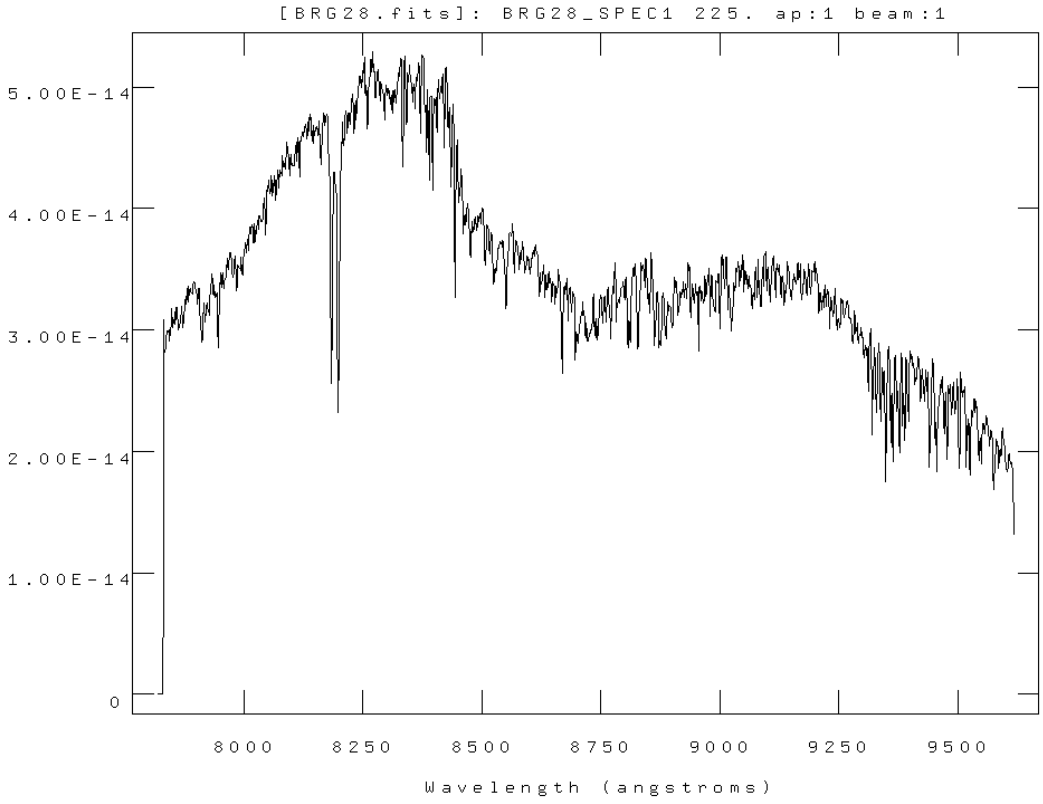

Figure D.28: The final flux calibrated spectrum of object BRG28 with flux in $\mathrm{erg}^{-2}\ \mathrm{cm}^{-2}\ \mathrm{s}^{-1}\ \text{Å}^{-1}$.

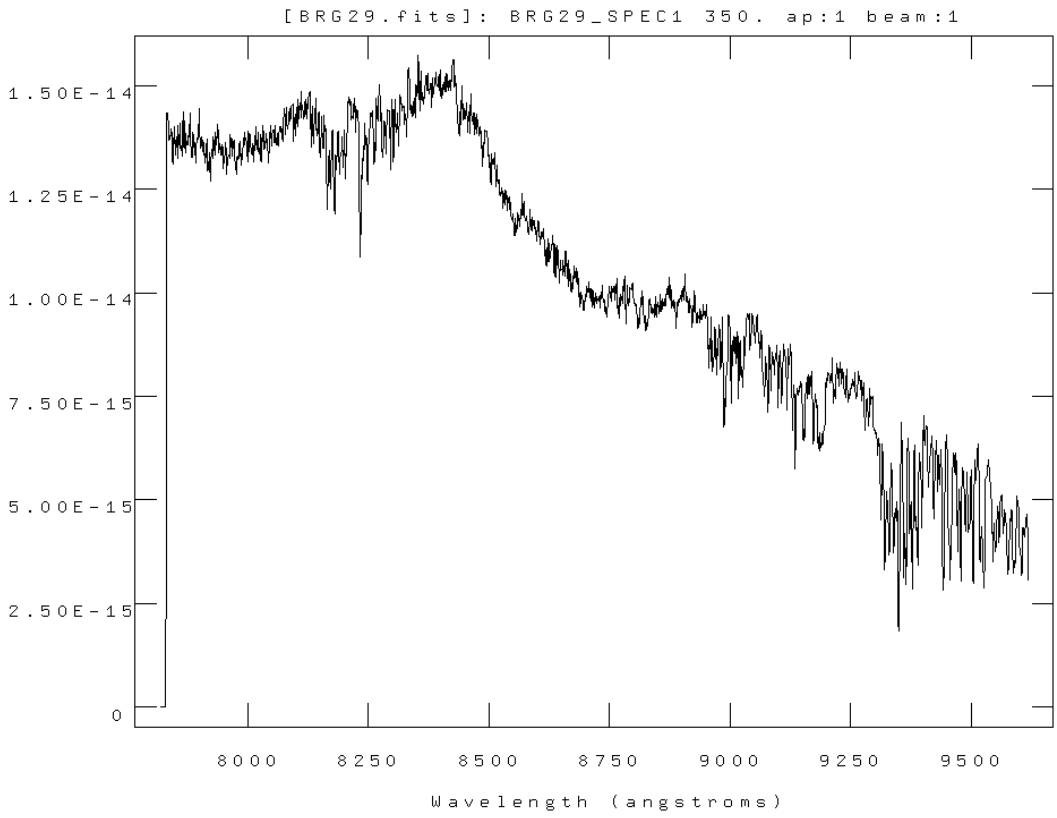

Figure D.29: The final flux calibrated spectrum of object BRG29 with flux in $\mathrm{erg}^{-2}\ \mathrm{cm}^{-2}\ \mathrm{s}^{-1}\ \text{Å}^{-1}$.

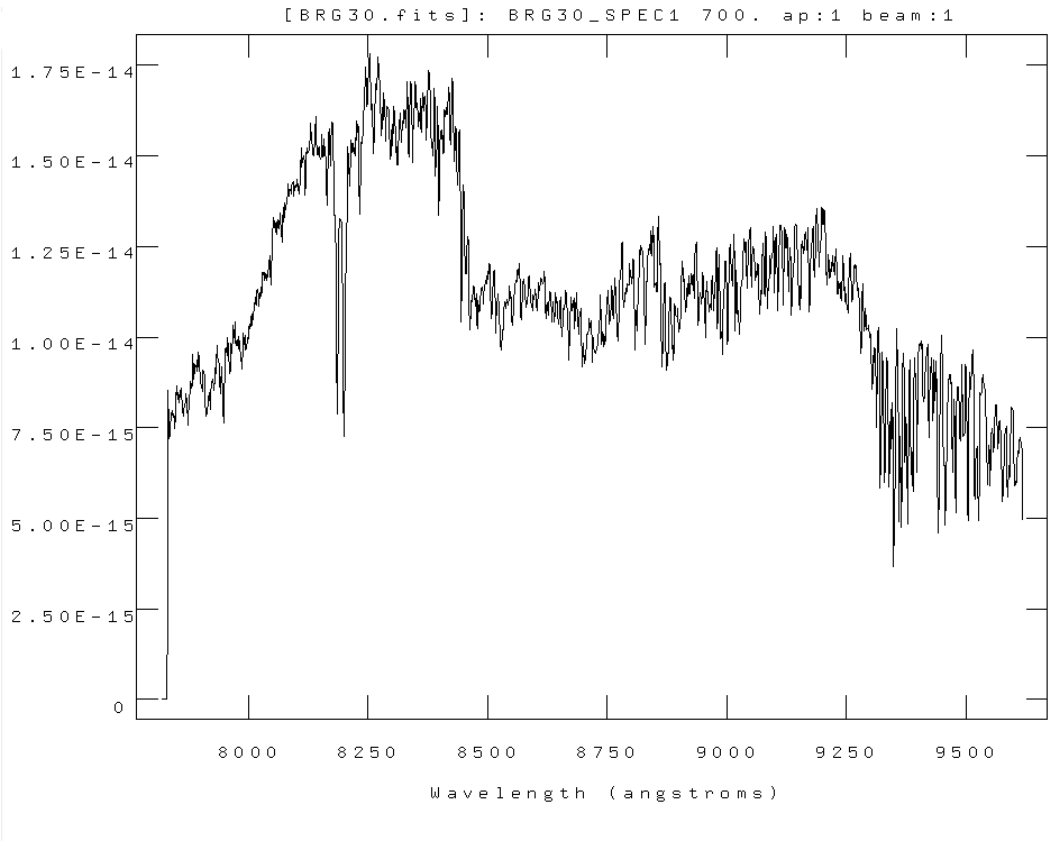

Figure D.30: The final flux calibrated spectrum of object BRG30 with flux in $\mathrm{erg}^{-2}\ \mathrm{cm}^{-2}\ \mathrm{s}^{-1}\ \mathrm{\AA}^{-1}$.

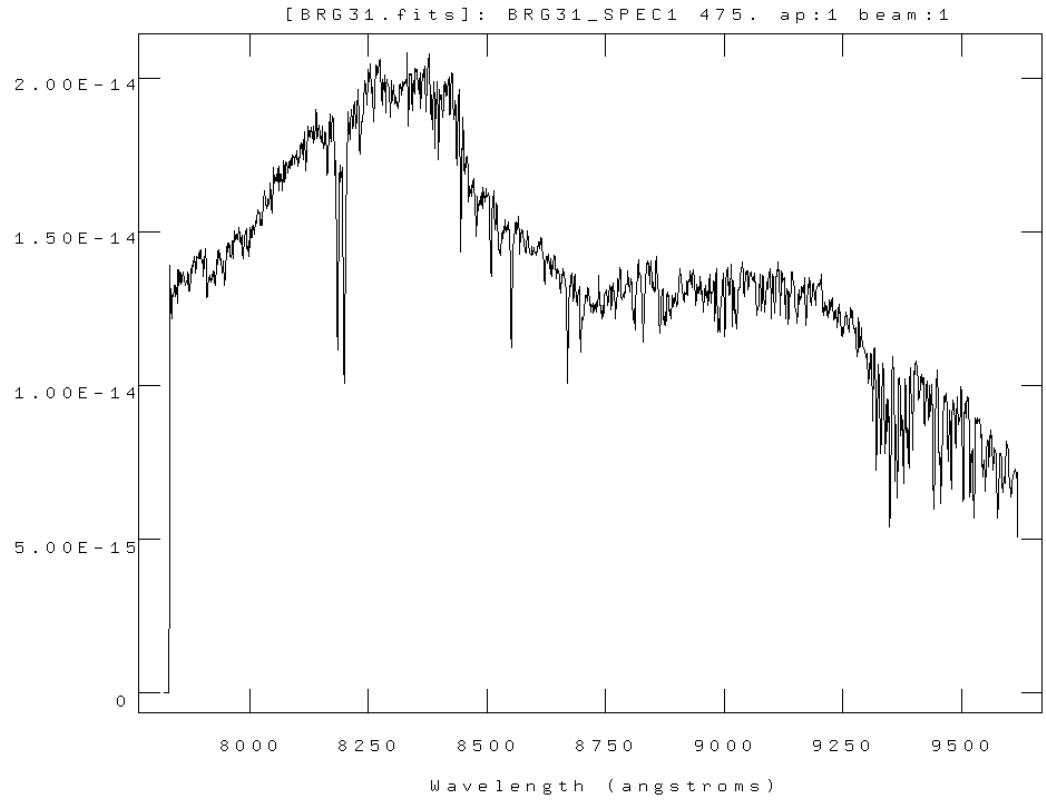

Figure D.31: The final flux calibrated spectrum of object BRG31 with flux in $\mathrm{erg}^{-2}\ \mathrm{cm}^{-2}\ \mathrm{s}^{-1}\ \mathrm{\AA}^{-1}$.

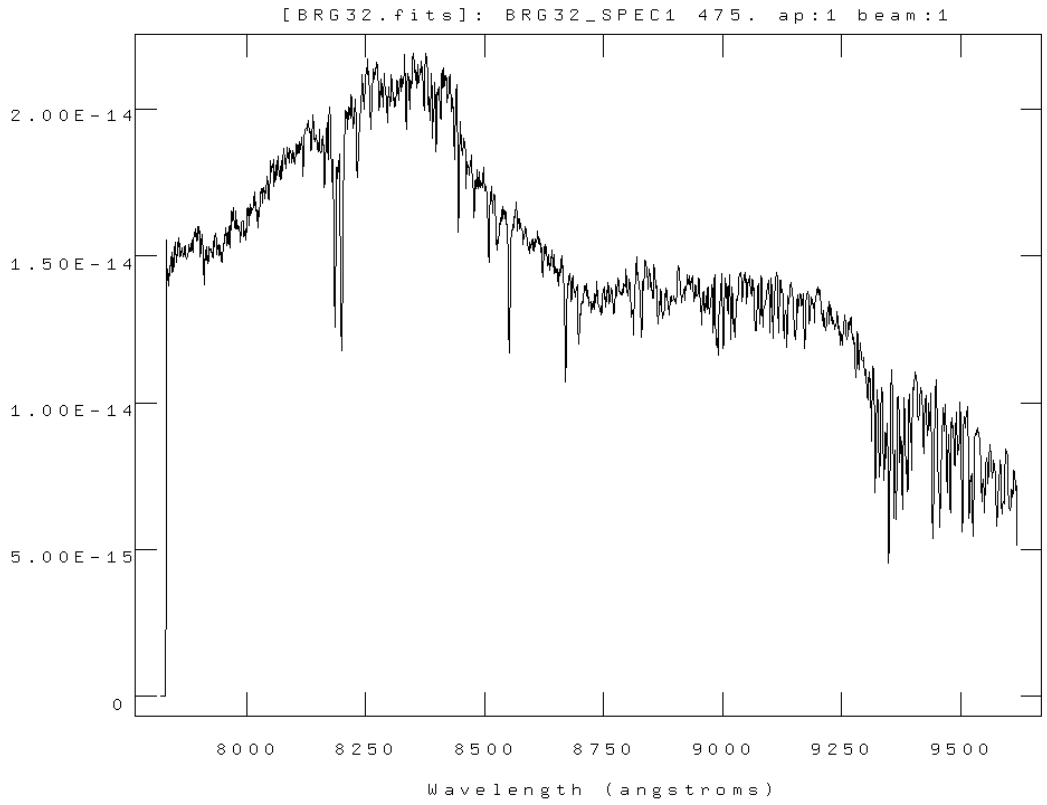

Figure D.32: The final flux calibrated spectrum of object BRG32 with flux in $\mathrm{erg}^{-2}\ \mathrm{cm}^{-2}\ \mathrm{s}^{-1}\ \mathrm{\AA}^{-1}$.

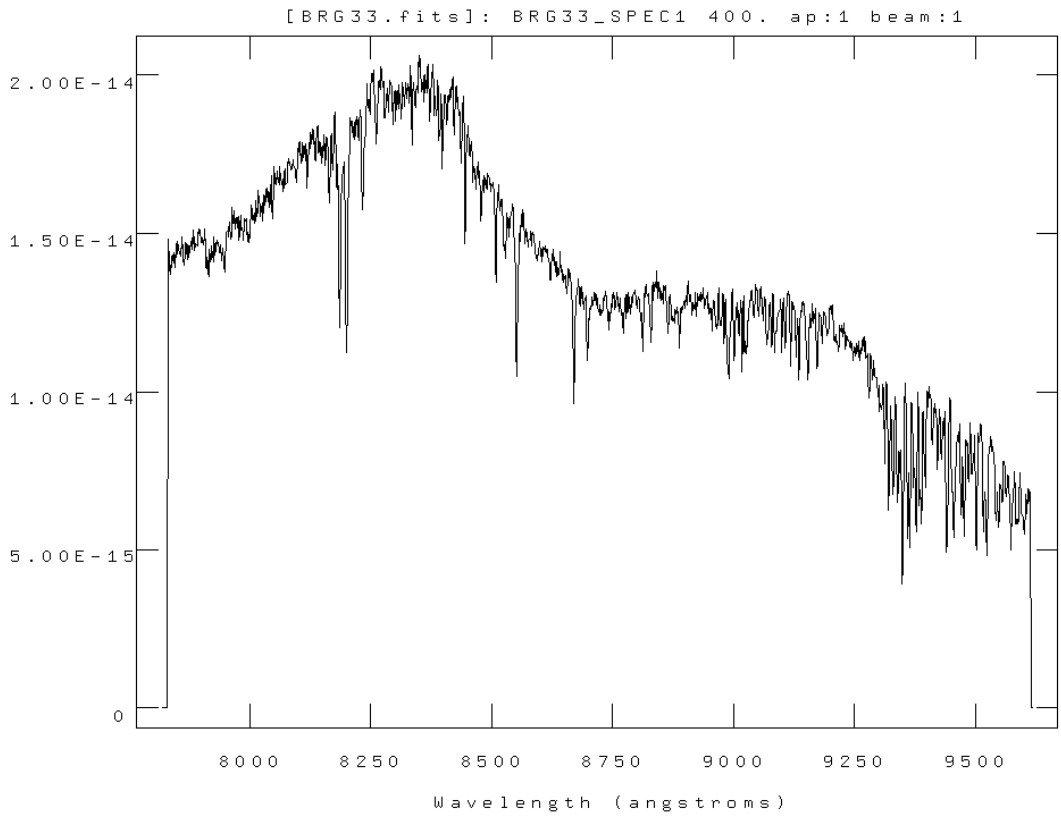

Figure D.33: The final flux calibrated spectrum of object BRG33 with flux in $\mathrm{erg}^{-2}\ \mathrm{cm}^{-2}\ \mathrm{s}^{-1}\ \mathrm{\AA}^{-1}$.

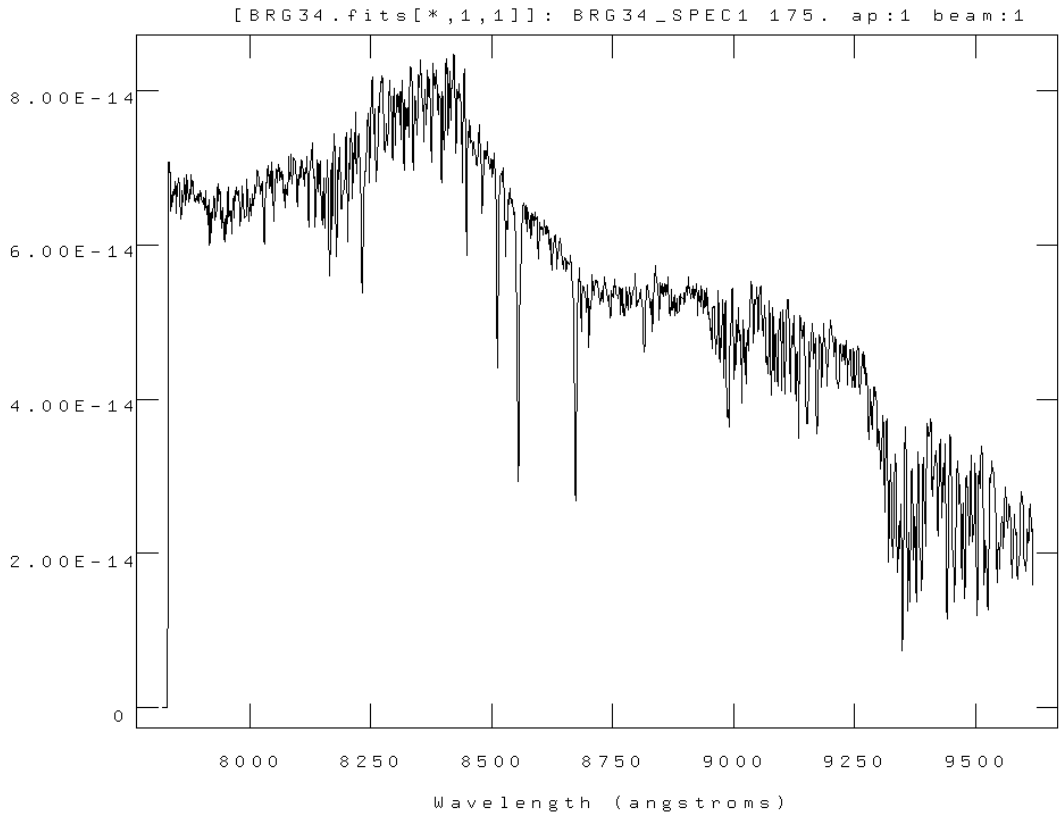

Figure D.34: The final flux calibrated spectrum of object BRG34 with flux in $\mathrm{erg}^{-2}\ \mathrm{cm}^{-2}\ \mathrm{s}^{-1}\ \mathrm{\AA}^{-1}$.